SYNTHESIS AND EVALUATION OF AHOKO KAOLIN DERIVED ZEOLITE A AND PHILLIPSITE SUPPORTED FERTILIZER ON SELECTED AGRONOMIC CHARACTERISTICS OF TOMATO (*Lycopersicon esculentum*)

BY

SALAKO, Oluwafemi

PhD /SEET/2015/791

A THESIS SUBMITTED TO THE POSTGRADUATE SCHOOL, FEDERAL UNIVERISRY OF TECHNOLGY, MINNA, NIGERIA IN PARTIAL FULFILMENT OF THE REQUIREMENTS FOR THE AWARD OF THE DEGREE OF DOCTOR OF PHILOSOPHY (PhD) IN CHEMICAL ENGINEERING

AUGUST, 2021

ABSTRACT

The high leachability of soluble conventional fertilizers causes environmental pollution and the low cation exchange capacity of farmlands reduces soil fertility and agricultural yields. The aim of this study was to synthesise and characterise Zeolite A and Phillipsite from Ahoko Kaolin and to evaluate their plant nutrient delaying capacity on tomato growth, fruit yield, nutritional quality and postharvest soil residues. Zeolite A and phillipsite were synthesised from Ahoko kaolin using hydrothermal methods. The zeolites synthesis parameters of aging time, crystallisation temperature and time were optimised using central composite design. The zeolites surfaces were modified with Hexadecyltrimethylammonium (HDTMA) through an adsorption process and further enriched with Nitrogen, Phosphorous, Potassium (NPK). The isotherms, kinetics and thermodynamics parameters of zeolite A and Phillipsite were determined. The desorption rate of the synthesised zeolite A and phillipsite based fertilizers were determined through percolating columns. The effect of Zeolite A, Phillipsite based fertilizers and NPK 15:15:15 fertilizers were evaluated on the agronomic characteristics of tomato crop. The results showed that the crystallinity of synthesised zeolite A and Phillipsite were 99.92 % and 72.26 % respectively. The specific surface area of Zeolite A and Phillipsite were 296.178 m^2/g and 361.50 m^2/g respectively. The regression model revealed that crystallization time contributed the highest to the crystallinity of zeolite A and phillipsite. The modification of zeolite A with HDTMA gave the maximum adsorption capacity of 3.10 mg/g with an initial concentration of 162.6 mmol/L, contact time 8 h and temperature at 25 ^{o}C while the modification of Phillipsite with HDTMA gave a maximum adsorption capacity of 3.40 mg/g with initial concentration of 195 mmol/L, contact time of 16 h and temperature 25 ^{o}C. The specific surface area of surfactant modified zeolite A and phillipsite were 65.257 m^2/g and 312.429 m^2/g, respectively. The Freundlich isotherm model represented the best fit for the experimental adsorption data of zeolite A with correlation coefficient R^2 = 0.7843 and the lowest error values of sum of square errors (SSE) (1.0377) and average relative error deviation (ARED) 24.5469. Dubinin Radushkevich isotherm model represented the best fit for the experimental adsorption data on Phillipsite with R^2 = 0.9633 and lowest values of the SSE (0.0004) and ARED (0.4142). The pseudo-first-order model with R^2 0.9992 and 0.7979 for zeolite A and phillipsite respectively represented the adsorption kinetics of the two zeolites. The Gibb's free energy for zeolite A and phillipsite were -27.045 kJ/mol and -61.799 kJ/mol respectively at temperature of 298K which points to the spontaneity of the adsorption processes. The negative enthalpies of -12.20 kJ/mol and -35.06 kJ/mol for zeolite A and Phillipsite showed that the adsorption processes were physical and exothermic. The phosphate loaded zeolite A based fertilizer showed slow release effect with the rate constant k_2 of 1.8 x 10-3h^{-1} higher than KH_2PO_4 with its rate constant of 3.84 x10-3 h^{-1}. The nitrate loaded zeolite A based fertilizer with rate constants 5.51 x 10-2 h^{-1} were slower than NH_3NO_3 fertilizer with rate constants 9.70 x 10-2 h^{-1} in the second phase of the leaching process. The slow release property of the zeolite A and Phillipsite based fertilizers were indicated through the leaf counts with mean value of 54.2 and 46.5 significantly higher to NPK 15:15:15 with a mean of 25.7 at 11 weeks after transplanting in 2018. Zeolite A and phillipsite based fertilizers produced fruit mean values of 84.69 and 83.36 g/plant significantly higher to NPK 15:15:15 with fruit mean value of 69.34 g/plant. Also, the vitamin C mean values 123.34 and 126.54 mg/100g of tomato fruit grown with Zeolite A and Phillipsite were significantly higher than those grown with NPK with mean 84.60 mg/100g. The results further showed that the soils with Zeolite based fertilizers significantly retained higher plant nutrients than soils treated with NPK at post harvest. The findings from this study revealed that zeolite based fertilizers significantly improved fruit yield, nutritive contents and postharvest soil content compared to NPK fertiliser.

TABLE OF CONTENTS

LIST OF TABLES

LIST OF FIGURES

LIST OF PLATES

ABBREVIATIONS, GLOSSARIES AND SYMBOLS

AEC	Anion exchange capacity
ANOVA	Analysis of variance
ASTM	American Society for Testing and Materials
AOAC	Association of Official Analytical Chemist,
BET	Brunanuer Emmett Teller
CCD	Central Composite Design
CEC	Cation Exchange Capacity
CRD	Completely Randomized Design
DMRT	Duncan's multiple range test
ECEC	External cation exchange capacity
EDS	Energy dispersive X-ray Spectroscopy
EDX	Energy dispersive X-ray
EDX	Energy dispersive X-ray spectroscopy
Fe	Iron
FTIR	Fourier transform infrared spectroscopy
FUE	Fertilizer use efficiency
ΔG	Gibb's free energy
ΔH	Enthalpy
HDTMA-Br	Hexa-decyltrimethyl ammonium bromide
K	Potassium
KOH	Potassium hydroxide
KH_2PO_4	Potassium dihydrogen Phosphate
LTA	Linde Type A

NaOH	Sodium hydroxide
N_2	Nitrogen
NaOH	Sodium hydroxide
Ni	Nickel
NH_4OH	Ammonium hydroxide
NPK	Nitrogen, Phosphorous Potassium fertilizer
OH^-	Hydroxyl group
P	Phosphorous
S	Entropy
SEM	Scanning electron microscopy
SMZ	Surfactant modified zeolite
SRF	Slow-release fertilizer
SSA	Specific surface area
TGA	Thermogravimetric Analyses
TEM	Transmission electron microscopy
WAT	Weeks After Transplanting
XRD	X-ray Diffraction
XRF	X-Ray Fluorescence

CHAPTER ONE

1.0 INTRODUCTION

1.1 Background to the Study

Future of agricultural activities is at risk as it has continued to grapple with lots of challenges such as soil erosion, water use and excessive fertilizer application (Liu *et al*., 2015). The loss of nutrients in soil leads to the deficiency of vital nutrients needed for plant growth thereby necessitating the use of fertilizers. Sources of soil nutrients include organic matter, chemical fertilizers, and some plants which fix atmospheric nitrogen that help in maintaining the soil fertility (Bharadwaj, 2016). All these make it possible for farmers to sustainably grow nutritious crops. Fertilizers are simply plant nutrients which are sources of Nitrogen, Phosphorous and Potassium nutrients for proper plant growth. Among the major plant nutrients, nitrogen is the most important for higher crop yields (Maheswari *et al*., 2017). These plant nutrients could be available as inorganic fertilizers and organic fertilizers.

Organic fertilizers generally require large amounts and extra investment of labour to have desired effects (Gao *et al*., 2017). Their availability is an obstacle, especially in remote areas where they need to be applied seasonally. Studies by Ali and Danafar (2015) revealed that improving fertilizer use efficiency is important not only for reducing the cost of cultivation but also to prevent soil and environmental degradation. Further studies have led to the search of natural materials that could be incorporated into the fertilizer mix to increase their plant nutrient efficiency. Natural occurring materials such as perlites and zeolites have drawn much attention. Zeolites are inorganic materials whose main properties of high cation exchange capacity, high water holding

capacity in the free channels, and high adsorption capacity are of great interest for agricultural purposes (Chen *et al*., 2017).

Zeolites are crystalline, micro-porous, hydrated aluminosilicates that are built from an infinitely extending three dimensional network of $[SiO_4]^{4-}$ and $[AlO_4]^{5-}$ tetrahedral linked to each other by the sharing of oxygen atoms (Gu *et al*., 2019). They form an important group of inorganic materials with valuable industrial interest, which is derived from their molecular sieving, ion exchange and catalytic properties (Sharma and Sanbi, 2010). The possession of these unique ion-exchange, dehydration-rehydration, and adsorption properties can contribute significantly in agricultural and aqua-cultural technology (Bumbac *et al*., 2016). These properties are inherent in this material because of the presence of extensive isomorphous substitution and three dimensional channeled framework of aluminates and silicates with permanent negative charge. The cage-like polyhedral units with a high cation exchange capacity and internal pores in the crystal lattices have resulted in high water adsorption, nutrient retention and increase cation exchange capacity of the soil. Zeolites have been widely used in agriculture for nitrogen capture, control release of plant nutrients, reduction in nitrogen nitrification, leaching, increment in the yield of agricultural crop and increased vitamin content (Jakkula and Wani, 2018). Zeolites have found relevance in improving nitrogen and phosphorous use efficiency, as fertilizer input in farming, soil amelioration, remediation of contaminated soil, removal of odour, as soil amendment and wastewater treatment (Jakkula and Wani, 2018). Manikandan and Subramanian (2016) had also demonstrated the high potential of zeolitic minerals as nitrogen fertilizers which consequently diminishes environmental problems such as high concentration of nitrogen and phosphorous in ground and surface water.

Zeolites are traditionally natural minerals which could presently exist in synthetic forms because the formation conditions in nature can be replicated in the laboratory at shorter duration. Synthetic zeolites are used commercially more often than natural zeolites due to the purity of crystalline products and the uniformity of particle sizes. The main barrier militating against zeolite synthesis is the availability and cost of raw material specifically the silica and alumina sources (Musyoka *et al*., 2014). Cheaper raw materials, such as clay minerals, coal ashes and municipal solid waste incinerating ashes are utilised as starting materials for zeolite synthesis (Ayele *et al*., 2016). Other sources of zeolite synthesis include fly ash, feldspar and rice husk are widely used for synthesis of zeolites (www.iza-online.org).

Kaolin is a clay mineral with SiO_4 tetrahedral sheets linked to $Al(O,OH)_6$ octahedral sheets through shared oxygen. It can be transformed into zeolite through two steps: (i) metakaolinization which involves converting kaolin into metakaolin by chemical activation of the kaolin clay and (ii) zeolitization which involves the treatment of the metakaolin with an alkali solution to form zeolite (Kovo, 2009). The uniqueness of zeolite structure gives it the ability for different functional groups to modify its surface. Zeolites surfaces can be modified by surfactants to act as slow release fertilizers to promote plant growth (Subramanian *et al*., 2015). Low cost cationic surfactants, such as tetraethylammonium bromide (TEA-Br), tetramethylammonium bromide (TMA-Br), hexadecyltrimethylammonium bromide (HDTMA-Br) are attached to the external surface of the zeolite and then subjected to the loading of cationic nutrients such as K^+ and NH_4^+ in the pores simultaneously with the anionic nutrients such as NO_3 or PO_4 on the zeolite surface (Bansiwal *et al*., 2006). The application of zeolite based fertilizers have found relevance in regulating the needed uptake of the appropriate plant nutrients,

reducing fertilizer applications, solving the problem of excess fertilizers applications which are washed off into water bodies and consequently minimizing environmental pollution (Ramesh *et al*., 2015). The use of zeolite as soil ammendements was reported by Lisa (2007) where a commercial zeolite product, ZeoPro was used to enhance plant yields. Several experiments were carried out on the effects of the zeolite on the growth of cucumber and tomato seedlings in the U.S for ZeoponiX in turf, floriculture and vegetable applications.

Further studies by Jami *et al*. (2019) reported that application of zeolite and cattle manure, in soils exposed to drought stress, could retain moisture content and improve plant growth and yield components of crops. Jie *et al*. (2015) mentioned that zeolite performed better in adsorbing and releasing anionic nutrients after modification with cationic surfactant HDTMA (SMZ) was added in propagating substrate for the germination of some vegetables. This present study focuses on the synthesis of zeolite A and Phillipsite from Ahoko Kaolin as fertilizer carriers and evaluation of their effects on growth, fruit yield and quality of tomato cultivated.

1.2 Statement of the Research Problem

Most agricultural farmlands are low in soil fertility because of low cation exchange capacity and continual depletion of soil nutrients from frequent farming. Soil fertility enhancers such as as ammonium salts, potassium nitrate and NPK fertilizers are also highly soluble and often leach beyond the root zone thereby reducing the plant nutrient use efficiency. The frequent and excessive use of inorganic fertilizers cause pollution of the ground and surface water leading to eutrophication in aquatic ecosystems. The materials used as fillers for handling purposes of conventional NPK 15: 15: 15 fertilizers do not adhere on the plant nutrients thereby act as bulk additions.

1.3 Aim and Objectives

The aim of this study is to synthesise and characterise zeolite A and phillipsite from Ahoko kaolin and evaluate their fertilizer carrying effects on growth, fruit yield and quality of tomato. The objectives are to;

i). Synthesise and characterise zeolite A from raw Ahoko kaolin as well as evaluate the effects of varying synthesizing parameters such as stirring time, ageing time, crystallisation time, and crystallisation temperature on percentage crystallinity of zeolite A;

ii). Synthesise and characterise phillipsite from raw Ahoko kaolin as well as evaluate the effect of varying synthesizing parameters such as ageing time, crystallisation time and crystallisation temperature on percentage crystallinity of phillipsite;

iii) Functionalise the surfaces of zeolite A and phillipsite with Hexadecyltrimethylamminiumbromide (HDTMA) and occlude with fertilizer nutrients;

iv). Evaluate the isotherm, kinetic and thermodynamic parameters of the adsorption of HDTMA on zeolite A and Phillipsite

v). Evaluate the desorption rate of the synthesised zeolite A and phillipsite based fertilizers;

v) Evaluate the release mechanism of the zeolite A and phillipsite based fertilizers on growth, fruit yield, quality and post-harvest soil parameters of tomato grown.

1.4 Justification of the Study

This research is important because the synthesis of zeolite A and phillipsite with its high cation exchange capacity would improve soil fertility on application. The modification of the surfaces of the synthesised zeolites would help to improve the adsorption capacity of negatively charged anions such as phosphates and nitrates on the surface of the

modified zeolite and consequently increase the adsorption intensity of the anions on the modified zeolite. The occlusion of plant nutrients in the pore openings of the zeolites would reduce the rate of release of plant nutrients to the crop and consequently reduce environmental pollution caused by plant nutrient leaching beyond the root zone. The production of zeolite based fertilizer would increase the nutrient use efficiency and handling characteristics of the fertilizer.

1.5 Scope of the Study

The scope of the study is limited to an optimised synthesis of zeolite A and phillipsite from Ahoko kaolin and an optimized adsorption process of HDTMA on the zeolites surface and consequently loaded with plant nutrients. The kinetics and thermodynamics of the adsorption of surfactant modifiers on the synthesised zeolites were studied. The characterisation of the synthesised zeolite A and phillipsite were done using X-ray Diffraction (XRD), Scanning electron microscopy (SEM), X-ray Fluorescence (XRF) and Brunanuer Emmett Teller (BET), Fourier transform infra-red spectroscopy (FTIR), Cation exchange capacity (CEC), External cation exchange capacity (ECEC) analysis were carried out during the adsorption process. The nutrient release mechanism of modified zeolite A and phillipsite based fertilizer carriers on the growth and fruit yield of tomato (*Lycopersycum esculentum*) were evaluated in a pot experiment.

CHAPTER TWO

2.0 LITERATURE REVIEW

2.1 Overview of Fertilizers

Globally, food security has been observed to be declining as a result of decreasing quality and quantity of the soil resource base (Bouakham, 2015). Most soils in the tropics are low in fertility because of low cation exchange capacity of the soil and continuous depletion of nutrients with inefficient farming practices. The efficient application of inorganic fertilizers, water, and other nutrients has been on the decrease. This development has necessitated the use of fertilizers to improve soil fertility (Jakkula and Wani, 2018|). Fertilizers are chemical or natural substances added to soil to increase its fertility (Manikandan and Subramanian, 2016). Fertilizers could be natural or synthetic. Synthetic fertilizers are man-made inorganic compounds usually derived from bye products of the petroleum industry. Examples are ammonium nitrate, ammonium phosphate, single super phosphate and potassium sulphate. Synthetic fertilizers are also known as inorganic fertilizers used in agriculture as low-cost and rapid source of plant nutrients that result in an enormous rise in plants productivity (Zahoor *et al*. 2015; Ahmed *et al*., 2017).

However, these synthetic fertilizers are prone to sorption, runoff, degradation and leaching processes. Leaching occurs when the water that fills the pores in the soil begin to move downwards by gravity with any plant nutrient present in the soil. The solubility of synthetic fertilizers worsens their propensity to damage the environment especially through eutrophication. The high concentration of phosphorous and nitrogen in surface water results to algae proliferation, increase in oxygen demand, decrease in waterways storage and transport capacity (Bhardwaj and Tomar, 2011). The need to reduce

groundwater pollution caused by phosphates and nitrates, and the need for fertilizer use efficiency had necessitated the concept of slow release fertilizers. Slow release fertilizers include synthetic anion and cation exchange resins and also plant nutrient carriers such as zeolites which are known for their high cation exchange capacity (Li *et al*., 2017). The advantage of synthetic zeolite over the natural one lies in their ability to control the uniformity of the pore sizes and the surface area of the zeolite. The advantage of synthetic zeolite based fertilizers over synthetic exchange resins are that zeolite based fertilizers are the most environmental friendly (Lateef *et al*., 2016). The unique zeolite properties of adsorption, ion exchange and dehydration-rehydration with its nanopores make the zeolite study relevant in fertilizer development in agriculture.

2.2 Zeolites

The term zeolite comes from a Greek word which means stone that boils. Swedish mineralogist Axel Fredrik Cronstedt introduced "zeolite" in 1756 for certain silicate minerals in reference to their behaviour on heating in a borax bead (Shah *et al*., 2016). The potential raw materials for zeolite synthesis include coal fly ash, oil shale ash, bagasse fly ash, high silicon fly ash, waste sandstone cake, paper sludge, waste porcelain, bentonite and kaolinite (Ayele *et al*., 2016).

Kaolinte is an aluminisilicate clay mineral that is made up of one silica tetrahedron sheet and one alumina octahedron sheet in a 1:1 stoichiometric ratio. The SiO_2/Al_2O_3 molar ratio (approximately 1) of kaolinite is very similar to zeolite A, thereby making kaolinite a good precursor for the synthesis of zeolite A. The application of kaolinite is closely related to its reactivity and surface properties, which depend strongly on surface modification (Arogundade, 2014). Kaolinite crystals are thermally broken down to partially disordered structure with a new phase called metakaolinte. The process is

called dehydroxylation or calcination which is the conversion of kaolinite into a shapeless state by the loss of its hydroxyl groups. Heller-kallai (2013) reported that the XRD interpreted the kaolinite mineral as amorphous even when some octahedral layer were preserved after dehydroxylation. Johnson and Arshad (2014) reported that the alkaline activation of the kaolinite enhances its reactivity so that it can be easily converted to zeolites. The authors also reported the effects of calcination at low range 300 to 500 ^{o}C, medium range 600 to 800 ^{o} C, and high range 800 to 900 ^{o} C. Kovo and Edoga (2005) reported the calcination of Ahoko kaolin to metakaolin at a medium temperature of 600 ^{o}C for 2 h. Metakaolin decomposes to spinnel at calcination temperature above 950 ^{o}C whereas no metakaolin would be formed at calcination temperatures below 300 ^{o}C. The medium range temperature maintains kaolin in its lowest stability when NaOH solution reacts with it, thereby producing an increase of the amount of $Al(OH)_4$ and SiO_4 species in solution. Furthermore, the specific surface area and pore volume of the kaolin calcined at medium temperature range are higher than those calcined at low and high temperature ranges (Johnson and Arshad, 2014). The interaction of the metakaolin with NaOH at 95^{o}C results in the formation of zeolite A according to the Equation 2.1

$$6Al_2Si_2O_7 + 12\ NaOH + 6H_2O \rightarrow (Na_{12}(AlO_2)_{12}(SiO_2)_{12}.\ 27H_2O) \qquad (2.1)$$

Various authors described the properties of zeolite minerals, to include adsorption properties, reversible cation exchange and dehydration (Jalil *et al*., 2013). These naturally occurring group of minerals contain cage-like structures which have the capacity to promote plant growth by enhancing nutrient availability, soil conditioning and improve soil moisture holding capacity. According to Yilmaz *et al*. (2017), zeolites

are often used in attempts to develop new substrates for plant growth, seedling production, rooting of cuttings and potting of ornamental plants.

Zeolites are microporous crystalline aluminosilicates, composed of TO_4 tetrahedral (T = Si, Al) with oxygen atoms connecting neighbouring tetrahedral (Khaleque *et al.*, 2020). For a completely siliceous structure, combination of TO_4 (T = Si) units in this fashion leads to silica (SiO_2), which is an uncharged solid. Upon incorporation of Al into the silica framework, the +3 charge on the Al makes the framework negatively charged, and requires the presence of extra framework cations (inorganic and organic cations can satisfy this requirement) within the structure to keep the overall framework neutral. The zeolite composition can be best described as having three components as shown in Equation 2.2

$$M^{m+}_{n/m} + \lceil Si_{1-n}\, Al_n O_2 \rceil + nH_2O \longrightarrow M^{m+}\lceil Si_{1-n}\, Al_n O_2 \rceil.nH_2O \qquad (2.2)$$

Cations framework sorbed phase Zeolite framework

The extra framework cations are ion exchangeable which give rise to the rich ion – exchange chemistry of these materials (Lozinska *et al*., 2020). The novelty of zeolites stems from their micro porosity and the topology of the framework. The amount of Al within the framework can vary over a wide range, with Si/Al = 1, the completely siliceous form being polymorphs of SiO_2**.** Fletcher *et al*. (2017) reported that Lowenstein rule proposed the lower limit of Si/Al = 1 of a zeolite framework. The value of 1 occurred as a result of placement of adjacent AlO_4 tetrahedral which is not favoured because of electrostatic repulsions between the negative charges. The framework composition depends on the synthesis conditions. Post synthesis modifications involved the inclusion of Si or Al into the framework. As the Si/Al ratio of the framework increases, the hydrothermal stability as well as the hydrophobicity

increases (Khivantsev *et al.*, 2021). Typically, in as-synthesised zeolites, water present during synthesis occupies the internal voids of the zeolite. The sorbed phase and organic non-framework cations can be removed by thermal treatment/oxidation, making the intra-crystalline space available. The fact that zeolites retain their structural integrity upon loss of water makes them different from other porous hydrates, such as Calcium tetra-oxosulphate (VI) $CaSO_4$ (Musyoka *et al.*, 2013). The crystalline nature of the framework ensures that the pore openings are uniform throughout the crystal and can readily discriminate against molecules with dimensional differences less than 1Å, giving rise to the name molecular sieves. Though the existence of natural zeolites was noted centuries ago, the field of zeolite science and technology grew in the 1950s, following the discovery of methods for large-scale industrial synthesis of zeolites by Union Carbide (Ozdemir and Piskin, 2013). Elements such as Boron (B), Zinc (Zn), Phosphorous (P), and transition elements, can also be incorporated into the framework and referred to as crystalline molecular sieves (Xia, 2015). Aluminophosphates (AlPOs) have strictly alternating AlO_2 and PO_2^+ units, and the framework is neutral, organophilic, and non-acidic. The alternation of Al or P leads to structures lacking in odd-numbered rings. Substitution of P by Si leads to silicoaluminophosphates (SAPOs), with cation-exchange abilities. Metal cations can also be introduced into the framework, including transition metal ions such as Cobolt (Co), Iron (Fe), Manganese (Mn) and Zinc (Zn).

2.3 Natural Zeolites

The current growing awareness of the phenomenon and availability of inexpensive natural zeolites in the world has aroused considerable commercial interest. The reason zeolites are now attracting attention lies in the honey comb structure of cavities and

minute channels in different directions, which works at the cellular level trapping heavy metals and associated forms in the soils and water (Ramesh *et al*., 2010). Zeolites are natural materials with the ability to exchange ions, absorb gases and vapours, act as molecular-scale sieves, and catalyse reactions due to fixed pore sizes and active sites in the crystal lattice. The unique physical and chemical properties of natural zeolites, based on their ion exchange, catalytic and molecular sieve properties, make them useful for many agricultural and horticultural applications and also for other environmental uses (Gholamhoseini and Gholamhoseini, 2018). By substituting metallic cations in the crystalline structure, it is possible to obtain modified zeolites for specific uses including the removal of NH_4^+ and toxic metal cations from waste water (Gupta *et al*., 2015). Zeolites are capable of adsorbing into their cavities or channels of different polar and non-polar inorganic or organic molecules but they are also agrochemical effective compounds and odouriferous compounds (Kam *et al.*, 2002).

The development of zeolitic materials with improved properties has provided the opportunity for various applications and new flexibility in the design of products and processes (Zheng, 2012). It was reported by Polat *et al*. (2004) that the most common zeolites studied among 40 naturally occurring zeolites were clinoptilolite, erionite, chabazite, mordenite, stilbite, and phillipsite. Chabazites and mordenite are relatively scarce in nature while erionite and stilbite are less abundant in nature. Their extra-framework cations such as sodium, potassium, calcium and magnesium are in order of abundance. These loosely bound cations facilitate fast ion exchange with other pollutant cations in water (Baruah *et al*., 2019).

Naturally clinoptilolite zeolite was observed to be the most abundant in soils and sediments and the most commonly used in agricultural practices as soil amendment for

promoting nitrogen retention in soils (Polat *et al*., 2004). Clinoptilolite is a member of the heulandite group of natural zeolites, a temperature stable heulandite which seems to be the most abundant zeolite in soils over a wide variety of pH conditions, from slightly acidic to strongly alkaline. Extensive deposits of clinoptilolite were found in United States, Bulgaria, Hungary, Japan, Australia, and Iran (Alsawalha, 2019). Clinoptilolite possesses a high cationic interchange capacity and a great affinity for NH_4 ions (Anari and Nezamzadeh, 2015).

The size of clinoptilolite channels controls the size of the molecules or ions that can pass through them and therefore clinoptilolite can act as a chemical sieve allowing some ions to pass through while blocking others. They also have large internal and external surface areas for ion exchange in the range of several hundred square meters per gram (Inan, *et al*., 2016). Ramesh *et al*. (2015) reported the sedimentation technique for separation of clinoptilolite from soils by combining the low specific gravity and fine particle-size characteristics of clinoptilolite in soils.

2.4 Comparison of Natural and Synthetic Zeolites

Natural zeolites such as clinoptilolite and chabazite occur in large deposits and they could be obtained at low cost, thereby making them alternatives to synthetic zeolites (Paolini *et al*., 2016). They are mostly impure because of the variable conditions that form them and their ores contain impurities such as quartz and feldspar. The benefits of synthetic zeolites are that they could be synthesised to improve certain properties over others (Musyoka, 2012). Moshoeshoe *et al*. (2017) reported some benefits of synthetic zeolites in the control of Nitrogen (I) oxide (N_2O) emissions and the removal of radioactive waste from the environment. He *et al*. (2016) reported the adsorption of various toxic metal ions (Cr^{3+}, Ni^{2+}, Zn^{2+}, Cu^{2+}, and Cd^{2+}) using natural and synthetic

zeolite. The authors noted that the synthetic zeolite showed much higher adsorption capacity for all the ions than the natural zeolite. The polarities of synthetic zeolites can be influenced by the zeolite's aluminum content. Zeolites with high aluminum content (low Si:Al ratio) are much more polar than those with higher Si:Al ratio. High polarity zeolites show stronger sorption capacities due to the presence of stronger (chemisorption) forces and high CEC values. The polarities of zeolites can be utilised to improve applications which may require hydrophilic/ hydrophobic environments (Moshoeshoe *et al*., 2017). Natural zeolites are usually hydrophilic due to the interaction of the dipole of the H_2O molecule with the electrostatic fields of the anionic aluminosilicate framework. Non-polar zeolites with higher Si/Al ratio do not possess this anionic property and are therefore hydrophobic. These "high silica zeolites" have a more homogeneous surface characteristic and exhibit high hydrophobic selectivity. They have been used in applications which have stopped working in the presence of water. An example is the direct esterification of acetic acid with n-, iso-, and tert-butyl alcohol. Water is an intermediate product of this reaction, which pollutes the acid sites of the catalysts. However, the pollution is lower in the presence of the more hydrophobic high-Si/Al-ratio ZSM-5 catalyst (Mohebbi *et al*., 2020).

The capability of synthetic zeolites to vary their pore sizes is an advantage over natural zeolites. Bandura *et al*. (2015) reported that synthetic zeolites have significantly larger pore volumes than their natural equivalents. Koshy and Singh (2016) showed that the increased pore sizes of synthetic zeolites locate them in an advantageous position as economically feasible sorbent minerals for trapping various contaminants from air and water. Furthermore, zeolites with smaller pore sizes usually experience pore blockage and eventually poisoning and deactivation as catalysts (Celik *et al*., 2010). Jiang *et al*.

(2015) reported that zeolites having large interconnected channels make allowance for shape selectivity and fast diffusion of large molecules through their channels.

2.5 Zeolite Synthesis

The zeolite synthesis involves the hydrothermal crystallisation of aluminosilicate gels. The gels are formed by the mixing of an aluminate and silica solution in the presence of alkali hydroxides. The crystallisation of the resulting mixture occurs is in a closed hydrothermal system at increasing temperature, autogenous pressure and varying time (few hours to several days). Georgiev *et al*. (2011) reported that the framework of zeolite formed was dependent on the composition of the reacting mixture, silica to alumina ratio, OH^-, and inorganic cations. Musyoka *et al*. (2014) observed that increasing the Si/Al ratio strongly affects physical properties of the zeolites. The hydroxyl group alters the nucleation time by influencing the transport of silicates from the solid phase to the solution. The inorganic cations acting as structure directing agents neutralise the framework charge. They also influence the purity of the crystal and product yield. The nature of the reactants (organic and inorganic) and their pre-treatments affects the zeolite synthesis. The inorganic precursors produce more surfaces with hydroxyl groups while the organic precursors simply integrate metals into the network. The rate of crystallisation is directly proportional to the temperature while the rate of nucleation is inversely proportional to the temperature (Selim *et al*., 2017). The crystallisation time is altered in such a way to reduce the time needed to produce the desired zeolite crystallinity and other side products. The process of zeolite formation occurs in an alkaline medium. The synthesis could be carried out on a continuous or semi continuous mode for industrial applications.

The main problem in zeolite synthesis is the availability and cost of raw material especially the silica source. The commercial silica made from sand is usually available in gel, sol, fumed or amorphous solid and it is known for its inconsistency in reactivity and selectivity. The preparation of synthetic zeolites from silica and alumina chemical sources is expensive. Yet, cheaper raw materials, such as clay minerals, natural zeolites, coal ashes, municipal solid waste incineration ashes and industrial slags, are utilised as starting materials for zeolite synthesis. The use of waste materials in zeolite synthesis contributes to the mitigation of environmental problems, water purification and removal of heavy metals (Shaila, *et al*., 2015).

2.6 Low and High Silica Zeolites

The proportion of silica and aluminum content determines the properties of zeolites. The development of zeolites commenced with the synthesis of low-silica zeolites with Si/Al ratio less than 2 and they show high ion exchange capacities (Jiang *et al*., 2018). Zeolite A, X and Y are examples of low-silica zeolites and they were synthesised by crystallisation from reactive aluminosilicate gels with alkali and alkaline hydroxides. The gels were characterised by high pH usually greater than pH 13 and crystallisation temperature with the range of 85 and 125 ^{o}C. Low silica zeolites are saturated by aluminum and have the highest cation concentration. They therefore promote optimal adsorption capacity, three dimensional channel system and pore size (Johnson and Arshad, 2014).

However, high-silica zeolite is a term used for zeolites rich in the silica component with Silicon to Aluminum ratio of 10 or higher. They are known for excellent heat resistance and hydrophobicity. They are prepared by dealuminating low silica zeolites (Burton 2018). In addition, mesopores are generated in a small portion of the zeolite external

surface area during the dealumination process (Burton 2018). ZSM-5, ZSM-8 and ZSM-11 are examples of high-silica zeolite with high chemical and thermal stability in industrial catalysis (Lin *et al*., 2015).

2.6.1 Zeolite linde type A (LTA)

Zeolite A is one of the most common commercial adsorbents. It was discovered by R. Milton at the Union Carbide Corporation (Gougazeh and Buhl, 2014). The zeolite A framework composition with a molar ratio of Si/Al = 1 is reported to possess the highest aluminium content among tetrahedral aluminosilicate frameworks (Tontisirin *et al*., 2017). It also contains the maximum number of cation exchange sites neutralising the aluminium framework and consequently the highest cation contents and exchange capacities. These compositional characteristics provide zeolites with the most highly heterogeneous surface known among porous materials, because of exposed cationic charges held in an aluminosilicate framework (Shaban *et al*., 2018). The zeolite A surface is highly selective for water, polar and polarisable molecules which serves as the basis for many applications mainly in drying and purification (www.asdn.net/asdn/chemistry/zeolites.php).

Zeolite A has been successfully synthesised by a hydrothermal method, using kaolin as the silica and alumina source. The hydrothermal method is the most used among zeolite synthesis methods reported in the literature (Lee *et al*., 2018). It is a multiphase reaction–crystallisation process, connecting at least one liquid phase and both amorphous and crystalline solid phases. The term hydrothermal is used in a wide sense and includes zeolite crystallisation from aqueous systems that contain the necessary chemical components. Zeolites have metastable phases, and slight changes in the synthesis conditions can bring about a pollution of the desired product by the co-

crystallisation of other phases with a similar composition but with completely different properties (for instance, zeolite A and zeolite X). Loiola *et al*. (2012) reported the preparation of zeolite A with high purity, by means of a hydrothermal route which was based on kaolinite as starting material, as well as its application in removing Ca^{2+} ions from solutions.

Zeolite A is generally synthesised in the Na^{+} form, $Na_{12}Al_{12}Si_{12}O_{48} \leqslant 27H_2O$, and it has a three-dimensional pore structure. The framework structure of zeolite A is shown in Figure 2.1. Its structure is composed of sodalite cages, which are similar to faujasite ones, but connected through double four-member rings (D4R) of $[SiO_4]^{4-}$ and $[AlO_4]^{5-}$. This connection shows the presence of three cages: D4R, sodalite cage, and α-cage. Zeolite A is a synthetic zeolite with very small pore diameter of 4 Å, that can be changed either to 5 or 3 Å by ion exchange with aqueous solutions of calcium or potassium salts (Loiola *et al*., 2012). The pore diameter is defined by an eight-member oxygen ring with diameters between 0.23 and 0.42 nm. Zeolite A has promising applications in separation processes and shape-selective catalysis because of its pore structure.

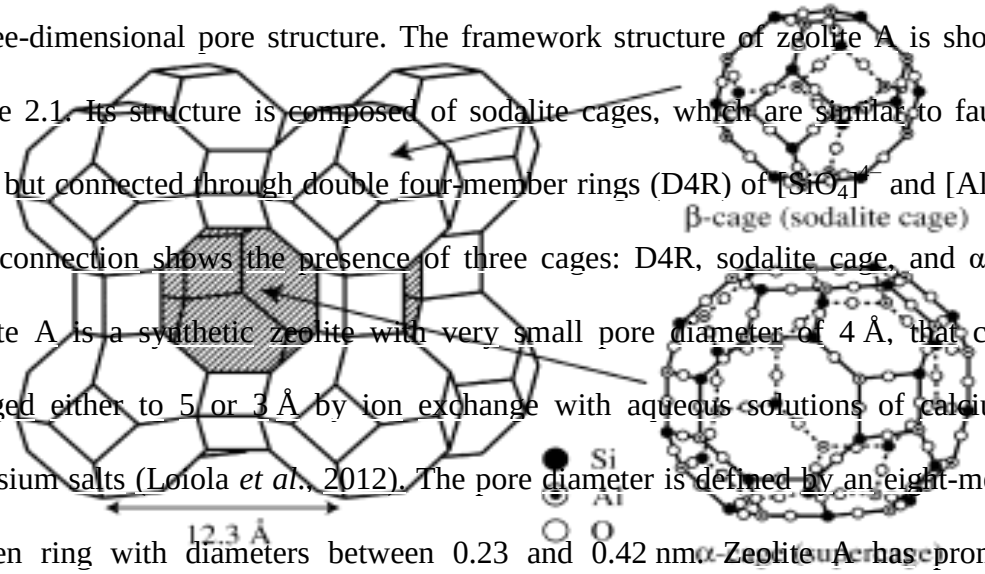

Figure 2.1: The framework structure of Zeolite A (Johnson *et al*., 2014)

Zhihui *et al*. (2014) also reported zeolite A synthesis from calcined kaolin, sodium hydroxide and deionised water vigorously stirred for 12 h at room temperature. The mixture was transferred into a stainless steel autoclave lined with Polytetrafluroethylene (PTFE) and subsequently placed into an oven for crystallisation at a temperature of 100 ^{o}C. The product was washed with deionized water and dried at 105 ^{o}C. A summary of zeolite A synthesis from kaolin is presented in Table 2.1.

Table 2.1: A summary of Zeolite A synthesis from Kaolin

References	Kaolin Source	Method of Synthesis	Synthesis Parameters	Overview of studies
(Gordina *et al*., 2017)	Prosko Resury, Ukraine	Hydrothermal	Metakaolin, Sodium Hydroxide, Aluminium oxide	The effect of ultrasonic treatment on the thermal behaviour of the mixtures from metakaolin, sodium hydroxide and alumina designed for LTA zeolites synthesis was studied. It was shown that after evaporation of the suspension, 24 % LTA zeolite was contained in the samples. It was established that the new phase (sodium aluminum silicate) was formed at a calcination temperature of about 600 ^{o} C. It was demonstrated that at a calcination temperature over 800 ^{o} C, nepheline was formed.
(Kwakye *et al*., 2014)	Volta region of Ghana	Hydrothermal	Metakaolin, Sodium Hydroxide, bauxite	A gelatinous solution was obtained from a mixture of sodium aluminate solution (from bauxite) and sodium silicate solution (from metakaolin). The gel was agitated vigorously for 20 mins and aged for 24 h in Teflon bottles. The resulting mixture was crystallized at 95^{o} C for 3 h. The synthesis method was repeated varying crystallisation time for 5, 24 and 94 h and dried at 100 ^{o} C. The main phases of zeolites obtained were zeolite LTA, zeolite X and analcime. A phase change of the zeolite A into sodalite as a result of longer crystallisation time. At crystallisation time of 5 hours, 87.2 % of

Table 2.1: Contd.

Reference	Kaolin source	Method of synthesis	Synthesis Parameters	Overview of studies
				zeolite LTA was obtained as the optimized zeolite synthesis. It was concluded that zeolite LTA is significantly influenced by crystallisation time.
(Ayele *et al*., 2016)	Bombowa kaolin, southern part of Ethiopia	Hydrothermal and fusion method	Metakaolin, NaOH, cryst temperature and time	The metakaolin was treated with alkaline solution by mixing 1.25 g of metakaolin with 25 ml of 3 M NaOH at 50 °C for 1 h under stirring at 500 rpm for gel formation. The gel formed was aged at room temperature in static conditions for different times (1, 3, 6, 12 and 24 h). In the alkali fusion synthesis, 1.25 g of raw kaolin was mixed with 1.5 g of NaOH (solid) for 30 min followed by calcination at 600^{o}C for 1h in a furnace. Then the fused product was ground in a mortar and further mixed with 12.5 ml of ultrapure (milli Q) distilled water at 50 °C for 1 h under stirring at 500 rpm for the gel formation. The conventional hydrothermal synthesis gave cubic crystal of zeolite A with rounded edge having optimum crystallinity of 75 % and CEC of 250 mg $CaCO_3$/g of anhydrous zeolite A. Whereas, the alkali fusion method yielded cubic crystal of zeolite A with rounded edge having optimum crystallinity of 84% and CEC of 300 mg

CaCO3/g of anhydrous.

Table 2.1: Contd.

Reference	Kaolin source	Method of synthesis	Synthesis parameters	Overview of studies

				zeolite A in the absence of purification steps. Hence alkali fusion method of synthesis was the best synthesis method in terms of time, energy cost and even in product quality compared to the conventional hydrothermal method of synthesis.
(Menezes *et al.*, 2017)	Kaolin waste from the state of Para	Hydrothermal	Kaolin waste	Zeolites A derived from kaolin waste were obtained by hydrothermal synthesis, under reflux as follows: 200 g of kaolin calcined at 700 °C was mixed with 600 mL of 5 mol/L NaOH solution at 95 °C in a 1 L glass reactor with mechanical stirring for 2 h, after reaction, the samples were rinsed until pH approximately 7 with distilled water and was dried at 105 °C for 24 h. The product was predominantly composed of sodium-type zeolite A and a small quantity of sodalite. The product showed an elevated percentage of sodium and a Si/Al ratio of approximately 1, which was typical of a zeolite with a low concentration of Si. The structure of zeolite A was maintained after the pigments were produced and that the crystalline Na_2SO_4 phase was formed in the process.

Table 2.1: Contd.

References	Kaolin source	Method of synthesis	Synthesis parameter	Overview of studies
(Abdullahi *et al*., 2017)	Mersing kaolin depost in Johor, Malaysia	Hydrothermal	Metakaolin, NaOH, crystallisation temperature and time	A gel solution was formed from metakaolin and NaOH solution. Ageing was achieved by continuous stirring the mixture for 12 h at 50 °C. The crystallisation was carried out in a 100 mL Teflon lined autoclave at a temperature of 90 °C with varying time of 6, 9 and 12 h, respectively. The conversion was carried out at 90 °C for a crystallisation time of 6, 9 and 12 h, respectively. The purity and grade of the synthesised products varies accordingly with the suitability of the crystallisation time. The synthesised product at 6 h crystallisation time, yielded an aluminosilicate rather than the targeted zeolite A. zeolite A replaced the amorphous aluminosilicate after prolonging the crystallisation time from 6 to 9 h which revealed the metastable nature of zeolite.
(Youssef *et al.,2008)*	Georgian USA Kaolin	Hydrothermal and microwave synthesis	Time	The study compared the synthesis of zeolite A from metakaolinite using microwave-assisted and conventional heating. Synthesis variables such as different NaOH molarities, temperatures, durations and percentage seeding were investigated on the crystallinity, rate of formation and percentage yield of zeolite

Table 2.1: Contd.

Reference	Kaolin source	Method of synthesis	Synthesis parameters	Overview of studies
				It was however found that rate of zeolite A production increased by 50 – 70% in the samples treated
(Chandrasekhar and Pramada, 2008)	Indian Kaolin	Microwave synthesis	Aging time	Microwave energy was used as a heating device for the synthesis of zeolite A from a combined source of silica and alumina. The optimized synthesis of zeolite A with high crystallinity was obtained from a crystallisation time and temperature of 2 h and 85 ^{o}C respectively under a microwave system. The authors concluded that the microwave energy reduces the formation of unwanted zeolite phases.
(Heller – Kallai and Lapides, 2007)	Kaolin from Makhtesh (Israel)	Hydrothermal synthesis	Kaolinities and aqueous sodium hydroxide	Different kaolinites and metakaolins were reacted with NaOH solution. The kaolinites produce hydrosodalite while metakaolinites produced primarily zeolite A. It was observed the metakaolinites became hydrosodalite after 5 days. The authors reported that no relationship was observed between the crystallinity of kaolinites and the rates of the reactions though the rates of the reactions of the samples were different

Table 2.1: Contd.

References	Kaolin source	Method of synthesis	Synthesis parameters	Over view of studies
(Chaudhuri *et al*., 2002)	Indian clay	Hydrothermal synthesis	Metakaolin, Sodium Hydroxide	Kaolin samples from locations in India have been studied and found to produce Detergent grade zeolite A. The synthesis variables of the calcination temperature were studied. It was observed that the calcium binding capacity, 170 mg of CaO/g was found to substitute phosphate in formulation of detergent
(Park *et al*. 2001)	Handong Kaolin deposit in Korea	Ultrasonic irradiation and hydrothermal method	Crystallisation temperature	Zeolite A was synthesised from a mixture of metakaolin, sodium hydroxide and distilled water immersed in a water bath irradiated at a frequency of 47 KHz for a certain duration. It was observed that zeolite A with 70% crystallinity was obtained from the ultrasonic method. The authors concluded that ultrasonic irradiation of aluminosilicate gel results to faster crystallisation rate for the synthesis of zeolite A

Table 2.1: Contd.

References	Source of Kaolin	Method of synthesis	Synthesis Parameter	Overview of studies
(Sanhueza et al., 1999)	Chilean Kaolin	Hydrothermal synthesis	SiO_2/Al_2O_3, ratio, temp, time of crystallisation	The Chilean kaolin were used to synthesis zeolite A. The reaction time of 15 h, crystallisation temperature of 100 ^oC and the ratios of SiO_2/AlO_2 at 1.9 were the synthesis parameters studied with respect to the textual and structural properties of zeolite A. The samples were characterized by XRD, FTIR and SEM to identify the zeolite phases.
(Rees and Chandrasekhar, 1993)	Cornwall kaolin	Hydrothermal synthesis	Alkalinity, synthesis time and temperature	The study reported the reaction of kaolinite, metakaolinite and sodium aluminosilicate gel with NaOH solution while keeping the molar composition of Na_2O-Al_2O_3-SiO_2-H_2O constant in the 3 systems considered. It was observed that zeolite A was formed from metakaolin and Hyroxsodalite was formed from kaolinite. It was further observed that crystallisation started before the complete conversion of the metakaolinite gel.

Table 2.1: Contd.

References	Source of Kaolin	Method of synthesis	Synthesis Parameter	Overview of studies
(Murat *et al*., 1992)	English Kaolin	Hydrothermal synthesis	Metakaolin, Sodium Hydroxide	The study revealed that the type of zeolite obtained was dependent on the zeolite nucleation process and it could be as a result of soluble potassium or high silica content from muscovite. The formation of zeolite A or Zeolite P or mixture of tetragonal and cubic zeolites could be traceable to low calcination temperature, low crystallized kaolinite and presence of iron atoms.
(Basaldella *et al*., 1990)	Argentina Kaolin	Hydrothermal synthesis	metakaolin, sodium hydroxide	Kaolin was activated by grinding and hydrothermally treated in NaOH solution. It was observed that hydroxysodalite, mixtures of hydroxysodalite and zeolite A were observed to be destroyed by grinding. However, the study showed that the activation of kaolin by grinding could also produce

				synthesis zeolite A

Table 2.1: Contd.

Reference	Kaolin source	Method of synthesis	Synthesis parameters	Overview of studies
(Bosch and Schitter. 1983)	Kaolin from Ventas, Teenicas, Mexico City, USA	Hydrothermal synthesis	Metakolinization temperature, Alkalinity, induction time.	The authors reported that the different calcination temperature chosen for kaolin is related to the synthesise A, X and Y. It was observed that some atoms of Al and Si in the kaolin constituents did not participate in zeolite formation. The XRD and TGA results of the zeolite were comparable to the the zeolite synthesised from conventional soluble salts.

2.6.2 Phillipsite

Phillipsite is found abundantly in nature especially in rocks of marine and continental deposits. It is mostly found as low-silica, alkali-rich rock (Comboni *et al*., 2016). It has 4-ring (Al-Si) unit as the smallest structural unit under Group I zeolite Meir's classification. The framework of the phillipsite is made up of layers of tetrahedral which contain 4 and 8 membered rings. Narimani and Kharamesh (2014) reported the synthesis of phillipsite from high-potassium, high-calcium volcanic glass with the treatment of potassium hydroxide solutions at temperature above 150 ^{o}C. The authors further reported the preparation of a synthetic phillipsite ZK -19 whose XRD pattern was similar to a phillipsite found in a marine environment. The ZK-19 phillipsite was found to crystallize from a composition of molar silica/alumina ratios between 4 to16. Abukhadra and Mostafa (2019) reported that the ratio of sodium ion to potassium ion was narrow (between K/(Na + K) of 0.10 to 0.20) in the reacting mixture and it was crucial in the synthesis of a single phase.

Phillipsite could also be synthesised from kaolinite of various sources (Minikara, 2017). It could also be synthesised from other methods such as the alkaline fusion procedure, sodium aluminate and sodium silicate solution by hydrothermal treatment in microwave oven. Rodrigues *et al*. (2016) reported that 12.7 g of metakaolinite mixed with sodium fluoride was prepared by dissolving 10.4 g of NaF powder in 87.7 mL of distilled water. The resulting synthesised slurry was aged at 50 ^{o} C by stirring the mixture for 4 h. After this ageing, the slurry was passed through a thermal treatment by heating at a temperature of approximately 100 ^{o} C under reflux system for 96 h. The solid product was filtered and washed with de-ionised water until the rinsing water has pH 9,

centrifuged at 3500 rpm and dried at 105 ^{o} C for 24 h. The obtained product was referred to as phillipsite.

Low-silica zeolites, such as phillipsites synthesised from kaolin with Si/Al ratio of 1 – 1.5 are known for their excellent ion-exchange properties and their adsorption capacities. They have a composition of $K_2(Na_2Ca_{0.5})_3(Al_5Si_{11}O_{32}).12H_2O$ with common cations as sodium, potassium or calcium (Comboni *et al*., 2016). Its exchangeable Na cation is usually found in complex twinned crystals, with smaller crystals generally showing the simple forms such as radiating, prismatic, spherical, and clusters of these forms (Ibrahim, 2014; Colella *et al*., 2015). The most relevant applications of phillipsites are based on its high cation exchange capacity and selectivity for ammonium ion.

Sangita *et al*. (2016) reported the synthesis of phillipsite using one factor at a time experiment from a slurry of 25 g fly ash sample and 100 mL of 2 N NaOH solution at a constant temperature of 105 ^{o} C. The authors varied the crystallisation time for 2 h, 3 h, 6 h, 12 h, 24 h, and 48 h respectively in a search for an optimum combination of levels of the factors. Abukhadra and Mostafa (2019) also reported the synthesis of pure phillipsite from a mixture of silica-alumina gel, sodium aluminate, sodium silicate solution and a reagent grade sodium and potassium hydroxide at a temperature range of 25 - 150 °C under autogenous pressure. Though the phillipsite was reported to be identical with natural phillipsite, the interactive effects of the independent variables on the crystallinity of the phillipsite were not recorded. A summary of Phillipsite synthesis from kaolin is presented on Table 2.2.

Table 2.2: A summary of Phillipsite synthesis from kaolin

Reference	Sources of aluminosilicates	Method of synthesis	Synthesis Parameters	Highlights of studies
Rujiwatra (2004)	Perlite from Amphur Lamnarai, Lopburi, Thailand	Hydrothermal	Perlite powder, NaOH, crystallisation temperature and time	Phillipsite and sodalite were selectively prepared from perlite (a glass with 70% silica and 13% alumina) through treatment with NaOH solution at 70 – 100 ^{o}C under autogeneous pressure. The effects of synthesis parameters on the type of product were investigated. It was observed that the treatment of perlite with 3 mol dm^{-3} at 70 and 100 ^{o}C for 5, 10 and 20 days gave the highest conversion to Phillipsite
Park and Choi (1995)	Fly ash from Youngwoel, Korea	hydrothermal	Fly ash, NaOH, reaction temperature and time	Phillipsite was synthesised from fly ash by hydrothermal treatment with NaOH solution at 105 ^{o} C between 2 – 6 h. The formation of phillipsite from fly ash was explained as a result of the dissolution of the silicate glass and the aluminum compounds. The product consisted of Phillipsite, mullite and quartz aggregates with their irregular forms in their shapes.

Table 2.2: Contd.

Reference	Sources of aluminosilicates	Method of synthesis	Synthesis Parameters	Highlights of studies
Chen *et al*. (2002)	Glasses with compositions comprising of Albite-anorthite, orthoclase-albite	hydrothermal	Albite-anorthite, orthoclase-albite, Na_2CO_3 NaOH, NaCl, KOH, crystallisation temperature and time	The phillipsite was synthesised from compositions representing 3 chemical systems namely, $Na_2O.Al_2O_3.nSiO_2$ (n = 2-10), albite-anorthite, and orthoclase mixed with alkaline solutions. The gel solutions were crystallized at 110 ^oC to 210 ^oC for a duration of 7 to 53 days. It was observed that a single phase of Phillipsite occurs at temperatures below 150 ^oC but above that temperature, other phases are mixed with it. It was further observed that the starting materials basically determine the Si/Al ratio and the cationic composition

Table 2.2: Contd.

Reference	Source of aluminosilicates	Method of synthesis	Synthesis of Parameters	Highlights of studies
McEvoy *et al.*, 1970	Kaolin	Hydrothermal	Concentration of NaOH, Aging time and time, Crystallisation temperature time	The kaolin was calcined at 450 ^{o}C. and added to aqueous NaOH solution and stirred. The slurry is allowed to age at 80 ^{o}C for a period of 10 – 35 h and crystallized for 5 to 120 h. The resulting product was washed with water and dryed at 40 ^{o}C

2.7 Zeolite Structure

The zeolite structure is described by a three dimensional material usually silicon and aluminium connecting tetrahedrally with four oxygen atoms. The sharing of oxygen atom between two tetrahedral forms a tetrahedron. Zeolite structures could be characterised by the secondary building units that was used for making three dimensional framework. The connection of the secondary building units through double -4 rings as in sodalite cage leads to zeolite A formation. The structure of zeolite can be further characterised by the dimensionality of the pore network which can be one, two or three dimensional depending upon the interconnectivity and the pore size. The pore structure is characterised by cages which are interconnected through channels approximately 0.8 nm in diameter. The pores are inter-linked and form channels of different sizes. These channels permit the passage of ions and molecules in and out of the zeolite structure. The empty spaces or cages within the zeolite structure resembles honeycomb structures.

The zeolite framework resulting from SiO_4 and AlO_4 tetrahedral have an anionic framework such that the extra framework cations such as potassium, calcium and sodium atoms compensate for the negative charges (Kovo, 2011). The Atlas of Zeolite Framework Types lists about 176 framework structures of zeolites (Baerlocher *et al*., 2007). The standard for differentiating zeolites and zeolite-like materials (porous tectosilicates) from denser tectosilicates is the number of tetrahedral coordinated atoms per 1000 x 10^{-30} m^3. This number is known as the framework density, with values ranging from 12.5 to 20.2 T atoms per 1000 x 10^{-30} m^3 for porous tectosilicates (Moshoeshoe *et al*., 2017). The angle around the T atoms in the TO_4 tetrahedral are near tetrahedral, whereas the T-O-T bond angles connecting the tetrahedral can vary over a

wide range approximately 125^{o} to 180^{o}. Lima *et al*. (2019) related a classification for porous tectosilicates that differentiates between aluminous (porolites) and siliceous (porosils) frameworks as well as (zeolites/zeosils) that do allow exchange of guest species and (clathralites/clathrasils) that do not allow exchange of guest species are summarized in Table 2.3

Table 2.3: Classification of Porous Tectosilicates

Porosils (SiO_2 based)		**Porolites (aluminosilicates)**	
Clathrasils	Zeosils	Clathralites	Zeolites
Silica sodalite	Silicalite	Sodalite	Faujasite
	Silica ZSM -22		Mordenite
Dodecasil	SSZ-24		ZSM-5
			Zeolite A

(Krivovichev, 2017)

IUPAC recommendations for nomenclature of structural and compositional characteristics of ordered microporous and mesoporous materials with inorganic hosts with particular attention to the chemical composition of both host and guest species, structure of the host, structure of the pore system, and symmetry of the material have been published (Krivovichev, 2017). The structure commission of the International Zeolite Association identifies each framework with a three-letter mnemonic code (Lima *et al*., 2019). Generally, these codes are derived from the name of the species type. For example, FAU for faujasite or SOD for sodalite. These symbols describe all variants of a framework with a given topology, irrespective of composition, Silicon, and Aluminium distribution, cell dimension and symmetry.

2.7.1 Zeolite pores

Zeolite pores are refered to as the three-dimensional void spaces formed by zeolite framework structures. They provide zeolites with the characteristics of molecular

sieving (Moshoeshoe *et al*., 2017). The faces of the three-dimensional void space are also called pore windows. The ability of a molecule larger than water (a circular window diameter of 2 Angstrom) to enter at least one window of the pore makes the pore to be referred as a cavity. Pores with windows too small to allow a molecule of water are referred to as cages (Dusselier and Davis, 2018). The extensions of cavities in more directions are referred to as channels. Cages, cavities and channels can contain guest species, ions and molecules in their void polyhedron. The framework of silica and alumina tetrahedron is referred to as host structure. The size of zeolite pores are determined by the number of tetrahedral that form rings and the kind of cations that occupy the pores of the zeolite. The pore sizes of zeolites with divalent cations are bigger than those with monovalent cations. It is the chemistry of the zeolite channels, cavities, and cages that describes the material's performance with respect to molecular sieving, ion-exchange, and catalytic selectivity (Moshoeshoe *et al*., 2017). Zeolite A synthesised in sodium form has pore opening of 0.34 nm, when ion exchanged with potassium its pore reduces to 0.30 nm whereas when exchanged with calcium the pore increases to 0.43 nm (Selim *et al*., 2017). These differences in pore windows are important in determining the best application for zeolite A.

2.8 Zeolites Properties

Generally, zeolites are colourless minerals. The properties of zeolites are determined by the specific crystal structure of each species, its framework and cationic composition. Quantifying physical and chemical properties is crucial in characterizing zeolitic materials for commercial uses. The following physical and chemical properties and tests are generally required: cation exchange capacity, catalytic property, specific gravity and bulk density, brightness, whiteness, colour, hydration/dehydration testing, gas

adsorption, attrition in water, and internal and external surface area (Inglezakis and Antonis, 2012). The most important properties of zeolites are the following: ion exchange, adsorption, dehydration and rehydration. These unique porous properties distinguished them as adsorbents for industrial purifications processes.

Many zeolites are able to lose water fairly continuously over a temperature range of 150 to 400 ^{o}C without collapse of the framework structure and re-absorb it from the atmosphere at room temperature. All zeolites are molecular sieves and they can selectively adsorb molecules on the basis of their size, shape or electrical charge. The ion exchange, catalytic and molecular sieves properties of zeolites make them useful in wide range of applications (Inglezakis *et al*., 2012).

2.8.1 Ion-exchange properties

Zeolites are widely applied in ion–exchange processes where cations on the zeolite structure are exchanged with cations in solution. Ion exchange property is the most important property of zeolites amongst others such as adsorption, hydration and dehydration (Li *et al*., 2017). Ion exchange capacity is often determined simply by equilibrating batchwise a sample of an ion exchanger with a solution of an ion and calculating the capacity from the up take value thus obtained. The exchangeable cations of a zeolite are loosely bonded to the tetrahedral framework and can be removed or exchanged from the framework structure easily by washing with a strong solution of another element. Therefore, crystalline zeolites are some of the most effective ion exchangers known to man, with capacities of 3 to 4 meq per gram (Ayele *et al*., 2015). Cation-exchange capacity is basically a function of the degree of substitution of aluminium for silicon in the zeolite framework: the greater the substitution, the greater the charge deficiency of the structure, and the greater the number of alkali or alkaline

earth atoms required for electrical neutrality. Zeolites with a negative charge provides an ideal trap for positive cations such as sodium, potassium; barium and calcium, and positively charged groups such as water and ammonia. Both carbonate and nitrate ions are attracted by the negative charge within zeolites. Therefore, alkali and soil alkali metallic cations are attracted in the same way water is absorbed by zeolites (Kovo *et al*., 2017). Absorbed cations are relatively mobile due to their weak attraction, and can be replaced using the standard ion exchange techniques, making zeolites good ion exchangers.

Ion-exchange is dependent on a number of factors. In certain species, cations can be trapped in structural positions that are relatively inaccessible, thereby reducing the effective exchange capacity of that species for that ion. In other species, cation sieving may take place if the size of the exchanging cation is too large to pass through the entry channels into the central cavities of the structure (Ham *et al*., 2018).

Unlike most non-crystalline ion exchangers, such as organic resins or inorganic aluminosilicate gels (mislabeled in the trade as “zeolites”), the framework of a crystalline zeolite dictates its selectivity toward competing ions. The hydration spheres of high-charge, small size ions (such as sodium, calcium, magnesium) prevent their close approach in the cages to the seat of charge of the framework; therefore, ions of low charge and large size (such as lead, barium, potassium), that normally do not have hydration spheres are more tightly held and selectively taken up from solution than are other ions (Khaleque *et al*., 2020). The small amount of aluminium in the composition of clinoptilolite, for example, results in a relatively low cation-exchange capacity (about 2.3 meq/g); however, its cation selectivity is:

Cesium > Rubidium > Potassium > Ammonium > Barium > Strontium > Sodium > Calcium > Iron > Aluminium > Magnesium >Lithium (Young, 2011). For instance, synthetic zeolite A, is more selective for calcium than for sodium, and thus, acts as a water softener in laundry detergents where it picks up calcium from the wash water and releases sodium (Gulten, 2014).

The cation exchange capacity of a zeolite depends on the structural characteristics of the particular zeolite. The affinity of an ion in solution for exchange of the extra framework cation depends on the charge of the the extra frame work cation, the degree of hydration, the pore size and shape of the zeolite. The mechanism of cation exchange reactions are basically due to the zeolite structure, chemical composition and the chemical elements of the aqueous solution in contact with the zeolite. Gu *et al*. (2019) reported the summary of the structural causes for cation exchange in zeolite minerals as follows;

i). The presence of broken bonds at zeolite surfaces and edges produces unsatisfied valences

ii). The isomorphous substitution of cations causes unbalanced charges as in the substitution of Al^{+3} for Si^{+4}

iii). The replacement of the H^{+} by a metallic cation when the structural OH^{-} radical dissociates

The variation in cation exchange capacity for zeolite minerals is traceable to the presence of exchange sites caused by the occurence of negatively charges on the particles, differences in particle size and the chemical compostion that caused the negative charges (Gu *et al*., 2019)

2.8.2 Adsorption properties

Adsorption may be defined as the process of buildup of a substance of higher concentration of molecular varieties on the surface of another substance as related to that in the bulk (Jiang *et al*., 2018). When a solid surface is exposed to a gas or a liquid, molecules from the gas or the solution phase accumulate or concentrate at the surface. The phenomenon of concentration of molecules of a gas or liquid at a solid surface is called adsorption. "Adsorption" is a well-established and powerful technique for treating domestic and industrial effluents. Adsorption is usually carried out as an operation and it comprises of three steps as reported by Tan and Hameed (2017) as follows,

i. Film diffusion (external diffusion) which is the transport of the adsorbate from the bulk phase to the external surface of an adsorbent.
ii. Pore diffusion (intra-particle diffusion (IPD) is the transport of the adsorbate from the external surface into the pores.
iii. Surface reaction which is the attachment of the adsorbate to the internal surface of the adsorbent.

Under normal conditions, the large cavities and entry channels of zeolites are filled with water molecules forming hydration spheres around the exchangeable cations. Once the water is removed, usually by heating to 300 to 400 ^{o}C for a few hours, molecules having diameters small enough to fit through the entry channels are readily adsorbed on the inner surfaces of the vacant central cavities (Gan *et al*., 2009). Molecules too large to pass through the entry channels are excluded, giving rise to the well-known "molecular sieving" property of most crystalline zeolites.

The internal surface area available for adsorption ranges up to several hundred square meters per gram, and some zeolites are capable of adsorbing up to about 30 weight percent of a gas, based on the dry weight of the zeolite. In addition to their ability to separate gas molecules on the basis of size and shape, the unusual charge distribution within a dehydrated void volume allows many species with permanent dipole moments to be adsorbed with selectivity unlike that of almost all other sorbents. Thus, polar molecules such as water, sulphur dioxide, hydrogen sulphide, and carbon dioxide are preferentially adsorbed by certain zeolites over nonpolar molecules, such as methane.

Nakhli *et al*. (2017) had reported the adsorption processes in agricultural technology which have been developed using natural zeolites by which carbon dioxide and other contaminants can be removed from impure natural gas or methane streams, allowing the gas to be upgraded to high energy products. In addition, the small, but finite, quadruple moment of nitrogen allows it to be adsorbed selectively from air by a dehydrated zeolite, producing oxygen-enriched streams at relatively low cost at room temperature.

In adsorption and separation applications, there has been a major growth in the use of pressure swing adsorption for the production of oxygen, nitrogen and hydrogen. Processes for the purification of gasoline oxygen additives were introduced (Kacem *et al*. 2015). Recent environmentally driven applications have arisen using the hydrophobic molecular sieves, highly siliceous Y zeolite and silicalite, for the removal and recovery of volatile organic compounds that offer promise for significant market growth.

A new exciting scientific direction emerged in the 1980s and 1990s for exploring molecular sieves as advanced solid state materials. Cornelius *et al.* (2019) speculated

that zeolites (molecular sieves) as microporous molecular electronic materials with nanometer dimension window, channel and cavity architecture represent a 'new frontier' of solid state chemistry with great opportunities for innovative research and development. The applications envisioned included molecular electronics, "quantum" dots/chains, zeolite electrodes, batteries, non – linear optical materials and chemical sensors. More recently there have been significant research reports on the use of zeolites as low k dielectric materials for microprocessors (Huang *et al*., 2018).

2.8.3 Functionalisation of zeolites with surfactants

Surfactants consist of both hydrophobic group (alkyl chains such as alkyl phenyl ethers, alkyl benzenes) and a hydrophilic group such as carboxyl, sulphate, sulphonates and phosphates. Surfactants are defined as compounds that lower the surface tension (or interfacial tension) between two liquids or between a liquid and a solid. They are used as detergents, foaming agents and dispersants (Onuche *et al*., 2016). They make aqueous solutions to spread and penetrate more easily. It is one of the components of topical antiseptic and widely used in hair conditioning products.

Surface properties, such as hydrophobicity, hydrophilicity can be controlled by organic Functionalisation of the internal and external surface of inorganic materials making them more suitable for different applications. Surfactant which are also known as surface-active agents are water soluble organic molecules which have a characteristic molecular structure consisting of a structural group that has a very little attraction for water, known as a hydrophobic group, together with a group that has strong attraction for water, called hydrophilic group. The hydrophobic group is usually a long-chain hydrocarbon, and the hydrophilic group is an ionic or highly polar group. According to the nature of the hydrophilic group, surfactants are classified as follows: anionic,

cationic, non-ionic and amphoteric (Kamal *et al*., 2017). The common surface Functionalisation of zeolites is via adsorption of cationic surfactants.

Cationic surfactants have a positively charged head group attached to a hydrocarbon moiety. Above the critical micelle concentration (*cmc*), individual surfactant molecules self-associate into micellular clusters. Several cationic surfactants have been used to prepare surface modified zeolites such as tetramethylammonium, tetraethylammonium bromide, hexadecyltrimethylammonium bromide or chloride, cetylpyridinium bromide, octadecyltrimethylammonium (Ruman *et al*., 2018).

2.8.3.1 Cationic surfactant selection

The selection of surfactant for zeolite modification is vital because the properties of the modified zeolite will affect its effectiveness. The following properties of cationic surfactants have the tendency to influence the behaviours of the modified zeolite as;

i). The alkyl chain length of the cationic surfactant

The adsorption efficiency of a surfactant modified zeolite is affected by the length of the alkyl chain in the cationic surfactant. Thakkar *et al*. (2017) studied the adsorption and desorption of quaternary amine compounds namely, nonyltrimethylammonium, dodecyltrimethylammonium and hexadecyltrimethylammonium on montmorillonite zeolite. The authors however reported that the degree of desorption increased with surfactants with only amine sorption but decreased with surfactant with alkyl chain length of the amines. The sorption capacity of surfactant modified zeolite was also reported to increase with increasing chain length of the alkyl group of the surfactant. Hexadecyltrimethylammonium with longer alkyl chain was found to adsorb more on a solid surface than the shorter alkyl length of dodecyltrimethylammonium bromide and tridodecylmethylammonium (Ibrahim, 2014).

Hailu *et al*. (2017) reported the sorption of benzene, toluene and ethylbenzene on zeolite modified with cationic surfactants of different chain lengths indicated that the sorption coefficients of organic contaminants increased with respect to the chain length of the cation surfactant. It was further observed by Hailu *et al*. (2017) that the longer the tail group of the cationic surfactant, the more stable the surfactant retained on the surface of the zeolite. Thus, HDTMA is commonly used for surface modification.

ii). The influence of the polar head group

The evaluation of cationic surfactants which have the same number of alkyl chain but with different polar head groups showed different adsorption capacities. Liu *et al*. (2016) reported the application of two surfactant modified zeolites for the removal of chromate and observed that the adsorption capacity for HDTMA – Zeolite and CPB-Zeolite was 10.19 and 12.76 mmol/kg, respectively. The higher adsorption capacity of CPB-Zeolite was attributed to the role of pyridinium group in the cationic surfactant adsorption.

iii), The concentration of the cationic surfactant

The concentration of the the cationic surfactant determines whether the surfactant would adsorb on the surface of the zeolite as either incomplete monolayer, complete monolayer, patchy bilayer and bilayer (Ibrahim, 2014). Liu *et al*. (2016) reported the amount of surfactant adsorbed at various concentrations of cationic surfactants using CPB and HDTMA for chromate removal. The authors used the concentration of the cationic surfactants of 0.5, 1.8 and 2.0 mmol/kg and the corresponding adsorption capacity of 3.44, 9.34 and 18.20 mmol/kg (CPB loaded zeolite) and 3.72, 7.43 and 13.94 mmol/kg for HDTMA loaded zeolite were observed. The trend of the results show that adsorption capacity increases with increase in catonic surfactant concentration.

iv). The influence of cationic surfactant counterion

The influence of the surfactant counterion must be taken into consideration in selecting surfactant modified zeolites. Xing *et al*. (2016) reported that in the competitive sorption between HDTMA-Cl and HDTMA-Br on clinoptilolite zeolite, preference for Br^- counterion was shown. The authors further added that the effect of counterions in stabilizing the sorbed HDTMA bilayer followed the lyotropic series $Br^- > Cl^- > HSO_4^-$

A variety of surfactants can be used for changing the zeolite surface chemistry (Wolowiec *et al*., 2017). The cationic surfactant, hexadecyltrimethylammonium (HDTMA), one of a group of quaternary ammonium compounds (QAC) is often preferred due to its ready availability and low cost. It is also preferred because of its high affinity to negatively charged mineral surfaces. HDTMA modified minerals are also known for high anion sorption capacity (Swarnkar and Tomar, 2013). The chemical formula is $(C_{16}H_{33})N\ (CH_3)_3Br$. CTAB (Hexadecyltrimethylammonium bromide). It is reported to be a severe surface water pollutant. It is highly toxic to algae. The threshold limit for algae is 0.09mg/L. In terms of persistence and degradability, HDTMA is biodegradable in water. HDTMA has a pH 5-7, melting point of 235 ^oC, a flash point of 244 ^oC and molecular mass of 364.46 g/mol. It is soluble in water, ethanol and methanol.

Jimenez *et al*. (2017) reported that surfactant modification levels were limited to the cation exchange capacity of the clay minerals. Ltifi *et al*. (2017) observed that HDTMA sorption plateau was reported when the concentration of HDTMA was equivalent to 200% of the CEC. Consequently, the adsorption of HDTMA on clay minerals was accredited to cation exchange process. Researchers have been able to show that sorption of a cationic surfactant onto negatively charged clay minerals involve both cation

exchange and hydrophobic bonding. It was reported that at low loading levels, surfactant monomers were retained by ion exchange, and form a monolayer. However, interactions among hydrocarbon tails lead to the formation of a bilayer as the amount of surfactant increases (Ahmadishoar *et al*., 2016).

2.8.4 Hexadecyltrimethylammonium sorption on zeolites

Adsorption is one of the main processes for adhesion of cationic surfactants on the surface of zeolites. Two mechanisms are feasible for the adsorption of the cationic surfactants such as, ion exchange and hydrophobic bonding. Ion-exchange mechanism could take place between the cationic surfactant and positively charged ions on the zeolite surface. Electrostatic interactions are active forces for HDTMA sorption on the adsorbent surface. Due to excess amount of HDTMA molecules in the solution, hydrophobic interactions could take place between hydrophobic sides of HDTMA molecules. It was found that the organo zeolites developed anion exchange properties when excessive HDTMA was present which could be used to adsorb anionic plant nutrients such as Nitrates and Phosphates from aqueous solution (Demircivi and Saygili, 2014). Sorption capacities of the zeolites were calculated by using Equation 2.4

$$q_e = \frac{C_o - C_e}{m} \times V \qquad (2.4)$$

Where C_o and C_e are the intial and equilibrium HDTMA concentration (mmol/L) in the solution, m is the amount of the adsorbent used (g) and V is the volume (L) of the aqueous phase.

Peng *et al*. (2017) reported that approximately 94% of HDTMA molecules bound to the external surface of clinoptilolite when the initial HDTMA concentration was below that required to satisfy the zeolite External Cation Exchange Capacity (ECEC). The authors further observed that at higher HDTMA concentrations, the sorbed HDTMA

concentration were twice as high as the ECEC. Studies on the first water rinse off of the HDTMA after the adsorption process showed that some HDTMA molecules desorbed. Therefore, for surface modification of zeolites above the ECEC, most of the second layer HDTMA molecules adsorbed through tail – tail interaction alone would be removed from the HDTMA-Zeolite (Bakhtiary *et al*., 2013). A zeolite modified with an amount of HDTMA equal to 200% of the external cation exchange capacity would retain only slightly more than the external CEC of the zeolite. Any excess of HDTMA molecule adsorbed to the zeolite after rinsing could possibly be removed during the anion batch isotherm experiments.

2.9 General Applications of Zeolite

2.9.1 Zeolite as Catalyst

The main applications of zeolites are in adsorption, catalysis and ion exchange processes (Seyed, 2015). Zeolites are used as catalyst in petrochemical industries. The unique shape, size of the micropores of the zeolites determine their useful function as catalysts (Moliner *et al*., 2015). ZSM – 5 was commercialised as an octane enhancement additive in Fluid Catalytic Cracking (FCC) where silicon (Si) – enriched Y zeolites serve as the major catalytic component in high – octane FCC catalysts. They are also used as catalysts in the production of organic chemicals (Clough *et al*., 2017)

2.9.2 Medical applications

Zeolites exhibiting impurity removal properties have been used in hemodialysis (Bilgin and Koc, 2013). The fact that zeolites can protect polymers from ultraviolet degradation opens a wide spectrum of external application of zeolites in cosmetics and dermatology. Zeolite powder has been found to be effective in the treatment of athlete's foot and to reduce the healing time of wounds and surgical incisions (Nigussie, 2018).

Zeolites have interesting effects on bone structure and formation. Zeolite A is a synthetic zeolite that may have therapeutic utility in osteoporotic individuals because of its ability to stimulate bone formation (Hadigavabar *et al*., 2018).

2.9.3 Zeolite application as building material

The most ancient use of zeolites is their use as construction materials or cementing agent. Zeolites were found in the ruins of Etruscan, Grecian and Roman walls. This use has continued until the present time especially in Italy (Tran *et al*., 2019). Zeolitic tuffs have mechanical properties comparable with those of other natural building materials. The main characteristic is their ability to act as a thermal store due to their ability to adsorb and desorb water molecules reversibly (Higashiyama *et al*., 2017). Nevertheless, buildings are cool during the day and warm at night since the zeolite removes heat from the environment by desorbing water molecules during the warmest hours of the day, and returns this heat during the coolest hours at night by re-adsorbing water. Thus, thermal regulation is combined with the environmental humidity (Nagrockiene and Girskas, 2016).

2.9.4 Zeolites application for radioactive specie removal

One of the first publications on the utilization of zeolites for the sorption of radioactive species was probably the patent of Yuna (2016) who proposed a method for the removal of Caesium from aqueous solutions by sorption with clinoptilolite. A mixture of synthetic zeolite A and natural chabazite was used to take up ^{137}Cs from contaminated waters after the nuclear accident at Three Mile Island (USA) and about 0.5 million curies of radiation was removed (Johan *et al*., 2015). Some of the main advantages of using zeolite for nuclear wastewater are their resistance to degradation in the presence of ionizing radiation, their low solubility and that they can be used for long term storage

of long-lived radio isotopes after drying the radionuclide-exchanged zeolite at 200 ^{o}C and sealing in a stainless steel containers. The saturated zeolite can be also transformed into concrete, glass or ceramic (Holler, 2010).

2.10 Zeolite Applications in Agriculture

Zeolites were reported to have potential uses in agriculture (Ramesh *et al*., 2010). Other potential applications being studied include application as carriers of fertilizers, fungicides, insecticides and herbicides, and as a trap for heavy metals in soils (Sangeetha and Baskar, 2016). The property of zeolites that makes them relevant for enhancing soil qualities include large internal pore volume fraction that retains water, a uniform particle-size distribution that allows them to be easily incorporated, and high cation-exchange capacity that retains nutrients (Ramesh and Reddy, 2011). The authors had reported the addition of zeolite to sand based root zones for nutrient status enhancement, especially selective retention of ammonium and potassium ion. Zeolites are environmentally friendly and inexpensive. They have been used as soil conditioners to improve soil physical and chemical properties including infiltration rate, water holding capacity and cation exchange capacity.

The toxicity of zeolites is tantamount to diatomaceous earth. The International Agency for Research on Cancer, (IARC) classified zeolites as non-toxic and Federal Department of Agriculture, (FDA), USA also affirmed that zeolite are non-poisonous for human consumption (Eroglu *et al*., 2017). Reeve and Fallowfield (2018) reported that the microbial toxicity studies of HDTMA to solution. The authors further reported that HDTMA adsorbed to soil indicated that aqueous HDTMA-Br added to soil increased the lag periods and decreased the rate and extent of mineralization of test compounds. However, the result was interpreted as selective toxicity towards gram negative soil

microorganisms. It was found that relative to aqueous HDTMA however, once HDTMA is bound to soil or clay, its toxicity was greatly reduced. It has been assumed that low levels of HDTMA would not be harmful to the environment since HDTMA has been approved as additive in hair conditioner, mouthwash and fabric softener. Wu *et al.* (2019) while considering the conceivable poisonous impacts of water solutions of some zeolite compositions inferred the non harmfulness of zeolites to humans and also animals.

2.10.1 Zeolites as organic manure efficiency enhancers

Cattle excrements are natural manures known to improve physical, chemical and biological properties of soils, particularly increasing the humus content and decreasing acidity (Manjaiah *et al.*, 2019). Zeolites with specific selectivity for ammonium (NH_4), can take up this specific cation from farmyard manure, composts, or ammonium-bearing fertilizers, thereby reducing losses of nitrogen to the environment. Ammonium-charged zeolites have also been tested successfully for their ability to increase the solubility of phosphate minerals. Ramesh and Reddy (2011) confirmed that zeolite blended with degraded compost increases the effectiveness of organic fertilizers on meadowland soils.

2.10.2 Zeolites as soil physio-chemical properties enhancers

The improvement of the quality of the soil as it relates to sandy texture as well as nutrient poor topsoil has been made possible with the addition of zeolite (Manjaiah *et al.*, 2019). Application of zeolite to the tune of one-fifth of the soil weight was found to be the best medium for tomato plants (Jankauskiene *et al.*, 2015). Aminiyan *et al.* (2015) emphasized that zeolites were commonly used as soil conditioners. Nokkoul and

Wichitparp (2015) demonstrated that zeolite application on soybean crop encouraged the initiation of vegetative phenology on allophonic soil. Zeolite has an effect to mitigate the salt damage to plants and that the leaching of calcium chloride substitutes adsorbed sodium in zeolite and replace with calcium. Calcium exchanged zeolite gives high productivity to sandy soil. Zeolite amendment is an effective way to improve soil condition in an arid and semiarid environment (Aminiyan *et al*., 2015). Application of natural zeolite increased the available nitrogen, phosphorus, calcium, and magnesium of the medium (Bumbac *et al*., 2016). A study by Manjaiah *et al*. (2019) concluded that the slight effect of zeolite application observed in a study suggested that its potential benefit might be realized only under poorer conditions where the needs for improvement in nutrient retention and moisture holding capacity were greater. Farmers apply zeolites to the soil to control soil pH and to improve ammonium retention. The CEC of soil may be increased by using zeolites as soil amendments (Mahesh *et al*., 2018). Ferretti *et al*. (2020) found an increase in soil microbial biomass and incorporation of added ^{14}C into microbial biomass after zeolite amendment. The microbial populations could respond to zeolite amendment in different ways.

2.10.3 Zeolites as herbicides, pesticides and fungicides use efficiency enhancers

Controlled release of inputs is being employed extensively in agriculture to deliver active substances like pesticides, herbicides and fertilizer material (Kulasekaran *et al*., 2010). The high adsorption capacities in the dehydrated state and the high ion-exchange capacities of natural zeolites make them effective carriers of herbicides, fungicides and pesticides. These porous materials with well-ordered structures are attractive candidates for storage and release of organic guest molecules. Clinoptilolite had been an excellent substrate for benzyl phosphorothiaoate to control stem blasting in rice. The use of

natural zeolites as a base lead to the fact that clinoptilolite was more than twice as effective as carrier of the herbicide benthiocarb in eliminating weeds in paddy fields as other commercial products. The controlled release of paraquat from zeolites can occur only via ion-exchange because of charge neutrality of the zeolite (Manjaiah *et al*., 2019).

2.10.4 Zeolites as water use efficiency enhancers

Zeolites possess high water holding capacities without reducing air filled pore space (Zhang and Chen, 2017). Zeolites may hold water up to 60 % of their weight due to a high porosity of the crystalline structure. Water molecules in the pores could be easily evaporated or reabsorbed without damage to such structures (Hoeung, *et al.*, 2011). Zeolites guarantee a permanent water reservoir, providing prolonged moisture during dry periods; they also promote a rapid rewetting and improve the lateral spread of water into the root zone during irrigation. This results in saving the quantity of water needed for irrigation. The results of field studies clearly showed that zeolites act as soil amendments for crop production and improve available water to the plants (Taheri-Soudejani *et al*., 2019). Zeolite improved the water use efficiency of strawberry plants (Jakkula and Wani, 2018).

2.10.5 Zeolites as crop yield enhancers

Addition of clinoptilolite increased yields of barley, potato, clover, and wheat after adding 15 ton /ha in a sandy loam soil (Hussain and Radi, 2019). Channbasavaraj and Reddy (2017) observed that the application of clinoptilolite in the field, reduced maize yields, and the material appeared to act as a slow-release fertilizer increasing the growth of radish crop after three successive harvests in the greenhouse experiment. Cairo *et al*. (2017) reported increased productivity of sugar cane with utilization of 6 ton /ha of

zeolite in an oxisol. Jumadi *et al*. (2019) observed that the application of 150 kg/ ha of urea coated with 5-10% of zeolite increased productivity of rice and tomato crops. *Yilmaz et al*., 2017) found that zeolite application did not affect cabbage yields, but pepper yields showed a quadratic response to zeolite application rate, primarily as an initial decrease than an increase in fruit size as rate increased. Highest green herbage yield of Alfalafa was obtained by Seif *et al*. (2016) when 20% zeolite, 180% soil was used. Zeolite (clinoptilolite) can retain nutrients in the root zone to be used by plants when required. Consequently this leads to the more efficient use of nitrogen and potassium fertilizers by reducing their rates for the same yield, by prolonging their activity or finally by producing higher yields.

2.10.6 Zeolites as heavy metal intake reducers

The decrease in the content of heavy metal and other toxic compounds in plants growing on heavily contaminated soils in industrial areas have been studied using natural zeolite as well as zeolitic fertilizers (Sangeetha and Baskar, 2016). Studies on the influence of higher doses of clinoptilolite and zeolitic fertilizers have shown the reduction of intake of heavy metals from contaminated soils. A zeolite of the clinoptilolite type at 600 kg/ha reduced the intake of cadmium and lead from the soil to 0.04 mg/kg in the plants. Zeolitic fertilizer proved effective in reducing the intake of heavy metals at 700 kg/ha but further increase of dosage led to a negative influence on the resulting plant biomass (Wyszkowski and Sivitskaya (2019)

2.10.7 Zeolites act as gas absorbers and removal agents of odour

Natural zeolites can absorb carbon II oxide, carbon (IV) oxide, sulphur (IV) oxide, hydrogen (II) sulphide, ammonia, argon, oxygen, nitrogen, hydrogen, water, methanol and many other gases can consequently be used to collect them or control odours

(Drekova *et al*., 2017). Therefore, those minerals are being used in intensive animal husbandry sheds, significantly reducing the content of ammonia and Hydrogen (II) sulphide, which cause undesirable odours. The ammonium ion (NH_4^+) adsorbed by zeolite becomes a natural enriched slow release fertilizer. The high amount of ammonia adsorbed by zeolites makes it an effective method to reduce the high concentrations of this gas produced in fish farms. It can be used to protect lettuce plants (*Sclerotinia sclerotiorum* against virus presence (Thakur, 2017).

The semi fluid droppings in large poultry houses usually release an unpleasant smell that is uncomfortable to chickens and farm workers. The harmful fumes of ammonia and hydrogen sulphide contribute to decrease resistance to respiratory diseases and result in smaller and less healthy birds (Felipe, 2015). In many areas of Japan, clinoptilolite is now mixed with the droppings directly or packed in boxes suspended from ceilings to remove ammonia and thereby improve the general atmosphere in chicken houses. The net result is reported to be an overall increase in egg production and healthier birds. Sebastian *et al*. (2015) reported a zeolite-packed air scrubber to improve poultry-house environments by passing ammonia-laden air over a series of trays containing crushed clinoptilolite. 15 to 45 % of the ammonium- nitrogen (NH_3-N) was removed even though the contact time was less than one second. There was an associated reduction in odour intensity. The use of such a scrubber could improve the quality of the air in poultry houses without the loss of heat that accompanies normal ventilation. The ammonium-loaded zeolite could then be used as a valuable soil amendment on disposal.

2.10.8 Zeolites as feed additives

The addition of natural zeolite (clinoptilolite) type to feed mixtures in low doses of about 1 – 2% has influences on very important functions that have not been recorded by other natural compounds (www.zeoinc.com). The zeolite of the clinoptilolite type from Nizny Hrabovec applied at the concentration of 0.9 – 1.7 kg/100 kg of feed was reported to breakdown the toxins in animal feeds. The effect was shown in the improved conditions of the animals and weight increases (Valpotic *et al*., 2017).

Based on the successful use of montmorillonite clay in slowing down the passage of nutrients in the digestive system of chickens and the resultant improvement in caloric efficiency, experiments have been carried out in Japan since 1965 on the application of natural zeo1ites as dietary supplements for several types of domestic animals (Alhawary *et al*., 2017). Fuerjierfu (2016) confirmed many of Onagi's observations and reported small increases in Feed Efficiency Values (FEV) for Leghorn roosters over a 40-day period, especially during the first 10 days. The birds were fed a diet containing 7.5% clinoptilolite crushed and mixed directly with the normal rations. Faeces were noticeably dryer and less odoriferous. Unfortunately, seventeen birds were used in the study and extensive statistical evaluation of the results could not be made. It is also known that the addition of clinoptilolite to the diet of pig, poultry and cattle, improves their weight gain and increases feed conversion ratios. Clinoptilolite acts as a mycotoxin binder, absorbing toxins which can be dangerous to animals. It also helps to control aflatoxins in animal feed, thus lowering mortality from digestive stress and reducing the need for antibiotics (Nadziakiewicza *et al*., 2019). It also absorbs other toxins produced in the feed by moulds and microscopic parasites and enhances food absorption by animals.

2.10.9 Zeolite application for soil amendment

Zeolite application as soil amendment are current ways to improve soil condition in dry and semi-dry environment (Kwakye-Awuah *et al*., 2013). Zeolites have been tested for use as soil amendment on various crops, including vegetables and in greenhouses in Russia, field crops in Japan, as constituents of golf course greens and tees in order to improve drainage and aeration, to improve compaction resistance, and reduce leaching of pesticides and fertilizers from the soil (Ferretti *et al*., 2020). Zeolites also increase the water–retention capacity of the soils (Sangeetha and Baskar, 2016). Unlike other soil amendments (e.g. lime) zeolite does not break down over time but remains in the soil to improve nutrient retention. Therefore, its addition to soil will significantly reduce water and fertilizer costs by retaining beneficial nutrients in the root zone. The porous structure of natural zeolite helps to keep the soil aerated and moist as well as active for a long time. Zeolite is not acidic but marginally alkaline and its use with fertilizers can help buffer soil pH levels, thus reducing the need for lime application (Chan *et al*., 2016). This mineral is therefore very beneficial in the construction of golf courses and sport fields where the resulting irrigation and maintenance costs can be very substantial.

2.11 Zeolites based Nano Fertilizers

The emergence of nanotechnology and the development of new nano-devices and nanomaterials open up potential novel applications in agriculture. Nanotechnology is defined as "the understanding and control of matter at dimensions of roughly 1-100 nm, where unique properties make novel applications possible (Preetha and Balakrishnan, 2017). Nanomaterials are obtained through the manipulation of individual atoms, molecules, or molecular clusters into structures to create materials and devices with new and vastly different properties (Hossain and Rameeja, 2015). The control of molecules

on the scale of billionths-of-a-meter have assisted scientists to create materials that exhibit "almost magical feats of conductivity, reactivity, and optical sensitivity. Nano-fertilizer technology is very innovative and scantly reported in literatures. Nutrient use efficiencies of conventional fertilizers hardly exceed 30 - 35%, 18 - 20% and 35 - 40% for N, P and K respectively. The data remain constant for the past several decade and research efforts did not yield fruitful results. Nano-fertilizers are nutrient carriers that are being developed using substrates with nano dimensions of 1 – 100 nm. Nano particles have extensive surface area and capable of holding abundance of nutrients and release it slowly and steadily such that it assists nutrients uptake corresponding to the requirements of the crop without any harmful effects of customized fertilizer inputs (Tarafdar, 2015). This also has the potential to drive an economic revolution. Subramanian *et al.* (2015) reported that nano-fertilizers and nanocomposites can be used to control the release of nutrients from the fertilizer granules so as to improve the nutrient use efficiency while preventing the nutrient ions from either getting fixed or lost to the environment (Preetha and Balakrishnan, 2017).

Nano–fertilizers are synthesised basically by loading soil nutrients such as Nitrogen, Phosphorous and Potassium on adsorbents with pores of nano dimensions of 1 to 100 nm (Kaushik *et al*., 2014; Naderi and Danesh-Shahraki, 2013). The soil nutrients are slowly and steadily released for elongated periods helping to improve the nutrient use efficiency and environmental safety. Adsorbents used as fertilizer carriers such as synthesised zeolites are usually preferred to natural zeolites because of their uniform pore size, high specific surface area (SSA) and thermal stabilities (Alaba *et al*., 2015; Manikandan and Subramanian, 2016). To load bulky molecules on adsorbents with averagely low pore size, strategies such as dealumination, desilication, synthesis of

mesoporous zeolites and microporous zeolites and use of structure directing agents have been used (Alaba *et al*., 2015). The leaching pattern have been characterized by two stages with the first stage described by first order kinetic law (Selva *et al*., 2017). In addition, the current awareness that precursors such as kaolin clays could be used to produce inexpensive zeolites have aroused some level of commercial interest. In agronomy and horticulture especially due to the fact that their surface area is huge and adsorptive sites help in retention and release of nutrients; (Mahesh *et al*., 2018).

2.11.1 Control release fertilizers

Controlled-release fertilizers have been known for several years. It has been estimated that the percentage of the fertilizer dose recovered by plants when applied in conventional forms may amount to 30 ± 50% (Naz *et al*., 2016). The control of fertilizer release keeps the fertilizer concentration at effective levels in the soil solution and releases the fertilizer when the plant mostly needs it. As a result of this control, maximal utilization of the fertilizer from plant systems, remarkable decrease with respect to fertilizer application rate, least possible losses of the fertilizer through volatilization or leaching, prevention of the seedling damage and full protection of the ecosystem in the case of biodegradable carriers (Volova *et al*., 2016). Most of the cases cited in literature have to do with reservoir-type formulations: systems where a fertilizing core is encapsulated inside inert carrier, in other words, coated fertilizers. The controlled-release of the fertilizer is regulated by diffusion through the coating. Sulphur-coated urea (SCU), polyethylene-coated urea, and coated superphosphate provide typical examples for this class of formulations. Another way of regulating the release of fertilizer is accomplished by means of chemically controlled releasing products, such as urea ± formaldehyde condensates (Guo *et al*., 2018). Matrix-type (monolithic)

formulations constitute the third major category of controlled-release device. The active agent is dispersed in the matrix and diffuses through the matrix continuum or intergranular openings, that is, through pores or channels in the carrier phase and not through the matrix itself. One of the advantages of monolithic formulations is their simple fabrication. (Manikandan and Subramanian, 2014).

There are many advantages of controlled release materials such as regular and continuous nutrient supply to plants, lower frequency of applications in soil, reduced nutrient loss due to leaching, volatilization and immobilization, mitigation of root damage by high concentration of salts, greater convenience over handling fertilizers , contribution to the reduction of environmental pollution by NO_3 and improved ecological health to agricultural activity (less contamination of groundwater and surface water) and reduction in production costs (Milani *et al*., 2017).

The expressions of controlled release fertilizers (CRFs) and slow-release fertilizers (SRFs) have been substituted for each other even though they are different. However, the expression CRF is generally used for fertilizers in which the components controlling the rate, pattern, and duration of release are understood and they could be regulated during CRF preparation (Rajan *et al*., 2021). SRFs on the other hand are characterized by the release of the nutrients at a slower rate than is usual but the rate, pattern, and duration of release are not well controlled. They may be strongly affected by handling conditions such as storage, transportation, and distribution in the field, or by soil conditions such as moisture content, wetting and drying, thawing and freezing, and biological activity (Sempeho *et al*., 2014) Thus, while in SRFs the nutrient release pattern is fully dependent on soil and climatic conditions and it cannot be predicted. The SRF release pattern, quantity, and time can be predicted within certain limits. The

sulphur-coated urea (SCU) is considered a SRF due to a significant variation in the release patterns between different batches of fertilizer (Sempeho *et al*., 2014).

Controlled release fertilizers (CRFs) are fertilizer particles incorporated within carrier molecules to control plant nutrients release thereby improving nutrient supply to crops and reduce environmental pollution. CRFs are an innovative way to deliver crop's nutrients owing to the pattern of nutrient release, which consequently improves fertilizer use efficiency (FUE) (Hawkesford *et al*., 2014). CRFs assist nutrients to be discharged over a prolonged period irrespective of the nutrient coatings, thereby controlling the rate and pattern of release. The function of the carrier molecule is to control nutrients release time and remove the need for regular fertilization and thereby give higher efficiency rate than conventional soluble fertilizers (Sempeho *et al*., 2014).

2.11.2 Zeolites as slow release fertilizers

A slow release fertilizer is a fertilizer containing a plant nutrient in a form which either delays its availability for plant uptake and use after application, or which is available to the plant significantly longer than a reference 'rapidly available nutrient fertilizer' such as ammonium nitrate or urea, ammonium phosphate or potassium chloride (Naz and Sulaiman, 2016). Slow release fertilizers are agricultural products developed to save fertilizer consumption and to minimize environmental pollution. They are made to release their nutrient contents gradually and to coincide with the nutrient requirement of a plant (Chen *et al*., 2016). These fertilizers can be physically prepared by coating granules of conventional fertilizers with various materials that reduce their dissolution rate. The varieties of slow release fertilizers are inorganic (magnesium ammonium phosphate), organic synthetic (Ureaforms and Nitroform) and coated forms. Of the coated forms, there are polymer and resin coated, but there have been lots of different

kinds of materials that have been used as coatings (Kusumastuli *et al.*, 2019). All sorts of products have been used as coatings for fertilizer nutrients such as sulphur coated urea (SCU), polymer-coated NPK (such as Osmocote) and petroleum-coated (such as Nutricote). Slow release fertilizers give up their nutrients depending on the type of coating materials, thickness of coating material, moisture content and temperature of the soil. Bacteria do play a role with some products, but even the bacteria need moisture and temperature in order to function. Generally, the higher the temperature and the more moisture available, the faster the release takes place. However, zeolites have attracted much attention by overcoming the disadvantage of high solubility of chemical fertilizers by functioning as slow release fertilizers (SRF). Previous studies on SRFs based on zeolites were limited to nutrients, which can be loaded in cationic forms such as NH_4^+ and K^+. However, if the nutrients are in anionic forms such as NO_3^- or PO_4^{3-}, the loading is negligible on unmodified zeolites. Therefore, it is imperative that the zeolite material should have adequate affinity for anions so that the anionic nutrients can be efficiently loaded for its use as SRFs. Anionic properties can easily be imparted on the zeolitic surface using the concept of surface modification using surfactant. Zeolite could also be modified by surfactant as SRF carriers to control nitrate, phosphate and sulphate release (Azman *et al*., 2018).

Commercial SRFs are classified into two basic groups namely: low solubility and polymer coated water soluble fertilizers (Mikula *et al*., 2020). The polymer coated SRFs are water soluble and can exhibit consistent nutrient release rates. However, average soil temperature and moisture need to be known. The fertilizers are characterized by one or more polymeric resins surrounding the fertilizer. The duration of nutrient release is controlled by the porosity of the resin coating. A more porous coating results in quicker

release. When polymer coated SRFs are applied to the soil, the water in the soil enters the fertilizer granule through micropores which dissolves the nutrients. Nutrients are then steadily released through the pores. The rates of nutrient release of polymer coated SRFs are influenced by soil temperature, the higher the soil temperature, the greater the release rate (Mikula *et al*., 2020). Release rate was reported as not significantly influenced by microbiological decomposition, soil moisture, soil type or pH. However, all polymers eventually degrade in soil and the degradation rate influences nutrient release from the polymer (Timilsena *et al*., 2015). Matrix based formulations cover a range of inorganic nitrogen and phosphorous in compounds that are relatively loosely bound (MBF 1) to more moderately bound (MBF 2) and more tightly bound compounds (MBF 3). Matrix application rates are based on the amount of nutrients released to meet plant growth, therefore their application rates will necessarily not be comparable to conventional or SRFs, which release their nutrients based on the amount applied (Lubkowski, 2014).

2.11.3 Zeolite as slow release nitrogen fertilizers

There are several reports in literature showing that the addition of zeolite to the source of nitrogen can improve the nitrogen use efficiency (Wu *et al*., 2019). Surface-modified zeolites offer a great promise as anion carriers for slow release of nutrients (Iqbal and Umar (2019). It has been reported that when zeolites are mixed with nitrogen, phosphorus and potassium compounds, zeolite enhances the action of such compounds as slow-release fertilizers, both in horticultural and extensive crops (Rabai *et al*., 2012). Zeolites are known for nitrogen capture, storage and slow release. It has been shown that zeolites, with their specific selectivity for ammonium (NH_4), can take up this specific cation from either farmyard manure, composts, or ammonium-bearing

fertilizers, thereby reducing losses of nitrogen to the environment (Ramesh *et al*., 2010). Natural zeolites, due to their structure and properties, inert and nontoxic material can be used as a slowly releasing carrier of fertilizer (Wu *et al*., 2019). It is possible to obtain an increase in the efficiency of nitrogen fertilizer in forage for crops when nitrogenated clinoptilolites are used in comparison with the use of urea (Latifah *et al*., 2017).

Urea is one of the most commonly used nitrogen fertilizers. It is highly soluble in water making it possible to leach through the root zones. Urea is converted into ammonia by an enzyme called urease found in many soils as shown in Equation 2.5

$(H_2N\text{-}CO\text{-}NH_2) + H_2O \rightarrow 2NH_3 + CO_2$ (2.5)

Urea water ammonia carbon (IV) oxide

A slow release nitrogen fertilizer can be produced by heating zeolite rock chips to about 400 ^{o}C to drive out all zeolitic and pore water and by replacing this water with molten urea, which solidifies at about 132 ^{o}C (Mehrab *et al*., 2016). Urea can be occluded in the zeolite framework thereby preventing leaching of urea into the root zone. The ammonium ions are released into the soil slowly over time (www. Austetute.com.au).

Mehrab *et al*. (2016) suggested that the effects of zeolite on Nitrogen (N) uptake and plant growth would vary with soil type, and that the maximum benefit would be expected on coarse-textured low cation-exchange capacity soils. The development of a slow nitrogen release system for fertilization technology could simultaneously contribute to the reduction of contamination and the improvement of crop yields. Use of soluble Nitrogen fertilizers is one of the major causes for groundwater contamination. Nitrogen liberation dynamics of the occluded form (in zeolites) are much slower than the surfactant-modified zeolite (SMZ) using hexa-decyltrimethylammonium as fertilizer carrier (Latifah *et al*., 2017). The nitrogen molecules are retained by electrostatic

attraction, modifications of molecular angles and single and double bonds occur within the molecule (Murray and Politzer, 2017). There are reports of urea-impregnated zeolite chips, which can be used as slow-release nitrogen fertilizers.

Azman *et al*. (2018) demonstrated the feasibility of using nitrate release and concluded that SMZ is a good sorbent for nitrate, while slow release of nitrate is achievable. These dual properties suggest that SMZ has a great potential as fertilizer carrier to control the release of nitrate and other anions. Ammonium (NH_4^+) occupying the internal channels of clinoptilolite should be slowly set free, allowing the progressive absorption by the crop which results in a higher dry matter production of crops (Latifah *et al*., 2017). Tiny pores in the clinoptilolite framework are large enough for small cations like ammonium and potassium to enter, but too small for nitrifying bacteria to enter. This means that once ammonium is held internally on the cation-exchange sites within clinoptilolite, it is not likely to be leached out easily as water passes through. It is more likely that it will move out slowly and be taken up in small amounts by the turfgrass plant, similar to the way a slow-release fertilizer works. Nitrification (conversion of ammonium to nitrate) was substantially reduced (Li *et al*., 2019). Not only does clinoptilolite improve nitrogen fertilization efficiencies, it also reduces nitrate leaching by inhibiting the nitrification of ammonium to nitrate (Li *et al*., 2018).

Several reports have suggested that increased Nitrogen use efficiency occurs on zeolite. Manure-ammonia sequestered in the zeolite is unavailable to nitrifying bacteria because of the small pore size (4.5Å) of the crystal lattice structure. Experiments conducted by Akbari *et al*. (2021) revealed that zeolite incorporated with poultry manure served as an effective fertilizer and soil conditioner. Adikari and Ramana (2019) reported the beneficial effect of zeolite fertilizers on mobile humus substances of Chernozem and on

biological productivity of maize. Natural zeolites are able to bind humic acid through the action of the surface extra-framework cations and that this ability would be strongly enhanced if the zeolitic material was enriched with divalent cations, especially calcium ion (Colella *et al*., 2015).

Chen *et al*. (2017) found increased nitrogen use efficiency in rice due to application of zeolites. Nitrogen dynamics in soil-air-water systems is of great interest in agriculture for its rational use. Higher nitrogen efficiency is an essential factor for reducing environmental contamination. Surface and groundwater contamination as a result of nitrogen fertilization has been demonstrated in Argentina (Ramesh *et al*., 2010). The pronounced selectivity of clinoptilolite for NH_4 ion was exploited in slow release of chemical fertilizers (Rabai *et al*., 2012). Soil-clinoptilolite-nitrogen dynamics are variable, depending on the physio-chemical soil characteristics; nitrogen doses applied and crop management (Omar *et al*., 2020). The high potential of the clinoptilolite has been demonstrated as a vehicle for nitrogen fertilizers, with the aims of decreasing negative impacts on the environment and increasing fertilizer efficiency (Latifah *et al*., 2019). Jones *et al*. (2017) showed in a pot experiment with clinoptilolite, an increase of around 130% in nitrogen use efficiency, nitrogen uptake, and dry matter yield of Signal grass *Brachiaria decumbens*.

2.11.4 Zeolites as slow release phosphorous fertilizers

A zeolite containing an exchange ion such as ammonium can be mixed with phosphate mineral (such as apatite, calcium phosphate) to produce a controlled release phosphorous fertilizer. The zeolite takes up Ca^{2+} from the apatite and releases phosphate and ammonium ions into the soil as shown in Equation 2.6

$$Ca_3(PO_4)_2 + 6NH_4\text{-zeolite} \rightarrow 3Ca\text{-zeolite} + 6NH_4^+ + 2PO_4^{3-} \quad (2.6)$$

As phosphate is taken up by plants, the zeolite will release more phosphate and ammonium ions in an attempt to re-establish equilibrium by Le Chatelier's Principle. (www.Austetute.com.au). The rate of P release is controlled by varying the P-rock /zeolite ratio. Phosphorous is also released from the apatite by a lowering of soil pH related to the nitrification of ammonium ions.

Just as zeolites have been used to control release of fertilizer components, ammonium-charged zeolites have shown their ability to increase the solubility of phosphate minerals, leading to improved phosphorus uptake and yields of crops. Studies conducted to examine solubility and cation-exchange relationships in mixtures of rock phosphate and NH_4^+ and K-saturated clinoptilolite revealed that mixtures of zeolite and phosphate rock have the potential to provide slow-release fertilization of plants in synthetic soils by dissolution and ion-exchange reactions. The power-function equation has been found to describe the transport kinetics of the nutrient release process in these systems (Mikhak *et al*., 2018). Investigation conducted to study the effects of the potassium and ammonium-saturated clinoptilolite on Phosphorous availability in Ferrosols revealed that potassium and ammonium-saturated clinoptilolite can increase Phosphorous solubility while providing Potassium and Ammonium ion to the soil, a concurrent positive effect for plant growth (Shi *et al*., 2016).

2.12 Adsorption of Surfactants and Plant Nutrients

The main reason for the use of zeolite A and Phillipsite in fertilizer formulation and as fertilizer carrier is its ion exchange property. The process of modifying the surface of zeolite with surfactants and occluding plant nutrients in the pores of the zeolites is an adsorption process (Selva *et al*., 2014). The adsorption process requires an understanding of the adsorption isotherm which consequently improves the adsorption

mechanism pathways and effective design of adsorption process (Ayawei *et al*., 2017). An adsorption isotherm describes the trend controlling the movement of a substance from the aqueous porous media to a solid phase at a constant temperature and pH. The establishment of a dynamic balance when an adsorbate phase has been made to contact with the adsorbent for a sufficient time is described as the adsorption equilibrium. Basically, there are two types of adsorption processes namely physisorption and chemisorption. Most adsorption processes are a combination of physical force (physisorption) and chemical force (chemisorption). A distinction of these two processes is very useful in understanding the factors that influence the rate of adsorption process (Younas *et al*., 2016).

Physical Adsorption occurs when the force of attraction existing between adsorbate and adsorbent are weak Van der waal forces of attraction, the process is called physical adsorption or physisorption. Physical adsorption takes place with formation of multilayer of adsorbate on adsorbent. It has low enthalpy of adsorption. Heat of adsorption is 20-40 kJ/mol. It takes place at low temperature below boiling point of the adsorbate. As the temperature increases, the process of physisorption decreases (Inglezakis and Zorpas, 2012).

Chemical adsorption occurs when the force of attraction existing between adsorbate molecules and the surface functional groups of adsorbent are chemical forces of attraction or chemical bond, the process is called chemical adsorption or chemisorption. Chemisorption takes place with formation of unilayer of adsorbate on adsorbent. It has high enthalpy of adsorption. It can take place at all temperature. With the increase in temperature, chemisorption decreases. Chemisorption is an exothermic process and the enthalpy values are higher (80 - 240 kJ mol^{-1}) as it involves formation of chemical

bonds (Kalotra *et al*., 2014). However, the activation energy for chemisorption is high and occurs slowly. Hence it is also called activated adsorption. It is practically irreversible. The dominant adsorption mode for chemisorption is known when the isosteric heat of adsorption has a magnitude between 40 and 125 kJ.

2.13 Adsorption Isotherm Models

Equilibrium isotherm models such as Langmuir, Freundlich, Brunauer-Emmett-Teller, Temkin, Dubinin-Radushkevich isotherms have been widely used to study adsorption processes. Linear forms of the models are often used in the studies.

2.13.1 Langmuir monolayer adsorption isotherm model

Langmuir is the most useful two parameter isotherm for physical and chemical adsorption. It had been used to quantify and contrast the adsorptive capacity of various adsorbents. Langmuir gives the explanation for the surface coverage of an adsorbent by balancing the relative rates of adsorption and desorption (dynamic equilibrium) (Nimibofa *et al*., 2017). The model is based on the following assumptions: that only a single layer of molecules on the adsorbent surface are absorbed and that the adsorbent surface consists of active sites having uniform adsorption energy. There is no transmigration of adsorbate in the plane of the surface. No molecule can be further adsorbed on a site already occupied by an adsorbate. As the distance between the adsorbate and adsorbent increases, the intermolecular attractive forces decrease quickly. Molecules adsorbed on localized and neighbouring sites have no interactions (Saadi *et al*., 2015). The linear form of Langmuir isotherm can be expressed in Equation 2.7

$$\frac{C_e}{q_e} = \frac{1}{q_m K_e} + \frac{C_e}{q_m} \qquad (2.7)$$

Given that C_e is concentration of adsorbate at equilibrium (mg/g), K_L is the Langmuir constant related to adsorption capacity (mg/g), which can be further related with the

variation of the suitable area and porosity of the adsorbent which implies that large surface area and pore volume will result in higher adsorption capacity.

The important characteristic of the Langmuir isotherm for predicting the adsorption efficiency and usability of the Langmuir equation is expressed by the dimensionless constant called separation factor in Equation (2.8)

$$R_L = \frac{1}{1 + K_L C_o} \quad (2.8)$$

R_L values between 0 and 1 show favourable adsorption, while $R_L > 1$, $R_L = 1$ and $R_L = 0$ indicates unfavourable, linear and irreversible adsorption process respectively.

2.13.2 Freundlich isotherm model

The Freundlich Isotherm model in contrast to Langmuir can be applied to multilayer adsorption (Ramadoss and Subramanian, 2018). It describes the non-ideal and reversible adsorption. The model is based on the assumption that the surface of the adsorbent is heterogeneous and its active sites and adsorption heat energies distribute exponentially. The model also assumes that the stronger binding sites are occupied first, until the binding strength or adsorption energy are exponentially decreased upon the completion of adsorption process.

Presently, the isotherm is applied in heterogeneous systems especially for organic compounds. The model has been observed to be the most suitable for describing the adsorption of different adsorbates from aqueous solutions (Saadi *et al*., 2015). The Freundlich isotherm in its linear form is as shown in Equation 2.9

$$\log q_e = \log K_F + \frac{1}{n} \log C_e \quad (2.9)$$

Where K_F is adsorption capacity (L/mg) and 1/n is adsorption intensity and it signifies the relative distribution of the binding energy and the heterogeneity of the adsorbate

sites. It is also known as the slope whose values are between 0 and 1 for favourable adsorption isotherm. As the value of the slope gets closer to zero, the surface of the adsorbent becomes more heterogeneous. When the value of 1/n is above 1, it signifies an unfavourable adsorption isotherm and it indicates a cooperative adsorption. As 1/n gets smaller than 0.1, the adsorption isotherm approaches irreversible isotherm and consequently its implication is that it is a chemisorption process. The demerits of the Freundlich isotherm is its lack of thermodynamic basis, not approaching the Henry's law at diminishing concentrations (Ruthiraan *et al*., 2018).

2.13.3 Temkin isotherm model

The Temkin isotherm model contains a factor that explicitly takes into account the adsorbent-adsorbate interactions in the adsorption process. It assumes that the heat of adsorption (ΔH_{ads}) of all molecules in the layer decreases linearly rather than logarithmic with increase with surface area or as equilibrium adsorption capacity increases because the b_T factor is related to adsorbent-adsorbate interactions. The Temkin isotherm is valid only for an intermediate range of ion concentration and ignores the extremely low and large value of concentrations. The model is characterized by a uniform distribution of binding energies up to some maximum binding energies of 34.61(L/mg) (Balarak *et al.*, 2017). Temkin equation is better for predicting the gas phase equilibrium rather than liquid – phase equilibrium. The linear form of Temkin isotherm model is given by the linear form in Equation 2.10

$$q_e = \frac{RT}{b} \ln K_T + \frac{RT}{b} \ln C_e \qquad (2.10)$$

Where b_T is Temkin constant which is related to the heat of sorption ($Jmol^{-1}$) and K_T is Temkin isotherm constant (Lg^{-1}**).**

2.13.4 Dubinin – Radushkevich isotherm model

The model is an equation in which its adsorption follows a pore filling mechanism. It assumes a multilayer character including Van Der Waals forces appropriate for physical adsorption processes (Atugoda *et al*., 2020). The Dubinin-Radushkevich model has the capacity to approximate the characteristic porosity and the seeming free energy of adsorption. The model expresses the adsorption mechanism onto a heterogeneous surface with a Gaussian energy distribution. The model can further differentiate the physical and chemical adsorption of adsorbate ions with its mean free energy, E per molecule of adsorbate given in Equation 2.11 for removing a molecule from its location in the sorption space to the infinity.

$$E = [\frac{1}{\sqrt{2B_{DR}}}] \quad (2.11)$$

Where B_{DR} is denoted as the isotherm constant. For the meantime, the parameter ε, the Polanyi potential can be related as

$$\varepsilon = RT \ln[1 + \frac{1}{C_e}] \quad (2.12)$$

Where R, T and C_e represent the gas constant (8.öö4 J/mol K) absolute temperature (K) and adsorbate equilibrium concentration (mg/L), respectively. The temperature dependent feature of the model distinguishes it especially when adsorption data at different temperatures are plotted as a function of logarithm of amount adsorbed versus the square of potential energy, all suitable data will lie on the same curve, known as the characteristic curve. The model can effectively fit intermediate range of concentrations data even though it cannot predict Henry's law at low concentration. The model can be represented in its linear form as shown in Equation (2.13)

$$\ln q_e = \ln q_m - K_{ads} E^2 \quad (2.13)$$

Where E is the mean adsorption energy and K_{ads} is Dubinin–Radushkevich constant, Determination coefficient, R^2 are used to determine the relationship between the experimental data and the isotherm model in most literatures.

2.13.5 Types of adsorption isotherm

The characteristics of five different types of adsorption isotherm given as Type I, II, III, IV and V are explained in Figure 2.2 to 2.7 as follows:

The graph of Type I Adsorption Isotherm in Figure 2.2 shows a monolayer adsorption which is easily explained by Langmuir Adsorption Isotherm. X represents the amount of adsorbate while m represents the amount of the adsorbent, P represents the pressure and Ps represents the saturation pressure. Given the BET equation, when P/P0<<1, then it leads to monolayer formation and Type I Adsorption Isotherm is obtained. Examples of Type I adsorption are Adsorption of Nitrogen (N_2) or Hydrogen (H_2) on charcoal at temperature near to 180 ^oC (Wang and Guo, 2020). The external surface is basically found inside of the microspores and when an adsorbate molecule occupies a pore, there is no room for the filling of another adsorbate.

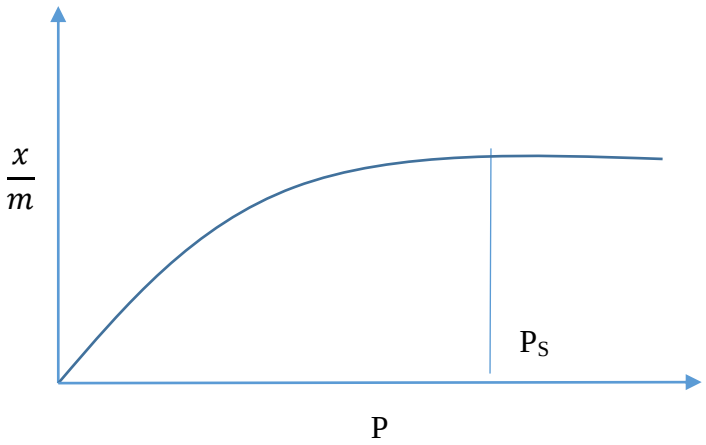

Figure 2.2: Type I Adsorption Isotherm

The graph of Type II Adsorption Isotherm in Figure 2.3 deviates from the Langmuir adsorption model. The intermediate flat region in the isotherm corresponds to

monolayer formation. Examples of Type II adsorption are Nitrogen (N_2) (g) adsorbed at -195 ^oC on Iron (Fe) catalyst and Nitrogen gas adsorbed at -195 ^oC on silica gel. Type II adsorption isotherm is often observed on nonporous powders or powders with diameters larger than micropores. The point of inflection is observed close to the completion of the first adsorbed monolayer.

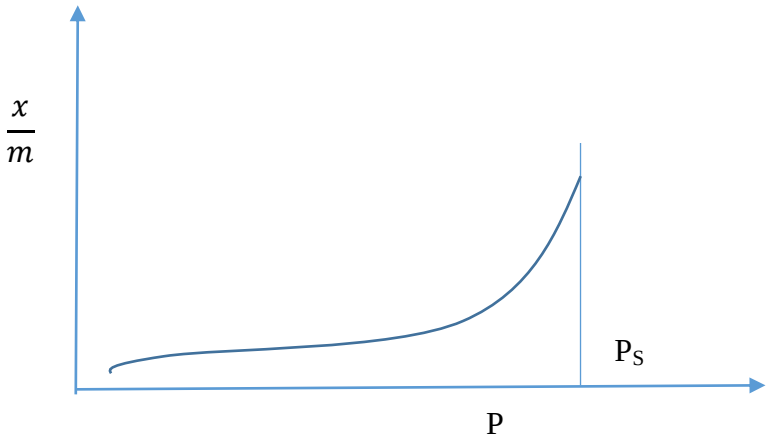

Figure 2.3: Type II Adsorption Isotherm

A large deviation from the Langmuir model is also shown in Type III Adsorption Isotherm in Figure 2.4. It gives the explanation for the formation of a multilayer. A flat portion is not observed as depicted in a monolayer formation. Examples of Type III Adsorption Isotherm are Bromine (Br_2) at 79 ^oC on silica gel or Iodine (I_2) at 79 ^oC on silica gel. The type III adsorption isotherm is characterized by heats of adsorption which are less than the adsorbate heat of liquification. The adsorption progresses as the adsorbate interaction with an adsorbed layer is greater than the interaction with the adsorbent surface

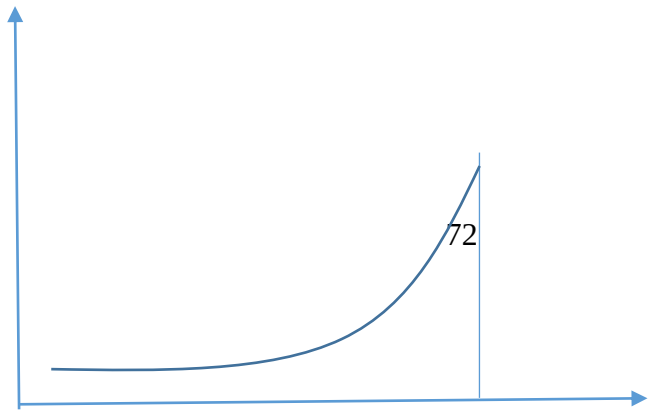

$\frac{x}{m}$

P_S

Figure 2.4: Type III Adsorption Isotherm

The graph is quite similar to Type II isotherm at a lower pressure region. This formation describes a monolayer followed by multilayer. The attainment of a pressure below the saturation vapour pressure signifies the saturation level. This can be explained on the basis of a possibility of gases getting condensed in the tiny capillary pores of adsorbent at pressure below the saturation pressure (P_S) of the gas. Examples of Type IV Adsorption Isotherm are of adsorption of Benzene on Iron Oxide (Fe_2O_3) at 50 ^oC and adsorption of Benzene on silica gel at 50 ^oC. Type IV adsorption isotherm as shown in Figure 2.5 occurs on porous adsorbents with pores in the range of 1.5 – 100 nm. At higher pressures, the slope shows increased uptake of adsorbate as pores become filled, inflection point typically occurs near completion of the first monolayer

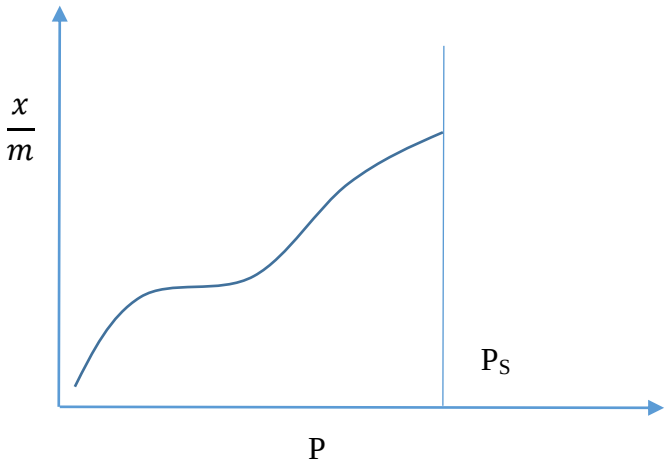

Figure 2.5: Type IV Adsorption Isotherm

Type V isotherm graph is similar to Type IV isotherm. The example of Type V adsorption Isotherm in Figure 2.6 is adsorption of water (vapours) at 100 ^{o}C on charcoal. Type IV and V adsorption isotherms show the occurrence of capillary condensation of gas. Type V adsorption isotherm are observed where there are small adsorbate absorbent interaction potentials (similar to type III), and they are also connected with pores in the 1.5 – 100 nm range.

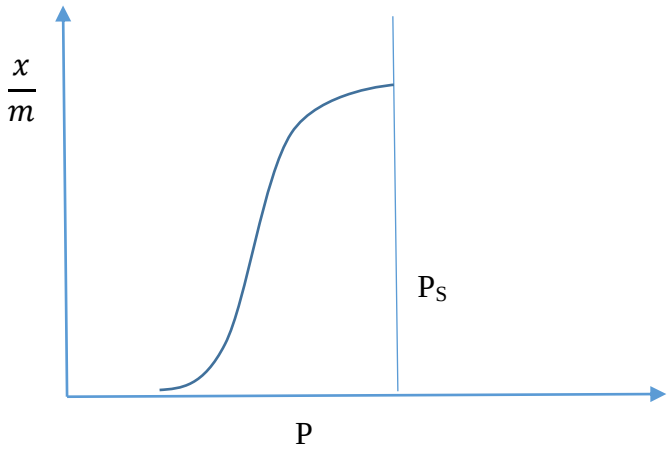

Figure 2.6: Type V Adsorption Isotherm

The study of the adsorption mechanism of cationic surfactant onto zeolites are not only limited to understanding adsorption isotherms, but also their rates of adsorption which is also referred to as adsorption kinetics.

2.14 Adsorption Kinetic Models

Kinetics is the study of reaction rates, or how fast they go under different conditions. The study also involves mechanisms of reactions which focus on how the reacting molecules break apart and then form new ones. The mechanism pathway helps in regulating reactions (Olutoye, 2012). Several kinetic models have been used to illustrate the adsorption and desorption of ions from soils minerals. The goodness of fit of the models is expressed by the coefficient of determination R^2. A relatively higher R^2 value

for the relationship between measured and predicted sorption and desorption data indicated that the model successfully described the kinetics of sorption and desorption. But a high R^2 value for a particular model does not necessarily mean that this model is the best. Therefore models producing r^2 values > 0.90 for most treatment levels are used for discussion (Riley *et al*., 2019).

The rate of adsorptive uptake of any adsorbent is dependent on the adsorption mechanism. The basis of kinetics study is the kinetic isotherm, which is obtained experimentally by tracking the adsorbed amount against time. Kinetic studies develop a model to describe the adsorption rate. The model should be able to show the rate limiting mechanism, and extrapolate the operating conditions of interest (Tan and Hameed, 2017).

2.14.1 Pseudo-first-order model

The equation for pseudo first order was proposed by Largergren for the adsorption of oxalic and malonic acid onto charcoal. The rate constant of adsorption is given from the first order rate expression as shown in the linearized Equation 2.14.

$$\ln\left(\frac{q_e}{(q_e - q)}\right) = k_1 t \qquad (2.14)$$

Where q_e and q are the amount of the adsorbate adhered on the adsorbent in (mg/g) at equilibrium and time t (min) respectively and k_1 is the rate constant of adsorption (L/min). Biswas and Mishra (2015) have reported that k_1 is an increasing function of C_o or independent of C_o. Systems that obey this model give a straight line that passes through the origin with a slope k_1 when ln (q_e – q) plotted against t.

2.14.2 Pseudo-second-order model

The model for pseudo second order model was based on the assumption that uptake rate is second order with respect to the available surface site. The linearized form of the model is given in Equation 2.15

$$\frac{t}{q} = \frac{1}{k_2 q_e^2} + \frac{t}{q_e} \quad (2.15)$$

The initial rate of adsorption, h (mg/g min), as t tends to 0 can given

$$h = k_2 q_e^2 \quad (2.16)$$

where the initial rate of adsorption (h), the equilibrium adsorption capacity (q_e) and the second-order constants k_2 (g/mg min) can be determined experimentally from the slope ($1/q_e$) and intercept ($\frac{1}{k_2 q_e^2}$) of plot t/q versus t. Comparably to Pseudo First Order (PFO)'s k_1, the constant k_2 is a time scale factor that decreases with increasing C_o. It has been observed that PFO is inferior in terms of fit to the pseudo–second order model by a least-square discrimination procedure Li *et al*., 2019).

2.14.3 Intra-particle diffusion model

This equation for modeling adsorption kinetics was proposed by Weber and Morris in 1963 and it is shown in Equation 2.17

$$q = k_{id}\sqrt{t} + B \quad (2.17)$$

Given that K_{id} is the Intra-Particle Diffusion (IPD) rate constant (mg/(g.min$^{0.5}$), and B is the initial adsorption (mg/g). The plot of q versus $\sqrt{t}$ should be linear; the k_{id} and B represent the slope and intercept respectively. K_{id} generally increases with increasing initial adsorptive concentration. For kinetics controlled by IPD, the line should pass through the origin. However, if the data describes multi-linear plots, then two or more steps describes the sorption process. The first sharper portion is attributed to the diffusion of adsorbate through the solution to the external surface of adsorbent or

boundary layer diffusion of solutes molecules. The extrapolation of the linear portions of the plots back to the y-axis gives the intercept and consequently the value of I which provides the measure of the boundary layer thickness. The larger the intercept, the larger the boundary layer effect (Tan and Hameed, 2017). The deviation of the straight lines from the origin may be attributed to the difference in rate of mass transfer in the initial and final stages of adsorption. Furthermore, such deviation of straight line from the origin indicates that the pore diffusion is not the sole rate controlling step. Therefore, the adsorption proceeds through a complex mechanism.

2.15 Adsorption Thermodynamics

The thermodynamics concept presumes that entropy change is the driving force in an isolated system where energy cannot be lost or gained. In environmental engineering, energy and entropy factors are taken into account in determining the processes that are likely to happen spontaneously. The Gibbs free energy change, ΔG^o is the fundamental criterion of spontaneity. Reaction occurs spontaneously at a given temperature if ΔG^o is a negative quantity (Ushakumary, 2013). Janda *et al*. (2016) reported that adsorption reactions depend on temperature and therefore the thermodynamic parameters considered in the determination of the adsorption processes are the changes in standard enthalpy (ΔH^o), standard entropy (ΔS^o) and standard free energy (ΔG^o) owing to transfer of unit mole of solute from solution onto the solid – liquid interface. The amount of heat evolved when one mole of the adsorbate is adsorbed on an adsorbent surface is called enthalpy of adsorption. Adsorption is always an exothermic process and enthalpy of adsorption is always negative. When adsorbate molecules are adsorbed on the surface of an adsorbent, their freedom of movement becomes restricted, and hence, entropy decreases. Adsorption is spontaneous, therefore at constant temperature

and pressure, Gibb's free energy (ΔG^o) decreases. The Gibbs free energy change (ΔG^o) shows the degree of spontaneity (naturalness, freedom, impulsiveness) of an adsorption process, and a higher negative value shows a more forceful favourable adsorption.

In accordance to thermodynamic law, ΔG^o of adsorption is shown in Equation 2.18

$$\Delta G^0 = -RT \ln K \quad (2.18)$$

Given that K is the thermodynamic equilibrium constant, T is the absolute temperature in kelvins; R is the gas constant with a value 8.314 $Jmol^{-1}$ K^{-1}. The relationship between the thermodynamic parameters is expressed in Equation 2.19

$$\Delta G^0 = \Delta H^0 - T\Delta S^0 \quad (2.19)$$

Substituting Equation 2.19 into Equation 2.18 gives

$$\ln K = \frac{-\Delta H^o}{RT} + \frac{\Delta S^0}{R} \quad (2.20)$$

The plot of the values of ln K against 1/T hypothetically gives a straight-line graph. The resulting slope and intercept allow the calculation of ΔH^o and ΔG^o respectively. These thermodynamic estimates provide information into the type and mechanism of an adsorption process. The heat given off during the physical adsorption is between the range of 2.1 to 20.9 kJ/mol whereas a chemical adsorption is between the range of 80 to 200 kJ/mol (Yousef *et al*., 2011). A negative value of ΔH^o means that adsorption would be an exothermic adsorption process while a positive ΔH^o denotes an endothermic adsorption process. A positive ΔS^o value signifies increased randomness at the solid–solution interface during adsorption while a negative ΔS^o usually indicate a no remarkable change in entropy during adsorption (Yousef *et al*., 2011).

2.16 Influence of Zeolites on Tomatoes

Vegetable production can be adopted as a strategy for improving livelihood and alleviating the nutritional status of the people. It is the answer to the perpetual problems

of hunger and malnutrition in the country. A lot of Nigerian children suffer from vitamin “A” deficiency, a nutritional problem that can be reduced by regularly eating fruit and green leafy vegetables (Szabo *et al*., 2018).

Tomato is one of the most important vegetable crops grown all over Nigeria. It is the world’s largest vegetable crop after potato and sweet potato but it tops the list of canned vegetables. It is an important condiment in most diets and a very cheap source of vitamins. It also contains a large quantity of water, calcium, and Niacin all of which are of great importance in the metabolic activities of man (Bamaniyan *et al*., 2019). Tomato is a good source of vitamin A, C, and E and minerals that are very good for the body and protect the body against diseases (Bamaniyan *et al*., 2019). Ugonna *et al*. (2015) reported that the yield level in Nigeria is low when compared to major producing countries like Ethiopia, Niger with average yield of 7.1 t ha^{-1}. Low soil fertility has been identified as one of the major problem facing small scale farmers in the tropics. The low fertility is caused by continuous cropping without additional soil fertility inputs (Ande *et al*., 2017). In the savannah agro-ecology, decline in crop yields are associated with the inability of most farmers to acquire inputs for optimum crop production (Wato, 2019). The yield of tomato in Nigeria is low, the average in Western part of the country being only about 5 tonnes per hectare and in growing areas of Northern Nigeria is 20 tonnes per hectare. One of the reasons for this low yield in Nigeria is poor fruit set resulting from temperatures that are generally above optimum range for good fruit set (Onyia *et al*., 2019). Soil fertility is a major overriding constraint that affects all aspects of crop production (Yadav and Sarkar, 2019). Most local farmers in Africa, use inadequate nutrient inputs, inappropriate quality and inefficient combinations of fertilizers, which eventually to high input cost (Biramo, 2018). A consequence of this

trend is a deeply unbalanced soil nutrient composition that ultimately leads to a reduction in crop yield potential (Elemike *et al*., 2019). Nutrients, when in adequate quantity, increases fruit quality, fruit size, colour, and fruit taste of tomato (Bazgau *et al*., 2021). It also helps in increasing desirable acidic flavour.

Plant nutrition research is highly useful in tackling low soil fertility, low levels of available mineral nutrients in soil and improper nutrient management. Removing these constraints improves the sustainability of food security and well-being of humans without harming the environment (Wu *et al*., 2017). As far as mineral nutrition of tomato is concerned, the effect of potassium (K) and phosphorous (P) are well established, Potassium plays a vital role in growth, plant productivity, metabolism, ionic balance, activation of several enzymes and plant defence systems (Hasanuzzaman *et al*., 2018). It is the most prominent inorganic plant solute and the only mineral nutrient that is not a constituent of organic structures. It is also of outstanding importance for crop quality as it improves fruit size and stimulates root growth. It is necessary for the translocation of sugars, formation of carbohydrates and provision of resistance against pest and diseases and drought, as well as frost stresses (Hasanuzzaman *et al*., 2018). Several studies have shown that K content during the growth period has a profound effect on sugars and acids. potassium nutrition strongly influences acid concentrations and especially ascorbic acid (vitamin C) levels. Fresh tomato fruits are an important source of vitamin C hence production practices, including adequate plant potassium fertilization, are important to determine how levels can be increased (Bernardi and Verruma, 2013).

The total potassium uptake in tomato plants after harvest is 70% in the fruit and 16% in the leaves (Cole *et al*., 2016). Fruits of Potassium deficient plants are not fleshy, their

ripening is uneven and their appearance is blotchy. The dry matter content of the ripe tomato fruit is about 5 – 7.5% of the total weight, a high proportion of this dry matter consisting of sugars and organic acids, both of which contribute to the taste of the fruit. The organic acid content, mainly citric and malic acids, increases during fruit development.

The importance of Phosphorous as a plant nutrient in tomato plants in general is less well recognized than that of Potassium, even though Potassium and phosphorous are both essential plant nutrients. The main reason for this is that lower amounts of Phosphorous (in the form of phosphate) are taken up by plants and tomato is particularly responsive to Potassium application by increased growth and quality. In tomato, the phosphorous content in fruit and vegetative tissue is less than one tenth that of potassium. After uptake, phosphate can remain as free inorganic phosphate as well as being bound with organic constituents of major importance, including sugar phosphates. When tomato plants are Phosphorous deficient, foliage size is greatly reduced and Phosphorous is transferred preferentially to the roots, photosynthesis is depressed, and the smaller leaves become a darker green. In extreme cases, the underside of the leaves become purple as a consequence of anthocyanin accumulation. Therefore the high cost of tomato in the Nigerian market justifies that the production is far lower than the demand. If proper nutrient management is adapted by the tomato producer, the production will certainly go up to meet the demand.

It has been reported by Preetha *et al*. (2017) that zeolite helped to retain a large amount of phosphate in the soil during the cultivation of tomatoes with the right conditions of watering and fertilizing. Irrigation was applied every 2 days for 2 hours using a trickle irrigation and application rate of irrigation water at 13.5 m^3/day. Though different ratios

of zeolite were added, it was observed that zeolite additions did not affect the fruit yield of the tomatoes. The authors however reported that the use of zeolite enhanced nutrients retention in soils. However, the study did not compare the effects of zeolite based slow release fertilizer with a conventional fertilizer on the tomato crop.

The evaluation of tomatoes grown in a pot experiment for their growth and nitrogen (N) losses through leaching was reported by (Wang *et al*., 2019). The plants were fertilized with ammonium nitrate and Georgia Pacific slow release nitrogen fertilizers. The fertilizer rate was at 112 low nitrate rate (L) and 224 high nitrate (H) kg N ha^{-1}. Sandy and loam soil were used. The authors observed that the net amount of N leached from the sandy soil was between 6.5 to 32.9%. The authors also reported that three slow release fertilizers had a much lesser tendency to leach than ammonium nitrate which was a traditional fertilizer. However, the research work did not evaluate the effect of synthesised zeolite based slow release fertilizers as fertilizer carrier that reduces most the leaching potential of nitrate-nitrogen in the sandy loam soil.

2.16.1 Studies on the effect of zeolites on tomato crops

The increase in yield and vitamin C levels of tomato grown on KH_2PO_4 – enriched zeolite in an inert-sand substrate was reported by (Bernardi and Verruma, 2013). The zeolite mineral was concentrated by a gravitational process and dispersed into solution (0.5 NaCl) to saturate the negative charges. This homo ionic material was dispersed into KH_2PO_4 solution and then centrifuged, filtered and dried. The authors reported that the evaluation of K and P addition to a zeoponic substrate for growth of tomato (*Lycopersicon esculentum L. Cv. Finestr*a) showed positive effects on fruit yield, quality and dry matter (DM) yield. The authors however concluded that increasing

levels of K and P supply to tomatoes plants, by addition to a zeoponic substrate in a pot experiment, increased fruit and total dry matter yields. Additionally, the concentration of vitamin C in the fruits was also increased by higher levels of K and P in the substrate. The authors reported the effects of the application of zeoponic system in the growth and yield of the tomatoes. The authors did not report the enrichment of the zeolite used with nitrogen and the Functionalisation of the zeolite used. The effect of the zeolite used on the soil at post harvest was also not reported.

The effects of zeolite utilization in the mixture of different growing media on the seed quality and nutrient contents of tomato (*Solanum Lycopersicon cv. Malike* F_1) were determined under the green house conditions (Sonmez *et al*. (2010). Natural zeolite, perlite, turf and their different mixture forms were used as growing media for growing of tomato seedlings. The effects of these substances on the seed germination, seedling height, stem diameter, seedling fresh weight and N, P, K, Ca, Mg, Fe, Zn, Mn and Cu contents were studied. Results of their findings revealed that the effects of growing media on the seedling quality parameters except for stem diameter were found to be significant and the best results were generally obtained from turf and zeolite mixtures. The nutrient contents of seedlings showed significant differences ($p<0.001$). Therefore, it was concluded that turf and zeolite mixtures could be used as alternative media instead of turf and perlite mixtures. However, the authors did not report the use of a synthesised zeolite based slow release fertilizer in the experiment.

The study on the effect of the natural clinoptilolite and bentonite additions on the tomato variety NEMO NETTA's growth was reported by (Cvetko *et al*., 2013). The study dealt with the agricultural use of the natural clinoptilolite from the Igros deposit near Brus and bentonite from the Meeji Do deposit near Vlasotince (Serbia) in the

tomato growth at an agricultural field near Novi Sad. The result of their preliminary study indicated that the minerals which were natural and non-toxic solids could improve the physical properties of soils and that they exhibit a positive effect on the tomato growth and yield. However, the authors did not report the effect of synthesised zeolite A and phillipsite based fertilizers in reducing leaching plant nutrients.

In another related work on the effect of zeolite in the culture substrate of tomato grown in a green house, Berar, (2011) reported that there was significant increase in the quality of fruit yield of tomato as was observed in the substrate mix with 75% zeolite. The author further added that there was significant increase in the content of calcium, magnesium and Potassium minerals for the treatment with 25% of the zeolite. Natural zeolite, clinoptilolite was applied on tomato crop. The author however did not report the use of a synthesised zeolite from a local clay source.

The influence of zeolite in the culture substratum, on the quality of tomato using variants of natural zeolite (clinoptilolite based), manure, garden soil, sand, and peat was reported by (Berar and Posta, 2011). The authors reported the average values of the quality index of tomato fruits from 6 variants for humidity, dry substance, titratable acidity, vitamin C and lycopene parameters. The authors also determined the tomato fruit compositions in essential macro and micro elements for calcium, magnesium, potassium, sodium, copper, zinc, manganese and iron in the 6 variants used in the experiments. The authors concluded that the zeolite applied had influence on the quality of tomato fruits which could also be observed on the nutritious mix that consists of 75% zeolite in vitamin C content and titratable acidity. It was also added that the use of 25% zeolite in the nutritious mix on tomato in the greenhouse resulted to significant differences in the fruit quality as regards the content in calcium, manganese, and

potassium. However, the authors did not report the use of a synthesised zeolite and the modification of the zeolite surface for oxyanions such as nitrates.

Treatments comprising four enrichment types of concentrated natural zeolite, pure concentrated zeolite (Z), zeolite + KNO_3 (ZNK), zeolite + K_2HPO_4 (ZPK) and zeolite + H_3PO_4 + apatite (ZP) were applied on successive crops of lettuce, tomato, rice and Andropogen grass carried out on the same substrate of each pot as reported by (Bernardi *et al*., 2010). The result indicated that nitrogen, phosphorous and potassium enriched zeolite was an adequate slow release source of nutrients to plants. Production of total dry matter of aerial biomass of four successive crops followed a descending order ZP>ZPK>ZNK>Z. The authors reported that the experiment was carried out in a greenhouse and evaluated in a randomized block design with three replications. The natural zeolite, stilbite was functionalized with H_3PO_4 and phosphate rocks (apatite). However, the authors did not report the use of a synthesised zeolite neither was Functionalisation of the surface of the zeolite reported.

The effect of ZeoPro (a commercial zeolite) on cucumber and tomato seedlings and its evaluation when 5%, 10% and 20% ZeoPro was mixed into the growth medium was reported by (Lisa, 2007). The results showed some increase in growth when ZeoPro was added to the growth medium. In cucumber, the growth increased with increasing amount of ZeoPro, generating the largest plants with 20% ZeoPro and the smallest in the control group without ZeoPro. In tomato, the largest plants were found in the 5 % group closely followed by the 10% and 20% groups. The plants in the control group, grown without addition of ZeoPro were clearly smaller than the other groups. However the study did not report the zeolite source nor the name of the zeolite synthesised and the use of the commercial zeolite as a slow release fertilizer.

The evaluation of zeolite as a component in organic growing substrates for tomato transplant production was reported by (Lafrenière *et al*., 2011). Initially twenty-five substrates were evaluated and the most promising were chosen for further investigation. In a second experiment, tomato (*Lycopersicon esculentum*'Matrix F1') seedlings, at two to three leaves stage, were transplanted into six organic growing substrates. Three of these substrates had zeolite incorporated at 7% (by volume) and Tomato seedlings were harvested at week five (first harvest) and week six (second harvest). At both harvests no significant differences in stem diameter, stem height and leaf area were found. However, shoot and root dry weights of seedlings grown in one of the three substrates containing zeolite were significantly lower than those grown in its non-zeolite counterpart. At the first harvest shoots and roots from the substrate with zeolite weighed 31 and 29% less respectively than shoots and roots from the non-zeolite substrate and 26 and 28% less respectively at the second harvest. Results suggested that it was not economically feasible to include zeolite at greater than 7% due to its high bulk density and consequently high shipping cost. Therefore, zeolite at greater than 7% (v/v) inclusion rate was not recommended for organic growing substrates as traditionally used for producing tomato transplants. The authors however did not report the use of an inorganic fertilizer and the name of zeolite used in the experiment.

The effect of Iron rich zeolite application on tomato yield and quality in soilless culture was reported by (Sherafatmand *et al*., 2014). The aim of the study was to compare some growing indexes of greenhouse tomato that were cultivated in some substrates such as perlite, zeolite and coco peat. The research was conducted in a completely randomized design with 4 replications. The treatments were coco peat + perlite (v/v = 50%), coco peat + perlite (v/v = 50%), + zeolite (v/v = 10%), coco peat + perlite (v/v = 50%), coco

peat + perlite (v/v = 50%), + zeolite (v/v = 5%). Comparison of means showed that the media had no significant effect on concentration of nutrient elements in fruits, stems and leaves such as iron and copper. Minimum and maximum amount of concentration of nutrient was rich in zeolite with cation + perlite + coco peat treatments. This had no significant difference with other treatments. The result showed that zeolite is an appropriate media for soilless culture with suitable physical and chemical properties, available at low cost. However, synthesised zeolite produced from kaolin clay was not reported in the experiment and oxyanions such as phosphates and nitrates were not incorporated into the zeolite used in the study.

The fruit yield and quality of tomato grown was evaluated in a zeolite substrate enriched with N, P and K as reported by (Benardi, 2007). Treatments comprised of four levels (20, 40, 80 and 160 g per pot) of zeolite enriched with H_3PO_4/apatite, KNO_3 and KH_2PO_4, and a control grown in a nutrient solution. Fruit production, firmness, total soluble solids, pH, titratable acidity and ascorbic acid contents were evaluated from 80 to 90 days of plant cultivation. Nutrients supplied through the mineral zeolite enriched with N, P and K was an adequate alternative to increase the production. Higher fruit production was obtained with addition of P and K and higher zeolite doses (160 and 80 g per pot). Fruit production was 17% higher when compared to the plants grown in nutritive solution. Good quality was observed in P-enriched zeolites in relation to fruit firmness, and negative effects over fruit pH. Fruit firmness varied among treatments, from 7.06 N (ZNK 160) to 14.38 N (ZPK 40). The increase of potassium availability increased the ascorbic acid levels of the fruits. However, the authors did not report the details of the zeolite used and the nutrient delaying effects of the zeolite studied.

A comparative study of the release of phosphorus and potassium ions from two phillipsite-based slow-release fertilizers and potassium di-hydrogen phosphate fertilizer (KH_2PO_4) was performed using the percolation reactor at constant solution flow (Yuvaraj and Subramanian, 2018). In all cases, the nutrient release takes place in several stages and followed a first – order kinetic law, whose rate constants were determined. It was observed that zeolite fertilizers supply available phosphorous after 70 days of continuous percolation, whereas phosphorous from KH_2PO_4 was exhausted after 50 days. A previous treatment of the zeolite with H_3PO_4 improved the phosphorous release pattern throughout the whole experiment. All fertilizers supplied available potassium throughout the whole experimental period unlike KH_2PO_4 which was exhausted after 50 days. However, the authors did not report the release of nitrates from optimized zeolite A and phillipsite based slow release fertilizers in the cases considered in the study.

The high selectivity and affinity of synthetic and natural phillipsite towards ammonium ion (NH_4^+) were compared and their potential as slow release fertilizers (Jakkula *et al*., 2011). The authors explained that Phillipsite (PHI) was synthesised in Na-K form, ion exchanged with NH_4NO_3 and compared with its natural counterpart. The zeolites were characterized before and after ion exchange by x-ray diffraction, x-ray fluorescence, thermo-gravimetric analysis and scanning electron microscopy. Ammonium exchanged Phillipsites were introduced as a soil amendment (2, 4 and 8% zeolite to soil loadings) to study the growth of maize (Zea mays) and compared with a control comprising NPK fertilizer added to soil. The affinity of the zeolite mineral Phillipsite for the presence of other cations was demonstrated by soil nutrient status. Results demonstrated that synthetic Phillipsite had a very high affinity when introduced as a soil amendment,

compared with its natural counterpart. Results were promising for ion exchange reactions in a zeolite-soil system, whereby cations present in soil exchanged for K^+ more freely than present in the synthetic Phillipsite framework. However, the authors did not report the enrichment of the phillipsites with phosphates and nitrates and the synthesised ammonium exchanged phillipsite was not applied as a slow release fertilizer on the test crop.

The response of Croton grown in a zeolite containing substrate to different concentrations of fertilizer solution was studied by (Munir *et al*., 2004). The authors reported that a growth chamber experiment was conducted to determine the response of croton grown in a substrate composed of a mixture of zeolitic tuff, peat, moss, and perlite at a ratio of 1:1.5:1.5 by volume respectively, to different concentrations of a fertilizer solution. Prior to the application of the fertilizer solution, the substrate was allowed to dry via evapo transpiration to a pre-irrigation moisture content equivalent to 55 % of available water. The plants were then fertigated with a complete fertilizer solution containing different concentrations of nitrogen (N) (0, 75, 150, and 225 mgL^{-1}), phosphorus (P) (0, 32.75, 65.5, or 98.25 mg L^{-1}), and potassium (K) (0, 62.5, 125 and l87.5 mgL^{-1}) to render the substrate to its container capacity and allow for 0.2 leaching fraction. The results indicated that there was no significant effect of the concentration of the fertilizer solution on plant growth. The highest concentration of the fertilizer solution resulted in the highest protein and N contents in the plant. Non-fertilized plants accumulated the highest amount of sodium (Na). At the end of the growth period, the concentrations of N, P, and K were the lowest in the non-fertilized substrates. The highest pH values were recorded for leachates collected from non-fertilized substrates at the end of the experiment. Substrate and leachate salinity and concentration of mineral

N were the highest when the highest concentration of fertilizer solution was used. It was concluded that the use of this substrate as a growth medium for croton can provide the plant with adequate amounts of N, P, and K for the given growth period investigated. However, the characteristic of the zeolite used was not reported in the study and the role played by the zeolite in the reduced concentrations of N, P and K in the leachates of the zeolite amended substrates was not studied.

The effect of synthetic zeolite application on morphology, grain yield and yield components of soybean grown on allophonic soils was reported by (Amir *et al*., 2011). A greenhouse experiment was carried out using three zeolite levels and three soils (two allophonic and one paddy) with two soybean cultivars. Zeolite levels of 0, 20 and 40 (g) were used to determine the growth of soybean cultivars on allophonic soil. Different morphological parameters including grain yield were significantly affected by various zeolite levels and soil type. Maximum leaf area and plant height were obtained from 40 g zeolite application with the allophonic soils. Both cultivars gave the highest grain yield at 20 g zeolite application and thereafter, the grain yield declined. A decrease in morphological and yield components were observed when soybean were grown on a paddy soil with zero (g) zeolite application. However, the authors did not report the nature or give the details of the zeolite used. They did not report the modification and the enrichment of the zeolite used with plant nutrients. Furthermore, they did not apply the zeolite as a slow release fertilizer in a sandy loam soil.

The characterization of the pattern of seed development in mature soybean seeds during its progression from germination to seedling growth and maturation as affected by synthetic zeolite application and allophonic soil was studied by (Amir *et al*., 2013). Changes in seed quality in terms of viability and germination were monitored from seed

initiation to physiological maturity of soybean under different zeolite level and allophonic soil. A pot experiment was conducted to study the influence of zeolite on nutrition, allophonic soil and seed developmental traits of soybean cultivars. Seeds were harvested at 12 days interval from 60 to 120 days with zeolite and allophonic soil treatments. The cultivars planted on allophonic soil and treated with 20 g and 40 g zeolite gave maximum fresh, dry seed weight and germination as compared to the second cultivar. A decrease in fresh and dry seed weight, and germination were observed with zero (g) zeolite application to paddy soil. Fresh and dry seed germination increased linearly in both varieties. Immature seeds in both cultivars during early developmental stage did not germinate in all treatments of zeolite and allophonic soil. However, the authors did not report the nature of synthetic zeolite and its use as a slow release fertilizer. They also did not report the effect of the zeolite on the agronomic growth of the crop and its nutritive contents in the study.

The characterization of natural phillipsite treated with orthophosphoric acid at several concentrations was studied by (Katsiki, 2019). Structural modifications arising from the treatment were studied by several techniques, including XRD, FTIR, XPS, SEM and porosimetry. Phillipsite became partially dealuminated as a consequence of the treatment. Aluminium accumulated on the zeolite surface as aluminiumphosphate, but also inside the zeolite pores. Both the surface area and the pore volume of the material increased with increasing concentrations of orthophosphoric acid, and this behaviour was more marked at the micro porosity level (below 2 nm). Results showed that CEC decreased with an increasing concentration of H_3P0_4, and the release of $A1^{3+}$ ions to solution caused the precipitation of amorphous $AlPO_4$. Phosphate ions have been observed to enter the zeolite pore system, whereas aluminum is lost from the surface.

Dealumination also increased the pore volume and the specific area of the material. XRD analysis showed that zeolites have been thinned as a consequence of the acid treatment, losing their original morphology. However, the study did not reveal that synthetic phillipsite produced from kaolin was used and plant nutrients of nitrogen, phosphorous and potassium were not loaded on the zeolite surface to enhance better plant growth and consequently reduce plant nutrients leaching.

The application of ammonium-loaded clinoptilolite (Acp), a slow-release nitrogen fertilizer on sweet corn *(Zea mays* L.) was reported by (Ditta and Arshad, 2016). In pot experiments, sweet corn were fertilized with either ammonium sulphate (AS) or one of three size fractions of (Acp), small (<0.25 mm), medium (0.25 to 2 mm), or large (2 to 4 mm), at rates of 112, 224, or 336 kg N ha^{-1} (Experiment #1) and 112 or 224 kg N ha^{-1} (Experiment #2). Ammonium (NH_4^+) and NO_3^- leaching from these pots were compared. Corn relative growth rates (RGR), leaf area ratio (LAR), and net assimilation rate (NAR) among all N fertilizers were also compared. Soil amended with AS leached 10 to 73% of the added N, depending on N rate, whereas < 5% of the added N leached from the A-Cp amended soil regardless of N rate and Cp particle size. No differences in corn growth were observed among N fertilizers, however, plants fertilized with A-Cp assimilated significantly more N than AS fertilized plants. Results indicated fertilization with A-Cp minimized Nitrogen leaching from sandy soils while sustaining normal corn growth. The extent of delaying nitrogen leaching from the sandy soils was not reported and synthesised zeolites were not applied in the study.

The application of zeolite pre-load with ammonium (NH_4^+) and potassium as a slow release fertilizer on spinach in order to evaluate spinach growth, yields and quality was reported by (Li *et al*., 2013). An increase in spinach yield with comparable vitamin C

content was achieved using the zeolite. However, a synthesised zeolite was not used and the tomato crop was not used in the study. Nitrogen and Phosphorous were not loaded on the zeolite surface as the cations in order to produce a complete fertilizer.

The synthesis of zeolites and their application as soil amendments to increase crop yield and potentially act as slow release fertilizers was reported by (Jakkula, 2005). Three glasshouse experiments were performed to study the effects of zeolite-amended soils on maize growth. Ion exchanged synthetic and natural phillipsites were first used as soil amendments (w/w 2, 4, 8% zeolite to soil). Synthetic phillipsite, at 2% loading, resulted in the most significant improvement in both plant growth and phased ammonium release. The synthetic ammonium-exchanged zeolites phillipsite and Linde-type F (at w/w 1, 2, 4 %) were then compared; synthetic phillipsite, at 2% loading, again resulted in the most significant plant growth response with an increase (≥15%) in shoot dry weight and a decrease (≥30%) in nitrate leaching. Experiments using un-exchanged synthetic Phillipsite (at w/w 2%), but with added NPK fertilizer, showed increased plant growth and decreased nitrate leaching, compared with parallel experiments containing un-exchanged synthetic Linde-type F (at w/w 2%) and a conventional fertilizer amended soil. This revealed the beneficial effect of phillipsite for soil amendment, even without ion exchange to the ammonium form. To study the chemical properties affecting the release of ammonium from the phillipsite framework; high crystalline/low aluminium and low crystalline/high aluminium forms were synthesised and ion exchanged. Both forms were introduced as soil amendments (at w/w 1 and 2%) and experiments showed that the lower zeolite crystallinity decreased cation exchange and therefore decreased nitrate leaching. Experimental results from the glasshouse experiments and cation exchange capacity (CEC) experiments suggest that synthetic

phillipsite, at lower loadings (1 and 2% w/w zeolite to soil) have most potential as soil amendments for both plant growth and controlled-release applications. However, Synthetic phillipsite produced were not sourced from kaolin and the optimum plant nutrients loaded on the zeolite were not studied using statistical process.

The study on the zeolite obtained by hydrothermal synthesis from Lipari pumice had been tested as soil conditioner in tomato cultivation (Faccini *et al*., 2018). The results have been compared with the raw pumice and a commercial 4A zeolite. The addition of the zeolite resulted in an average yield of tomato higher than 50 % in comparison with the control plant. It is suggested that the exchange properties of the aluminosilicates did not play an important role in tomato-growing and the beneficial effect has to be ascribed to other factors such as the presence of Fe and K. However, the zeolite obtained was not synthesised from kaolin precursor and details of the pore which influences the cation exchange capacity was not reported. The zeolite produced was used as a soil conditioner and not as zeolite carrier for slow release fertilizer nutrients.

The production of ammonium-exchanged zeolite X (NH_4-LTX) and its soil amendment activity was reported (Musyoka *et al*., 2013). The ammonium-exchanged zeolite X was characterized by X-ray diffraction (XRD) analysis, scanning electron microscopy (SEM), energy dispersive X-ray (EDX) analysis, particle size analysis and Fourier transformed infrared (FTIR) spectroscopy. The addition of NH_4-LTX increased the pH, total nitrogen, potassium, sodium content and water retention capacity of the soil. Consequently, the fresh weight, dry weights, plant heights, stem thickness, stem length, number of leaves, leaves areas was remarkably greater for both maize and okro planted in soils containing NH_4-LTX compared to plants in soil without NH_4-LTX. However, the author did not report the ammonium exchanged zeolite A and Phillipsite and the

maximum ammonium ion adsorbed on the zeolite synthesised. The ammonium exchanged zeolite X was not applied on tomato crop.

It has been observed that series of research had been conducted on the utilization of zeolite as soil amendment and nutrient carrier for effective and efficient crop growth and yield. However, little information is available on the synthesis of zeolite A and phillipsite from locally source Ahoko kaolin as nutrient carrier. It can be further inferred from various literatures that the basic nutrients required by tomato plant are nitrogen, phosphorous and potassium.

2.16.2 Importance of nitrogen, phosphorous and potassium to tomato crop

Nitrogen encourages leaf growth in tomatoes, excess leaf growth discourages blossoms and fruit. Excessive use of nitrogen can produce a crop that is too vigorous, having poor flowering and excessive large fruit (Leghari *et al*., 2016). Some nitrogen fertilizer is normally broadcast preplanting or at transplanting, unless rainfall patterns are likely to lead to leaching. This is followed by side dressing prior to flowering. High nitrogen fertilizers such as urea, ammonium sulfate or fresh manure have produced dark green tall tomato plant with fewer tomatoes (Souri and Dehnavard, 2018).

Phosphorus is the second number in the N-P-K ratio. It encourages flowering, and therefore fruiting. Most Phosphorus is required early in the plant's development to ensure good root growth and flowering. Energy transfers in plant processes are carried out with the use of phosphorous molecules. It is relevant for optimum growth and reproduction of plant root formation, respiration and photosynthesis in plants (Malhotra *et al*., 2018).

Potassium is needed in greater quantities than nitrogen. The tomato plant needs a higher ration of potassium once it starts flowering. The highest plant uptake occurs during fruit

bulking (Agbede *et al*., 2018). Base applications of potassium are usually followed by regular applications throughout the season. Good organic sources of potassium are granite dust and wood ash.

2.17 Optimization of an Adsorption Process

The use of statistical experimental design in optimising zeolite synthesis is on the increase. Optimisation would give the process more informed decisions at every stage of the synthesis and also provide less experimental runs and costs. The Engineering career employs natural principles to build useful objects. Engineers are usually interested in best designs and not minor ones. The process of achieving the best design is called optimisation. Optimisation involves minimizing or maximizing a certain function in a finite dimensional design space over a subset of that space (Ogunleye *et al*., 2016). The optimisation of a process usually leads to maximum benefit and consequently leads to a decrease in cost and consumption of energy and materials. Optimisation problems have been solved traditionally by the one variable at a time method before the advent of statistical design approach. The One Variable At a Time (OVAT) method involves successive study of the influence of one variable while keeping the values of the other variables constant. However, this method does not give information about the interactive effects of the variables studied and therefore it cannot give the holistic effects of the process variables. Generally, the OVAT method has the tendency to give large number of experimental runs thereby making the method time consuming and expensive (Rodrigues and Iemma, 2014). In view of the above, statistical design of experiment has found relevance in overcoming these challenges. Statistical design of experiments is a well ordered method to determine the relationship between variables influencing a process and the response of that process. The statistical

design of experiment is preferred to the OVAT method in the provision of the same information in fewer experimental runs and estimation of interactive effects among the process variables. The pictorial view of the statistical design of experiment has resulted to the response surface (Nair *et al*., 2014).

2.17.1 Response surface methodology

Response Surface Methodology (RSM) is a set of mathematical and statistical techniques that is used for modeling and problem analyses. The purpose is to optimise a response of interest that is dependent on several factors (Ghadamnan *et al*., 2019). The values of the optimized response could be maximised, minimised or targeted. Several statistical designs for doing experiment vary in experimental points selection and number of experimental runs. Commonly utilized statistical experimental designs are the full three level factorial design, Box-Behnken design and the Central composite design (Ferreira *et al*., 2018). The Box-Behnken design and Central Composite design can contain factors with three levels namely (Upper level, Lower level, and Centre point.

2.17.2 Central composite design

The central composite design is a response surface design similar to the Box-Behnken with 3 factor levels but it has additional axial and star points. The inclusion of axial and star points make the 3 earlier factors levels add up to 5 factor levels and therefore make the experimental design flexibile. The advantage central composite design has over Box-Behnken is the provision of information on the response of interest for levels below or above the chosen factor levels (Maleki *et al*., 2016).

The CCD has found relevance in determining the interactive effects in zeolite synthesis and optimizing the adsorption of cationic surfactants onto the surface of zeolites. The relationship between the amount of HDTMA adsorbed and HDTMA concentration remaining in solution is described by an isotherm. Therefore, adsorption isotherms are used to understand and make the decision of the sorption parameters that would be used for best synthesis design.

2.18 Zeolite Characterization

2.18.1 X-Ray Diffraction (XRD)

XRD is often used in the description of members of zeolite groups. It gives information on structures, phase purity, structural parameters such as average grain size, crystallinity, strain and crystal defects (Bunaciu *et al*., 2015). The theory is based on the elastic scattering of X-rays from structures that have long range order (Watt *et al*., 2016). XRD is based on the principle of scattering phenomena where a crystal is bombarded with X-rays of a fixed wavelength at certain incident angles. Intense reflected X-rays are produced when the wavelengths of the scattered X-rays interfere constructively. In order for the waves to interfere constructively, the differences in the travel path must be equal to integer multiples of the wavelength. When this constructive interference occurs, a diffracted beam of X-rays will leave the crystal at an angle equal to that of the incident beam. The general relationship between the wavelengths of incident X-rays, angle of incidence and spacing between the crystal lattice planes of atoms is known as Bragg's law:

$$n\lambda = 2d \sin \theta \qquad (2.21)$$

here: n (an integer) is the "order" of reflection, labda (λ) is the wavelength of the incident X-rays d is the inter-planar spacing of the crystal and θ is the angle of incidence.

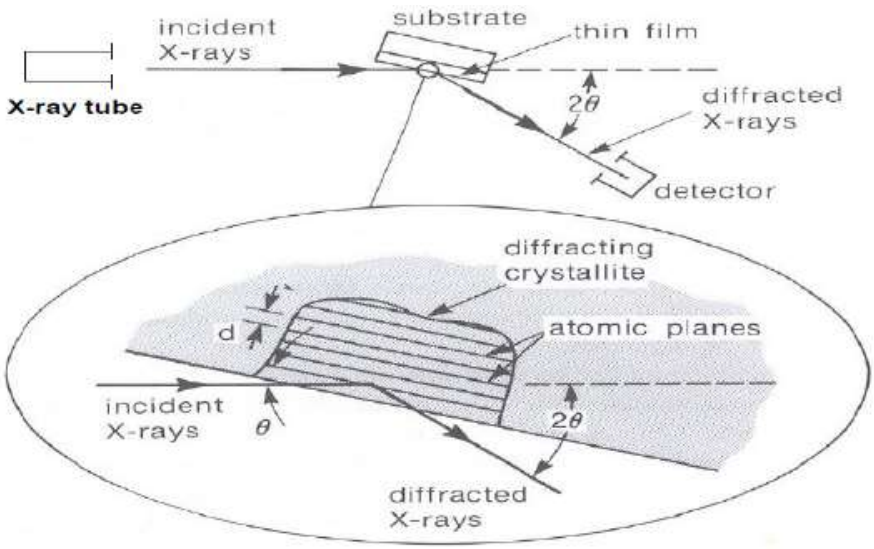

Figure 2.7: Basic features of an X –ray Diffractometer

A diffraction pattern results when x-ray interacts with a crystalline material. X –ray is a non-destructive tool. It is a powerful procedure for the study of material with one of its dimensions in the range of 1 – 100 nm. The XRD is a tool for investigating nanomaterial. The intensities measured with XRD have the potential to provide accurate information on the atomic arrangements at the interfaces. The areas under the diffraction peak are related the amount of each phase present in the sample. The diffraction pattern reflects the finger print of the crystal structure. It is a rapid technique for identification of an unknown material that are homogeneous and single phase material (Epp, 2016). The interpretation of the data is relatively straight forward.

Four main components of a typical powder XRD instrument consists of X-ray source, specimen stage, receiving optics and x-ray detector as shown in Figure 2.2

2.18.2 Scanning electron microscopy

Scanning Electron Microscopy (SEM) is a versatile and well-established complementary technique to light optical microscopy (Muraoka *et al*., 2016). By scanning with a beam of electrons instead of photons, samples can be imaged at far higher magnifications. The electrons interact with atoms in the sample, producing various signals that can be detected and contain information about the sample's surface topography and composition. SEM can use different signals to generate contrast mechanisms. The back-scattered electron and secondary electron signals can be used to form images that can give information about the structure, topography and compositional features of a sample. Accelerated electrons in an SEM carry significant amounts of kinetic energy, and this energy is dissipated as a variety of signals produced by electron-sample interactions when the incident electrons are decelerated in the solid sample (Muraoka *et al*., 2016).

As the excited electrons return to lower energy states, they yield X-rays that are of a fixed wavelength (that is related to the difference in energy levels of electrons in different shells for a given element). Thus, characteristic X-rays are produced for each element in a mineral that is "excited" by the electron beam. SEM analysis is considered to be "non-destructive"; that is, x-rays generated by electron interactions do not lead to volume loss of the sample, so it is possible to analyze the same materials repeatedly (Schulze *et al*., 2018).

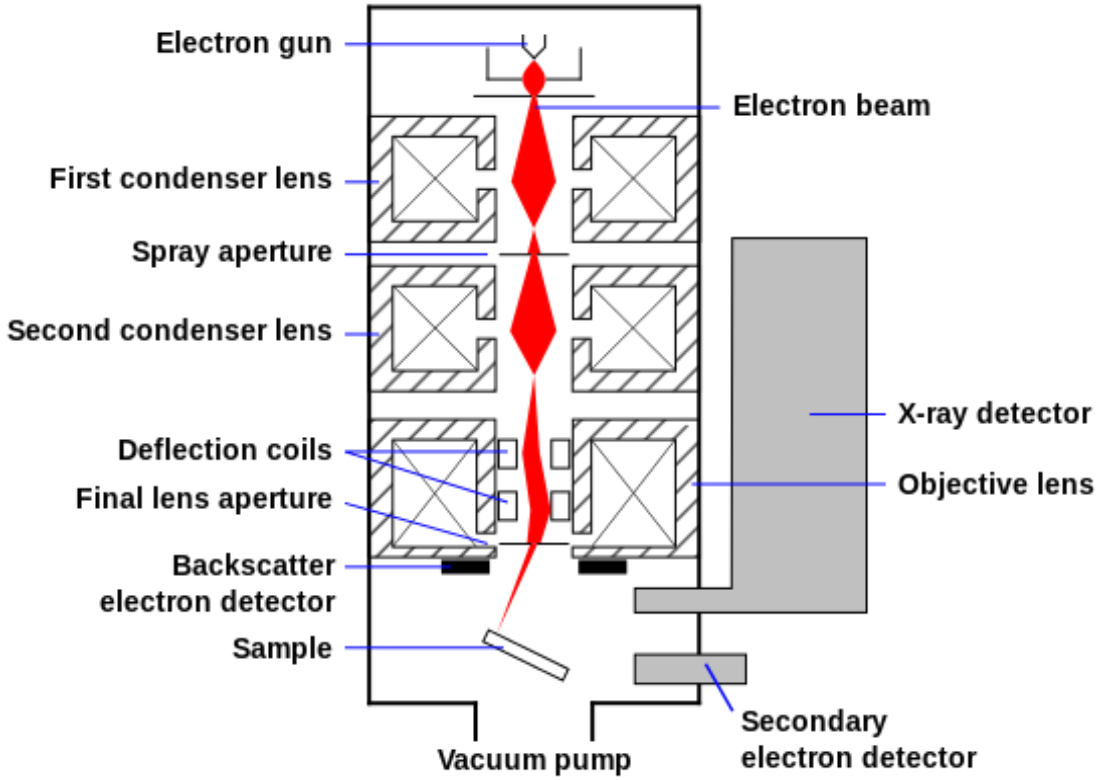

Figure 2.8: Schematic diagram of a Scanning Electron Microscope

2.18.3 X-Ray Fluorescence

Electromagnetic radiations having wavelength in the range of 0.01 to 10 nm, corresponding to frequencies in the range 30 peta hertz to 30 hexa hertz (3×10^{16} Hz to 3×10^{19} Hz) and energies in the range 100 eV to 100 keV are known as X-Rays. Meaning there are different kinds of x-rays. When atoms of any chemical element are irradiated with x- or low-energy rays, they emit energy in the form of fluorescence x-rays; the energy is characteristic of each element involved (Schulze *et al*., 2018). The intensity of each fluorescence line varies according to the quantity of the element present in the investigated sample. The term “fluorescence” is applied to phenomena in which the absorption of radiation of a specific energy results in the re-emission of radiation of a different lower energy.

Ionization of a material's component atoms may take place when the material is exposed to short-wavelength X-rays or to gamma rays. Ionization consists of the ejection of one or more electrons from the atom, and may occur if the atom is exposed to radiation with energy greater than its ionization potential. X-rays and gamma rays can be energetic enough to expel tightly held electrons from the inner orbitals of the atom. The removal of an electron in this way makes the electronic structure of the atom unstable and electrons in higher orbital "fall" into the lower orbital to fill the hole left behind. In falling, energy is released in the form of a photon, the energy of which is equal to the energy difference of the two orbitals involved (Acquafredda, 2019). Thus, the material emits radiation, which has energy characteristic of the atoms present. The fluorescent radiation can be analysed either by sorting the energies of the photons or by separating the wavelengths of the radiation.

2.18.4 Fourier transform infrared spectroscopy

Infrared spectroscopy has become a tool useful for the characterization of the zeolite adsorbent with its functional groups. This includes the different building units of the framework, the cations and the hydroxyl group in addition to any other molecule adsorbed on the internal surface of this group of porous solids (Bortolatto *et al*., 2017).

The use of Fourier Transform Infrared Spectroscopy has made available some useful information on the interaction of light and vibrational motion of the covalent chemical bonding of the molecules and lattice vibrations of ionic crystals. Two different compounds could only produce different infrared spectrums. Generally, two main areas, FTIR could be separated into are; ID region (from 4000 cm^{-1} to approximately 1500cm^{-1}) which is the functional group region useful for correlating peak location with bonds, and fingerprint region from 1500 to 600 cm^{-1} which is typically complex bond and

thecan only provide less meaningful information. FTIR spectrum containing several peaks could be assigned to; C=O groups streltching mainly of carboxylic and traces of ketones and esters at 1712 cm^{-1}, OH stretching vibrations of H-bonded hydroxyl groups of phenol (at 3418 cm^{-1}), C-O stretching (at 1032 cm^{-1}), CH_3 weak stretching (at 2922 cm^{-1}), peaks of OH stretching hydroxyl group (wide band at 416 cm^{-1}) and C-O at 1041 cm^{-1} (Taaca *et al*., 2020). Table 2.4 further shows the FTIR frequencies of common vibrational modes and assigned functional groups of zeolites.

Table 2.4: FTIR frequencies and some common modes of vibration for zeolites

Locations	**Type of vibration modes and functional groups**	**Frequency range (cm^{-1})**
Internal Tetrahedral	OH- stretch	3200-3700
	OH- deform, (bending)	1700-1600
	Adsorbed water	1640
	CH_3 of $N(CH_3)_3$ symmetric bending	1410
	CH_3 of $N(CH_3)_3$ asymmetric bending	1490
	Aluminum containing entities; $Al_xO_y^{n+}$	1438 – 1452
	Asymmetric stretch (Si-O-Si), T-O stretch	1250-950
	Symmetricalstretch (O-T-O) group	720-650
	(Si-O-Al), T-O bend	420-500
External linkage	Double Ring	650-500
	Pore opening	300-420
	Symmetric stretch	750-820
	Asymmetric stretch	1050-11
	Cationic vibration; far infrared region	200 – 50

(Iqra *et al*., 2014)

2.18.5 Textural analysis by nitrogen adsorption

The surface area is an important characteristic of porous materials, especially for applications in adsorption separations. For physical adsorption, the energetic interaction of guest molecules with surface atoms is usually much more important than guest-guest interactions, so it is expected that a higher surface area per mass of material should

correlate with a higher amount adsorbed (per mass). Several groups have reported a linear relationship between surface area and the amount adsorbed for different types of porous materials (Villarroel-Rocha *et al*., 2020)

Surface areas are commonly reported as BET surface areas obtained by applying the theory of Brunauer, Emmett, and Teller to nitrogen adsorption isotherms measured at 77 K. This is a standard procedure that allows for comparisons among different materials and with benchmark materials from the literature. However, the BET method relies on several assumptions that may break down for microporous materials with very open structures and ultrahigh surface areas such as zeolites. The BET analysis assumes that adsorption occurs by multilayer formation and that the number of adsorbed layers is infinite at the saturation pressure which means adsorption occurs as if on a free surface. Appreciable overlap of monolayer and multilayer adsorption would invalidate this assumption (Suek *et al*., 2018).

BET stands for Brunauer, Emmett and Teller-the men who proposed a theory to measure the surface area of solid particles like porous powders. The basic principle involved is the adsorption of gas molecules to the surface of the solid whose surface area is required. From the area of each molecule, the whole area of the solid can be calculated. Samal, (2014) reported on the BET theory that is based on multilayer adsorption with the following assumptions

1. Gas molecules can be physically adsorbed on the solid surface and form infinite layers.
2. There is no interaction between the layers
3. Langmuir theory is applied to each layer. The BET equation is given by:

$$\frac{1}{v}\left[\left(\frac{P_o}{P}\right)-1\right]=(c-1)\left(\frac{\frac{P}{P_o}}{V_m C}\right)+\frac{1}{V_m C} \quad (2.22)$$

P_o = Saturation pressure of the adsorbate

P = Equilibrium pressure of the adsorbate

V = Volume of gas adsorbed

V_m = Volume of gas adsorbed in the monolayer

C = BET constant given by exp $(E_1 – E_L)/RT$

E_1 = Heat of adsorption for adsorption for the first layer

E_L = Heat of adsorption for higher layers

A plot of $1/v\ [(P_o/P)$ versus (P/P_o) is obtained from the BET analysis. From the slope and intercept of the line, V_m and C are obtained. Surface area S of the solid sample is given by

$S = (V_m N_s)/(VX)$

N = Avogadro's number

S = adsorption cross-section of the gas being adsorbed

V = molar volume of the gas being adsorbed

X = mass of the adsorbent.

CHAPTER THREE

3.0 RESEARCH METHODOLOGY

3.1 Materials

All the chemicals used in this study were of analytical grade with percentage purity in the range of 96 – 99.9% as shown in Table 3.1. Ahoko kaolin was sourced from Kogi State, Nigeria. The list of equipment used in this study is as shown in Table 3.2.

Table 3.1: List of Chemicals/Reagents used for the experimental work

S/N	Item	Manufacturer	Purity %
1.	Sodium Hydroxide	BDH laboratory	96.0
2.	Potassium Hydroxide	BDH laboratory	96.0
3.	Calcium Hydroxide	BDH Chemicals	99.0
4.	Potassium dihydrogen Phosphate	BDH Chemicals	99.0
5.	Potassium Nitrate	BDH Chemicals	99.0
6.	Phosphoric Acid	BDH Chemicals	99.0
7	Sodium Chloride	BDH Chemicals	99.9
8	Potassium Sulphate	BDH Chemicals	99.9
9.	Hexadecyltrimethylammonium Bromide	BDH Chemicals	99.9

Table 3.2: List of Apparatus /Equipment used for the Experimental Work

S/N	Apparatus/ Equipment	Model	Manufacturer
1	Mortar and Pestle	Porcelain	SEDI, Minna
2	Electric weighing balance	Pro SP 202	Ohaus Corp., pine Brook, NJ USA
3.	Magnetic Stirrer	Model 400	Gallenkamp, England
4.	Muffle furnace	Size 1 (1000^{o}C)	Gallenkamp, England
5	Sieve (75µm)	ASTM No.100	Interlab, Sethi
6.	pH meter	PHB-4	Rex, Shanghai, China
7.	Beakers	Pyrex	Pyrex, England
8.	Measuring Cylinders	Pyrex	Pyrex, England
9.	Crucibles	Porcelain	SEDI, Minna
10.	TEM	Taecnai G2 F20-ZTwin	FEI company, Czech republic
11.	SEM	MEL-30000	SCO teen, Germany
12.	XRD	XRD-6000	Shimadzu scientific instrument
13	FTIR	Frontier FT-IR	Perkin Elmer, UK
14	BET	NOVA 4200e	Quantachrome instruments, UK
14	Teflon-lined Stainless Steel Autoclave		
15	Desiccator	Pyrex	England

16	Filter Paper	Whatman	England

Table 3.2: Contd.

S/N	Apparatus/Equipment	Model	Manufacturer
17	Funnel	Ok plast	Nigeria
18	Watch glass	Pyrex	England
19	Glass stirrer	Pyrex	England
20	Oven	Gallenkamp Sanyo	United Kingdom

3.2 Methodology

3.2.1 Zeolites synthesis and characterisation from Ahoko Kaolin

Locally sourced Ahoko Kaolin with compositions predominantly aluminosilicates were pretreated, calcined and hydrothermally processed through different receipes to produce zeolite A and phillipsite.

3.2.1.1 Refinement of Ahoko Kaolin

Kaolin from Ahoko in Kogi State, Nigeria was used as the starting material in the zeolite synthesis. The procedure used for the refinement of Ahoko was as reported by (Kovo, 2011). A 829 g of Ahoko clay was disaggregated by crushing with the aid of mortar and pestle. The crushed kaolin was sieved with a 75 µm mesh (Tyler fraction or Micro sphere) of which the screened mixture was beneficiated by soaking it in deionised water using a 1000 cm^3 measuring cylinder. The method of refinement was applied as reported by Kovo (2017). Kaolin was filled to the 2 cm^3 mark of the cylinder and deionised water was filled to the height of 28 cm and stirred vigorously. The particles of the solution were allowed to settle with quartz settling in 4 mins according

to the Atterberg software which used the principle of stroke's law (Gougazeh and Buhl, 2014). The supernatant was decanted into another container and allowed to finally settle. The washed clay was dried in an oven set at 45 ^{o}C for two days.

3.2.1.2 Synthesis and characterisation of Zeolite A from refined Ahoko Kaolin.

Zeolite A was synthesised through a procedure reported by (Kovo, 2011). The refined kaolin was calcined in a muffle furnace with a heating rate of 100 ^{o}C/min. The kaolin sample in a crucible was placed in the furnace for 3h when the furnace had attained 600 ^{o}C. Then the furnace was allowed to cool down to room temperature after switching off the furnace. The metakolin product was weighed and subsequently used in zeolite preparation by varying four synthetic parameters such as stirring time, aging time, crystallisation temperature and crystallisation time. The molar composition of Zeolite A recipe is as reported by (Oyinade *et al*., 2015);

3.75 Na_2O : Al_2O_3 : 2.5 SiO_2 : 243.7H_2O

Typically, 62.64 cm^3 of deionized water was measured and divided into two equal parts. 4.17 g of sodium hydroxide pellet was dissolved in the first part of the precursor, and then followed by dissolving 3 g of Ahoko metakaolin to the second part of the deionized water. The procedure of gel formation was obtained as reported by (Kovo, 2011). Both sets of precursors were subsequently mixed together to form a homogenous aluminosilicate gel. The synthesis calculation for zeolite A is shown in Appendix C. Four factors were varied in the synthesis process with aid of response surface methodology in design expert software version 7.0 as shown on Table 3.3. The gel was stirred at a stirring speed of 150 rpm at room temperature using magnetic stirrer for a range of 0.5 to 2.5 h. The resulting gel was allowed to age under static condition for 3 to 21 h. The aged gel was crystallized at a temperature of 85 to 105 ^{o}C for 0 to 4 h in a

Teflon inserted in a steel autoclave. At the end of the hydrothermal treatment, the autoclave was removed from the oven and the sample taken out, filtered and washed with deionized water until the pH was within 7– 8. The sample was dried at 80 ^{o}C for 24 h in an oven. The zeolite A sample was characterized by XRD and SEM. The process conditions for designing the experiment for zeolite A synthesis were as reported by (Ayele *et al*., 2016). The experimental design matrix was produced using the boundaries of -1 and +1 for each of the synthesis variables in Table 3.3.

Table 3.3: Experimental design for zeolite A using central composite design

Variables	**-α**	**-1**	**0**	**+1**	**+α**
Stirring time (hours)	0.5	1	1.5	2	2.5
Aging time (hours)	3	12	15	18	21
Crystallisation temperature (^{o}C)	85	90	95	100	105
Crystallisation time (hours)	0	1	2	3	4

3.2.1.3 Phillipsite synthesis from refined Ahoko Kaolin

The synthesis of phillipsite was carried by a procedure reported by (Jakkula *et al*., 2011). The aluminosilicate gel used for the synthesis of phillipsite was prepared by dissolving 3 g of metakaolin produced from refined kaolin in 14.40 mL of deionised water with 1.39 g of NaOH and 0.98 g of KOH pellets. The synthesis calculations for phillipsite are presented in appendix B. The mixture was stirred for 0.5 h at room temperature at 150 rpm using a magnetic stirrer. The gel formed was allowed to age for a period of 15.82 to 56.18 h under static condition (Jakkula *et al*., 2011). The gel formation was heated in a 100 mL closed Teflon-lined stainless steel autoclave, and varied for crystallisation time 0.66 to 150.34 h at crystallisation temperature within

84.77 – 135.23 ^{o}C at autogenous pressure as provided as within the region of operation of the design space by the software. The autoclave was allowed to cool when it was taken out of the oven. The resulting materials were filtered out, rinsed with deionized water until a pH of 7- 8 was achieved. It was further dried in an oven at a temperature of 80 ^{o}C overnight. The resulting product were characterized by XRD and SEM spectrometry. Optimization of the synthesis parameters consisting of aging time, crystallisation temperature and crystallisation time) were investigated in the synthesis of Phillipsite using RSM with central composite design which gave 20 experimental runs. Once the zeolite was identified as Phillipsite zeolite on the smaller scale, bulk synthesis was scaled up making use of the same gel molar composition. The boundary conditions were used as reported by (Jakkula *et al*., 2011). The experimental design matrix was produced using the boundaries of -1 and +1 for each of the synthesis variables in Table 3.4

Table 3.4: Experimental design of phillipsite synthesis using central composite design

Variables	**-α**	**-1**	**0**	**+1**	**+α**
Aging time (h)	15.82	24	36	48	56.18
Crystallisation temperature (^{o}C)	84.77	95	110	125	135.23
Crystallisation time (h)	0.66	31	75.50	120	150.34

3.2.1.4 X- Ray Diffraction analysis

X – ray diffraction (Bruker D8 Phaser) with Cu-Ka (1.542 Å) radiation was used for phase identification of the crystalline material after the samples were crushed into powder. The XRD procedure applied for the analysis was obtained from (Ayele *et al*.,

2016). The powder samples were placed and clipped into the rectangular aluminium sample holder. The diffractograms were recorded under the following conditions. Such as 2 (theta) range of 20 – 90^{o}, x-ray operating voltage of 40 kv and x-ray operating current of 40 mA. The XRD tool is also used in calculating crystallinity of crystal samples.

Determination of crystallinity of Zeolite A and Phillipsite

The percentage crystallinity of synthesised zeolites was estimated by comparing characteristic peak areas appearing at 2θ from 12^{o} to 75^{o} to that of the reference sample with characteristic XRD peaks of zeolite A at 2θ-: 7.0^{o}, 10.1^{o}, 12.5^{o}, 16.2^{o}, 21.9^{o}, 24.0^{o}, 27.2^{o}, 30.1^{o} and 34.2^{o} and the characteristic XRD peaks of Phillipsite at 2-theta (degree)-: 12.40, 24.23, 33.43, 42.23, 51.47, 57.56, 62.41, 68.81 using the relationship reported in Equation 3.1.

Percentage Crystallinity = $\frac{\Sigma P}{\Sigma P_S} \times 100$ (Ayele *et al*, 2015) (3.1)

Where P is the total area of seven (7) characteristics peaks pattern of pure sample

P_s is the total area of seven (7) characteristics peaks of standard sample

3.2.1.5 Scanning electron micrograph analysis

The method of sample preparation for SEM analysis was as reported by (Muraoka *et al*., 2016). Synthesised zeolite materials, 0.05 mg were sprinkled on a sample holder with carbon adhesive tape and sputter coated with Au-Pd using Quorum T15OT for 300 seconds prior to analysis. The sputter coated samples were characterized using Zeiss Auriga SEM. The microscope was operated with electron high tension (EHT) of 5 kV for imaging.

Electron Dispersive X-ray Analysis

The elements that consititute a material would be determined using electron dispersive X-ray equipment attached to a JEOL 7500F SEM electron microscopy (SEM/EDX). The method for analysis was as adopted by (Lateef *et al*., 2016) The detector was turned to 150 ^{o}C prior to measurement and the electron high voltage was reduced to 5 KV. The data generated from the sample introduced into the equipment reveals peaks that are in agreement with the elements and the composition of the sample being analysed.

3.2.1.6 Functionalisation of zeolite A and phillipsite using Hexa-decytrimethyl ammonium bromide

The surfactant modified zeolite A sample was prepared according to a procedure described by (Schick *et al*., 2010) by treating 5 g of raw zeolite A by 25 mL of 25 – 299 mmol/L surfactant (HDTMA) solution at temperature between 25 to 65 ^{o}C for a period of 8 to 24 h using a central composite design. The mixture was continuously stirred at 150 rpm to achieve equilibrium. After filtration, the sample was washed with 50 mL distilled water to remove the excess of HDTMA and dried at 80 ^{o}C overnight.

Phillipsite sample was also modified according to procedure described by (Schick *et al*., 2010) by treating 5 g of raw phillipsite with 25 mL of 25.87 – 299.33 mmol/L surfactants (HDTMA) solution at temperature between 25 to 65 ^{o}C for a period of 8 to 29.45 h using central composite design. The mixture was continuously stirred at 150 rpm to achieve equilibrium. After filtration, the sample was washed with 50 mL distilled water to remove the excess of HDTMA and dried at 80 ^{o}C overnight.

3.2.1.7 Phosphate and nitrate loading on surfactant modified zeolites

Potassium dihydrogen phosphate (KH_2PO_4) and Ammonium nitrate were used as the reagents to carry out ion exchange for phosphates and nitrates on surfactant modified

zeolite A and phillipsite as reported by (Subramanian *et al*., 2011). A surfactant modified zeolite to reagent mixture of 1:20 (w/w) was stirred continuously at 150 rpm in a plastic container for 16 h at room temperature for surfactant modified Zeolite A and 8 h for surfactant modified phillipsite as also reported by (Jakkula *et al*., 2011). Each of the zeolite A and philipsite solutions was filtered and washed repeatedly with distilled water to remove the excess soluble nutrients loaded on the extra lattice framework (Zhaohu *et al*., 2013).

3.2.1.8 Fourier Transform Infra-red spectroscopy analysis

The sample preparation for FTIR analysis was carried out by using Perkin Elmer 100 FT- IR Spectrometer model "Spectrum Two". The sample preparation was as described by (Maina, 2016). The instrumental settings were as follows: Force gauge: 50, scan wavelength: 4000-400 cm^{-1}, scan number 4, Percent transmittance was used for the analysis. The FTIR probe was first cleaned with ethanol and the baseline was run to guard against interference. A sample of 0.005 g was put under the focus of the probe condidering the earlier mentioned instrumental conditions. The light spectrum specific to infra red region was used to scan the sample and corresponding peaks of functional groups were recorded.

3.2.1.9 Brunauer Emmett Teller (BET) surface area analysis

The surface area and pore size of the synthesised sample materials were measured with A BET TRISTAR 3000 analyser. The preparation of zeolite sample analysis for surface area determination was as modified from (Fungaro and Magdalena, 2014). An estimate of 0.2 g of the sample was degassed under nitrogen gas for specific time period of 4 h under ambient temperature of 150 °C to remove moisture before the analysis. The

degassed sample at a temperature of 250 ^{o}C was later analysed for physisorption of the adsorbate nitrogen molecules on the surface of the zeolite

3.2.2.1 Evaluation of nutrient release pattern by percolation reactor

The experimental set up was designed to estimate the release tendency of fertilizers similar to the percolation reactor reported by (Thirunavukkarasu and Subramanian, 2014) except with few modifications in Plate I. The percolation reactor was made of a polyethylene column with internal diameter = 1.5 cm; height = 25 cm and rain water with pH = 7.23 was continuously supplied at a flow rate of 100 mL day^{-1} from 1 to 25 days. 10 g of soil was overlaid with 1.0 g of fertilizer inside the column. The experiment consists of 7 treatments comprising of HDTMA modified zeolite A loaded with phosphate, HDTMA modified zeolite A loaded with nitrate, HDTMA modified phillipsite loaded with phosphate, HDTMA modified phillipsite loaded with nitrate, ammonium nitrate, and potassium dihydrogen phosphate along with control (soil alone). The phosphates and nitrates concentrations were determined by collecting the leachates every 24 h and analyzed by the colorimetric method. The leachates collection continued until the concentration of the leachates were constant. The room temperature during the experiment was 30 ^{o}C. The experimental site sandy loam soil was used to simulate the actual field conditions. The physicochemical properties of the initial experimental soil were also characterized for various soil parameters in Table 4.27.

Plate I: Experimental setup for the percolating reactor column used in the study of the desorption rates of phosphates and nitrates from the soil and different fertilizer sources

3.2.2.2 Evaluation of the effects of zeolite A, phillipsite based fertilizers and NPK fertilizer application on growth, fruit yield and quality of tomato (Lycopersicon esculentum) in pots.

Introduction

A pot experiment was conducted to evaluate the efficacy of the synthesised zeolite A, phillipsite based fertilizers and NPK fertilizer on the growth, fruit yield and quality of two cultivars of tomato (Roma VF and UC82B) during the 2018 and 2019 rainy season.

Experimental site: - The experiment was conducted at teaching and research farm of the Federal University of Technology, Minna

Treatment and experimental design: The treatments consist of four levels each of the synthesised zeolite A, phillipsite and NPK fertilizer laid out in complete randomized design with three replications.

Soil preparation: Soils were collected from a depth of 0 – 20 cm, mixed thoroughly to achieve a uniform status. The soil samples were analyzed using standard procedure reported by Agbenin (1995).

Sowing and transplanting: The seeds were initially sown in nursery using germination

The seeds were initially sown in germination trays and later transplanted into pots, 3 weeks after sowing the seeds.

Cultural practices: Synthesised zeolite A and phillipsite based fertilizers and NPK 15:15:15 at four levels each (Soil alone 0% as control, 0.66 g, 1.33 g, 2.66 g which is equivalent to 0, 150, 300 and 600 kg/ha) were applied at 5 weeks after transplanting. Weeds were controlled by hand pulling.

Fruit Harvesting: Fruits were harvested at 10 and 12 WAT

Data collection: At 6 weeks after transplanting (6WAT), data on growth parameters viz; number of leaves, plant heights were measured using meter rule, plant girth was

measured with venier caliper, number of leaves, branches, flowers, and fruits were counted at 6, 8, and 10 WAT. Fruit yield was measured after harvesting at 10 and 12 WAT.

Fruit quality: Samples from the harvested fruit from each treatment were oven dried at 60 ^{o}C until constant weight was achieved and analyzed for fruit nitrogen, potassium, calcium, magnesium and vitamin C according to standard procedure described by AOAC (2002).

Data Analysis: Data collected were subjected to Analysis of variance using Statistical Analysis Software (SAS). The mean values were separated using Duncan's Multiple Range Test (DMRT) at 5% level of probability.

CHAPTER FOUR

4.0 RESULTS AND DISCUSSION

4.1 Synthesis and Characterisation of Zeolite A and Phillipsite based Fertilizers

4.1.1. Crystallisation of zeolite A

The study is focused on the optimized synthesis of zeolite A from Ahoko kaolin and the results of various crystallisation are hereby presented in Table 4.1. The highest percentage crystallinity was obtained as 99.92%.

4.1.2 Characterization of zeolite A

The synthesised zeolite A from Ahoko kaolin was characterised with XRD to determine percentage crystallinity. The XRD patterns are shown in Figure 4.1 a, b, c, d, e, f, g, h, i. Crystals of zeolite produced as shown on Table 4.1 were also characterised with scanning electron microscope to determine its morphology.

4.1.2.1 XRD analysis

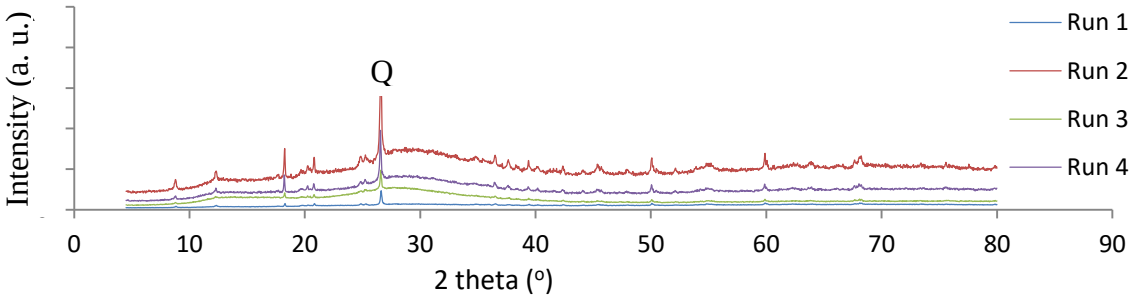

Figure 4.1a: X-ray diffraction pattern for the synthesised zeolite

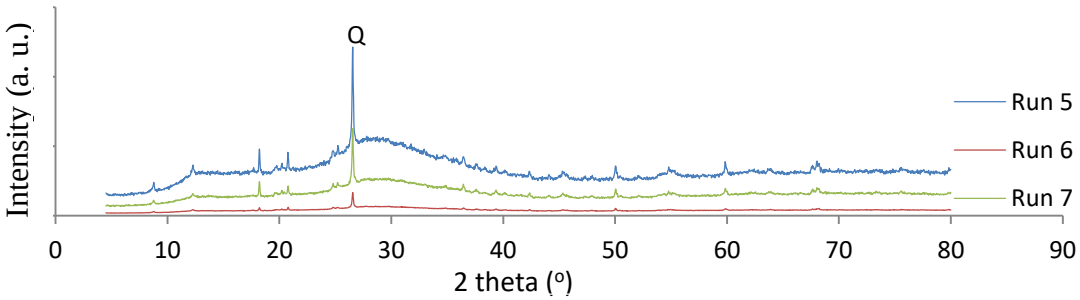

Figure 4.1b: X-ray diffraction pattern for the synthesised zeolite A

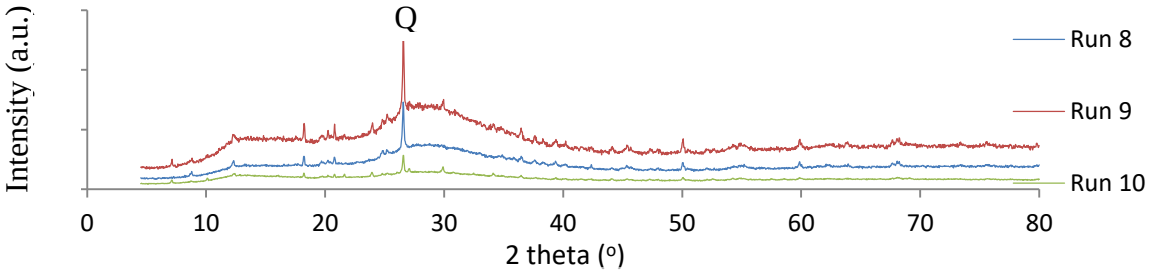

Figure 4.1c: X-ray diffraction pattern for the synthesised zeolite A

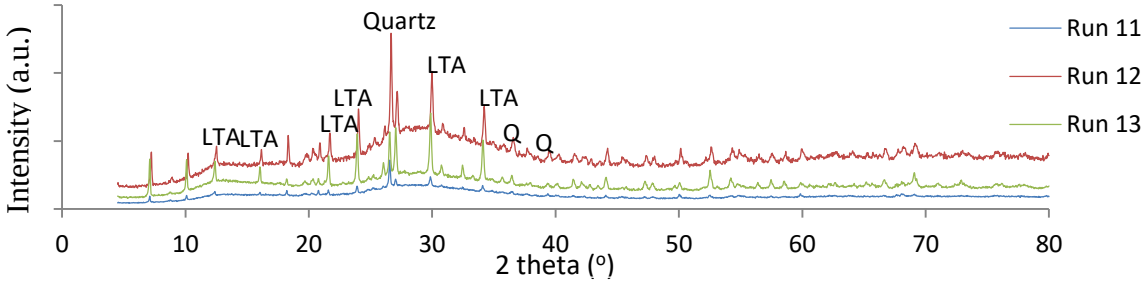

Figure 4.1d: X-ray diffraction pattern for the synthesised zeolite A

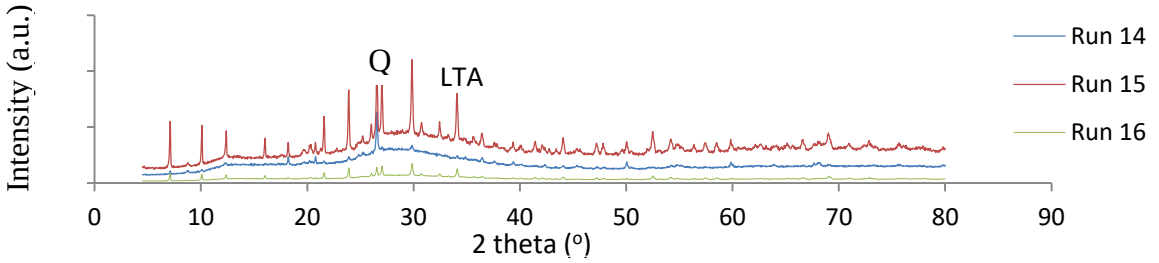

Figure 4.1e: X-ray diffraction pattern for the synthesised zeolite A

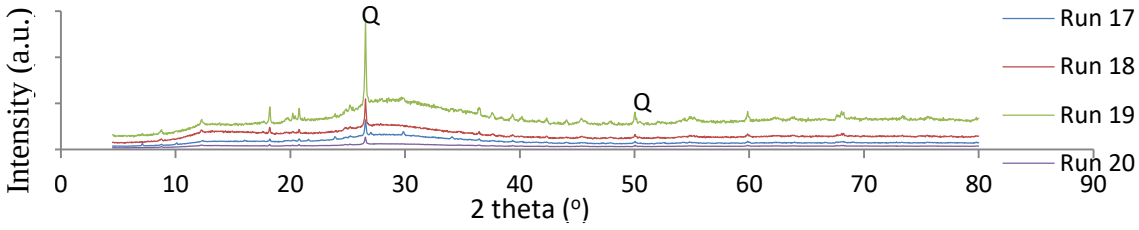

Figure 4.1f: X-ray diffraction pattern for the synthesised zeolite A

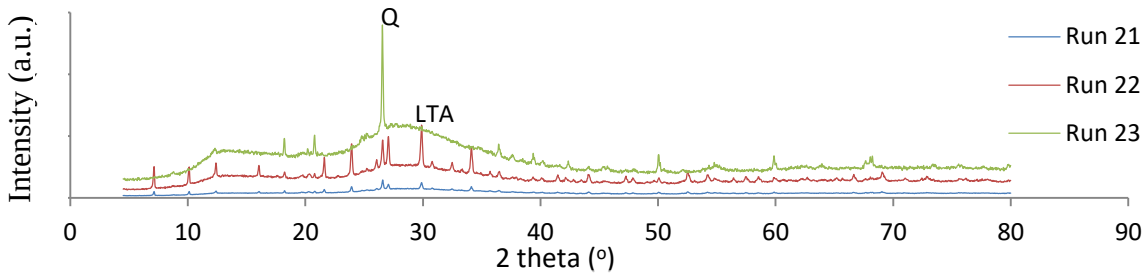

Figure 4.1g: X-ray diffraction pattern for the synthesised zeolite A

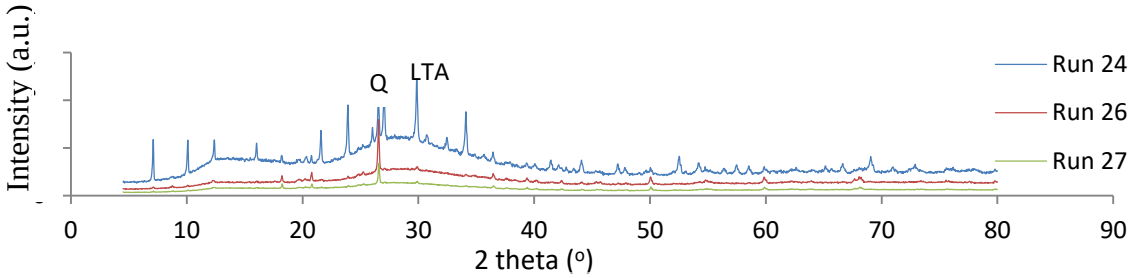

Figure 4.1h: X-ray diffraction pattern for the synthesised zeolite A

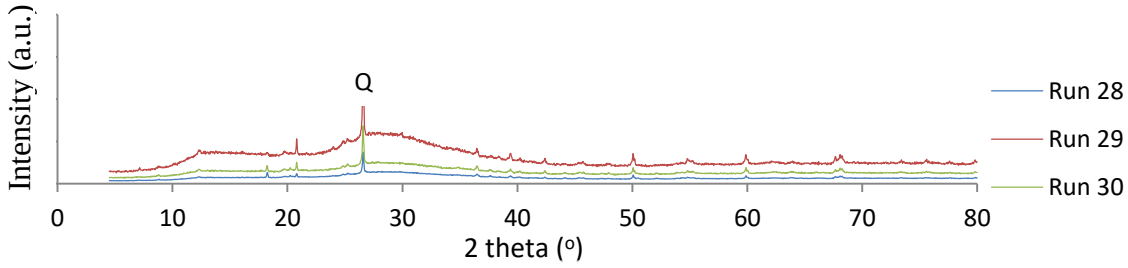

Figure 4.1i: X-ray diffraction pattern for the synthesised zeolite A

The results show that zeolite A was crystallized as the main zeolite phase in the reaction product similar to the report by Mostafa *et al*. (2011) where zeolite A was synthesised from Egyptian kaolin calcined at 850 ^{o}C. Zeolite A was associated with some side reaction mineral phases such as quartz and anatase. The prominent diffraction peaks at diffraction angle 26.55^{o} corresponds to the crystalline phase of quartz in the synthesised zeolitic material. It was observed for the first 8 runs that Zeolite A peaks were not prominent. This was traceable to the fact that the crystallisation time was less than 2 h.

Kovo (2010) attributed the lack of formation of zeolite A to incomplete dissolution of the metakaolin. However, the zeolite A characteristics peaks became larger as the crystallisation time increased from 3 to 4 h. Though zeolites crystals were formed for the crystallisation temperature range used in the experiment, the zeolite with the highest crystallinity was taken as the zeolite with the optimum set of synthesis conditions. It was also observed in Figure 4.1i and runs 28 to 30 that the zeolite peaks were reducing in intensity as crystallisation time reduced from 3 to 2 h. The XRD results showed that the spectra of synthesised zeolite A agreed well with the spectra of reference zeolite A (Treacy *et al*., 1996) and that pure crystalline zeolite A was formed in the work.

4.1.2.2 Scanning electron microscope analyses

The SEM micrographs of the synthesised zeolite A at different conditions are presented in Plate II - VI. The SEM micrographs were observed to complement the XRD analysis. The micrographs of the synthesised zeolite A were similar to those reported in previous studies (Iqbal *et al*., 2019). The observations in Plate II illustrated spherical crystals which are cotton-ball like and yam-like morphologies which represent sodalite and cancrite. The morphology of the product from experimental run 8 in Plate II was in agreement with the XRD Run 8 where there was no characteristic peak of zeolite A. There was also the twining growth and intergrowth of polycrystals which was explained as early agglomeration of nuclei (Iqbal *et al*., 2019).

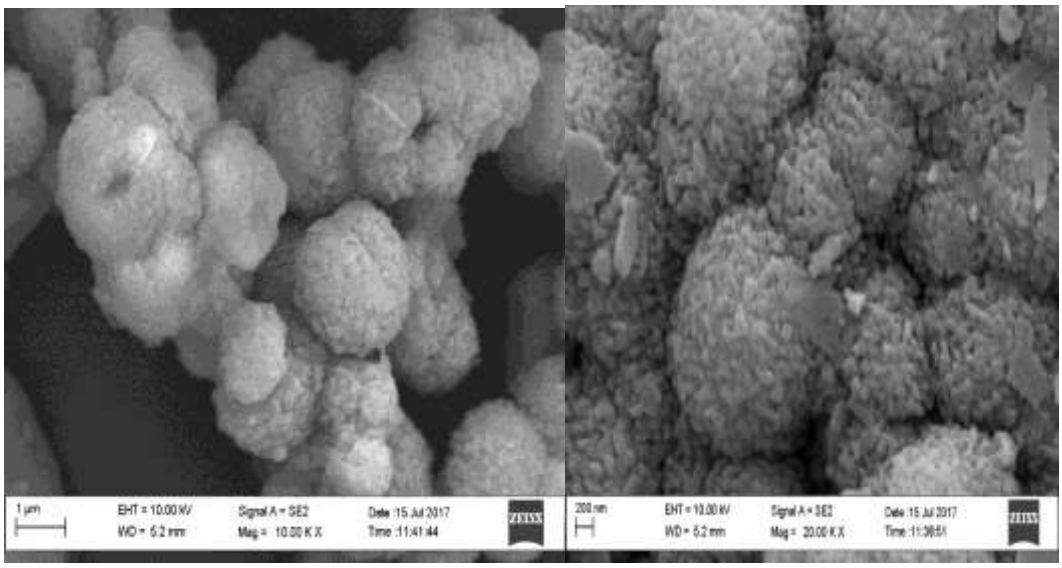

Plate II: SEM micrographs of zeolite A synthesised from run 8 at 100 ˚C for 1 h when stirring time was 2 h and ageing time was 2 h. Shown on the scale of 1µm and 200µm

Plate III and IV showed spherical agglomerates of sodalite growing out onto the surface of well-developed cubes of zeolite A. Unreacted metakaolin that did not react with NaOH also co-existed with zeolite A was shown as parallel plates. Generally, the results were in agreement with the report of Ayele *et al.* (2015) which reported that the morphological characteristics of the crystalized zeolite A depend on the synthesis conditioning reaction mixture.

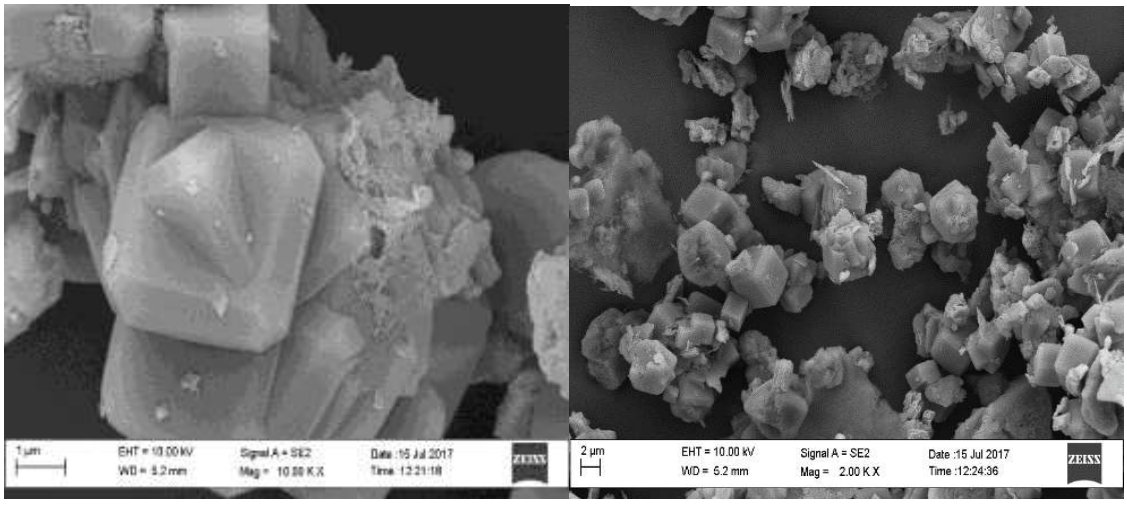

Plate III: SEM micrographs of zeolite A synthesised from run 15 at 100 ˚C for 3 h when stirring time was 1 h and ageing time was 18 h. Shown on the scale of 1µm and 2µm

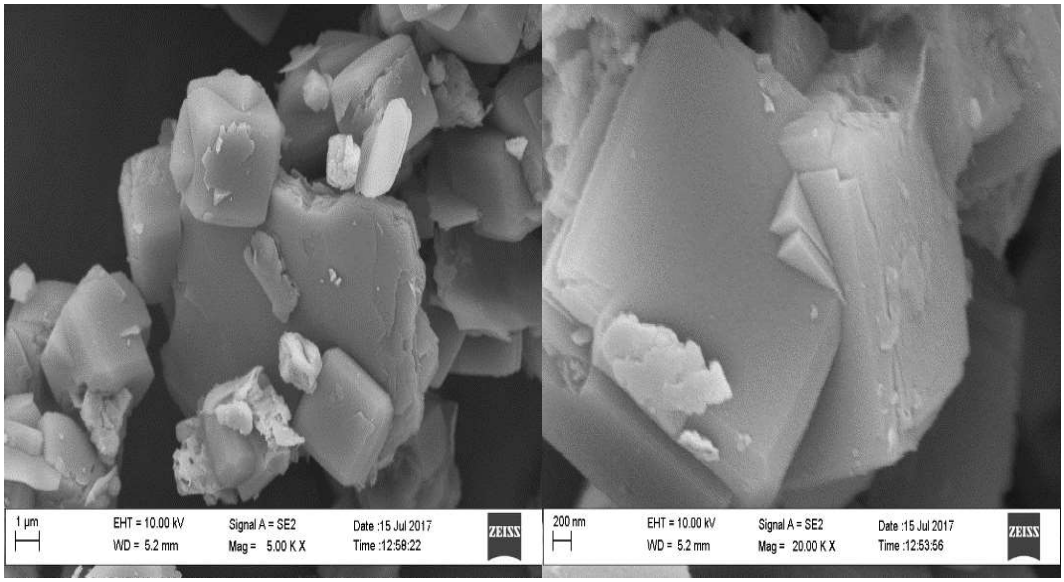

Plate IV: SEM micrographs of zeolite A synthesised from Run 22 at 105 ˚C for 2 hours when stirring time was 2 h and ageing time was 18 h. Shown on scale 1µm and 200µm

The micrographs of Plate V and VI illustrated the zeolite A characteristics of sharp edged cubic crystals. The SEM micrographs in Plate VI reveal that optimum cubic shaped crystals of zeolite A with rounded edges was obtained from runs 24 using aging time 15 h, crystallisation temperature 95 ^{o}C and crystallisation time 4 h to give the highest crystallinity of 99.92%.

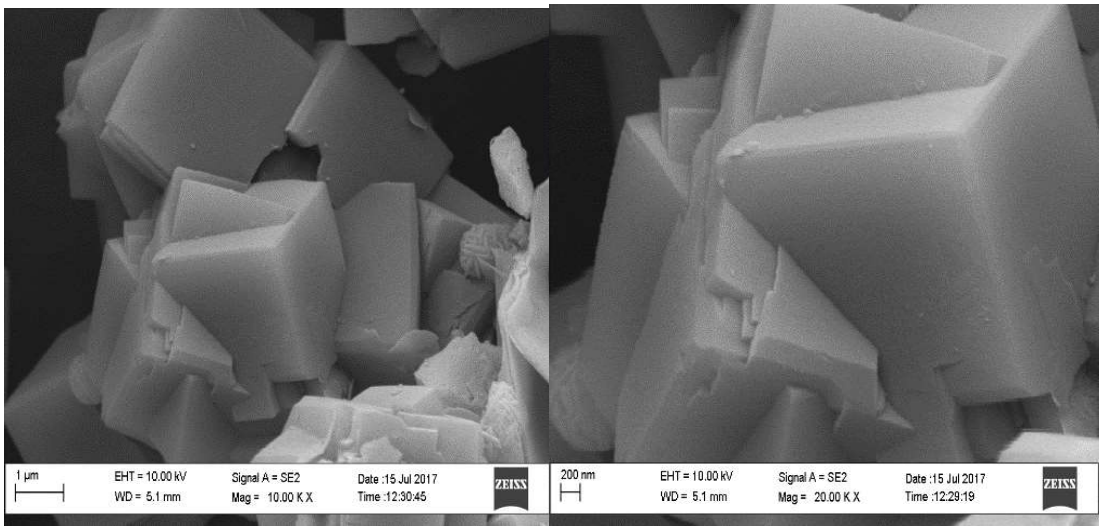

Plate V: SEM micrographs of zeolite A synthesised from run 16 at 100 ˚C for 3 h when stirring time was 2 h and ageing time was 18 h. Shown on the scale of 1µm and 200µm

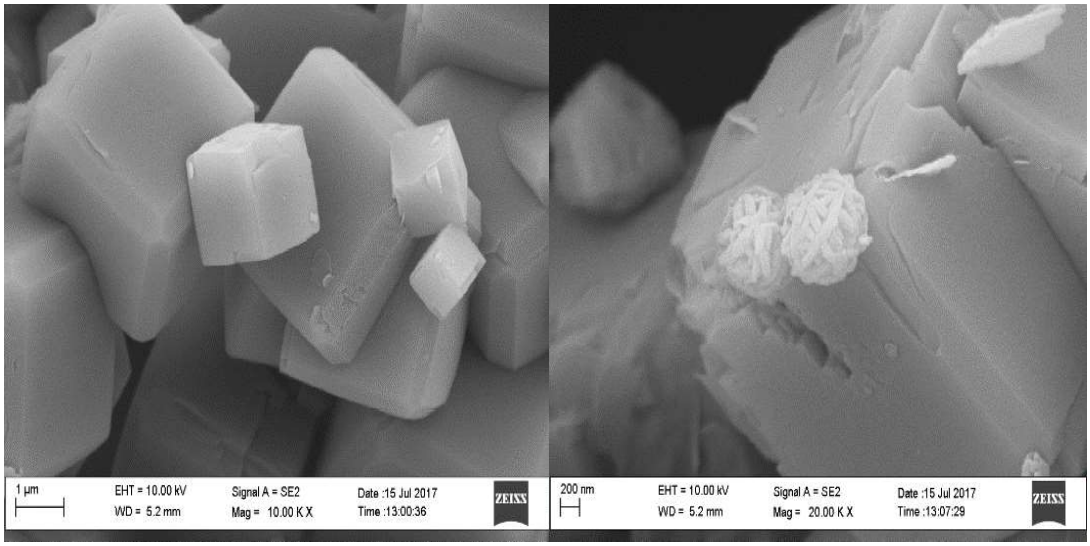

Plate VI: SEM micrographs of zeolite A synthesised from Run 24 at 95 ˚C for 4 h when stirring time was 2 h and ageing time was 18 h. Shown on the scale of 1µm and 200 µm

4.1.2.3 Energy dispersive X-ray spectroscopy analysis

The Energy Dispersive X-ray in Figure 4.2 gave the chemical composition of the synthesised product for the metal ions such as Sodium, Potassium, Aluminum, Silicon, titanium, Iron. The Si/Al ratio of 1.09 which was calculated from the EDX is a characteristics of low silica zeolites.

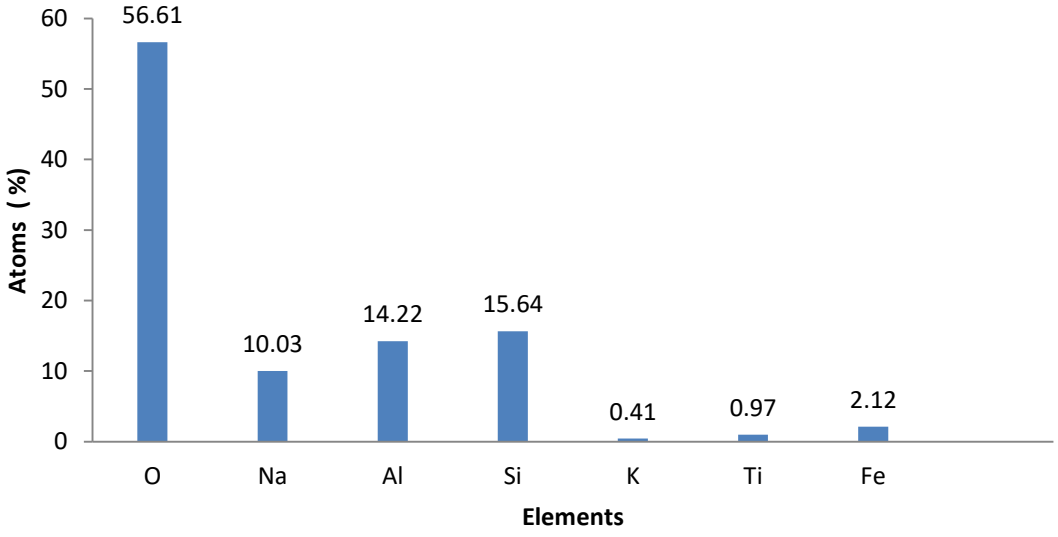

Figure 4.2: EDX showing the atomic percentage of the synthesised zeolite A

4.1.3 Optimisation study of zeolite A crystalisation

The central composite design provides the potential of maximising the crystallinity of zeolite A.

4.1.3.1 Experimental design for the zeolite crystallisation

The experimental design matrix for the zeolite A percentage crystallisation with the synthesis variables of stirring time, aging time, crystallization temperature and crystallization time is shown on Table 4.1

Table 4.1: Experimental design matrix for zeolite A synthesis

Std	Run	A: Stirring time (h)	B: Aging time (h)	C: Cryst temp (Celsius)	D: Cryst time (h)	% Crystallisation
1	16	1	12	90	1	1.26
2	2	2	12	90	1	1.29
3	6	1	18	90	1	1.77
4	27	2	18	90	1	2.62
5	13	1	12	100	1	2.83
6	23	2	12	100	1	3.76
7	3	1	18	100	1	3.86
8	5	2	18	100	1	4.04
9	7	1	12	90	3	32.30
10	14	2	12	90	3	77.26
11	11	1	18	90	3	87.03
12	12	2	18	90	3	85.70
13	1	1	12	100	3	88.09
14	28	2	12	100	3	89.38
15	26	1	18	100	3	93.99
16	24	2	18	100	3	94.73
17	17	0.5	15	95	2	68.42
18	21	2.5	15	95	2	75.72
19	15	1.5	9	95	2	54.05
20	4	1.5	21	95	2	62.09
21	19	1.5	15	85	2	86.06
22	29	1.5	15	105	2	94.09
23	10	1.5	15	95	0	0.00
24	20	1.5	15	95	4	99.92
25	22	1.5	15	95	2	83.71
26	9	1.5	15	95	2	71.42
27	18	1.5	15	95	2	64.10
28	30	1.5	15	95	2	69.74
29	25	1.5	15	95	2	63.56
30	8	1.5	15	95	2	65.87

4.1.3.2 Effect of process parameters on zeolite crystallisation

The contribution of crystallisation time has the most impact on the crystallininty of zeolite A amongs factors such as stirring time, aging time.

Main effects of stirring time on percentage crystallinity of zeolite A

The stirring time refers to the period of vigorous agitation between gel formation and the beginning of crystallisation. Abdullahi *et al*. (2017) reported that stirring during aging improved the uniformity of the gel formation and the selectivity of the different zeolite phases. Figure 4.3 revealed the main effect of stirring time on percentage crystallinity of zeolite A when ageing time was 15 h, crystallisation temperature was 95 ^{o}C, and crystallisation time was 2 h that as stirring time increased from 1 to 2 h, the percentage crystallinity increased from 60.78 to 65.80%. However, in Table 4.2, as stirring time increases from 0.5 to 2.5 h, the percentage crystallinity increased from 68.42 to 75.72%. The slight increase of 7.30% in percentage crystallinity indicated the level of contribution the stirring time variable adds to the zeolite A synthesis. This observation probably explains the reason the stirring activity is referred to as aging time (Maia *et al*., 2019).

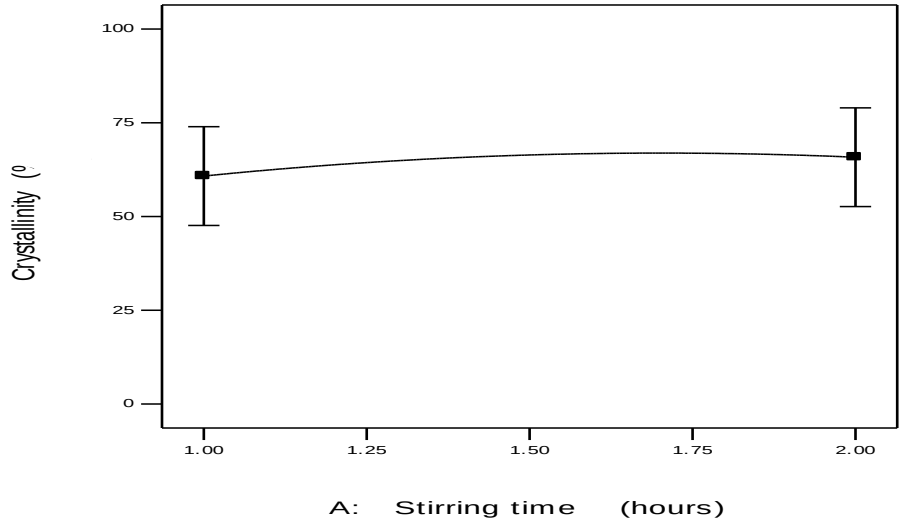

Figure 4.3: The main effect of stirring time on percentage crystallinity of zeolite A

Main effects of aging time on percentage crystallinity of zeolite A

The aging time in this study was referred to as the period between the gel formation and the start of crystallisation without stirring activity. There was generally a slight increase in percentage crystallinity of 57.36 to 62.22% for an increase in aging time from 12 to 18 h in Figure 4.4, however percentage crystallinity attained a maximum value of 66.89% at an aging time of 15.62 h when stirring time was 1.5 h, crystallisation temperature was 95 ^{o} C, and crystallisation time was 2 h. In Table 4.2, as aging time increased from 9 to 21 h, the percentage crystallinity increased from 54.05 to 62.09%. The slight increase of 8.04 % in percentage crystallinity indicated the contribution of aging time to zeolite A synthesis. Lima *et al*. (2019) reported that the seed nuclei needed for crystallisation were developed during the aging period. It was generally observed in the study that increases in aging time lead to increase in crystallinity. The observed trend was also supported by Kovo and Holmes (2009) who reported the production of kaolin based zeolite via a novel calcination process that aging of the aluminosilicate gel with stirring for 48 h resulted in an increase in crystallinity of the zeolite. Kovo (2011) also reported the formation of zeolite A even when the synthesis mixture was not subjected to aging with stirring. The author attributed it to the reactivity of the Ahoko Nigerian kaolin metakaolin which might be higher than kaolin used in other works. Johnson *et al*. (2014) reported a review on the hydrothermal synthesised zeolites based on kaolinite and stated that optimum aging conditions were 12 h at 20 ^{o}C.

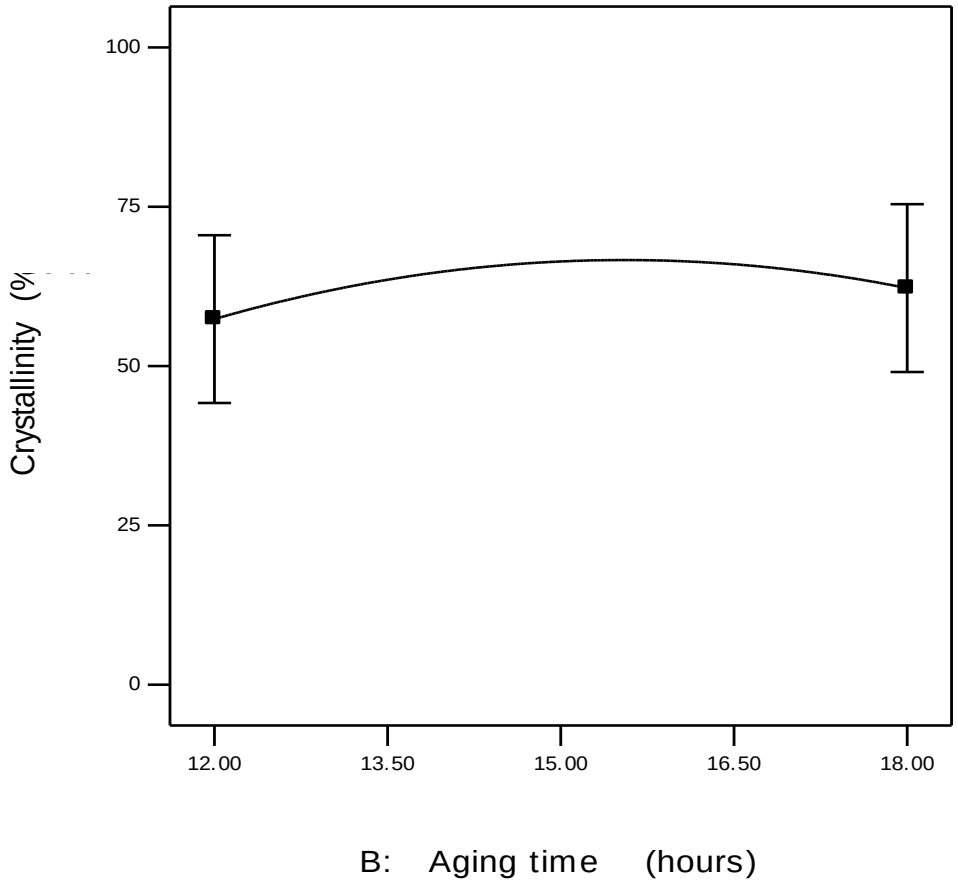

Figure 4.4: The main effect of aging time on percentage crystallinity of zeolite A

Main effects of crystallisation temperature on percentage crystallinity of zeolite A

In Figure 4.5, it was observed from the plot of crystallisation temperature on percentage crystallinity of zeolite A that percentage crystallinity increased linearly from 63.63 to 71.96% as crystallisation temperature increased from 90 to 100 ^{o}C. It was however observed in Table 4.1 that as crystallisation temperature increased from 85 to 105 ^{o}C, percentage crystallinity increased from 86.06 to 94.09%. The percentage crystallinity difference of 8.03%, indicates the contribution of crystallisation temperature to zeolite A synthesis. Mirfendereski and Mohammadi (2016) also reported similarly that crystallinity of zeolite A increased with an increase in temperature from 80 to 100 ^{o}C.

Johnson *et al*. (2014) also reported that crystallisation temperature should be in a range of 70 and 200 ^{o}C because the temperature lower than 70 ^{o}C was not adequate to synthesise crystalline species. The difference of 8.33% between the lower limit and upper limit of percentage crystallinity was higher for crystallisation temperature than aging time and stirring time. However, the result showed that crystallisation temperature was more important than aging time and stirring time in zeolite A synthesis.

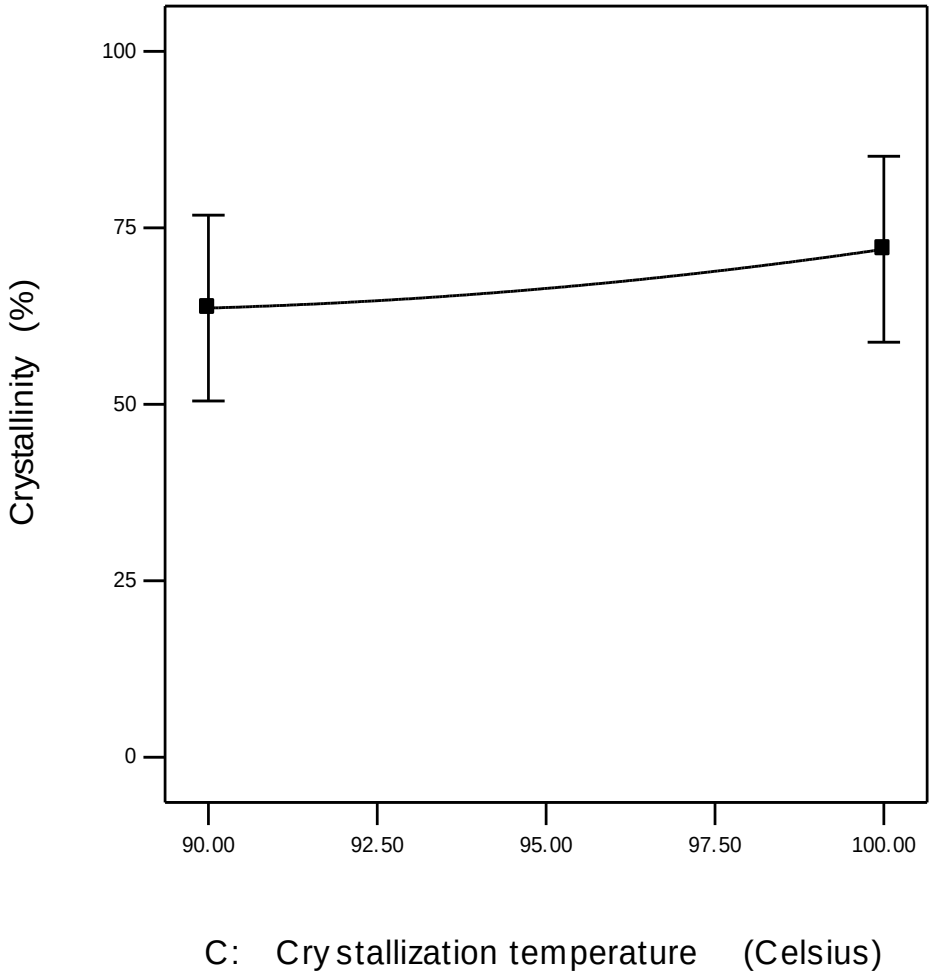

Figure 4.5: The main effect of crystallisation temperature on percentage crystallinity of zeolite A

The main effect of crystallisation time on the percentage crystallinity of zeolite A

Figure 4.6 revealed the main effect of crystallisation time on the percentage crystallinity of zeolite A at stirring time 1.5 h, aging time 15 h and crystallisation time of 95 ^{o}C. It was observed that the percentage crystallinity of zeolite A increased from 22.67 to 93.16% as the crystallisation time increased from 1 to 3 h. There was a huge difference of 70.49 % in percentage crystallinity of zeolite A in 2 h which showed that crystallisation time was the most significant variable in the synthesis of zeolite A. This trend was shown as the highest coefficient value in the regression model for the zeolite A synthesis in Equation 4.1. It was also shown in Table 4.1 that percentage crystallinity of 99.92% was observed when crystallisation time increased to 4 h. It was further observed from Table 4.1 that there was no appreciable zeolite formation for crystallisation time below 1 h. The plausible reason might be insufficient time for the dissolution of metakaolin in the initial period of crystallisation (Kovo, 2011).

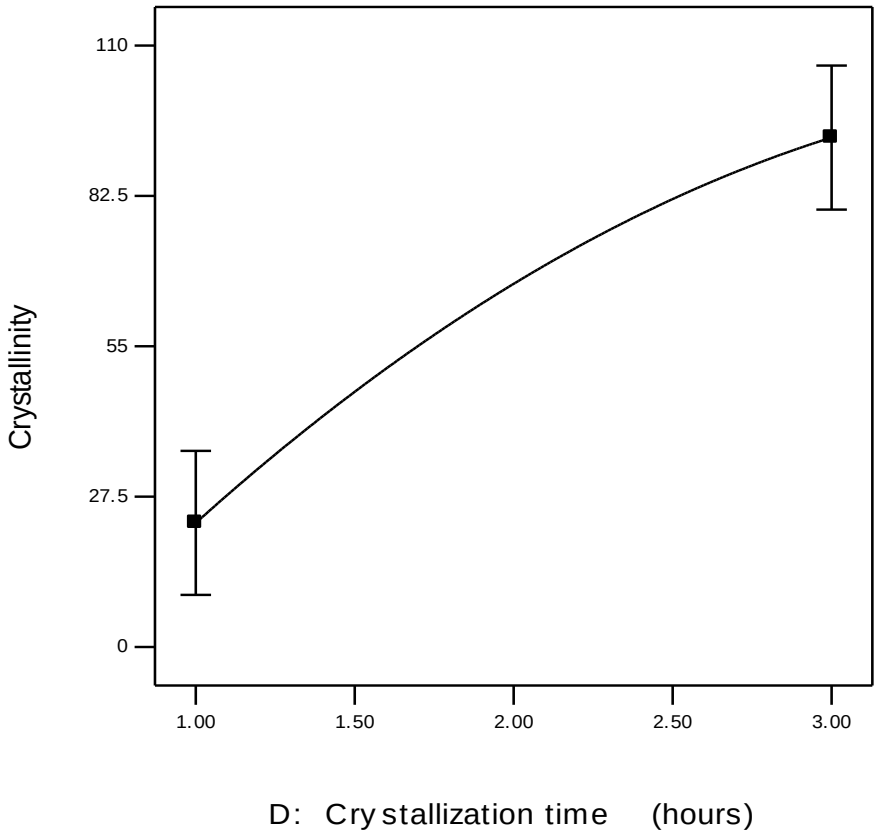

.

Figure 4.6: The main effect of crystallisation time on percentage crystallinity of zeolite A

Effect of synthetic variables interaction on zeolite A crystallinity

The interactive effect of the stirring time, aging time, crystallisation temperature and time on percentage crystallinity of zeolite A are shown in Figure 4.7 to 4.13.

Figure 4.7 showed the effect of stirring time and aging time on the percentage crystallinity of zeolite A. Percentage crystallinity of synthesised zeolite A increased as aging time increased from 12 to 18 h while the percentage crystallinity was observed to initially decrease and subsequently increased as stirring time increased from 1 to 2 h. The interactive effect of aging time at 15.50 h and stirring time at 1.77 h gave the maximum percentage crystallinity of 61.81% when crystallisation time at 2 h and crystallisation temperature at 95 ^{o}C were kept constant.

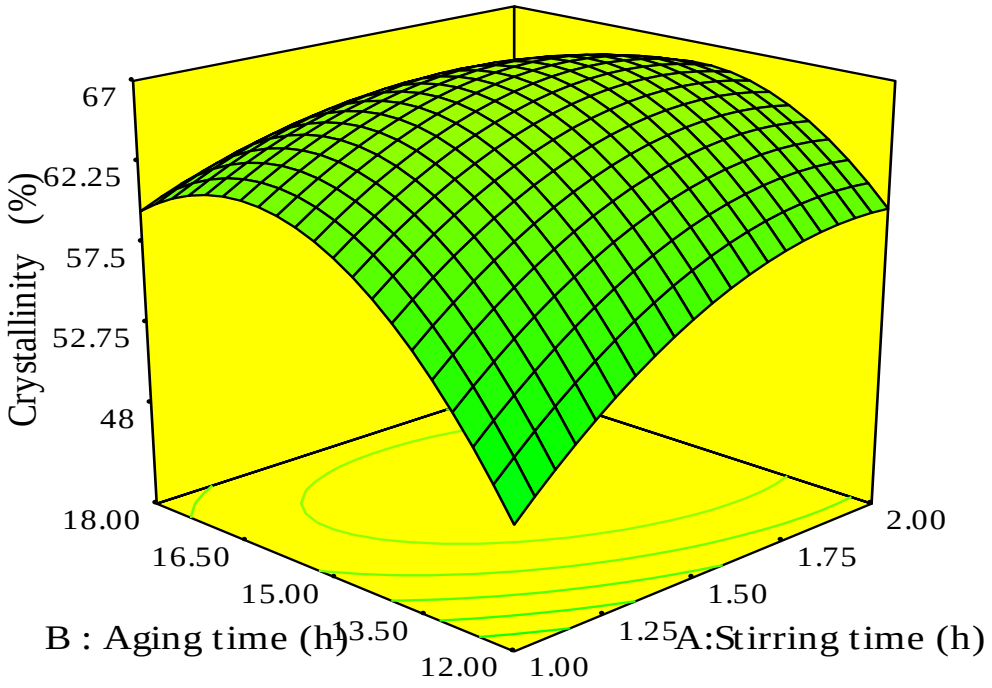

Figure 4.7: Effect of 3D plot showing the relationship between aging time, stirring time on percentage crystallinity of zeolite A

Figure 4.8 showed the interactive effect of crystallisation temperature and stirring time on percentage crystallinity of synthesised zeolite A. It was observed that both crystallisation temperature and stirring time increased uniformly with percentage crystallinity of the synthesised zeolite. At a constant aging time of 15 h and crystallisation time of 2 h, the synergetic effect of crystallisation temperature at 99.95 ^{o}C and stirring time at 1.47 h was observed to give a maximum percentage crystallinity of 71.89%.

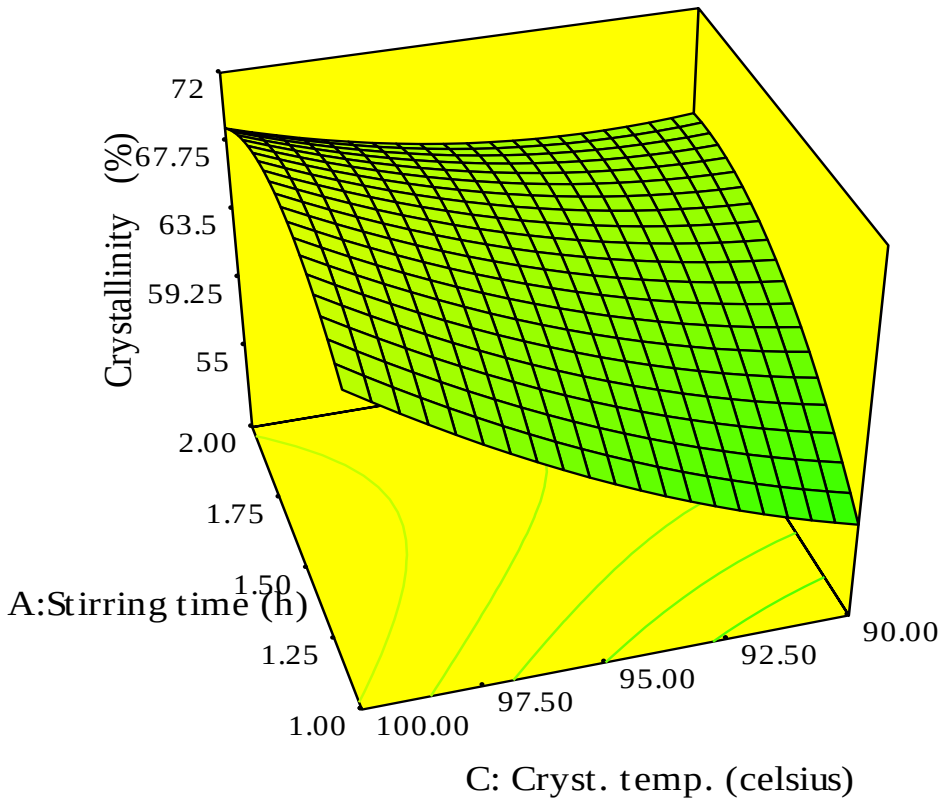

Figure 4.8: Effect of 3D plot showing the relationship between crystallisation temperature, stirring time on percentage crystallinity of zeolite A.

The Figure 4.9 depicted the relationship between crystallisation time, stirring time and percentage crystallinity of synthesised zeolite A. The Figure 4.9 illustrated that as stirring time increases from 1 to 2 h, the percentage crystallinity increased but not as much as the effect of crystallisation time from 1 to 3 h whose increase was more prominent. However, a percentage crystallinity of 95.34% for the synthesised zeolite A was obtained for the interactive effect of crystallisation time of 2.99 h and stirring time of 1.96 h when aging time of 15 h and crystallisation temperature of 95 ^{o}C were held constant.

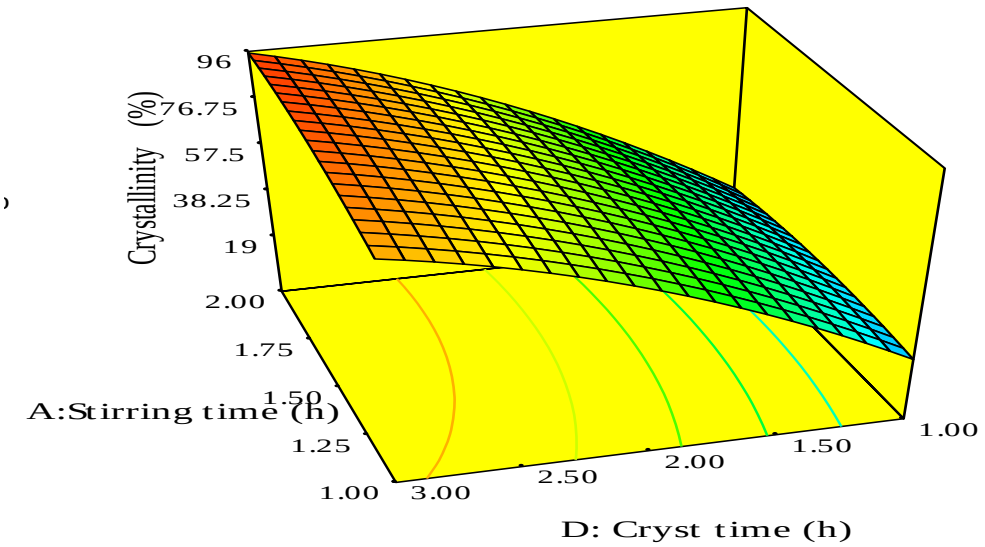

Figure 4.9: Effect of 3D plot showing the relationship between crystallisation time, stirring time on percentage crystallinity of zeolite A

The Figure 4.10 showed the relationship between crystallisation temperature, aging time and percentage crystallinity. The Figure 4.10 showed that as aging time increased from 12 to 18 h, the percentage crystallinity increased. It was also observed that as crystallisation temperature increased from 90 to 100 ^{o}C, the percentage crystallinity decreased, became constant before increasing. The maximum interactive effect was observed when the crystallisation temperature at 99.73 ^{o}C and aging time at 14.96 h gave 71.59% crystallinity keeping crystallisation time 2 h and stirring time 1h constant.

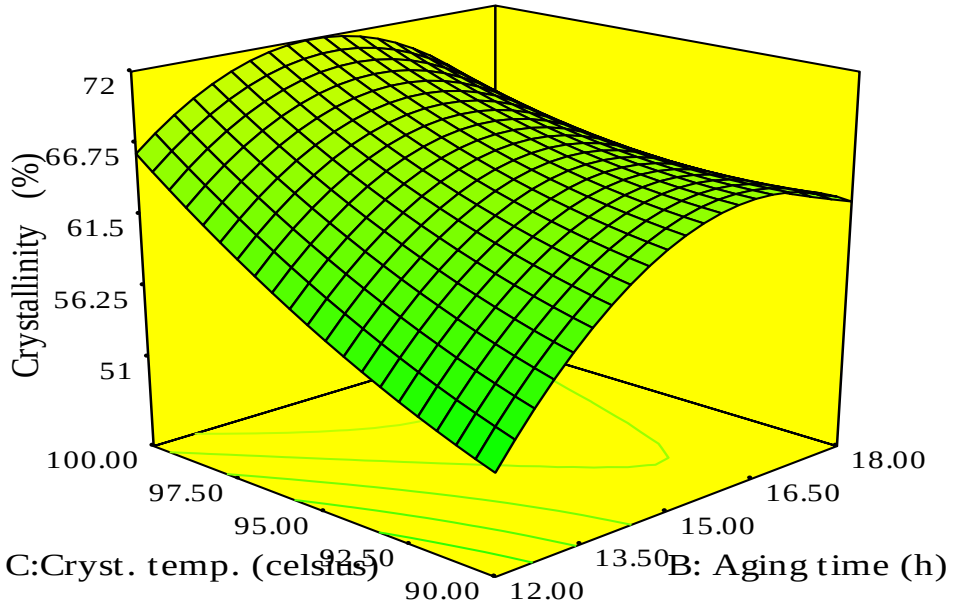

Figure 4.10: Effect of 3D plot showing the relationship between crystallisation temperature and aging time on percentage crystallinity of zeolite A

Figure 4.11 showed the effect of crystallisation time and aging time on the percentage crystallinity of zeolite A. The plot showed that as the aging time increased from 12 to 18 h, the percentage crystallinity increase was low while the response of percentage crystallinity increased sharply with increase in crystallisation time as it was also observed by (Silva *et al*., 2017). The net effect of both the crystallisation time at 2.81 h and aging time at 16.68 h when crystallisation temperature at 95 ^{o}C and stirring time of 1.5 h was kept constant was 90.73% crystallinity.

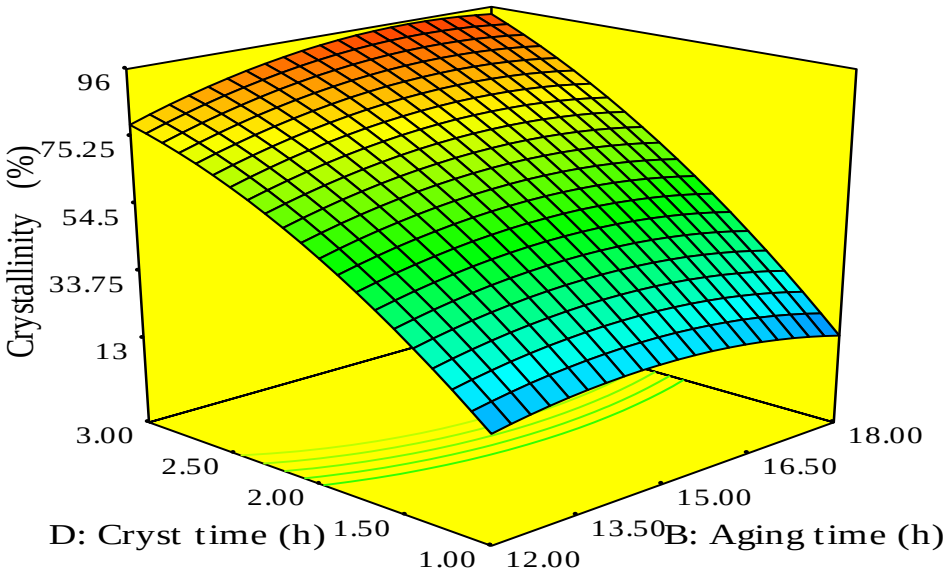

Figure 4.11: Effect of 3D plot showing the relationship between crystallisation and aging time on percentage crystallisation of zeolite A

Figure 4.12 showed the interactive effect of crystallisation time and crystallisation temperature on percentage crystallinity. The plot showed that the percentage crystallinity was relatively constant at the initial increase of crystallisation temperature from 90 to 95 ^{o}C. Then it was followed by a gradual increase in crystallinity. It was however observed that as crystallisation time increased from 1 to 3 h, the percentage crystallinity increased sharply more than the corresponding result of the crystallisation temperature. The maximum interactive effect of crystallisation temperature at 96.54 ^{o}C and crystallisation time at 2.85 h was observed at a crystallinity of 92.55% when stirring time at 1.50 h and aging time at 16 h were kept constant as it was observed in (Kovo *et al*., 2017).

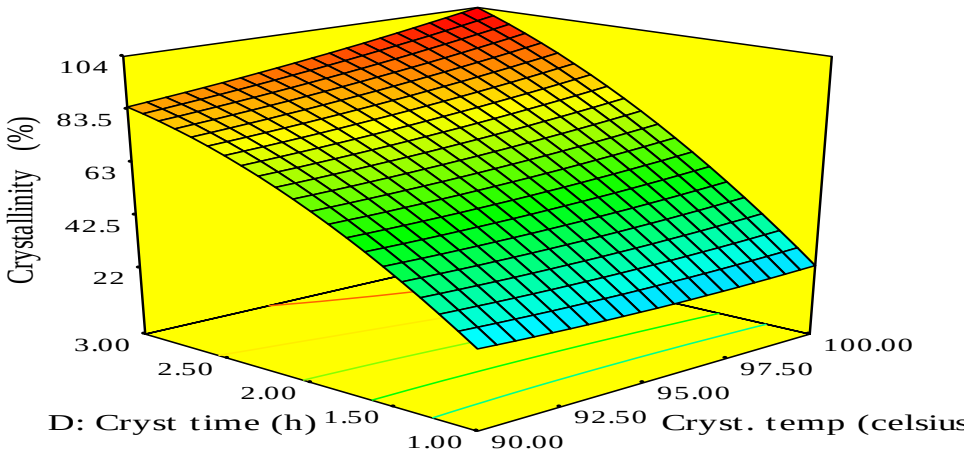

Figure 4.12: Effect of 3D plot showing the relationship between crystallisation time and crystallisation temperature on percentage crystallinity of zeolite A

4.1.3.3 Response equation development for zeolite A crystallisation

Response equation for zeolite A in terms of coded factors:

Given that A = Stirring time, B = Aging time, C = Cryst temp, D = Cryst time

Crystallinity = +7.35 +2.51 A +3.10 B + 4.17C +35.24 D -2.93AB -2.60 A C +2.85 AD - 3.24BC +4.65BD +5.24 CD + $14.07A^2$ - 3.95 B^2 + 18.57 C^2 +8.70D^2 (4.1)

Equation 4.1 showed that the crystallisation time was the most significant factor followed by the crystallisation temperature in the synthesis of zeolite A by reason of the magnitude of their coefficients.

4.1.3.4 Test for adequacy of the model for zeolite A crystallisation

The analysis of variance for the response surface quadaratic model was presented in Table 4.2. The Model F-value of 10.96 implied the model was significant. There was only a 0.01% chance that a "Model F-Value" this large could occur due to noise. Values of "Prob > F" less than 0.0500 indicated model terms were significant. In this case D^2, A^2, C^2, D were significant model terms. The "Lack of Fit F-value" of 0.94 implies the

Lack of Fit was not significant relative to the pure error. There was a 56.55% chance that a "Lack of Fit F-value" this large could occur due to noise. Non-significant lack of fit is good because it gives a model that fits.

Table 4.2: ANOVA for response surface quadratic model

Source	**Sum of Squares**	**Df**	**Mean Square**	**F Value**	**p – value Prob > F**	**Coeff of terms**	**Remarks**
Model	47758.98	14	3411.35	10.96	< 0.0001		signific.
A-Stirring time	151.39	1	151.39	0.48	0.4963	2.51	
B – Aging time	230.76	1	230.76	0.74	0.4027	3.10	
C- Cryst temp	416.33	1	416.33	1.33	0.2655	35.24	
D – Cryst time	29811.63	1	2981.63	95.80	0.0001	4.17	
AB	137.12	1	137.12	0.44	0.5169	-2.93	
AC	108.16	1	108.16	0.34	0.5642	-2.60	
AD	130.30	1	130.30	0.41	0.5273	2.85	
BC	168.48	1	168.48	0.54	0.4732	-3.24	
BD	346.14	1	346.14	1.11	0.3082	4.65	
CD	439.95	1	439.95	1.41	0.2529	5.24	
A^2	5431.18	1	5431.18	17.45	0.0008	14.07	
B^2	427.05	1	427.05	1.37	0.2592	-3.95	
C^2	9461.57	1	9461.57	30.40	<0.0001	18.57	
D^2	2075.07	1	2075.07	6.6688	0.0208	8.70	
Residual	4667.41	15	311.16				
Lack of Fit	3046.74	10	3046.74	0.93	0.5655		Not signific.

Table 4.3: Statistical prameters for the percentage crystallinity of zeolite A data analysis from the model

Std.Dev	Mean	C.V. %	PRESS	Pred R-Squared	Adj R-Squared	R-Squared	Adeq Precision
17.64	37.27	47.33	19883.01	0.6207	0.8279	0.9110	11.302

The value of R- squared (0.9110) explained that 91.10 % of variation obtained within the experimental data for zeolite A synthesis. The "Predicted R-Squared" of 0.6207 was not as close to the "Adj R-Squared" of 0.8279 as expected. The ratio of 11.302 indicated an adequate signal. This model explains the best scanario of high R squared close to 1.0 and low p-value less than the cut off for significance of $p < 0.05$.

4.2 Synthesis and Characterisation of Phillipsite

4.2.1 Production of phillipsite

The response of percentage crystallinity to synthesis vaiables such as aging time, crystallisation temperature, crystallisation time using central composite design is presented in Table 4.4

4.2.2 Characterisation of phillipsite

4.2.2.1 Phillipsite XRD spectra

The X-ray diffraction spectra for the synthesised phillipsites zeolites for 20 experimental runs are shown in Figure 4.13

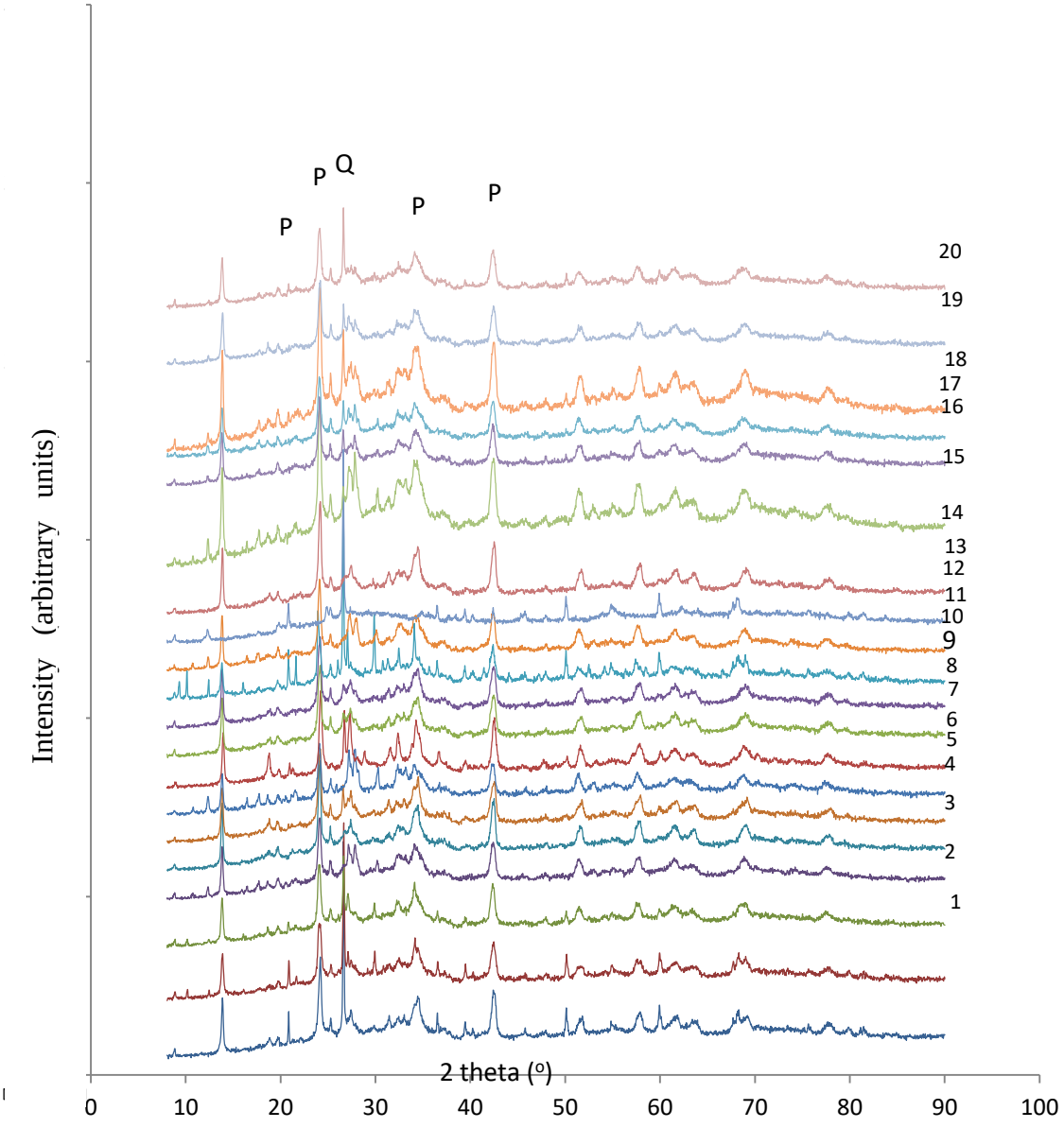

Figure 4.13: X-ray diffraction pattern for the synthesised phillipsites showing P for Phillipsite peaks, Q for Quartz peaks

The peaks designated (P) refer to phillipsite peaks. The prominent highest diffraction peaks at diffraction angle 26.55^{o} corresponds to quartz in the synthesised zeolitic material. The results showed that the spectra of synthesised zeolite agreed well with the spectra of phillipsite at the characteristic XRD peaks of Phillipsite at 2-theta (degree)-: 12.40, 24.23, 33.43, 42.23, 51.47, 57.56, 62.41, 68.81. They were consistent with the reference sample from the Acta Crystallographica, showing that phillipsite crystalline zeolite was formed in the work (Kowalak *et al*., 2015).

4.2.2.2 Scanning electron micrographs for synthesisied phillipsite

Micrographs of the crystal growth of the phillipsite have been observed to be made up of complex twinned crystals, with smaller crystals generally showing the simple forms such as fourling, prismatic and spherical clusters of these forms (Mattioli and Cenni, 2020).

i). Prismatic crystals are shown in Plate VII. Most phillipsite were seen as cracked or broken shapes. (Adisaputra and Kusnida, 2010) reported that phillipsite crystals occur as broken shapes because of the spread of the zeolite nuclei and the insufficiency of soluble aluminium in the liquid phase thereby inhibiting the growth of large zeolite crystals. Prismatic crystals were observed to have characteristics of 25 µm long and 0.2 µm thick and have length to width ratios of about 1.5 – 10. It was also observed that these prismatic phillipsites occur as radial aggregates as shown in Plate VIII. (Mattioli and Cenni, 2020) also described the rare occurrence of capped prisms as phillipsite.

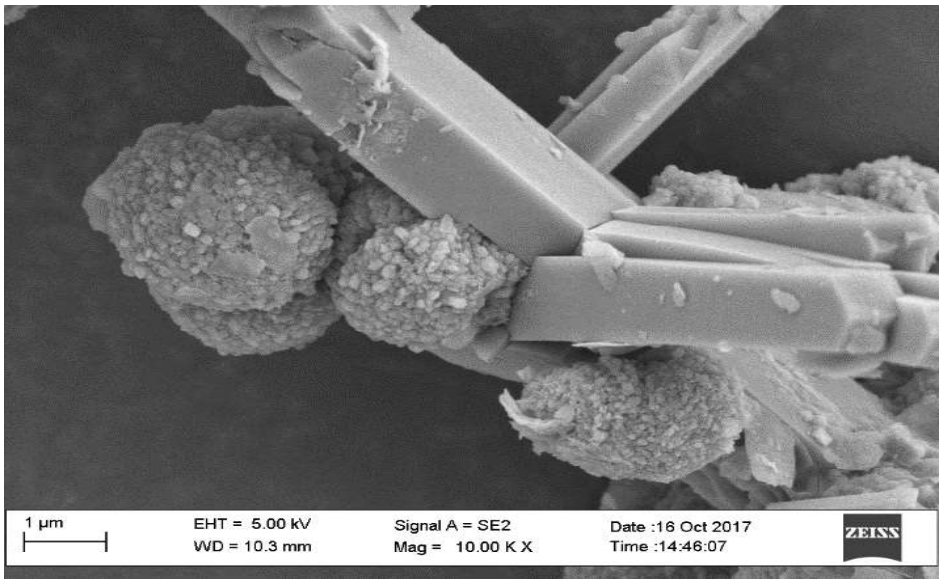

Plate VII: SEM micrographs of phillipsite synthesised from run 13 at 110 ˚C for 75 h when ageing time was 36 h.

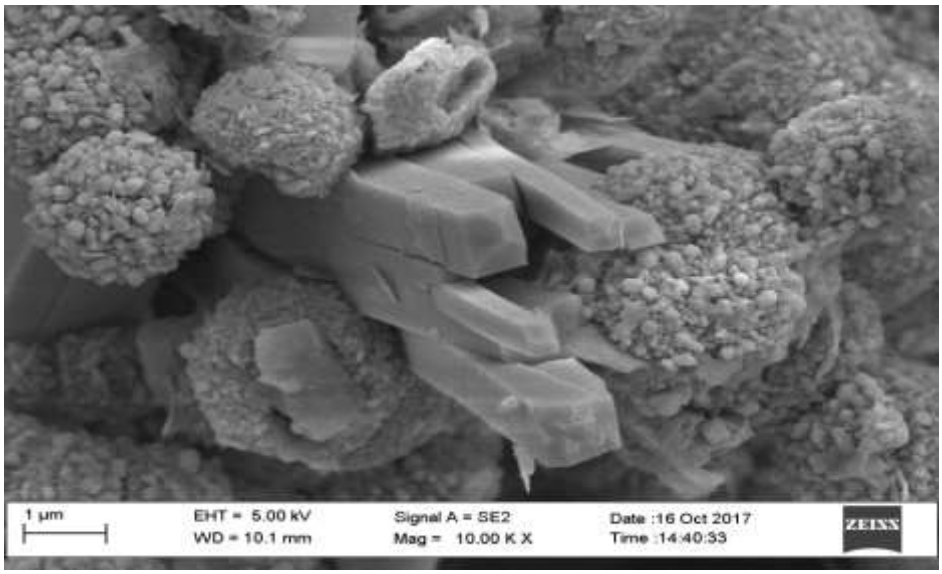

Plate VIII: SEM micrographs of phillipsite synthesised from run 4 at 135 ˚C for 75 h when ageing time was 36 h.

ii). Spherical crystal aggregates as illustrated in Plate IX and X show well developed crystal terminations around their peripheries. Cluster of several mutually interfering spherulites are common and some of the spherulites are malformed (Mees, 2018).

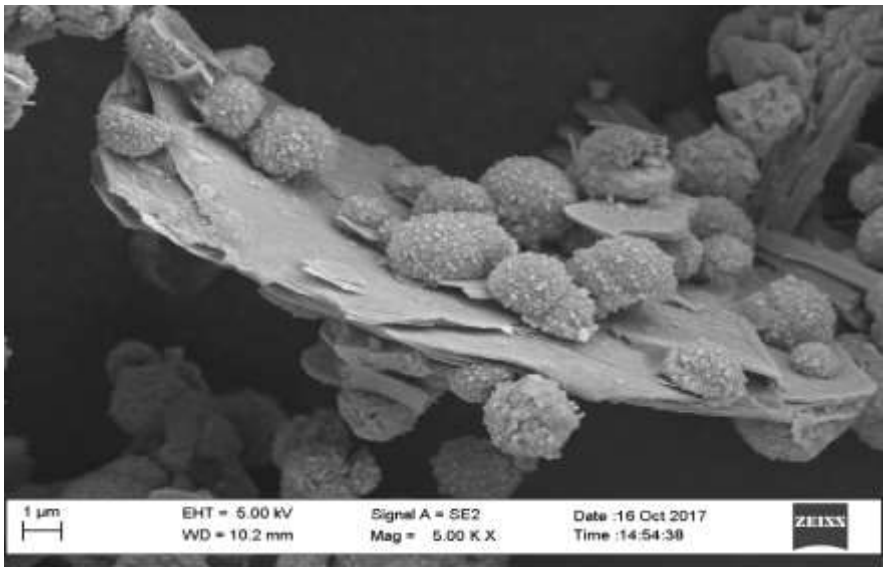

Plate IX: SEM micrographs of phillipsite synthesised from run 13 at 110 ˚C for 75 h when ageing time was 36 h

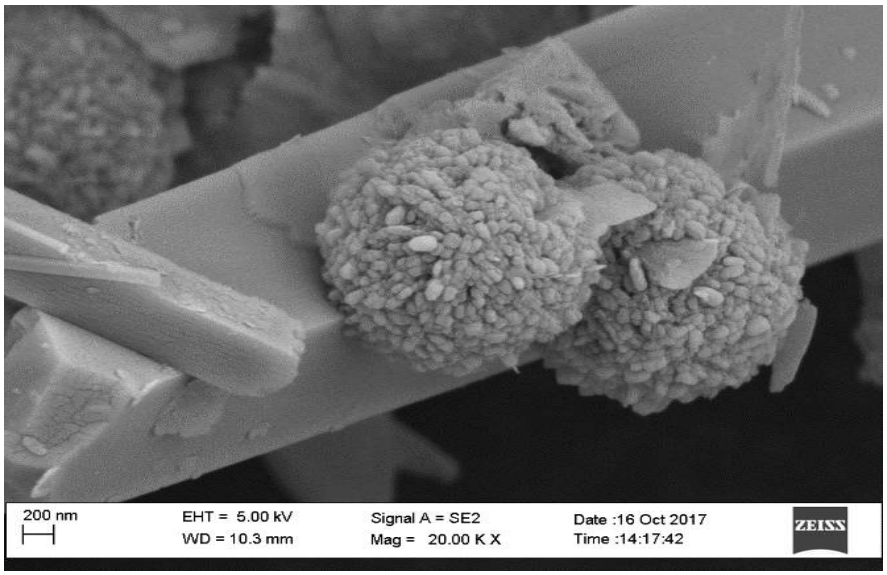

Plate X: SEM micrographs of phillipsite synthesised from run 6 at 125 ˚C for 31 h when ageing time was 48 h

iii). Twinned crystals of phillipsite were observed in Plate XI with scale 200µm.

From the SEM micrographs in Plate XI, scale 1µm, it could be observed that spherical crystals were obtained using 36 h of gel aging, 84.77 ^{o}C crystallisation temperature and 75 h crystallisation time gave the crystallinity of 33.89%.

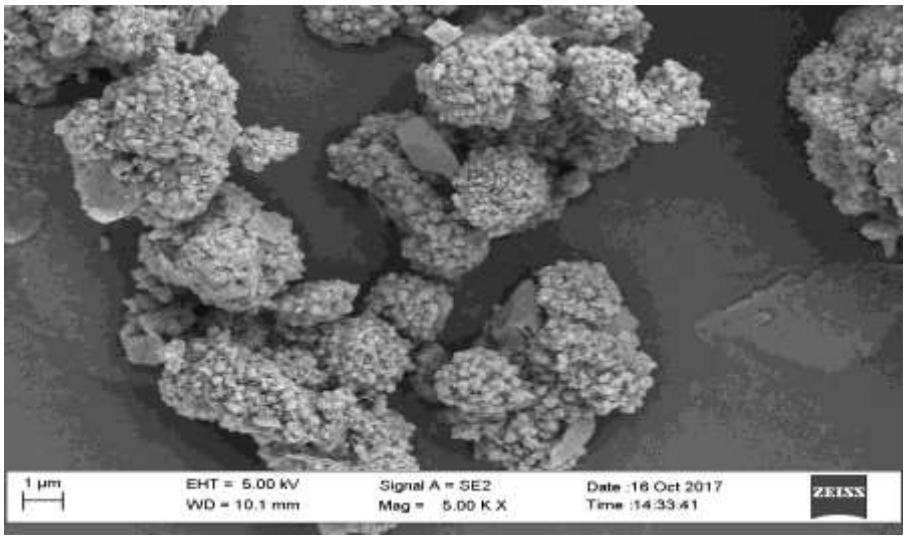

Plate XI: SEM micrograph of phillipsite synthesised from run 9 at 84.77 ˚C for 75 h when ageing time was 36 h

4.2.2.3 EDX analysis of phillipsite

The Si/Al ratio of 1.15 as calculated from the EDX represented in the Figure 4.14 is another characteristic of low silica zeolite. The percentage of potassium atoms in the EDX analysis for phillipsite with 2.9% was higher than that of zeolite A with 0.41%. This could be traceable to the introduction of potassium hydroxide during the gel formation of phillipsite.

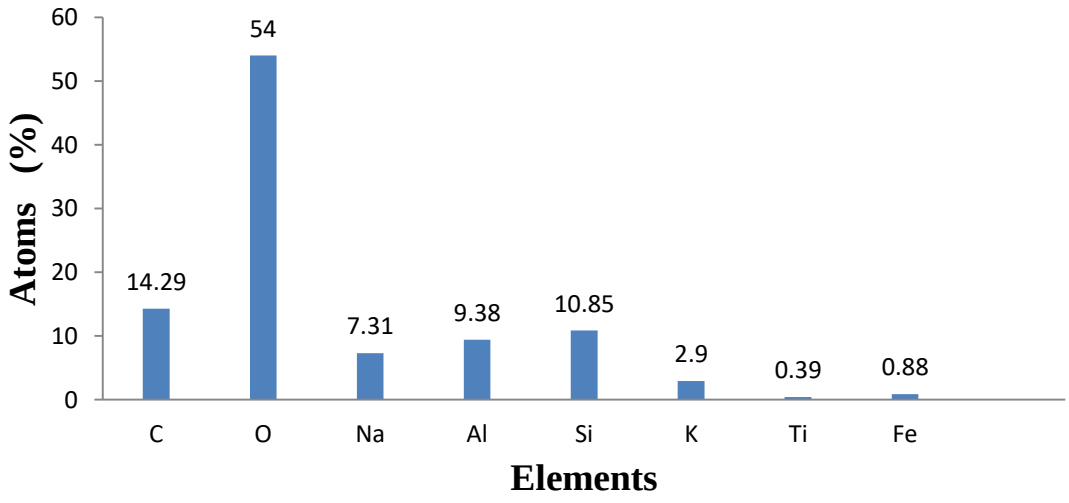

Figure 4.14: EDX result for the optimum synthesised phillipsite

4.2.3 Optimisation study of phillipsite production

4.2.3.1 Experimental design for the phillipsite production

The central composite design was used to make the experimental design of phillipsite as shown on Table 4.4.

Table 4.4: Experimental design matrix for phillipsite synthesis

Std	Runs	A: Aging time (h)	B: Cryst temp (°C)	C: Cryst time (h)	Crystallinity (%)
1	3	24.00	95.00	31.00	36.64
2	8	48.00	95.00	31.00	10.86
3	15	24.00	125.00	31.00	34.32
4	6	48.00	125.00	31.00	40.74
5	14	24.00	95.00	120.00	64.97
6	19	48.00	95.00	120.00	48.74
7	2	24.00	125.00	120.00	53.31
8	10	48.00	125.00	120.00	63.45
9	1	15.82	110.00	75.50	53.17
10	20	56.18	110.00	75.50	51.1
11	9	36.00	84.77	75.50	33.89
12	4	36.00	135.23	75.50	57.42
13	12	36.00	110.00	0.66	8.20
14	7	36.00	110.00	150.34	64.85
15	17	36.00	110.00	75.50	72.26
16	18	36.00	110.00	75.50	60.13
17	13	36.00	110.00	75.50	59.58
18	5	36.00	110.00	75.50	66.30
19	16	36.00	110.00	75.50	47.19
20	11	36.00	110.00	75.50	49.83

The effect of aging time on the percentage crystallinity of synthesised phillipsite

It was observed from the plot of aging time versus crystallinity in Figure 4.15 that as aging time increased from 24 to 48 h, percentage crystallinity decreased from 58.87 to 54.63% at crystallisation temperature of 110 ^{o}C and crystallisation time of 75.50 h. However it was observed in Table 4.4 that as aging time increased from 18.52 to 56.18 h, the percentage crystallinity decreased slightly 53.17 to 51.10%. It could therefore be infered that lower aging time favours higher percentage crystallinity. This observation was in agreement with Mirfendereski and Mohammadi (2018) who reported that percentage crystallininty decreases with increasing aging time. The authors further explained that the low crystallinity was a function of the quantity of aluminosilicate nuclei available in the precursor gel. Abdullahi *et al*. (2017) attributed the decrease in crystallinity to the seed nuclei that were formed during the aging period were loosing energy and gradually becoming inactive during zeolitization.

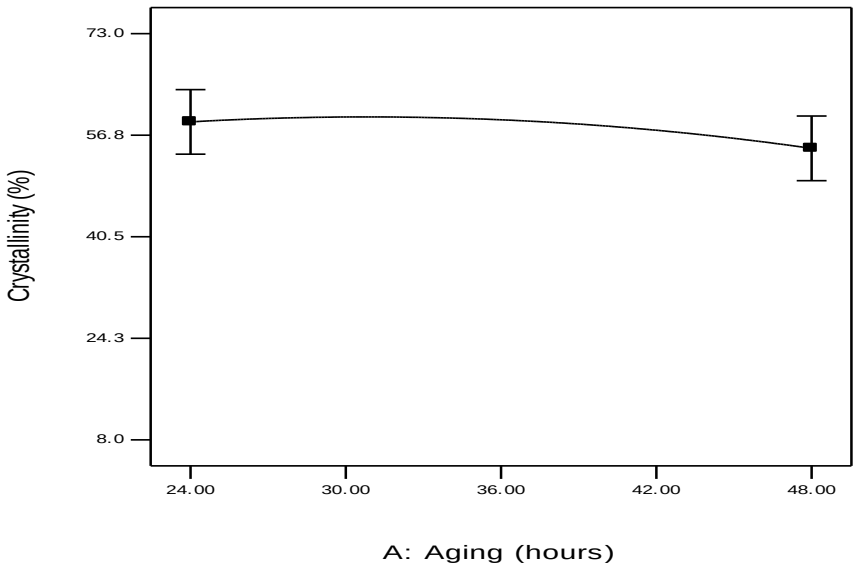

Figure 4.15: The effect of aging time on percentage crystallinity of Phillipsite

The effect of crystallisation temperature on percentage crystallinity of phillipsite

The plot of crystallisation temperature and percentage crystallinity in Figure 4.16 showed that there was an increase in crystallinity from 49.32 to 60.63% as crystallisation temperature increased from 95 to 118 ^{o}C. However the percentage crystallinity began to decline to 59.60% at 125 ^{o}C. It was observed from Table 4.4 that as temperature increased from 84.77 to 135.25%, there was an increase from 33.89 to 75.50% crystallinity of phillipsite. Similarly, Johnson *et al*. (2014) had reported that increase in crystallisation temperature would increase crystal growth rate and nucleation rate. Abdullahi *et al*. (2017) had further reported that crystallisation temperature was necessary for a specific type of zeolite synthesis because the desired zeolite phase can only be synthesised under a defined range of temperature. Kowalak *et al.* (2015) had reported that different temperature ranges determines the type of phillipsite synthesised.

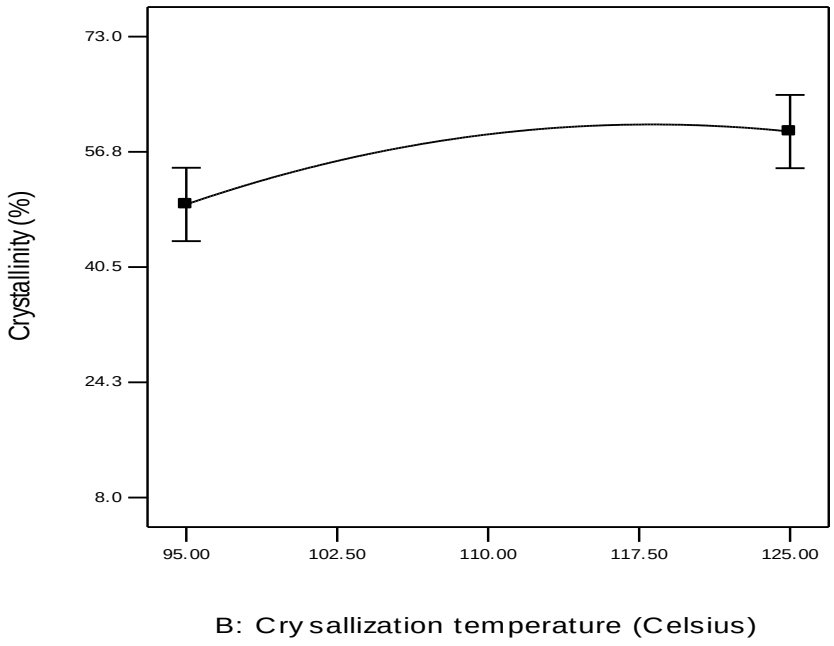

Figure 4.16: The effect of crystallisation temperature on the percentage crystallinity of phillipsite

The effect of crystallisation time on the percentage crystallinity of phillipsite

It was generally observed in Table 4.4 that as crystallisation time increases from 0.66 to 150.34 h, percentage crystallisation increased from 8.2 to 64.85 %. Figure 4.17 showed the effect of crystallisation time on the percentage crystallinity of Phillipsite under aging time of 36 h and crystallisation temperature of 110 ^{o}C. It was observed that percentage crystallinity of phillipsite increased from 38.36 - 66.11% when crystallisation time increased from 31 - 120 h. The difference of 27.75% was significantly high and it revealed the most important variable in the synthesis of Phillipsite. Ayele *et al*. (2016) observed that crystallisation time influences greatly, the quality of zeolite produced and not just the type of zeolite obtained. Abdullahi *et al*. (2017) reported that percentage crystallinity of zeolite should increase under a long crystallisation time. Kowalak *et al*. (2015) had also reported that in order to produce a highly crystalline phillipsite, crystallisation time had to be longer than 24 h.

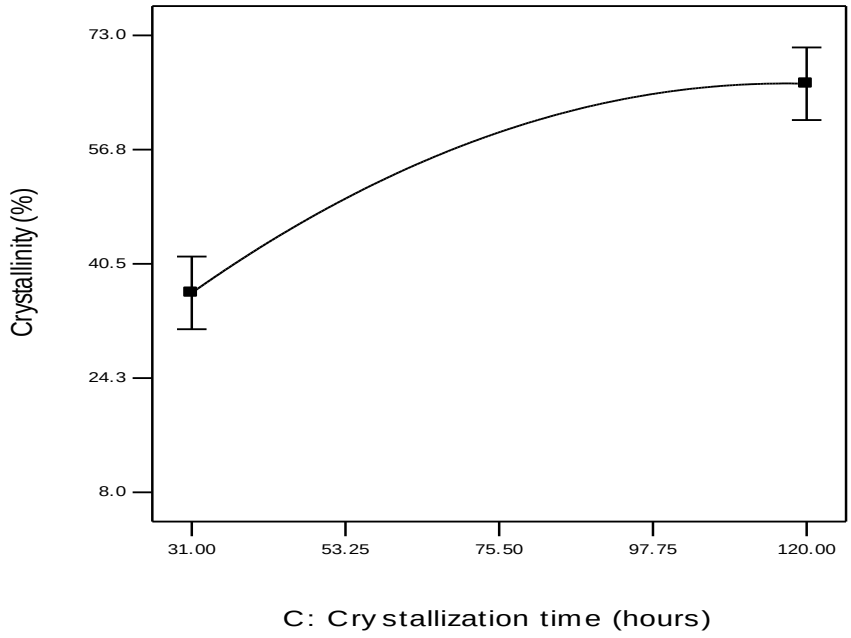

Figure 4.17: The effect of crystallisation time on percentage crystallinity of phillipsite

Effect of interactive variables on phillipsite crystallinity

The Figure 4.18 shows the relationship between crystallisation temperature, aging time and percentage crystallinity. The 3D plot shows that as aging time increased from 24 to 48 h, the percentage crystallinity decreases while as crystallisation temperature increase from 95 to 125 ^{o}C, the percentage crystallinity began to increase slightly. It was observed that the crystallisation temperature of 121.82 ^{o}C and aging time at 43.91 h would interact to give 61.65% crystallinity when crystallisation time at 75.50 h was kept constant.

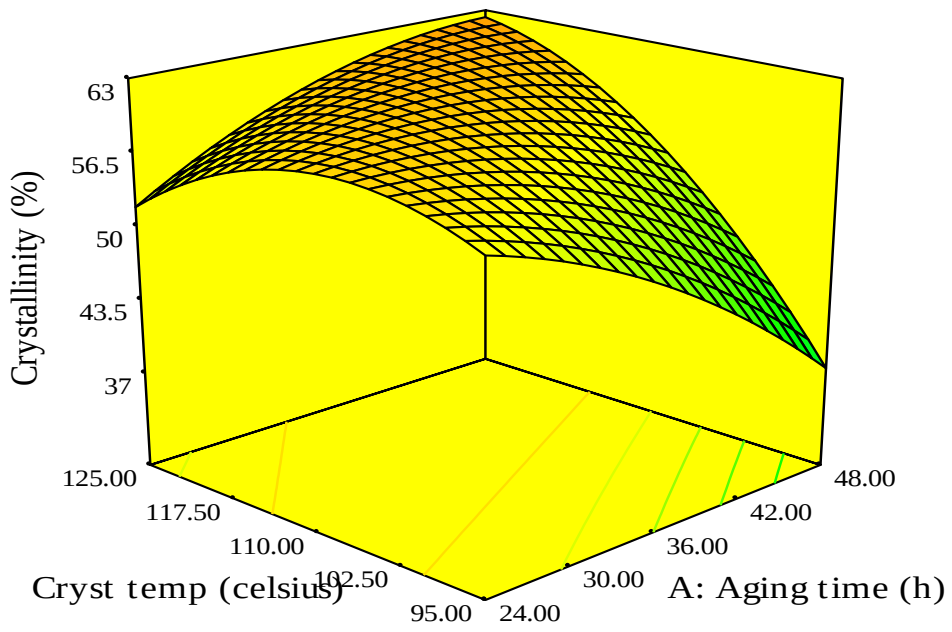

Figure 4.18: Effect of 3D plot showing the relationship between aging time, and crystallisation temperature on percentage crystallinity for phillipsite

Figure 4.19 shows the interactive effects of crystallisation time and aging time on the percentage crystallinity of phillipsite. The Figure 4.19 showed that as the aging time increased from 24 to 48 h, the percentage crystallinity decrease was low while the

response of percentage crystallinity increased immensely with increase in crystallisation time from 31 to 120 h. The interactive effect of both the crystallisation time at 113.78 h and aging time at 34.42 h gave 66.15% crystallinity when crystallisation temperature at 110 ^{o}C was kept constant.

e

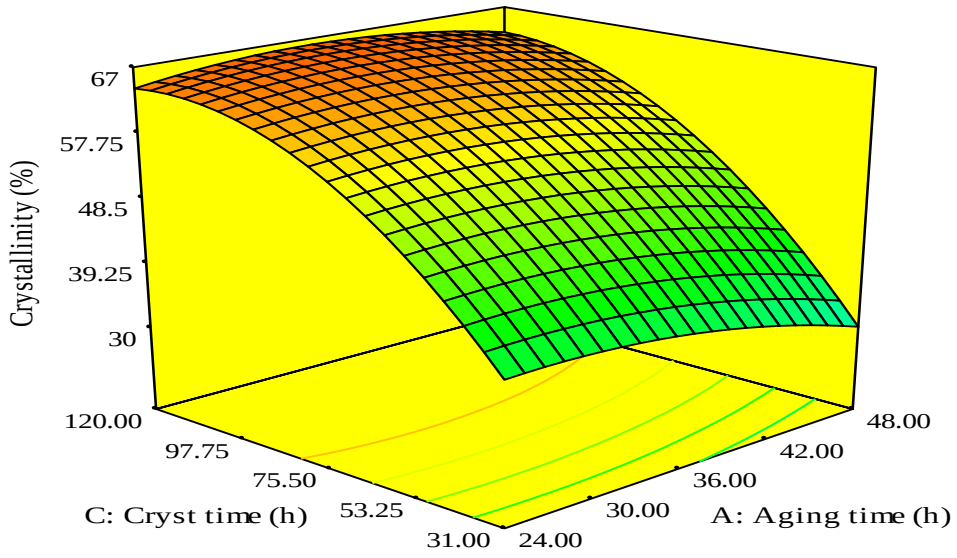

Figure 4.19: Effect of 3D plot showing the relationship between aging time, and crystallisation time on percentage crystallinity for phillipsite

Figure 4.20 showed the interactive effect of crystallisation time and crystallisation temperature synthesis variables on percentage crystallinity of phillipsite. The figure showed that the percentage crystallinity of the synthesised phillipsite increased remarkably as crystallisation temperature increased from 95 to 125 ^{o}C. It was however observed that as crystallisation time increased from 31 to 120 h, the percentage crystallinity increased sharply more than the corresponding result of the crystallisation temperature. The interactive effect for crystallisation time at 111.56 h and crystallisation

temperature at 114.59 ^{o}C gave 66.40% crystallinity when aging time at 36 h was kept constant.

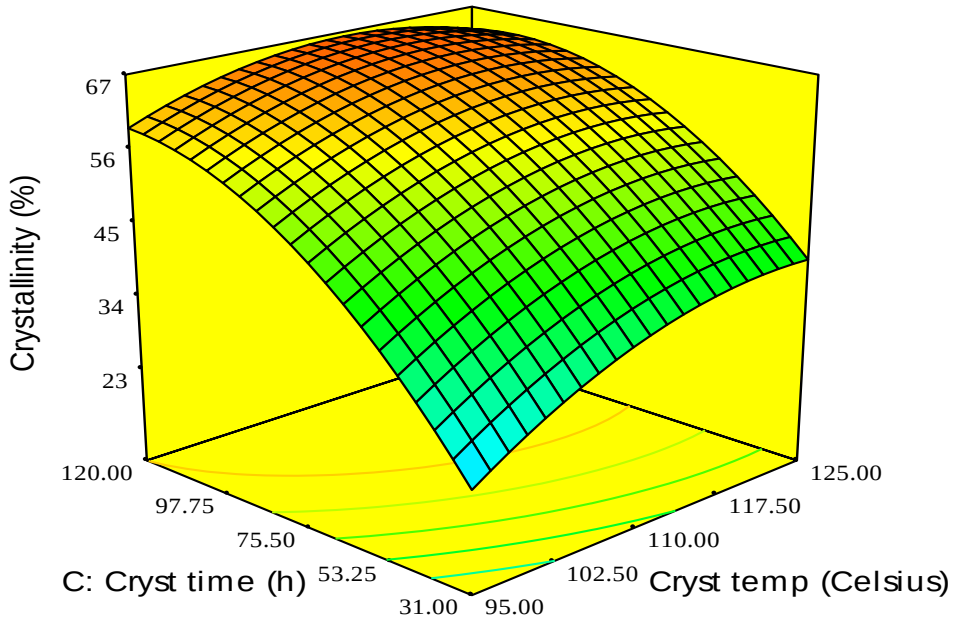

Figure 4.20: Effect of 3D plot showing the relationship between crystallisation time and crystallisation temperature on percentage crystallinity for Phillipsite

4.2.3.2 Response equation development for phillipsite production

The regression equation developed for the crystallinity of Phillipsite is shown in Equation 4.2. The most significant term in the synthesis of phillipsite as observed from the regression equation was the crystallisation time followed by the crystallisation temperature. The response equation in terms of coded factors is given in Equation 4.2

Crystallinity = 59.2 + 5.14 B + 14.88 C + 7.32 AB - 4.74 B^2 - 7.97 C^2 (4.2)

Given that A = aging time, B = Crystallisation temperature , C = Crystallisation time

4.2.3.3 Test for adequacy of the model for phillipsite production

The accuracy and statistical significance of the regression model was estimated using the analysis of variance (ANOVA) (Ogunleye *et al*., 2016) as shown in Table 4.5

Table 4.5: ANOVA for response surface quadratic model of phillipsite synthesis

Source	Sum of Square	df	Mean Square	F-Value	P-Value	Coeff. Of terms	Remark
Model	5139.34	9	571.04	10.37	0.0005		Signific.
A- Aging	61.29	1	61.29	1.11	0.3163	-2.12	
B-Cryst Temp	360.67	1	360.67	6.55	0.0284	5.14	
C-Cryst Time	3022.92	1	3022.92	54.88	0.0001	14.88	
AB	428.81	1	428.81	7.79	0.0191	7.32	
AC	22.01	1	22.01	0.40	0.5415	1.66	
BC	75.09	1	75.09	1.36	0.2700	-3.06	
A^2	86.78	1	86.78	1.58	0.2379	-2.45	
B^2	324.47	1	324.47	5.89	0.0356	-4.74	
C^2	916.09	1	916.09	16.63	0.002	-7.97	
Residual	550.80	10	55.08				
Lack of Fit	96.79	5	19.36	0.21	0.9425		Not signific.

The Model F-value of 10.37 implies the model was significant. There was only 0.05% chance that the "Model F-Value" this large could occur due to noise. Values of "Prob > F" less than 0.0500 indicated model terms were significant. In this case B, C, AB, B^2, C^2 were significant model terms. P - values greater than 0.1000 indicate the model terms were not significant. The "Lack of Fit F-value" of 0.21 implied the Lack of Fit

was not significant relative to the pure error. There was a 94.25% chance that a "Lack of Fit F-value" this large could occur due to noise. Non-significant lack of fit was good.

Table 4.6: Statistical parameters for the percentage crystallinity of phillipsite data analysis from model

Std.Dev	Mean	C.V. %	PRESS	Pred R-Squared	Adj R-Squared	R-Squared	Adeq Precision
7.42	48.85	15.19	1395.21	0.7548	0.8161	0.9032	11.051

The "Pred R-Squared" of 0.7548 is in reasonable agreement with the "Adj R-Squared" of 0.8161. "Adeq Precision" measures the signal to noise ratio. A ratio greater than 4 is desirable. The ratio of 11.051 indicated an adequate signal. The regression equation for the percentage crystalliinty of Phillipsite in terms of coded factors is given in Equation 4.2

4.3 Functionalisation of Zeolite A

The porous nature of zeolite confers on it high adsorptive and cation exchange property. The negative charged porous surface of zeolites makes them easily attract and carry alkaline metals in its pores by ion exchange mechanism. The process of carrying oxyanions (phosphates and nitrates) requires reverting the negative surface charge of the zeolite to positive to cause an intense attraction between the surfactant (HDTMA) and the zeolite adsorbent. It is this adsorptive process that requires optimisation in the development of a zeolite based slow release fertilizer. The adsorption process is further enhanced by the statistical design of experiment using Response surface methodology to provide the optimum conditions for the efficient utilisation of the adsorbent. The desired product with its optimum conditions is obtained with fewer experimental runs using

central composite design, a tool used to optimise any process especially multiple variables with their interactive effects on the response indicators. Table 4.7 shows the experimental design matrix for the adsorption of HDTMA on to zeolite A.

4.3.1 Optimisation study of the adsorption of HDTMA on zeolite A

4.3.1.1 Experimental design for the adsorption of HDTMA on zeolite A

The central composite design used for the adsorption of HDTMA on zeolite A has three independent variables which are initial concentration of HDTMA, adsorption temperature and contact time to give a total of 20 experimental runs in a standard order as shown in Table 4.7 of the test results.

Table 4.7: Experimental design matrix of the adsorption of HDTMA on zeolite A

Std	HDTMA conc mmol/ kg	Temp Celcius	Contact time (h)	Amount adsorbed (q) mg /g
1	81.3	25	8	3.75
2	243.9	25	8	5.95
3	81.3	65	8	0.50
4	243.9	65	8	2.00
5	81.3	25	24	0.50
6	243.9	25	24	5.25
7	81.3	65	24	0.35
8	243.9	65	24	2.00
9	25.87	47.5	16	1.95
10	299.33	47.5	16	5.85
11	162.6	25	16	7.55
12	162.6	65	16	1.30
13	162.6	47.5	2.55	0.00
14	162.6	47.5	29.45	0.60
15	162.6	47.5	16	1.10
16	162.6	47.5	16	0.70
17	162.6	47.5	16	1.35
18	162.6	47.5	16	0.60
19	162.6	47.5	16	1.00
20	162.6	47.5	16	1.25

4.3.1.2 Effect of process parameters on the adsorption of HDTMA on zeolite A

The observation shown in Figure 4.21 revealed that as the concentrations of HDTMA increase from 81.3 - 243.90 mmol/kg, the amount adsorbed on zeolite A increased from 0.72 – 3.16 mg/g indicating a positive main effect on adsorption capacity. This trend is similar to Demircvi and Saygili (2014) who reported that HDTMA sorption percentages on vermiculite, perlite, and zeolite clays increased with increasing the initial concentration of HDTMA.

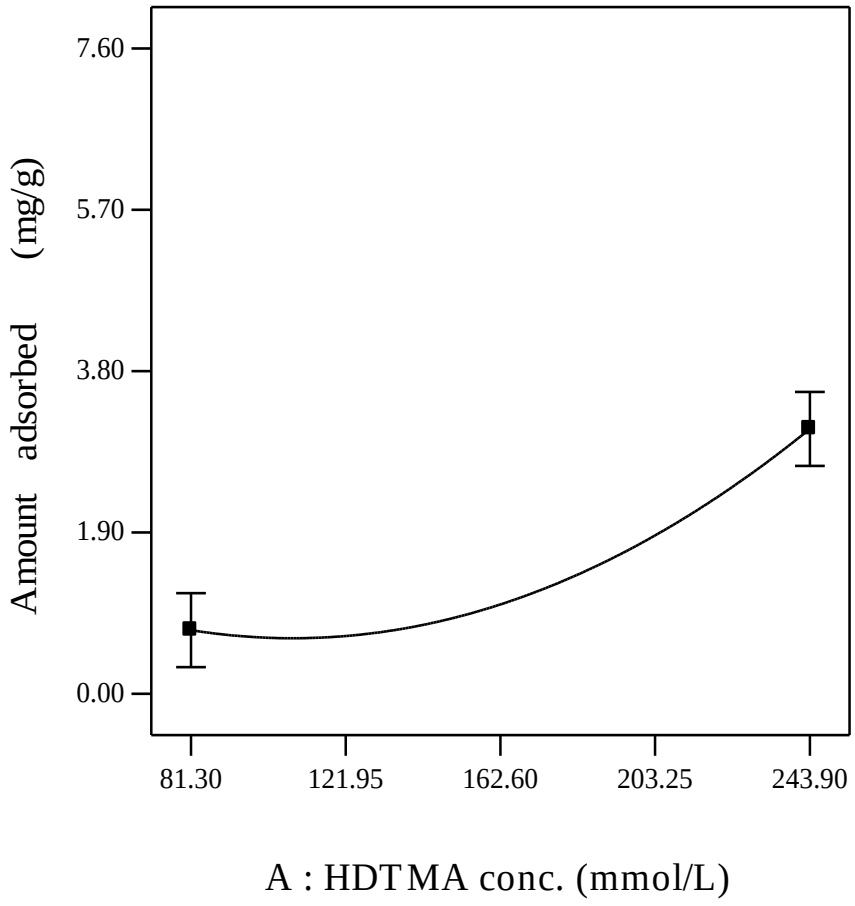

Figure 4.21: Main effect of HDTMA concentration of the amount adsorbed on Zeolite A

It was also observed in Figure 4.22 that as temperature increased from 25 to 65 ^{o}C the the amount adsorbed on zeolite A decreased from 3.68 to 0.58 mg/g. The increase in

temperature had a main negative effect on adsorption capacity on zeolite A. This trend is similar to Ghomashi *et al*. (2020) who reported that though the optimum temperature was found to be 25 ^{o}C, an increase in temperature lead to HDTMA surfactant desorption from the zeolite.

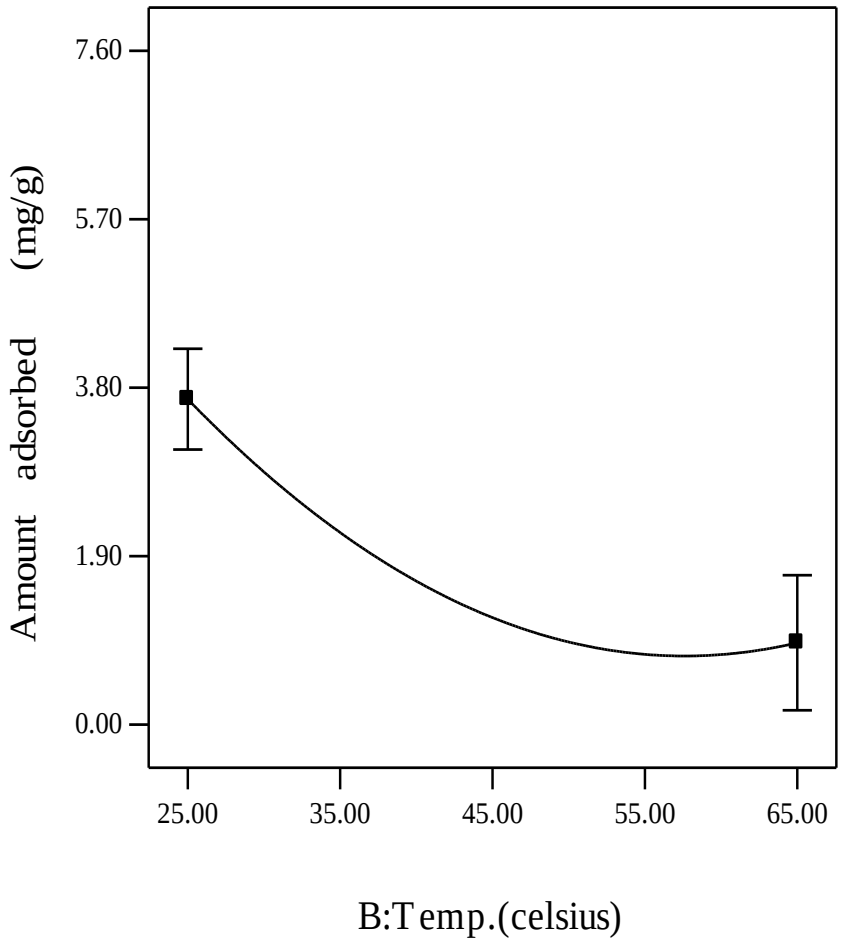

Figure 4.22: Main effect of temperature on the amount adsorbed on Zeolite A

Figure 4.23 showed the plot of the amount adsorbed and contact time. It was observed that there was a slight increase in adsorption from 8 to 13.78 h and thereafter a noticeable decrease in amount adsorbed as contact time increased from 16 to 24 h. The reduction of the amount adsorbed at higher HDTMA concentration may have been as a result of excess, loosely bound HDTMA from admicelles on the organo-zeolite into the aqueous solution (Anari and Nezamzadeh, 2015).

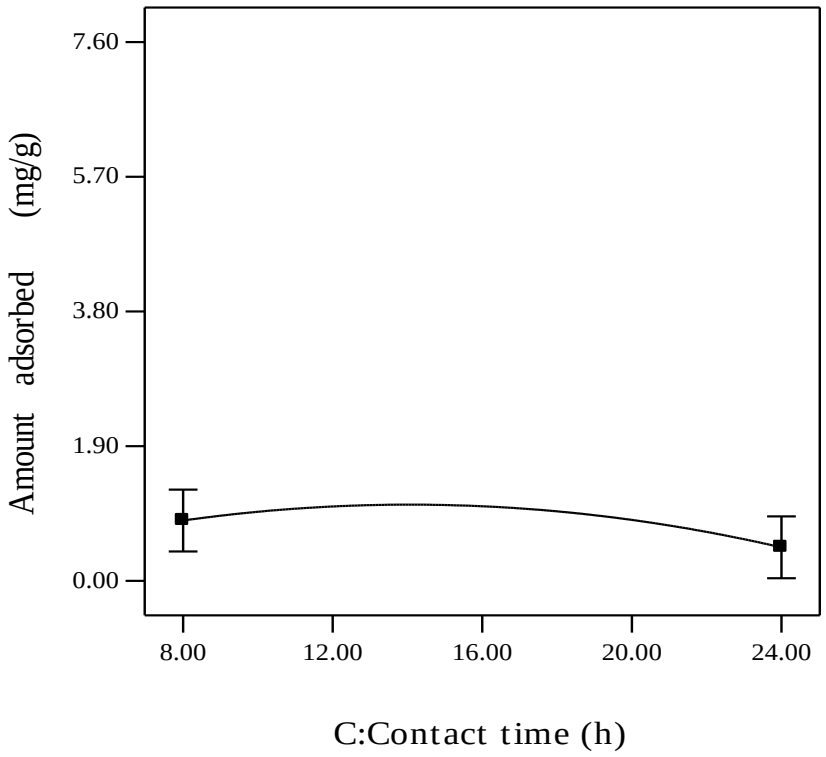

Figure 4.23: Main effect of contact time on the amount adsorbed on Zeolite A

The effect of interactive variables on the amount of HDTMA adsorbed on zeolite A

Response surface methodology is a statistical approach used to maximize the adsorption process by optimization of operational variables. The interactive effects among the adsorption process were also determined by this statistical technique in contrast to conventional methods which could not determine interactive effects among adsorption process variables.

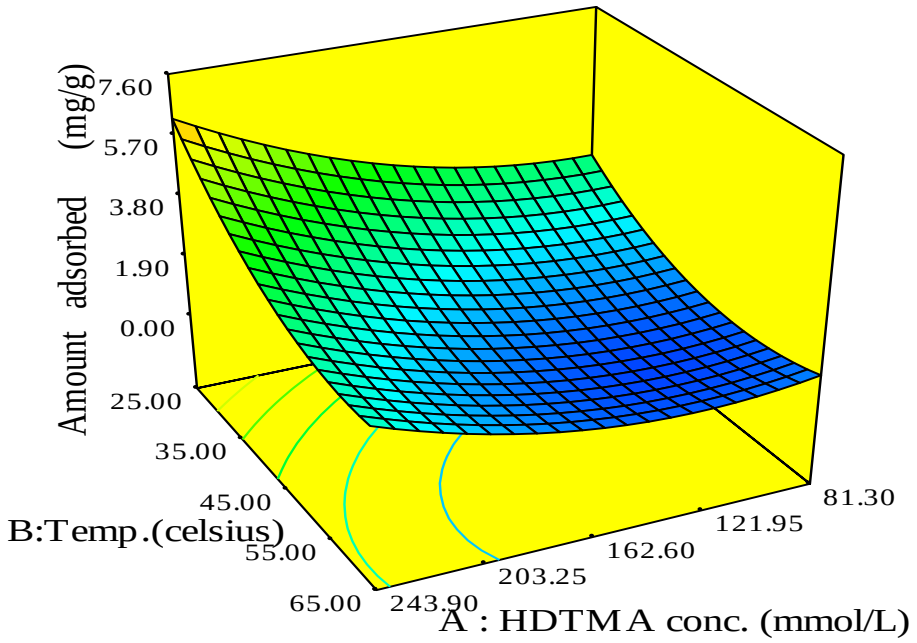

Figure 4.24: Effect of 3D response surface plot showing the interactive effect of temperature and HDTMA concentration on the amount adsorbed on zeolite A

The Figure 4.24 showed the relationship between amount adsorbed, temperature and concentration of HDTMA on zeolite A. The 3D plot showed that as temperature increased from 25 to 65 ^{o}C, the amount adsorbed decreased while as the concentration of HDTMA increased from 81.30 to 243.90 mmol/L, there was generally an increase in the amount adsorbed on zeolite A. The amount of HDTMA adsorbed for the interactive effects was 6.27 mg/g when the HDTMA concentration was 243.80 mmol/L and temperature was 25.21 ^{o}C.

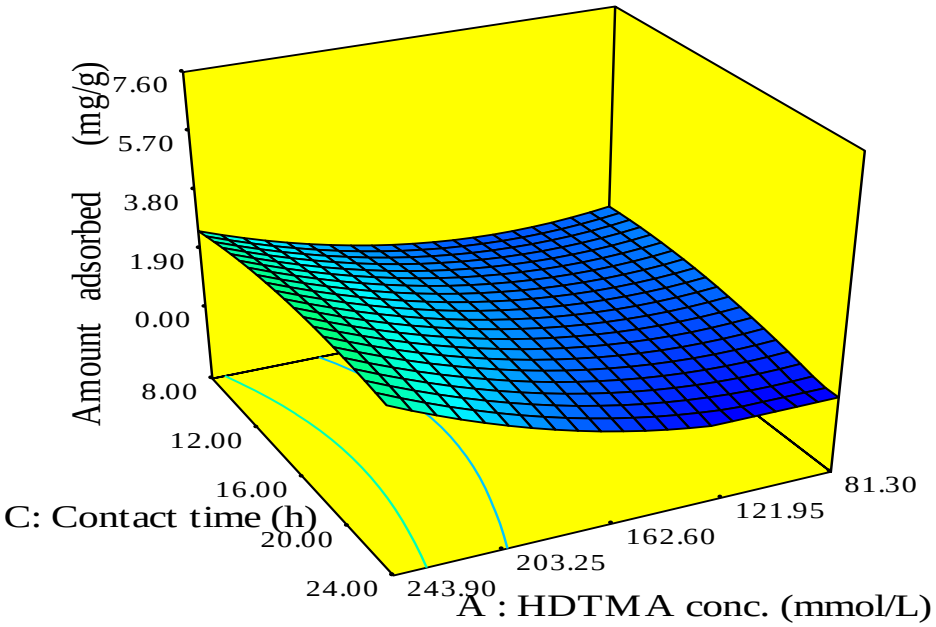

Figure 4.25: Effect of 3D response surface plot of contact time and concentration of HDTMA on the amount adsorbed on zeolite A

Figure 4.25 showed the interactive effects of contact time and HDTMA concentration on amount adsorbed on zeolite A. The response surface showed that as contact time increased from 8 to 24 h, the amount adsorbed on zeolite A decreased and simultaneously as the HDTMA concentration increased from 81.30 – 243.90 mmol/L, the amount adsorbed increased. The maximum effect of these two variables interaction resulted to an adsorbed amount of 2.72 mg/g when HDTMA concentration was 243.75 mmol/L and contact time was 8.15 h.

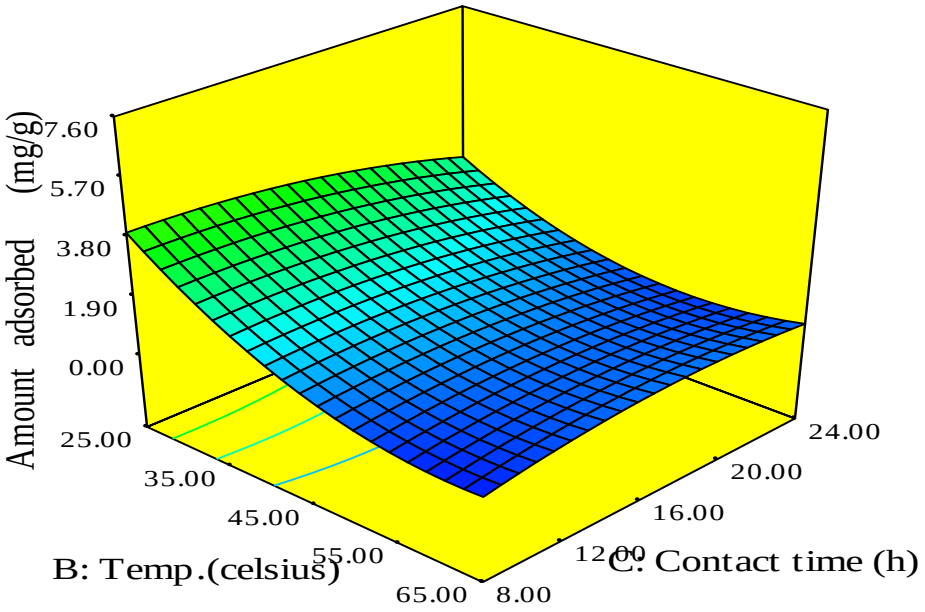

Figure 4.26: Effect of 3D plot of the interactive effect of contact time and temperature on the amount adsorbed on zeolite A

Figure 4.26 showed the interactive effects of contact time and temperature on the amount adsorbed on zeolite A. It was observed that as temperature increased from 25 to 65 ^{o}C, the amount adsorbed reduced while as contact time increased from 8 to 24 h, the amount adsorbed increased. However, it was observed that the maximum interactive effect of the two variables gave an adsorbed amount of 4.02 mg/g when contact time was 8.05 h and temperature was 25.09 ^{o}C.

4.3.1.3 Response equation development for the adsorption of HDTMA on zeolite A

The response of the amount of HDTMA adsorbed zeolite A was proposed by Design Expert software derived from the experimental adsorption process.

Amount adsorbed (q) = +1.01 + 1.22 A – 1.55 B + 0.93 A^2 + 1.12 B^2 (4.3)

Given that A = HDTMA concentration, B = Adsorption temperature and C = Contact time. Equation 4.3 is valid within the range of HDTMA concentration of 25.87 to 299.33 mmol/kg, Adsorption temperature of 25 – 65 ^{o}C and contact time of 2.55 to 29.45 h. The most significant term in the adsorption process is the adsorption temperature as observed from the highest coefficient of the regression equation. The highest F-value from the ANOVA table also shows the adsorption temperature as the most significant model term

4.3.1.4 Test for adequacy of the model for the adsorption of HDTMA on zeolite A

The ANOVA table validates the response equation 4.3 as shown in Table 4.8.

Table 4.8: ANOVA for the model of the adsorption of HDTMA on zeolite A

Source	**Sum of Square**	**df**	**Mean Square**	**F-Value**	**P-Value**	**Coeff of terms**	**Remark**
Model	89.97	9	10.00	22.85	0.0001		Signific
A-HDTMA conc	20.32	1	20.32	46.46	0.0001	1.22	
B- Adsorption Temp	32.63	1	32.63	74.61	0.0001	1.55	
C-Contact Time	0.70	1	0.70	1.60	0.2347	-0.23	
AB	1.80	1	1.80	4.13	0.0696	-0.48	
AC	0.91	1	0.91	2.08	0.1795	0.34	
BC	1.80	1	1.80	4.13	0.0696	0.48	
A^2	12.47	1	12.47	28.50	0.0003	0.93	
B^2	17.94	1	17.94	41.01	0.0001	1.12	
C^2	1.69	1	1.69	3.87	0.0775	-0.34	
Residual	4.37	1	0.44				

Lack of Fit	3.93	5	0.79	8.83	0.0160

The Adequate Precision measures the signal to noise ratio. Ahmadkhaniha *et al*. (2015) reported a statistical analysis that showed a ratio greater than 4 was desirable. The ratio of 15.19 obtained with the model indicated an adequate signal. The model can therefore be used to navigate the design space. The coefficient of determination (R^2) with value 0.9536 obtained for the model in Table 4.9 indicated that only 95.36% of the experimental data are well represented within the range of the study. The optimized conditions obtained from the design expert software were suitable for the various types of adsorption process carried out. The value of coefficient of variation (CV) of 30.37 indicated a better precision and reliability of the experimental runs (Peng *et al*., 2018)

Table 4.9: Statistical parameters for the amount of HDTMA adsorbed on zeolite A data analysis from the model

Std.Dev	**Mean**	**C.V. %**	**PRESS**	**Pred R-Squared**	**Adj R-Squared**	**R-Squared**	**Adeq Precision**
0.66	2.18	30.37	31.59	0.6652	0.9119	0.9536	5.194

The "Predicted R-Squared of 0.6652 is not as close to the Adjusted R-Squared of 0.9119 as one might normally expect. This may indicate a large block effect with the model.

4.4 Functionalisation of Phillipsite

4.4.1 Experimental design for the adsorption of HDTMA on phillipsite

The central composite design used for the adsorption of HDTMA on phillipsite made use of three independent variables namely: initial concentration of HDTMA, adsorption temperature and contact time to give a total of 20 experimental runs in a standard order as shown in Table 4.10

Table 4.10 Experimental design matrix for the adsorption of HDTMA on phillipsite

Std	Run	HDTMA Conc. (mmol/L)	Temp. (Celcius)	Contact time (h)	Amount adsorbed (mg/g)
1	15	65	25	8	5.95
2	11	195	25	8	9.55
3	18	65	65	8	2.6
4	1	195	65	8	5.4
5	12	65	25	24	3.07
6	16	195	25	24	5.00
7	2	65	65	24	4.55
8	9	195	65	24	5.56
9	3	20.68	42.50	16	1.00
10	17	239.32	42.50	16	5.15
11	19	130	13.07	16	3.01
12	13	130	65	16	0.60
13	10	130	42.50	2.55	5.55
14	8	130	42.50	29.45	4.46
15	6	130	42.50	16	1.55
16	4	130	42.50	16	3.20
17	14	130	42.50	16	0.20
18	7	130	42.50	16	3.15

19	20	130	42.50	16	3.60
20	5	130	42.50	16	4.55

4.4.2 Effect of process parameters of the HDTMA adsorbtion on Phillipsite

The observation shown in Figure 4.27 revealed that as the concentrations of HDTMA increased from 65.00 to 195 mmol/kg, the amount adsorbed on phillipsite increased from 2.4 to 4.7 mmol/kg indicating a positive main effect on the amount adsorbed.

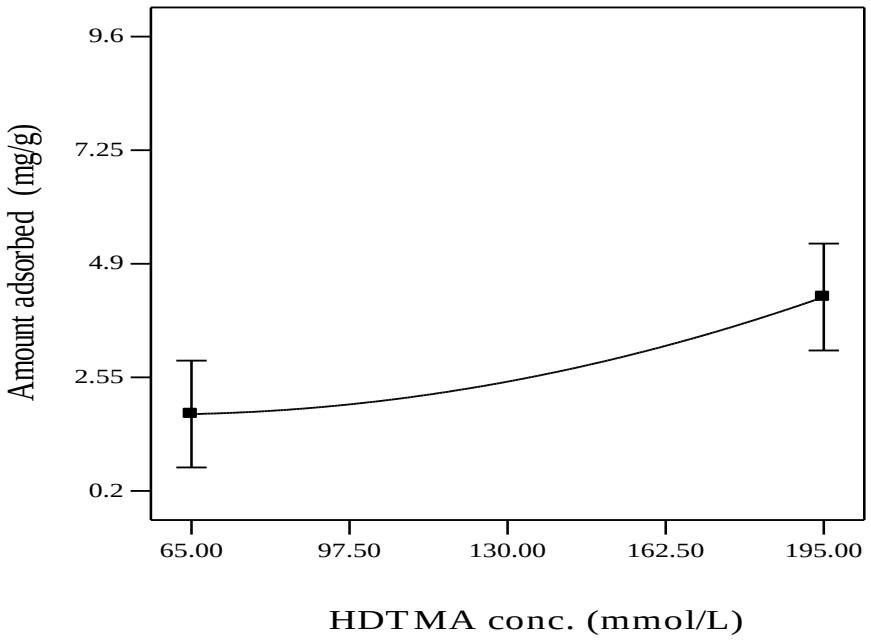

Figure 4.27: Main effects of HDTMA concentration on amount adsorbed on phillipsite

It was also observed in Figure 4.28 that as temperature increased from 25 to 65 ^{o}C the amount adsorbed on the phillipsite decreased from 3.42 to 2.03 mg/g. The increase in temperature had a main negative effect on amount adsorbed on phillipsite.

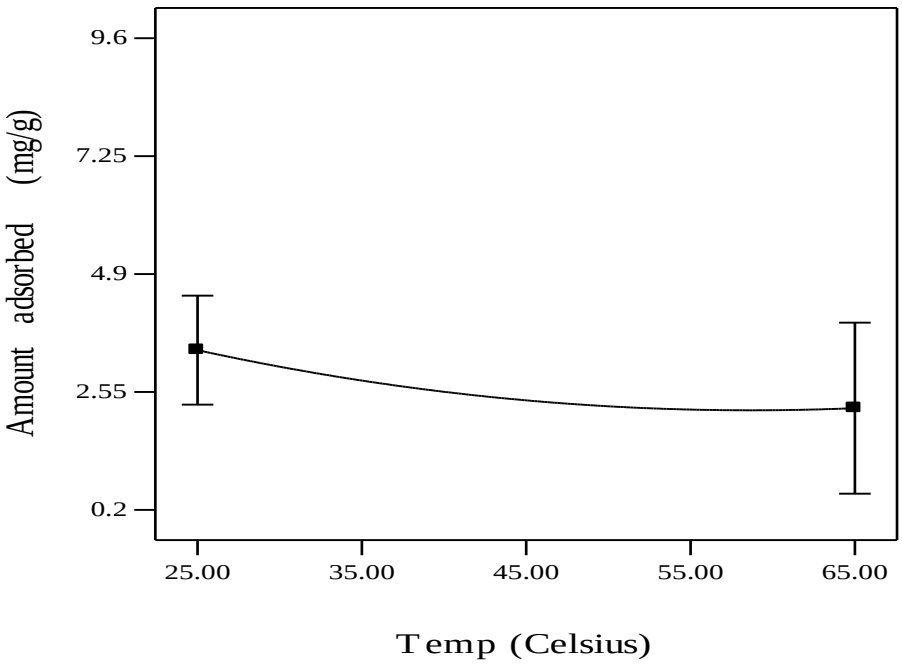

Figure 4.28: Main effects of temperature on the amount adsorbed on phillipsite

Figure 4.29 showed the plot of the amount adsorbed and contact time. It was observed that there was a decrease in adsorption as contact time increased from 8 to 17.29 h and thereafter a slight increase in amount adsorbed as contact time increased from 16 to 24 h. However, the plot showed the highest amount adsorbed occurred at contact time of 8 h. This trend may be attributed to the fact that the bulky HDTMA molecules have saturated the adsorption sites and therefore require more time to remove them from their adsorption sites in order for other molecules to get attached. This activity explains the initial decrease in adsorption capacity. The slight increase in the amount adsorbed could be traced to the formation of a bilayer on the existing monolayer by hydrophobic bonding.

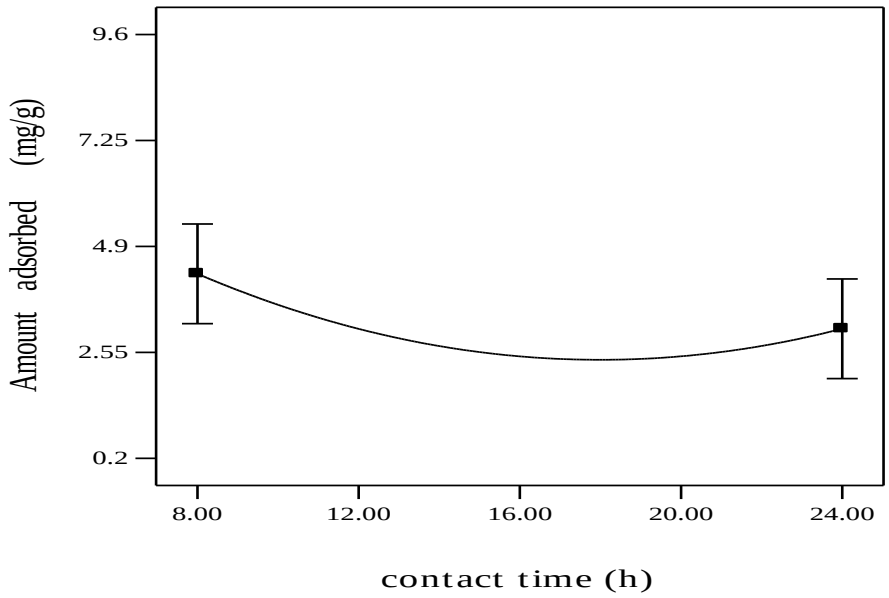

Figure 4.29: Main effects of contact time on the amount adsorbed on phillipsite

The effect of Interactive variables on the amount of HDTMA adsorbed on phillipsite

3D plots from Response Surface Methodology with the aid of statistical tools showed the interactive effects of variables involved in the maximization of the adsorption process involving HDTMA and Phillipsite

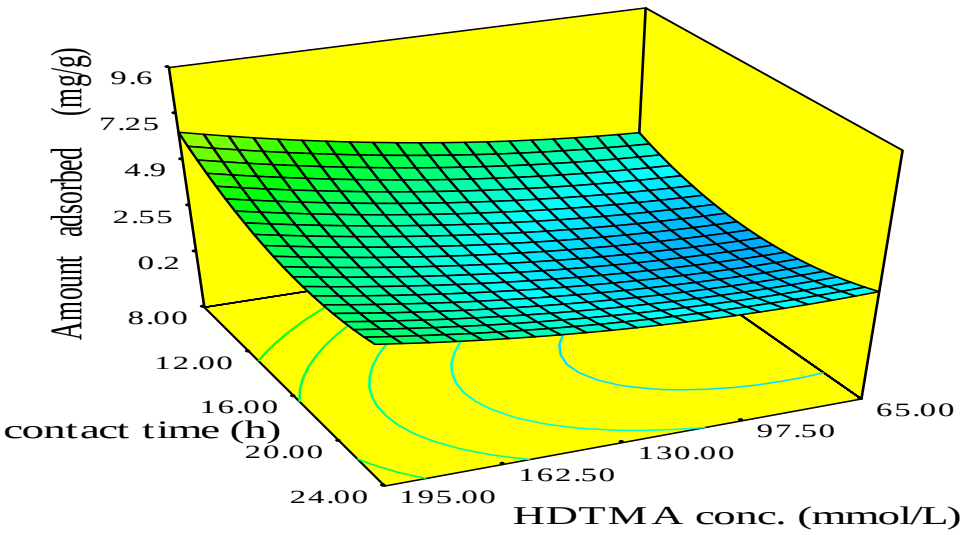

Figure 4.30: Effect of 3D response surface plot showing the interactive effect of contact time and HDTMA concentration on the amount adsorbed on phillipsite

The Figure 4.30 showed the relationship between amount adsorbed, contact time and concentration of HDTMA on Phillipsite. The 3D plot showed that as contact time increased from 8 – 24 h, there was a decrease in amount adsorbed and as concentration of HDTMA increased from 65 – 195 mmol/kg, and there was an increase in the amount adsorbed on Phillipsite. The net effect of the interactions between HDTMA concentration at 194.63 mmol/kg and contact time at 8.09 h produced an adsorbed amount of 6.48 mg/g when contact time at 8.09 h and HDTMA concentration at 194.61 mmol/L was kept constant.

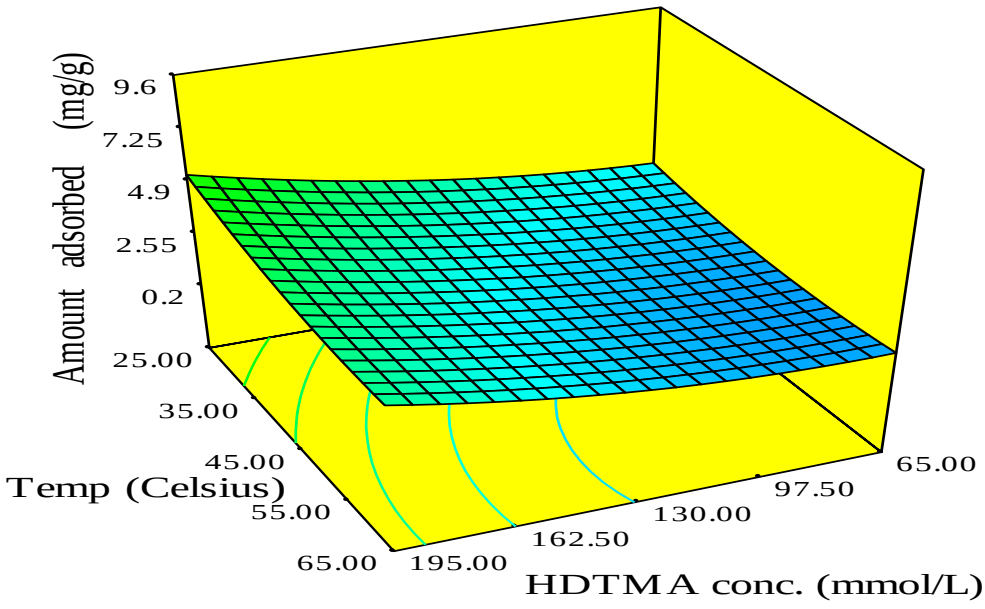

Figure 4.31: Effect of 3D response surface plot of the interactive effects of temperature and concentration of HDTMA on the amount adsorbed on phillipsite

Figure 4.31 showed the interactive effects of temperature and HDTMA concentration on amount adsorbed on phillipsite. The response surface showed that as temperature increased from 25 to 65 ^{o}C, the amount adsorbed on phillipsite decreased while as the

HDTMA concentration increased from 65 to 195 mmol/L, the amount adsorbed increased to 4.37 mg/g. The maximum interactive effect of temperature at 25.25 ^{o}C and HDTMA concentration at 194.77 mmol/L gave an adsorbed amount of 5.34 mg/g when contact time was 16 h.

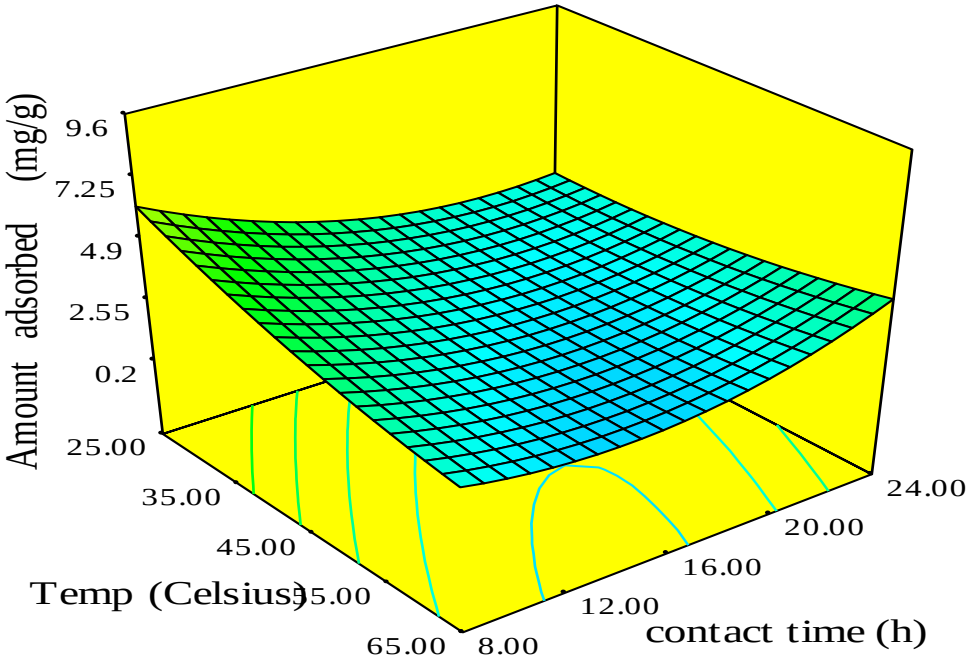

Figure 4.32: Effect of 3D surface plot of the interactive effect of contact time and temperature on the amount adsorbed on phillipsite

Figure 4.32 showed the interactive effects of contact time and temperature on the amount adsorbed on phillipsite. It was observed that as temperature increased from 25 to 65 ^{o}C, the amount adsorbed decreased while as contact time increased from 8 to 24 h, there was generally an increase in amount adsorbed. The net effect of the interaction of temperature at 25.23 ^{o}C and contact time at 8.05 h gave an adsorbed amount of 6.29 mg/g when HDTMA concentration was 130 mmol/kg.

4.4.3 Response equation development for the adsorption of HDTMA to Phillipsite

The regression model representing the experimental adsorption of HDTMA to phillipiste is given as in Equation 4.4

Amount adsorbed $(q) = +1.01 + 1.19 + 1.19\ BC + 1.20\ C^2$ (4.4)

Given that A = HDTMA concentration, B = Adsorption temperature and C = Contact time. Equation 4.4 is valid within the range of HDTMA concentration of 25.87 to 299.33 mmol/L, Adsorption temperature of 25 – 65 ^oC and contact time of 2.55 to 29.45 h. The most significant term in the adsorption process is the adsorption temperature as observed from the highest coefficient of the regression equation. The highest F-value from the ANOVA table also shows the adsorption temperature as the most significant model term followed by the HDTMA concentration and eventually the contact time. The Adequate Precision measures the signal to noise ratio. Ahmadkhaniha *et al*. (2015) reported a statistical analysis that showed a ratio greater than 4 was desirable. The ratio of 15.19 obtained with the model indicated an adequate signal. The model can therefore be used to navigate the design space. The coefficient of determination (R^2) with value 0.9536 obtained for the model in Table 4.11 indicated that only 95.36% of the experimental data are well represented within the range of the study. The optimized conditions obtained from the design expert software were suitable for the various types of adsorption process carried out.

Table 4.11: Analysis of variance of the response surface model for HDTMA adsorption on phillipsite

Source	Sum of Square	df	Mean Square	F-Value	P-Value	Coeff of terms	Remark
Model	66.66	9	7.41	3.09	0.0466		Sig.
A-HDTMA conc	19.50	1	19.50	8.14	0.0171	1.19	
B- Adsorption Temp	6.63	1	6.63	2.77	0.1272	-0.70	
C-Contact Time	3.75	1	3.75	1.56	0.2394	-0.52	
AB	0.37	1	0.37	0.15	0.7026	-0.21	
AC	1.50	1	1.50	0.62	0.4475	-0.43	
BC	11.38	1	11.38	4.75	0.0543	1.19	
A^2	3.99	1	3.99	1.67	0.2257	0.53	
B^2	0.08	1	0.08	0.036	0.8535	0.07	
C^2	21.05	1	21.05	8.79	0.0142	1.20	
Residual	23.94	10	2.39				
Lack of Fit	11.69	2.3	0.95		05202		Not sig.

The Model F-value of 3.09 signifies that the model is significant and that there is only a 4.66 % chance that a “Model F – value” this large could occur due to noise. The values of “Prob > F” less than 0.0500 indicate model terms are significant. Table 4.12 showed that A, C^2 are significant model terms. The values greater than 0.1000 indicate the model terms are not significant. The model could be reduced when its insignificant model terms are removed.

The "Lack of Fit F-value" of 0.95 implies the Lack of Fit is not significant relative to the pure error. There is a 52.02% chance that a "Lack of Fit F-value" this large could occur due to noise. Non-significant lack of fit gives a good fit for the model. The coeffiecients of the response surface given by Equation (4.5) were evaluated and the p-values showed that the model term coefficients of A, BC, and C^2 were more significant compared to the interactive terms AB, AC, BC and the quadratic terms. The regression model representing the adsorption of HDTMA molecules on Phillipsite fitted into the second order polynomial equation as shown in Equation 4.5

Table 4.12: Statistical parameters for the amount of HDTMA adsorbed on phillipsite data analysis from model

Std.Dev	Mean	C.V. %	PRESS	Pred R-Squared	Adj R-Squared	R-Squared	Adeq Precision
1.55	3.88	39.83	105.85	0.1683	0.0.4979	0.7357	6.428

A negative "Pred R-Squared" implies that the overall mean is a better predictor of the response than the current model.

4.4.4 Functional groups of the synthesised zeolites and modified zeolites

4.4.4.1 FTIR of zeolite A and HDTMA modified zeolite A.

The FTIR spectrum of the synthesised zeolites in Figure 4.33 showed vibrational bands with different types of functional groups present. The overall spectrum of FTIR is divided into two general regions: 4000 –1300 cm^{-1} (the functional group region) and 1300 – 400 cm^{-1} (the fingerprint region (Iqra *et al*., 2014). The frequency assignment approach was used for the interpretation of the spectrum.

The OH stretch and the asymmetric stretching of internal T-O bonds are characteristic peaks of zeolite A in Figure 4.33. The absorption bands near 3380 cm^{-1} represent OH groups on the surfaces of zeolite A and HDTMA-modified zeolite A. This showed that zeolites are hydrated materials. The OH band in the modified zeolite A spectrum also suggests that HDTMA only adsorbs on partial surface of the zeolites (Chao and Chen, 2012). The weak absorbance of signals near 1000 cm^{-1} for the zeolite A and HDTMA modified zeolite A in Figure 4.33 represents the presence of asymmetric stretching vibration modes of internal T-O bonds in TO_4 tetrahedral (T = Si and Al) on the surface. The strong absorbance signal near 1000 cm^{-1} for the HDTMA modified zeolite A is considered as the CN group on the surface. The absorbance of the HDTMA modified zeolite A located in the region below 1000 cm^{-1} are likely to have resulted from the alkyl groups of HDTMA on the zeolite surface (Chao and Chen, 2012). It is important to note that HDTMA molecules adsorb on the external surface of the zeolite and do not react completely with all the surface hydroxyl groups and HDTMA molecules are too big to enter the internal pores of zeolite A (Baniswal *et al*., 2006). The net effect of the adsorption leads to HDTMA modified zeolite A having the positive charge on the external surface and also the negative charge on the internal pore surface.

The bands observed at 2900 cm^{-1} and 2840 cm^{-1} in the modified zeolite A spectrum were attributed to symmetrical stretching vibration of C-CH_2 of alkyl chain while the band around 1400-1490 cm^{-1} was assigned to the trimethylammonium quaternary group vibration C-N$(CH_3)_3$ (Aroke and El-Nafaty, 2014; Maina, 2016). These spectra bands could be correlated with antisymmetric and symmetric C-H stretching of the methylene group. The extra peaks suggest that the HDTMA surfactant successfully modified the zeolite surface. There was no change in band positions after modification in Zeolite A and this showed that the basic zeolite structure was kept unchanged (Aseidu, 2016).

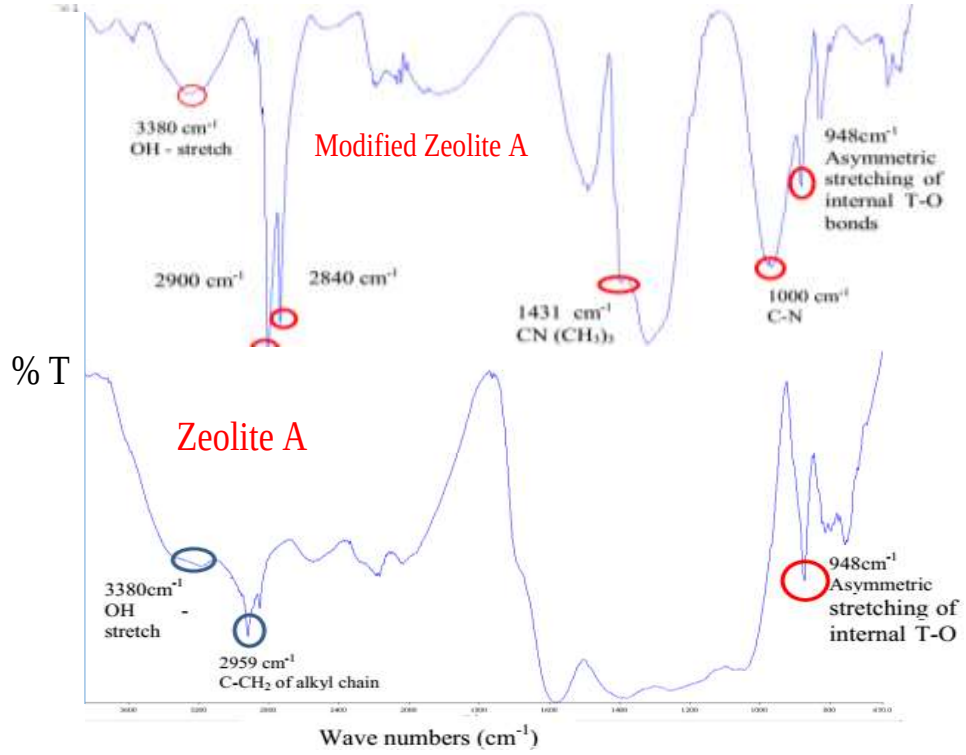

Figure 4.33: FTIR spectrum of synthesised zeolite A and modified zeolite A

4.4.4.2 FTIR of phillipsite and HDTMA modified phillipsite

The FTIR vibrational bands on phillipsite and HDTMA modified phillipsite in Figure 4.34 show structural stability of Phillipsite by the presence of characteristic peaks of OH- stretch group at 3380 cm^{-1}, Si – O group at 948 cm^{-1} and aluminium entities at the range of 1760 - 1240 cm^{-1} even after HDTMA modification (Chojnacka *et al.*, 2018). The absorption bands observed between 950 – 1250 cm^{-1} in Figure 4.34 were assigned to asymmetric stretch of the internal tetrahedral (Si – O – Si). Vibrational bands occurring between 1240 and 1610 cm^{-1} were attributed to OH deform (bending). The frequency band at 1490cm^{-1} in the modified phillipsite is assigned to antisymetric bending mode of the quaternary ammonium (alkyl) mode of the head methyl group $(CH_3)_3CN^+$ (Musyoka, 2012). It was also observed that as the adsorption of HDTMA on the external surface of the zeolite does not lead to the complete reaction of all the OH -

groups on the surface of the phillipsite as also reported by (Chao and Chen, 2012). The comparism of the FTIRs of zeolite A and Phillipsite before and after modification are presented in Table 4.13

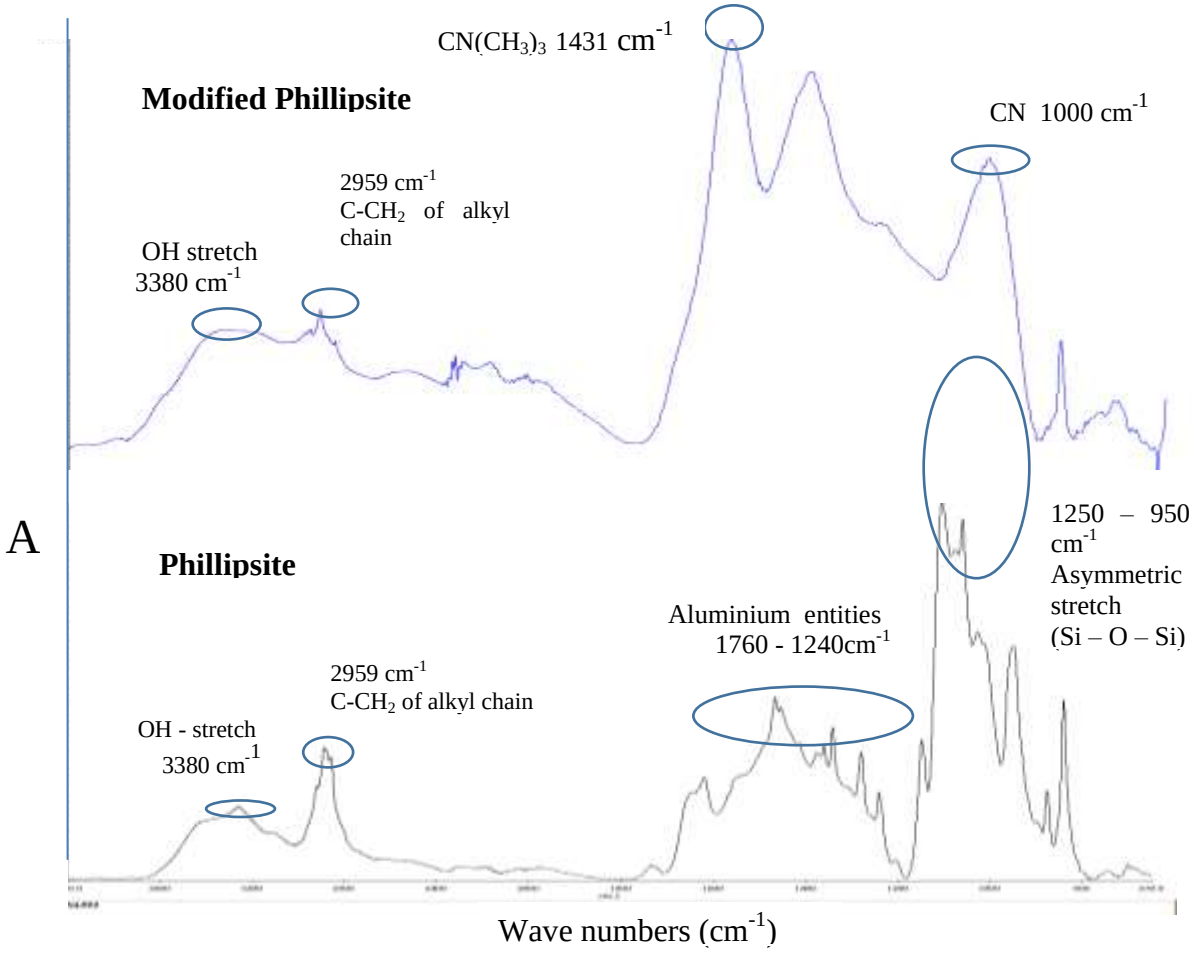

Figure 4.34: FTIR spectrum of phillipsite and modified phillipsite

Table 4.13: Comparison of FTIRs of zeolite A and phillipsite before and after modification

	Spectra band 1	Spectra band 2	Spectra band 3	Spectra band 4
Synthesised Zeolite A	OH – group 3700 – 3200 cm^{-1}	C-CH_2 bond symmetric stretching at 2959 cm^{-1}	Al containing entities and OH groups at 1650 -1050 cm^{-1}	Si – O group at 948 cm^{-1} Al – O at 780 cm^{-1} asymmetric stretching
Modified HDTMA Zeolite A	OH – group with high intensity	2900 and 2840 cm^{-1} attributed to symmetrical stretching of alkyl ammonium bromide	CN group at 1000 cm^{-1} and $CN^{+}(CH_3)_3$ at 1431 cm^{-1}	Si – O group at 948 cm^{-1} with peaks with lower intensities
Synthesised Phillipsite	OH – group 3200 – 3700 cm^{-1}	C – CH_2 of alkyl chain 2700 – 3000 cm^{-1}	Si–O-Si group symmetric and asymmetric bending 1240 - 950 cm^{-1}	Si – O group at 948 cm^{-1} asymmetric stretching
HDTMA modified Phillipsite	OH – group at 3380 cm^{-1} is within 3200 - 3700 cm^{-1}	C – CH_2 of alkyl chain at 2959 cm^{-1} with lower peaks	Quaternary ammonium alkyl mode of the head of $CN(CH_2)_3$ group 1400 – 1490 cm^{-1}	Si – O group at 948 cm^{-1} asymmetric stretching with lower peaks intensities

4.4.4.3 Textural analysis by Nitrogen adsorption

Surface areas and porosity are important characteristics responsible for the description of the adsorption process in zeolites. The BET surface area analyses were performed on the synthesised zeolites and their modifications as shown in Table 4.14. The samples were degassed under vacuum at 250 ^{o}C for 3 h to remove any residual moisture. It was observed that the specific surface areas of zeolite A and phillipsite reduced with HDTMA modification. The HDTMA modification of zeolite A decreased the specific surface area of zeolite A by 77.96% and the HDTMA modification of Phillipsite decreased the specific surface area of phillipsite by 13.57%. The high decrease observed in zeolite A could be attributed to the higher cation exchange capacity of zeolite A as shown in Table 4.15. Subsequent loading of phosphate ions (KH_2PO_4) and nitrate ions (NH_4NO_3) loading on the HDTMA-zeolite modifications reduced the surface areas of zeolite A and phillipsite further. Similarly, Fungaro and Magdalena, (2014) had observed that the modified zeolites show lower total BET surface area than the unmodified zeolite. The internal area of the zeolites was blocked and the miropore surface area decreased when the bulky molecules of the HDTMA are adhered on the external surface and pore openings of the zeolites. Chao and Chen, (2012) reported that similar trend was observed in reduction in the surface area and pore volume of the zeolites when surface modification took place.

Table 4.14: The BET results of specific surface area, porosity and pore size

	Specific Surface Area (m^2/g)	Porosity (%)	Pore Size (nm)
Raw Kaolin	340.73	1.322	2.2610
Zeolite A	296.178	1.025	0.4523
Modified Zeolite A	65.257	0.127	0.3488
Phosphate loaded Zeolite A	46.724	0104	0.3423
Nitrate loaded Zeolite A	62.272	0.134	0.3469
Phillipsite	361.510	1.137	0.4523
HDTMA modified Phillipsite	312.429	1.033	0.3523
Phosphate loaded Phillipsite	49.728	0.097	0.3469
Nitrate loaded Phillipsite	34.985	0.089	0.3423

Table 4.15: Cation Exchange Capacity (CEC) and External Cation Exchange Capacity (ECEC) values of Raw Ahoko Kaolin, Zeolite A and Phillipsite

	CEC (cmol/kg)	ECEC (cmol/kg)
Raw Ahoko Kaolin	50.87	0.43
Zeolite A	69.65	16.26
Phillipsite	64.08	12.60

4.5 Adsorption Isotherms

The adsorption isotherm studies showed how the HDTMA molecules distribute between the solid phase and the liquid phase when the adsorption process attains an equilibrium state. The curve gave essential physiochemical data for assessing the applicability of the adsorption process as a complete unit operation. The isotherm data were analysed by fitting them to different isotherm models in order to discover a suitable model for

optimizing the design parameters (Auta and Hameed, 2011). It further provided the basis of information needed for optimizing the design parameters for an adsorption process. The influence of various parameters such as surface coverage, contact time and temperature on the amount of HDTMA adsorbed on the synthesised zeolite A and phillipsite were studied.

4.5.1 Effect of surface coverage, contact time and temperature of HDTMA on adsorption capacity of Zeolite A and Phillipsite

An optimized zeolite A and Phillipsite require an isotherm to show the optimum surface coverage. Figure 4.35 illustrates that the increase in surface coverage of HDTMA on the zeolite in the range of 25 – 150% of the external cation exchange capacity (ECEC) for Zeolite A and Phillipsite resulted to a steady increase in the amount adsorbed. It was observed that as surface coverage of the adsorbate concentration increased to a value of 200% of the ECEC, an optimum adsorbed amount was attained and further increase surface coverage did not lead to significant adsorbed amount. The reason for the observed trend might be that the percentage of surface coverage which was greater than 200% exceeds the surfactant critical micelle concentration which results in the formation of another new layer (Hommaid and Hamdo, 2014). The increase in the amount of HDTMA molecules led to hydrophobic interactions between the hydrophobic sides of HDTMA molecules and second layer was formed on the zeolite surfaces. Negative surface charge of the zeolites reversed to positive by sorption of cationic surfactant molecule. Phillipsite with maximum adsorbed amount of 4.90 mg/g was higher than Zeolite A with 4.15 mg/g. The difference in the surface coverage of the two zeolites can be attributed to their chemical composition and and their initial HDTMA

concentrations. The initial concentration of HDTMA adsorbed on Phillipsite was 195 mmol/L while zeolite A was 162 mmol/L

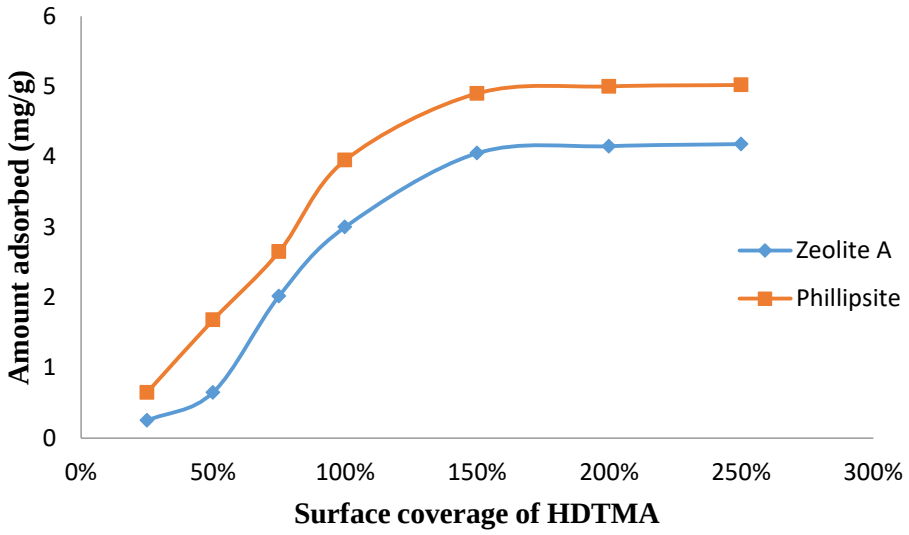

Figure 4.35: The effect of surface coverage of HDTMA concentration on the amount of HDTMA molecules adsorbed on zeolite A and phillipsite (Experimental conditions: stirring speed (150 rpm), temperature (25 ^{o}C) and stirring time (24 h))

Figure 4.36 illustrated that amount adsorbed increased steadily with increase in contact time for the first 8 h for zeolite A and the first 16 h for phillipsite. Thereafter, the two adsorbents exhibited constant adsorbed amount respectively until the contact time of 24 h. The time required to reach this state of constant adsorbed amount was described as the equilibrium time. The concentration of HDTMA adsorbed at the equilibrium time indicates the maximum adsorbed amount of zeolite A and phillipsite under the operating conditions. The remaining part of the curve with relatively constant adsorbed amount signified the non-availability of active sites for more positively charged HDTMA molecules to attach themselves. The variation in contact time of zeolite A and phillipsite may be attributed to the initial concentrations of HDTMA used. 162 mmol/L and 195 mmol/L of HDTMA were used for zeolite A and phillipsite respectively. The lower concentration of 162 mmol/L of HDTMA attained equilibrium with zeolite A faster

than the higher concentration of 195 mmol/L of HDTMA with Phillipsite under the same temperature and revolutions per minute. The contact time for Phillipsite is longer than that of zeolite A due to the larger pore volume. The attainment of 8 h for the equilibrium time for zeolite A is similar to the value obtained by Li *et al*. (2000) who reported the surface modification of clinoptilolite rich zeolitic tuff with Hexa-decyltrimethyl ammonium bromide (HDTMA-Br) at an agitation period of 8 h, 25 ^{o}C and 150 rpm.

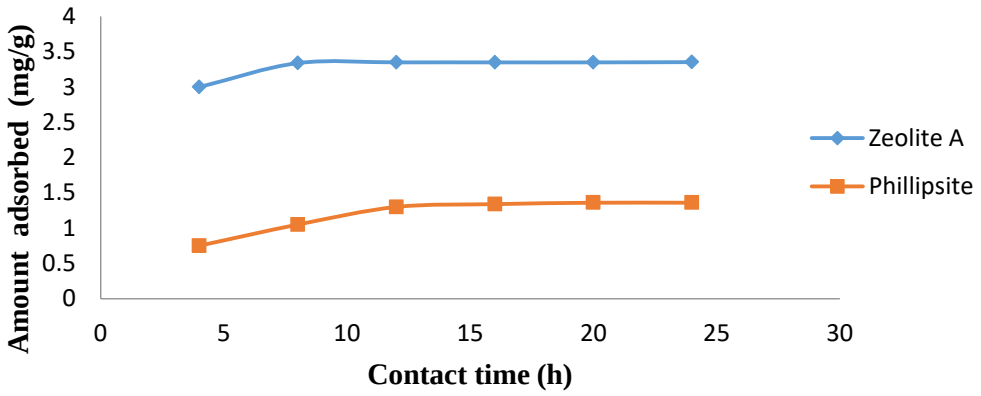

Figure 4.36: The effect of contact time on the amount of HDTMA adsorbed on zeolite A and phillipsite (Experimental conditions include adsorbent dosage (5 g), stirring speed (150 rpm), temperature 25 ^{o}C and HDTMA surface coverage of 162 mmol/L for zeolite A and 195 mmol/L for phillipsite)

The effect of temperature on the amount of HDTMA adsorbed on zeolite A and phillipsite was shown in Figure 4.37. It was generally observed that as temperature increased from 25 – 65 ^{o}C, the amount of HDTMA adsorbed decreased for the zeolites. The explanation for the observed trend may be traceable to the fact that as temperature increases, the solubility of HDTMA increases. Consequently, the interaction forces between the HDTMA molecules and the liquid solution were stronger than those within the HDTMA molecule and the zeolites' surfaces. Therefore, the HDTMA molecule is more difficult to adhere to the adsorbents (Saha and Chowdhury, 2011). This implies

that the optimum temperature for the adsorption of HDTMA molecules to zeolite A and phillipsite is favoured at lower temperature 25 ^{o}C. The amount of HDTMA molecule 3.4 mg/g adsorbed on phillipsite was higher than the amount of 3.10 mg/g adsorbed on zeolite A might be treacable to the differences of their specific surface areas where BET surface area for Phillipsite and zeolite A are 361.510 and 296.178 m^2/g respectively.

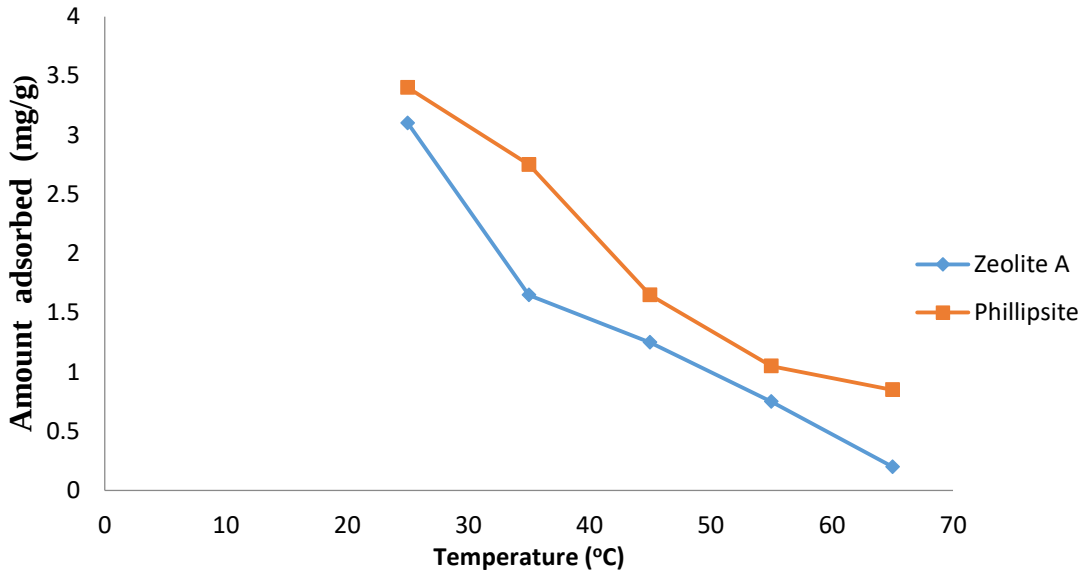

Figure 4.37: The effect of temperature on the amount adsorbed on zeolite A and phillipsite (Experimental conditions: adsorbent dosage (5 g), agitation speed (150 rpm), percentage of surface coverage for zeolite A and phillipsite was (100% of CEC))

4.5.2 Parameters of the isotherm models for the adsorption of HDTMA onto zeolite A and phillipsite

Four adsorption isotherm models such as Langmuir, Freundlich, Temkin and Dubinin-Radushkevich were used to fit the experimental data of the adsorption of HDTMA on zeolite A and phillipsite. The linear form of the isotherm models were used to determine the isotherm parameters of the adsorption process from their slope and intercept as presented in Table 4.16. The isotherm models are explained in (i), (ii), (iii) and (iv).

(i). The Langmuir isotherm model

The Langmuir isotherm model is used to measure and compare the adsorptive capacity of zeolite A and phillipsite. The description of the langmuir model based on the assumption that maximum adsorption corresponds to a saturated monolayer of the adsorbate molecule on the adsorbent surface tends to fit the modification of zeolite surface with cationic surfactant such as HDTMA (Saadi *et al*., 2015). The bulky molecules of HDTMA are adsorbed on a set of distinct localized adsorption sites on the zeolite surface especially when the initial concentration of HDTMA molecules is below the critical micelle concentration (cmc) or the external cation exchange capacity (ECEC) (Szala *et al*., 2015). The plot of Ce/qe against Ce from the linear form of Langmuir model gives a straight line whose slope and intercept is represented by adsorption capacity q_m and energy of adsorption b (L/mg). The calculated adsorption capacity from Langmuir isotherm model was observed to be 19.4530 mg/g for zeolite A and it was higher than phillipsite with 11.2310 mg/g. The plausible reason might be traceable to the maximum adsorbed amount on the surface coverage of zeolite A and phillipsite which was 4.15 and 4.90 mg/g respectively.

The essential characteristics of the Langmuir isotherm which is expressed by the separation factor R_L which shows the type of the isotherm to be either unfavourable ($R_L > 1$), linear ($R_L = 1$), favourable ($0 < R_L < 1$) and irreversible ($R_L = 0$). The value of zeolite A with $R_L = 0.2380$ and Phillipsite with $R_L = 0.0374$ show that zeolite A and

Phillipsite are favourable for the adsorption of HDTMA molecule under the conditions used in the study.

The correlation coefficient R^2 of zeolite A (0.9064) was closer to unity than correlation coefficient R^2 of Phillipsite (0.5700). According to the correlation coefficient, R^2 values, Langmuir isotherm model represents a better fit to the experimental data for the sorption of HDTMA to zeolite A than Phillipsite surface.

(ii). Freundlich isotherm model

The Freundlich isotherm model which is known for its applicabitlty for multi-layer adsorption of the components in solution can be used to describe the formation of bilayer of the adsorbate when the initial concentration of HDTMA is higher than the critical micelle concentration (Darvanjooghi *et al.*, 2018). The concentration of HDTMA above the external cation exchange capacity will result to the formation of patchy bilayers on the surface of zeolite A and phillipsite. The Freundlich constant would further serve as a measure of heterogeneity of adsorption sites in the zeolites (Ramadoss and Subraman, 2018). The Freundlich isotherm parameters shown in Table 4.16 were obtained from a linear plot of ln (qe) against ln (Ce). The Freundlich constant, K_F is an approximate indicator of the adsorption capacity that was obtained from the slope of the graph while the parameter 1/n gives the information on the adsorption intensity or surface heterogeneity as obtained from the intercept of the graph drawn from the linear form of the Freundlich equation. The adsorption process is said to be linear when the value of n is equal to unity. The adsorption process is unfavourable when the value of n is below unity and when it is above unity, the adsorption process is said to be favourable. The result of the present study in Table 4.16 showed the value of n = 1.6151 at equilibrium for zeolite A and it therefore suggests that the adsorption

process was favourable. The interaction between HDTMA and phillipsite gave an n value of 0.7962 which was below unity and therefore suggests that the adsorption process was unfavourable.

The adsorption capacity K_F for the adsorption of HDTMA to zeolite A and phillipsite was given as 3.1313 mg/g and 0.9856 mg/g respectively. The correlation coefficient R^2 of zeolite A with value 0.7843 closer to unity can represent a better fit to the experimental data for the adsorption of HDTMA than Phillipsite with the value of 0.7486. Further more, the sum of square error (1.0377) and average relative error deviation (ARED) 24.5469 were the lowest values compared to the values of langmuir and Dubinin- Radushkevich models. Based on the three error functions with respect to HDTMA and zeolite A, Freundlich model can used to describe the adsorption process favourably.

(iii). Temkin isotherm model

The Temkin isotherm model does not give information on the maximum adsorption capacity rather it describes the effect of indirect adsorbate – adsorbent interaction (Asgari *et al*., 2012). The model finds its relevance in the adsorption of HDTMA on the zeolite A and phillipsite respectively by giving insight to the type of bond formed between the adsorbate and adsorbent through the range of values of the heat of adsorption. The plot of ln (Ce) against qe presents the Temkin constants for slope and intercept as the binding constant K_T (L/g) and heat of adsorption B_L (J $gmol^{-2}$) respectively. The Table 4.16 showed the Temkin adsorption potential K_T of zeolite A with 34.8142 (L/mg) greater than phillipsite with 11.2499 (L/mg).

The second Temkin parameter called Heat of adsorption, B_L (kJ/mol) for zeolite A with 2.1559 kJ/mol is observed to be greater than Phillipsite with 1.9702 kJ/mol. The heat of adsorption values for zeolite A and phillipsite were lower than 20 kJ/mol which showed that the bond between the adsorbate and adsorbent are weak and they therefore indicate physical adsorption.

The Temkin's correlation coefficient R^2 of phillipsite with a value of 0.8916 represents a better fit to the experimental data for the sorption of HDTMA than zeolite A with a value of 0.8829. Both correlation coefficients are higher than the R^2 0.8420 obtained in the adsorption of ampicillin onto montmorilonite nanoparticles by Balarah *et al*. (2017).

(iv). Dubinin – Radushkevich isotherm model

The Dubinin – Radushkevich isotherm model is often used to distinguish whether the adsorption process has chemical or physical basis. The Dubinin – Radushkevich (D-R) two parameters are obtained from the plot of ln qe against E^2. The qs is the adsorption capacity (mg/g) and K_{DR} is a constant related to adsorption energy obtained from the intercept and slope respectively. The mean adsorption energy E that is derived from the Dubinin – Radushkevich constant is indicative of either chemisorption or physisorption between HDTMA and zeolite A and Phillipsite respectively. The adsorption capacity qs of zeolite A with178.8236 mg/g was observed to be higher than phillipsite with 4.8797 mg/g in Table 4.16. The K_{DR} constant related to mean adsorption energy, E for zeolite A with 0.0900 (mol^2/kJ^2) was higher than phillipsite with 0.0100 (mol^2/kJ^2). The correlation coefficient R^2 of phillipsite was 0.9633 and zeolite A was 0.7157. However, the mean adsorption energy E (kJ/mol) for zeolite A is 2.35 kJ/mol and phillipsite value is 0.14kJ/mol are less than 8 kJ/mol that reveals the predomination of physical adsorption (Naranjo *et al*., 2013). The correlation coefficient R^2 (0.9633) for phillipsite

was the most closest to unity compared to langmuir, Freundlich isotherm models. The values of sum of squares error (SSE) and average relative error deviation (ARED) for Phillipsite were 0.0004 and -0.4142 respectively. Therefore, based on the highest value of correlation coefficient R^2 and the lowest value of sums of squares (SSE) of Phillipsite, Dubinin- Radushkevich isotherm model could best describe the relationship between HDTMA and Phillipsite.

Table 4.16: Isotherm parameters for the adsorption of HDTMA onto zeolite A and phillipsite

Model		**Zeolite A Value**	**Phillipsite Value**
Langmuir constants	q_m (mg/g)	19.4530	11.2310
	b(L/mg)	0.1679	0.1318
	R_L	0.0238	0.0374
	R^2	0.9064	0.5700
	SSE	234.1818	40.0810
	ARED	368.74	129.2000
Freundlich constants	K_F(mg/g)	3.1313	0.9856
	n	1.6151	0.7962
	R^2	0.7843	0.7486
	SSE	1.0377	15.3225
	ARED	24.5469	79.8800
Tempkin constants	K_T (L/mg)	34.8142	11.2499
	B_L(kJ/mol)	2.1559	1.9702
	R^2	0.8829	0.8916
Dubinin R	qs (mg/g)	178.8236	4.8797
	K_D (mol^2/kJ^2)	0.0900	0.0100
	E (kJ/mol)	2.3500	0.1414
	R^2	0.7157	0.9633
	SSE	30,510.8665	0.0004
	ARED	4,209.0000	-0.4142

4.6 Adsorption Kinetics

The adsorption kinetics is the measure of the adsorption uptake with respect to time under constant pressure or concentration and it is usually employed to measure the diffusion of adsorbate onto the pores. The adsorption kinetics of cationic surfactant, nutrient uptake and release were determined by the ion-exchange and structural properties of zeolites. In order to describe the controlling mechanism of HDTMA adsorption onto zeolite A and Phillipsite, pseudo-first-order, pseudo-second-order and intra-particle diffusion were applied as shown in Table 4.17.

Table 4.17: Kinetic parameter for the adsorption of HDTMA by zeolite A and phillipsite

Kinetic Models and Parameters	**Zeolite A**	**Phillipsite**
q_e (exp) (mg/g)	3.4000	1.3000
Lagergren pseudo-first-order		
q_e(calculated) (mg/g)	0.6999	1.6856
K_1(g.mg^{-1}min^{-1})	0.0375	0.1017
R^2	0.9992	0.7979
SSE	7.2900	0.1488
ARED	79.4100	29.6600
Pseudo-second-order		
q_e (calculated) (mg/g)	0.1876	14.8730
K_2 (g.mg^{-1}min^{-1})	0.4045	3.5010
R^2	0.4286	0.2532
SSE	10.3100	184.2200
ARED	94.4800	1044.0000
Intra-particle diffusion		
K_3 (g.mg^{-1}min$^{-0.5}$)	0.2121	1.3727
C (intercept)	0.4277	5.9064

R^2	0.8509	0.9332

The kinetics of adsorption process for HDTMA on zeolite A and phillipsite describes the rate of adsorbate adherence on the adsorbent and it controls the equilibrium time. The kinetic parameters are helpful for the prediction of adsorption rate which gives important information for designing and modelling the processes. The kinetics of adsorption is important on the basis that it controls the process efficiency.

4.6.1 Pseudo-first-order model

The adsorption kinetics of HDTMA on to zeolite A and phillipsite could be described by pseudo first order model presented in Equation 2.13. The rate constant, k_1 (min^{-1}) is the adsorption rate constant of pseudo first order reaction. ln ($q_e - q_t$) was plotted against t. The application of kinetics parameters of adsorption of HDTMA onto zeolite A and Phillipsite according to pseudo first order model Equation 2.13 were presented in Table 4.17. The plot of ln ($q_e - q_t$) against time gave a straight line for pseudo first order equation. K_1 and q_e represent the slope and intercept, respectively. The comparison of the theoretical adsorption capacities and the correlation coefficients of the pseudo-first-order for zeolite A showed that correlation coefficient of 0.9992 was closer to unity than correlation coefficient 0.4286 obtained from the pseudo-second-order. The sum of square error (SSE) 7.2905 and average relative error deviation (ARED) -79.4100 were lower than the values of pseudo second order (Shahmohammadi-Kalalagh and Babazadeh, 2014). Similarly, the theoretical adsorption capacity of 0.6999 mg/g from the pseudo-first-order was closer to experimental adsorption value of 3.4000 mg/g than theoretical adsorption capacity of 0.1876 mg/g of the pseudo-second-order. Therefore, the adsorption of HDTMA on zeolite A can be better described by pseudo-first-order kinetic model.

4.6.2 Pseudo-Second-order model

The adsorption kinetics of HDTMA on to zeolite A and phillipsite based on pseudo second order model in Equation 2.14 is provided in Table 4.17. k_2 (g/mg/min) is the rate constant of second-order adsorption. The plot of t/q versus t shows a linear relationship if the second-order kinetics is applicable. q_e and k_2 were determined from the slope and intercept of the plot respectively. The observation of the kinetic parameters of phillipsite in Table 4.17 shows that the correlation coefficient R^2 of 0.7979 from pseudo-first-order model was closer to unity relative to 0.2532 obtained from the pseudo-second-order. The sum of squares (SSE) and average relative error deviation (ARED) with values 10.3100 and 94.4800 respectively were higher than the values obtained in pseudo first order model. The calculated adsorption capacity of 1.6856 mg/g from the pseudo-first-order was closer to the experimental of 1.3000 mg/g than 14.873 mg/g of pseudo-second-order. The adsorption of HDTMA to phillipsite data is better described by the pseudo-first-order due to better fitting of the kinetic parameters in Table 4.17. This suggest that the rate of adsorption of HDTMA on phillipsite can be controlled by pseudo first order and consequently inclined to physical adsorption (Tan and Hameed, 2010).

4.6.3 Weber-Morris Intraparticle diffusion model

The intraparticle diffusion model proposed by Weber and Morris gave the relationship between q_t and square root of time, $t^{0.5}$ as shown in Equation 2.16 to identify the influence of diffusion on adsorption. k_{id} (mg/g $h^{0.5}$) represent the intraparticle diffusion rate constant and C_i is obtained from the intercept which gives a clue about the boundary layer thickness. Intraparticle diffusion reports that when qt versus $t^{0.5}$ is linear and the plot passes through the origin, then the rate limiting process is simply attributed

to the intraparticle diffusion. The plots of qt versus $t^{0.5}$ did not pass through zero for both zeolite A and Phillipsite. The intercept value (0.4277) for zeolite A shows a low boundary layer thickness and its deviation from the origin may be attributed to the difference in rate of mass transfer in the initial and final stages of adsorption. The intercept value (5.9064) for phillipsite shows a larger boundary layer thickness and that pore diffusion is not the only rate controlling step. The values of correlation coefficients (R^2) from the intra-particle diffusion were higher than pseudo first order and pseudo second order. This indicates that the adsorption process of the two zeolites can be followed by intra-particle diffusion. Therefore, adsorption process progresses through a complex mechanism that explains that more than one process mechanism affects the adsorption of the two zeolites (Darvanjoeghi *et al*., 2018).

4.7 Adsorption Thermodynamics

The Gibbs energy change (ΔG^o) indicates the degree of spontaneity of an adsorption process and a higher negative value implied a more energetically favourable adsorption as shown in Table (4.18). Gibbs energy change, (ΔG^o) of adsorption is calculated using the relation in Equation 4.10

$$\Delta G^o = -RT\ln K_d \qquad (4.10)$$

Given that K_d is the thermodynamic equilibrium constant without units, T is the absolute temperature in kelvin and R is the universal gas constant with a value of 8.314 KJmol $^{-1}$ K^{-1}. The relation of ΔG^o to enthalpy change (ΔH^o) and entropy (ΔS^o) of adsorption is expressed in Equation 4.11

$$\Delta G^o = \Delta H^o - T\Delta S^o \qquad (4.11)$$

The values of (ΔH^o) and (ΔS^o) were calculated from the slope and intercept of plot between ln K_d versus 1/T for HDTMA initial concentration of 243.90mmol/L for zeolite A and 195 mmol /L for phillipsite.

Thermodynamic parameters enhance the study of the feasibility of the adsorption process (Das *et al*., 2013). The values of thermodynamic parameters for the adsorption of HDTMA on zeolite A and Phillipsite are listed in Table 4.18. The Gibb's free energy change (ΔG^o) values of zeolite A (-27.045) and Phillipsite (-61.799) were observed to be negative. The negative sign indicates the feasibility and spontaneity of the adsorption process at temperatures studied. The decrease in the negative values of Gibb's free energy change for zeolite A and Phillipsite with increase in temperature shows the degree of spontaneity and that the lower temperature makes the adsorption process easier. (Saha and Chowdhury, 2011).

The negative enthalpy change (ΔH^o) value -12.208 kJ/mol of zeolite A implies that the adsorption phenomenon is exothermic. The total energy released in an exothermic process when the bond between the water in the pore and the surface of the zeolite is broken is higher than the total energy absorbed in bond making between the adsorbate HDTMA and the adsorbent zeolite A. The resulting difference leads to a negative enthalpy change (Hongxia *et al*., 2014). The magnitude of enthalpy change (ΔH^o) in zeolite A with value (12.208 kJ/mol) falls within a range < 50 kJ/mol that is reported as physical adsorption (Yousef *et al*., 2011).

The Phillipsite negative enthalpy value of (ΔH^o) -35.066 kJ/mol shows that the adsorption process is exothermic. The total energy released in the desorption of the water molecules from the pores of phillipsite is higher than the total energy released in the sorption of HDTMA and phillipsite resulting to the release of heat energy. The

magnitude of phillipsite enthalpy gives the idea that the heat released from the adsorption process belongs to a range that is < 50 kJ/mol and consequently refered to as physical adsorption (Yousef *et al.*, 2011)

Zeolite A's positive entropy change (ΔS^o) value of (49.789 kJ/mol) indicates that the adsorption of HDTMA to zeolite A is enthalpy driven. The positive value of entropy change (ΔS^o) also suggests an increased disorder at the zeolite / HDTMA liquid interface during the adsorption process. Therefore, the amount of HDTMA molecules that can adsorb on the zeolite A's surface would decrease.

The phillipsite positive entropy change (ΔS^o) value indicates the affinity of phillipsite towards the HDTMA molecules. The positive value further suggests the increased randomness at the phillipsite / HDTMA liquid interface. The positive entropy change (ΔS^o) value also corresponds to an increase in the degree of freedom of the HDTMA molecule in the adsorption process (Tan and Hameed, 2010).

Table 4.18: Thermodynamic parameters derived from the adsorption of HDTMA on zeolite A and phillipsite

Samples	**T (kelvin)**	**Δ G (kJ/mol^{-1})**	**Δ H (kJ/mol^{-1})**	**Δ S (J/mol^{-1}K^{-1})**
Zeolite A	298	-27.045	-12.208	49.789
	308	-27.543		
	318	-28.041		
	328	-28.539		
	338	-29.037		
Phillipsite	298	-61.799	-35.066	89.708
	308	-62.696		

318	-63.593
328	-64.490
338	-65.387

4.8 Desorption Studies

The synthesised Phosphate and Nitrate loaded Zeolite A and Phillipsite based fertilizers respectively were subjected to desorption studies using the percolation chemical reactor to study the desorption rates. Desorption is a process of removing an adsorbed substance from a surface on which it is adsorbed (Thirunavukkarasu and Subramanian, 2014).

4.8.1 Slow release of phosphorus

The potassium dihydrogen phosphate (KH_2PO_4) fertilizer, phosphate loaded zeolite A fertilizer and phosphate loaded phillipsite fertilizer were subjected to leaching using the percolation reactors. Detectable concentrations of phosphate above 0.13 mg/L of phosphate were not released from the leachate of soil alone. Therefore, most of the phosphate measured from the leachates obtained from the reactors having soil and fertilizer can be attributed to the fertilizer sources. The variation in phosphates concentration with time for the three fertilizers is presented in Figure 4.38 to 4.41. The first order rate equation for the desorption process was used for the two stages of oxyanions leaching experiment can be expressed in Equation 4.5 (Li, 1999).

$$\ln \frac{S_t}{S_o} = -kd_t \quad (4.5)$$

Where S_t is the amount of solute adsorbed at time t, S_o is the amount of solute adsorbed at zero time of desorption and k_d is the apparent desorption rate constant. If the rate of

phosphate desorption by the zeolite based fertilizers follows first order kinetics, then a plot of ln (S_t/S_o) against desorption time t should give a linear relationship. It was observed that the concentration of phosphates released from the first leachates of potassium dihydrogen phosphate fertilizer was 20.5 mg/L (49.38%) while phosphate loaded zeolite A based fertilizer was 30.4 mg/L (28.65%) and phosphate loaded phillipsite based fertilizer was 23.8 mg/L (16.94%) of the total released leachates respectively. The low concentrations of phosphates observed in phosphate loaded zeolite A and phillipsite based fertilizers relative to potassium dihydrogen phosphate (KH_2PO_4) fertilizer could be attributed to the presence of the zeolite material inherent in the fertilizers which serve as carriers for the phosphate nutrients.

It was further observed from the first stage of Figure 4.38, that 76.98% of phosphates desorbed from the KH_2PO_4 fertilizer in the first three leachates collected. This observation is in agreement with Baniswal *et al*. (2006) who reported that the maximum concentration of 44.5 mmol/L. P was observed in pure KH_2PO_4 relative to the unmodified zeolite and surfactant modified zeolite-3 respectively. The rate constant, k_1 and the release factor for the first part of the curve is given as 8.00 X $10^{-2}h^{-1}$ and 0.31 respectively. However, the second part of the curve stabilizes progressively at a concentration of 1.62 mg/L (3.90%) to 0.20 mg/L (0.48%) from the leachate at 96 h to 600 h respectively. The release factor for the second part of the plot is 0.0028. The potassium dihydrogen phosphate fertilizer arrived at decay time of 72 h and consequently slow release was observed.

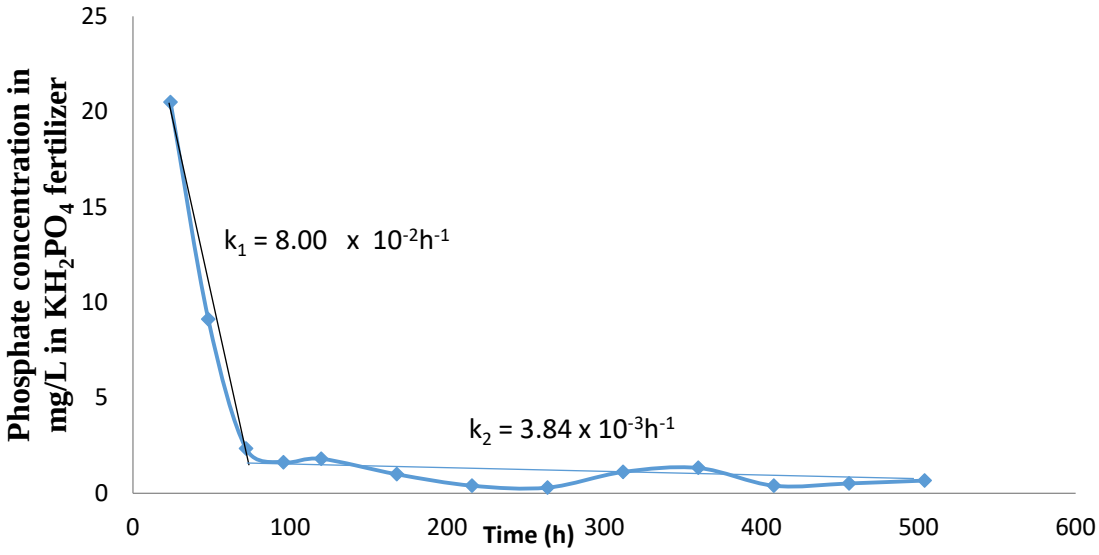

Figure 4.38: Phosphate release from Potassium dihydrogen Phosphate fertilizer

The first part of the plot of the desorption of phosphate from phosphate loaded zeolite A based fertilizer in Figure 4.39 occurred in the first six leachates (168 h). The release factor (slope) and rate constant of the first part of the curve were 0.16 and 1.26 x 10^{-2} h^{-1} respectively. It was observed that the first of the plot was less steep compared to that of Figure 4.39. The reason might be traced to occlusion of the phosphate nutrients in the zeolite. The second part of the desorption curve flattened out from 1.92 (1.8%) to 0.15 (0.45%) at 216 to 600 h. The rate constant and release factor is 1.8 x 10^{-3} h^{-1} and 0.0046 respectively.

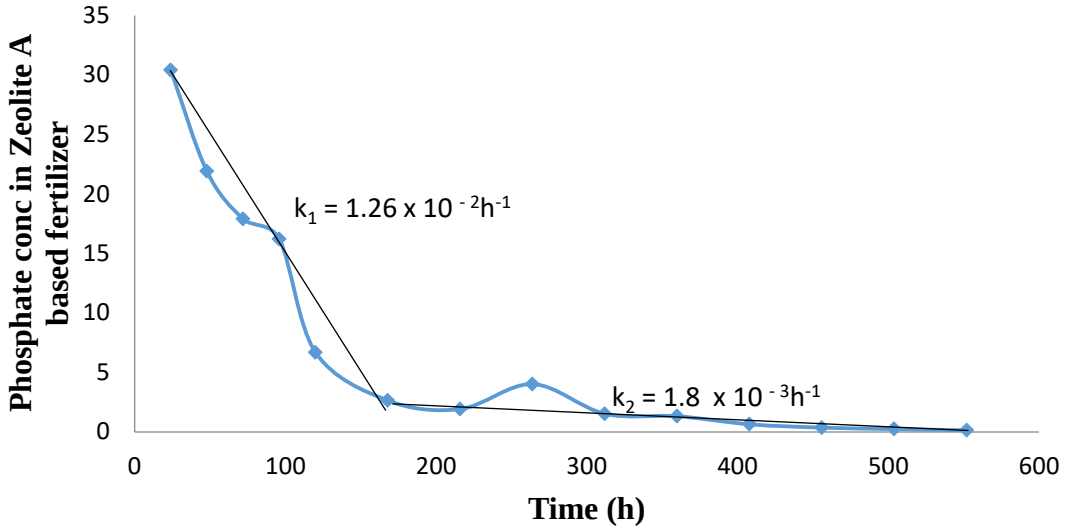

Figure 4.39: Phosphate release from phosphate loaded zeolite A based fertilizer

The rate constant for the first and second stages of the curve are 1.1 x 10^{-2} h^{-1} and 4.40 x 10^{-3} h^{-1} respectively in Figure 4.40. The release factor for the first and second stages are 0.11 and 0.61 respectively. Two different stages that correspond to different nutrient fractions were observed for each fertilizer as also reported for other slow release fertilizers (Baniswal *et al*., 2006). The rate constants in the first stages of the zeolite based fertilizers were higher than their respective second stages as shown in Figure 4.39 and 4.40. The first stage corresponds to the readily soluble forms of KH_2PO_4 that makes up most of the phosphates fertilizers. The high quantity of these phosphates in the first 168 h is explained as the soluble salt that were not bonded to any positive site of the HDTMA-zeolite molecule and were not completely rinsed off after adsorption process (Notario *et al*., 1995). The phosphate release of the zeolite A based fertilizer was slower than the Phillipsite based fertilizer in first 168 h as shown by their respective rate constants. The zeolite based fertilizers in Figure 4.39 and 4.40 provide higher phosphate concentrations at a given time than conventional Potassium dihydrogen phosphate in Figure 4.38.

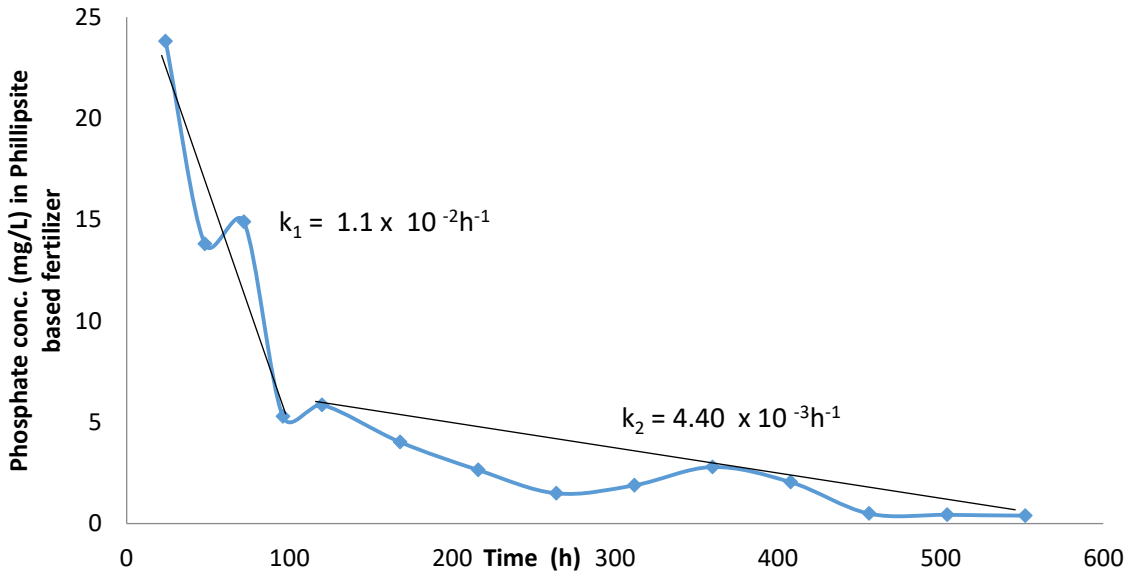

Figure 4.40: Phosphate release from phosphate loaded Phillipsite based fertilizer

4.8.2 Slow release of nitrate

Slow release fertilizers have been observed to follow a first order kinetics. The first order rate equation for the desorption process as reported by Li (1999) can be expressed in Equation 4.7 where S_t is the amount of solute adsorbed at time t, S_o is the amount of solute adsorbed at zero time of desorption and k_d is the apparent desorption rate constant. If the rate of nitrate desorption by the nitrate loaded zeolite based fertilizers follows first order kinetics, then a plot of ln (S_t/S_o) against desorption time t should give a linear relationship. This is in agreement with the nitrate release rate from nitrate loaded modified zeolite A which follows a first order kinetics especially with a linear plot of ln (natural logarithm) versus time (Li and Zhang, 2010). Results presented in Figure 4.41 showed that the release of nitrates takes place in two different stages. The first stage was observed for pure ammonium nitrate characterized by a steep slope to a decay time of 72 h after which the nitrate concentration reaches below detectable limits.

The rate constant for the the first stage of desorption of the ammonium nitrate fertilizer was the fastest among the nitrates fertilizers considered for the leaching experiment.

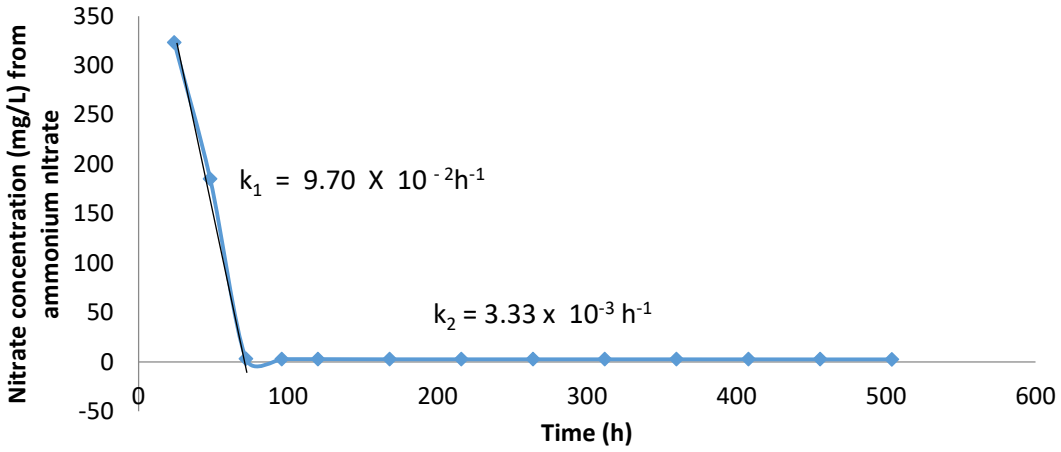

Figure 4.41: Nitrate release from ammonium nitrate fertilizer

The nitrate released from nitrate loaded zeolite A fertilizer showed a leaching pattern characterized by a fast and a slow stage. Results presented in Figure 4.42 showed that the first stage was described by a steep slope to a decay time of 72 h after which the nitrate concentration becomes un-detectable. The time required for the nitrate to desorb from the modified surface of the zeolite carrier was enlongated because the strength of sorption between the negative and positive charges had to be broken. Furthermore, the relatively slow dissolution rate for a soluble salt such as ammonium nitrate occluded in zeolite pores is traceable to the zeolite pore system that forms a diffusion barrier for the release of the nitrate salt.

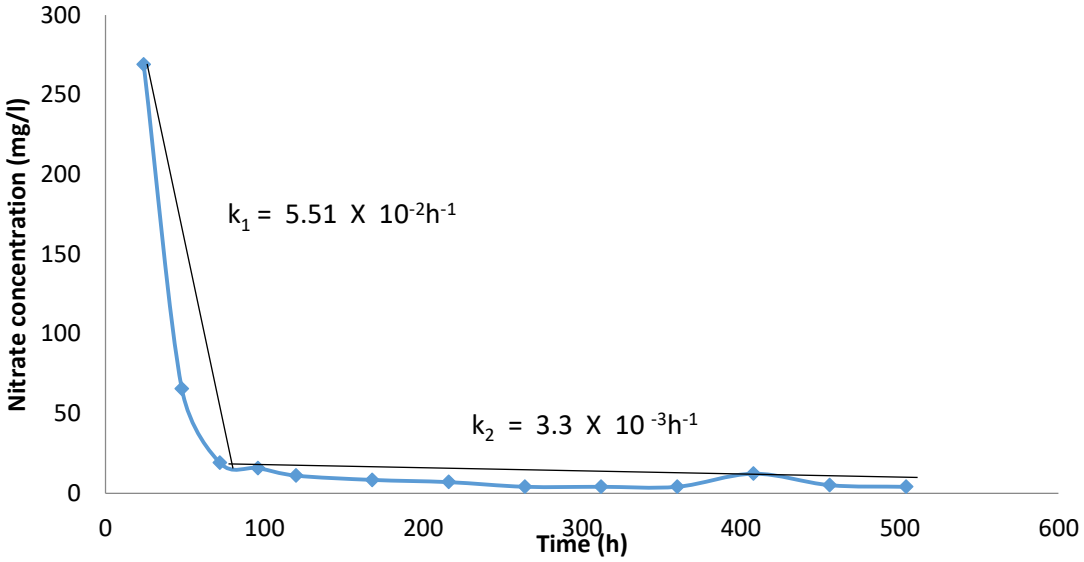

Figure 4.42: Nitrate release from nitrate loaded zeolite A based fertilizer

The nitrate loaded phillipsite based fertilizer showed a leaching pattern which resembled release patterns characterized by two stages. Results presented in Figure 4.43, showed that the first stage was described by a slope to a decay time of 48 h after which the nitrate concentration becomes un-detectable. The rate constants in the first stages of the zeolite based fertilizers were higher than their respective second stages. It was observed that 154 mg/L of nitrate was recorded from the nitrate leached from the nitrate loaded phillipsite fertilizer in the first leachate. The first stages of leaching correspond to the readily soluble forms of NH_4NO_3 that makes up most of the nitrate fertilizers. The high quantity of these nitrates in the first 72 h explains the soluble salt that was not bonded to any positive site on the HDTMA molecule and it was not completely rinsed off after adsorption process (Notario *et al*., 1995). The nitrate release of the Phillipsite based fertilizer is slower than the zeolite based fertilizer in first 168 h as shown by their respective rate constants.

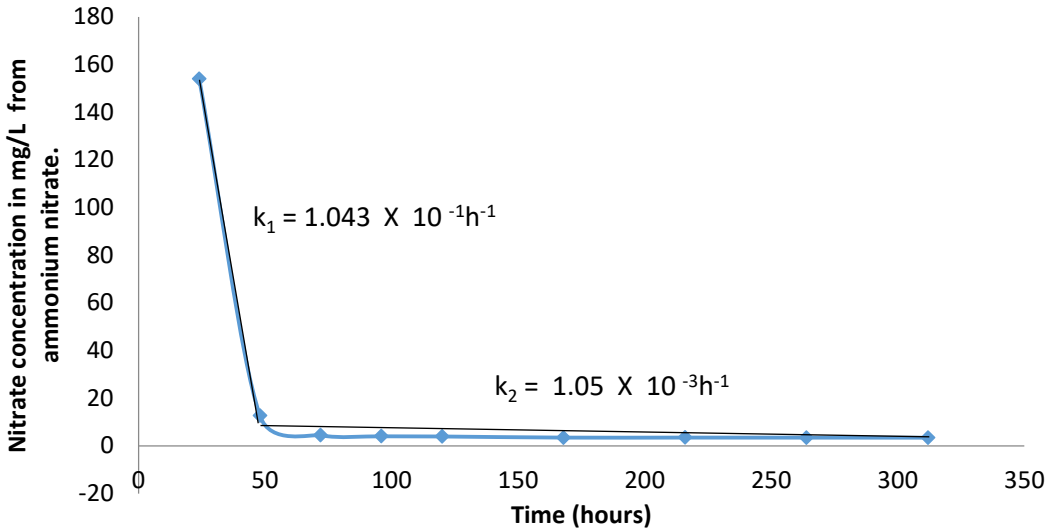

Figure 4.43: Nitrate release from nitrate loaded phillipsite based fertilizer

4.9 Agronomic Evaluation of the Application of Zeolite A, Phillipsite based fertilizers and NPK Fertilizer on Growth, Fruit Yield on Tomato Crop

The effectiveness of the synthesised zeolite A and phillipsite based fertilizers were evaluated when they were applied to the two varieties of tomato crop in a completely randomized design to determine their effects on the growth parameters such as the leaf count, plant height, stem girth, branch count, fruit count and fruit yield. The extent to which the synthesised zeolite based fertilizers delay the leaching of plant nutrients were also evaluated by analysing the soil parameters at post harvest.

4.9.1 Leaf count

In Table 4.19, it was observed that the mean of UC82b variety were higher than the Roma VF variety in the leaf counts from 6 to 10 weeks after transplanting in 2018 and 2019. However, there was no significant difference between the leaf counts of the two varieties in 2018. Variety UC82b produced significantly greater number of leaves at 6 and 10 WAT (62.08 and 127.65) than Roma VF (35.31 and 82.75) respectively in 2019.

There was an increase in the number of leaves from week 6 to 8 with respect to the three fertilizer sources; however, there was a drop in the leaf counts at 10 and 11 WAT in 2018. This trend might be traceable to the fact that the plant diverts the nutrients to the development of the fruits. At 11 WAT, the zeolite based fertilizer treatment plants were observed to have greener leaves than the conventional NPK fertilizer treated plants. The means of zeolite A (54.25) and Phillipsite (46.52) based fertilizers were significantly different at 11 WAT when compared to the mean of conventional NPK fertilizer (25.73) in Table 4.19. It was observed that the leaves of the conventional NPK fertilizer were wilting and dying as a result of aging and depletion of plant nutrients in the soil. The greener leaves on the plants with zeolite based fertilizer applications indicated the presence of more nutrients retained in the soil by the zeolite carriers in the fertilizer. The zeolite based fertilizers release their nutrients slowly for a longer period of time than the conventional fertilizers. The slow release trend could be attributed to to the strong bonding of the plant nutrients to the pore of the zeolite as observed by (Rajonee *et al*., 2016). In the conventional NPK fertilizer, nutrient carriers or fillers have no adherence to the plant nutrients and therefore their nutrients leach easily beyond the root zone with percolated water.

In 2019, there was an increase in the number of leaves from 6 to 11WAT for the three fertilizer sources although NPK fertilizer were significantly higher than the zeolite based fertilizers. The lower mean value of leaves for the zeolite based fertilizers in 2019 for 6 to 11WAT could be attributed to the controlled release of the plant nutrients from the zeolite carriers to the tomato plants. In 2019, the tomato crop displayed a general delay in crop growth compared to the growth in 2018. The low mean values of the leaf count for the zeolite based fertilizers compared to the NPK fertilizer could also be

attributed to the delayed release property of the zeolite carrier thereby preserving the nutrients for the fruiting stage (Nakhli *et al*., 2017).

The rates of application were not significantly different at 150, 300 and 600 kg/ha at 11 WAT in 2018. The highest number of leaves with mean 143.37 was observed at 8 WAT in 2018 with the application of 600 kg/ha. Statistically significant differences in terms of interaction between fertilizer source and rate of application was observed at 6 and 8 WAT in 2018 and 2019 respectively. The interactive effect of fertilizer source and rate of application on leaf count at 6 – 8 WAT is shown in Table 4.20. At 6 and 8 (WAT) in 2018 and 6 WAT in 2019, the highest interactive values were obtained when NPK 15:15:15 were applied at the rate of 600 kg/ha. The mean values recorded were however not significantly higher than other interaction values when zeolite A and Phillipsite based fertilizers were applied at 300 kg/ha in 2018 and 2019 respectively. The interactive effect recorded when NPK 15:15:15 was applied at 150 kg/ha at 8 WAT in 2019 was significantly different to zeolite A applied at 150 kg/ha at the same 8 WAT

Table 4.19: Effects of varieties, fertilizer sources and rates of fertilizer application on leaf count of tomato during 2018 and 2019 rainy seasons at Minna

	2018				2019			
Treatment	**6**	**8**	**10**	**11**	**6**	**8**	**10**	**11**
Variety(V)								
UC82b	124.92a	137.56a	80.35a	41.61a	62.08a	66.78b	127.65a	131.63b
Roma Vf	120.94a	133.54a	79.19a	32.23a	35.31b	107.22a	82.75b	84.86b
SE±	5.74	5.53	1.84	5.65	4.19	7.28	7.70	7.65
Fertilizer Source								
Zeolite A based fertilizer	99.56b	113.17b	81. 35a	54.29a	49.30a	72.21b	97.88b	102.67b
Phillipsite based fertilizer	97.43b	113.24b	77.84a	46.54a	50.60a	73.21b	89.58b	92.96b
NPK15:15;15	122.22a	133.19a	82.36a	25.76b	46.21a	105.58a	128.15a	129.10a
SE±	3.36	3.13	2.37	7.44	5.98	9.37	9.94	9.98
Rate (kg/ha)								
0	111.54b	123.67b	78.45abc	31.5a	42.67a	65.50b	82.06b	85.28b
150	129.83ab	143.17a	83.87ab	46.58a	55.07a	87.56ab	107.22ab	110.06
300	119.38ab	131.79ab	72.53c	32.21a	46.61a	84.89ab	102.22ab	105.69ab
600	130.96a	143.37a	84.25a	37.29a	50.44a	110.06a	129.31a	131.94
SE±	7.36	6.92	2.52	6.43	6.83	10.91	11.63	11.71
Interactions								
V*F	NS	NS	NS	NS	NS	NS	NS	NS
V*R	NS	NS	NS	NS	NS	NS	NS	NS
F*R	*	*	NS	NS	NS	*	*	NS
V*F*R	NS	NS	NS	NS	NS	NS	NS	NS
CV (%)	19.03	16.60	14.51	15.09	49.39	48.23	36.29	35.79

Means with unlike letter(s) in columns are significantly different at $p \leq 0.05$ by Duncan's Multiple Range Test (DMRT), NS stands for not significant, * stands for significant at 5%, V for variety, F for fertilizer source, and R for rate.

Table 4.20: Interaction of fertilizer source and rate of fertilizer application on leaf count in 2018 and 2019

			2018			
		6 WAT			8 WAT	
	Zeolite A	Phillipsite	NPK	Zeolite A	Phillipsite	NPK
0	92.83b	96.50b	124.50ab	111.33ab	109.67b	134ab
150	97.83b	93.33b	118.17ab	109.50b	113.33ab	129.50ab
300	99.17ab	97.83ab	113.83ab	110.50ab	112.83ab	127.00ab
600	108.17ab	102.00ab	132.67a	121.00ab	117.17ab	141.33a
SE+	7.37	7.37	7.37	6.49	6.49	6.49
			2019			
0	45.33ab	38.00ab	39.33ab	81.33bc	61.67bc	56.00c
150	35.00ab	50.17ab	28.17b	51.00c	61.33bc	167.00a
300	62.67ab	53.67ab	47.67ab	98.83bc	89.50bc	105.80bc
600	54.17ab	60.50ab	69.67a	85.67bc	80.33bc	120.00ab
SE	3.42	3.42	3.42	5.79	5.79	5.79

Means with unlike letter(s) in columns or rows are significantly different at $p \leq 0.05$ by Duncan's Multiple Range Test (DMRT).

4.9.2 Plant height

The analysis of variance for plant height did not significantly differ for the two varieties (Roma VF and UC82b) from 6 – 10 WAT during 2018 and 2019 as shown in Table 4.21. Roma VF variety had higher mean values at 6 – 10 WAT during 2018 and 8 and 10 WAT during 2019.

The effect of fertilizer sources on the plant height of tomato showed significant difference between NPK fertilizer and the zeolite based fertilizers only at 8 WAT in 2019. It was observed that there was an increase in plant height from 6 to 10 WAT for the three fertilizer sources for 2018 and 2019. The maximum plant height with mean of 62.82 at 10 WAT and 54.45 at 8 WAT was recorded in 2018 and 2019 respectively for NPK fertilizer though there was no significant difference between their means. In 2019, the mean for the application of NPK fertilizer was significantly higher than the means of zeolite A and Phillipsite based fertilizers at 8 WAT.

The rate of fertilizer application on plant height at 300 and 600 kg/ha for 6 – 10 WAT for 2018 and 2019 was observed to be significantly different to the rate of application at 0 and 150 kg/ha at 8 – 10 WAT in 2018 and 2019 respectively. It was observed that there was a growing trend in the plant heights from 6 -10 WAT with increase in rates of the different fertilizer application. This was expected because of the increase of fertilizer quantity at each subsequent level of application. It was obsevered that there were no significant interactions in Table 4.21.

Table 4.21: Effect of varieties, fertilizer sources and rates of fertilizer application on plant height of tomatoes in 2018 and 2019 seasons at Minna.

	2018			2019		
WAT	**6**	**8**	**10**	**6**	**8**	**10**
Variety (V)						
UC82b	52.86a	62.14a	63.33a	18.36a	49.06a	48.56a
Roma VF	53.05a	63.94a	64.85a	16.25a	51.05a	51.94a
SE±	1.04	0.83	0.85	0.83	1.89	1.81
Fertilizer source						
Zeolite A based fertilizer	52.73a	61.55a	63.06a	23.79a	48.23b	48.75a
Phillipsite based fertilizer	50.24a	61.54a	62.65a	25.98a	47.48b	48.82a
NPK 15 : 15: 15	50.67a	62.03a	62.82a	25.54a	54.45a	54.18a
SE±	1.21	1.32	1.23	1.62	2.21	2.13
Rate of application (kg/ha)						
0	53.13a	60.97b	61.55b	22.73a	44.37b	44.65b
150	53.15a	62.34ab	63.44ab	27.39a	44.99b	49.70ab
300	51.84a	63.44ab	65.13a	25.91a	53.35a	53.57a
600	52.76a	65.42a	66.57a	24.38a	52.50a	53.07a
SE+	1.37	1.14	1.13	1.92	2.55	2.48
Interaction						
V*F	NS	NS	NS	NS	NS	NS
V*R	NS	NS	NS	NS	NS	NS
F*R	NS	NS	NS	NS	NS	NS
V*F*R	NS	NS	NS	NS	NS	NS
CV (%)	10.48	8.11	7.93	29.21	24.31	19.20

Means with unlike letter(s) in columns are significantly different at $p \leq 0.05$ by Duncan's Multiple Range Test (DMRT), NS stands for not significant, * stands for significant at 5%, V for variety, F for fertilizer source, and R for rate

4.9.3 Stem girth

Table 4.22 showed that the stem girth's means for variety Roma VF were significantly different than variety UC82b at 6, 8 and 10 WAT in 2018 while there was no significant difference in 2019. The highest mean value for Roma VF's stem girth were 0.94 and 0.60 at 10 WAT for 2018 and 2019 respectively while variety Roma VF had the lowest stem girth of 0.75 and 0.43 at 6 WAT for 2018 and 2019 respectively

There was no significant difference in the stem girth for the fertilizer sources for 8 and 10 WAT in 2018 and 6 WAT in 2019. The mean values of the stem girth for NPK and phillipsite based fertilizers were significantly different to the means of zeolite A at 6 WAT in 2018 at 8 and 10 WAT in 2019. However, phillipsite based fertilizer produced the highest stem girth mean of 0.88 at 6 WAT in 2018 while NPK fertilizer treated plants produced the highest stem girth of 0.65 at 10 WAT in 2019. There was significant difference in the mean of the stem girth with respect to the rates of application of the fertilizer sources for 2018 and 2019 at 10 and 6 WAT respectively.

The rate of application with the highest stem girth occurred at the 10 WAT in 2018 with a mean value of 0.96 at a rate of 600 kg/ha and the lowest stem girth occurred at 10 WAT with a mean value of 0.82 at rate 150 kg/ha. However, there was no significant difference in the interactions of the stem girth.

Table 4.22: Effect of varieties, fertilizer sources and rates of fertilizer application on the stem girth of tomatoes during 2018 and 2019 season at Minna

	2018			2019		
Treatment	**6**	**8**	**10**	**6**	**8**	**10**
Variety (V)						
UC82b	0.83a	0.82b	0.82b	0.45a	0.56a	0.60a
Roma VF	0.75b	0.93a	0.94a	0.43a	0.57a	0.60a
SE±	0.02	0.02	0.03	0.02	0.02	0.02
Fertilizer Source						
Zeolite A based fertilizer	0.79b	0.83a	0.82a	0.42a	0.55b	0.57b
Phillipsite based fertilizer	0.88a	0.86a	0.87a	0.45a	0.56ab	0.57b
NPK15:15:15	0.87a	0.85a	0.85a	0.46a	0.61a	0.65a
SE±	0.02	0.02	0.02	0.02	0.02	0.01
Rate (kg/ha)						
0	0.85a	0.86a	0.96a	0.40b	0.54a	0.56a
150	0.87a	0.89a	0.82b	0.47a	0.59a	0.60a
300	0.84a	0.88a	0.83b	0.45a	0.58a	0.61a
600	0.85a	0.87a	0.96a	0.45a	0.59a	0.62a
SE±	0.03	0.02	0.03	0.01	0.02	0.03
Interaction						
V*F	NS	NS	NS	NS	NS	NS
V*L	NS	NS	NS	NS	NS	NS
F*L	NS	NS	NS	NS	NS	NS
V*F*L	NS	NS	NS	NS	NS	NS
CV (%)	13.69	11.74	12.07	24.35	13.94	13.51

Means with unlike letter(s) in columns are significantly different at $p \leq 0.05$ by Duncan's Multiple Range Test (DMRT), NS stands for not significant, * stands for significant at 5%, V, Fand L stand for variety, fertilizer source and rate respectively.

4.9.4 Branch count

The means of the variety UC82b were significantly higher than the means of Roma VF at 6, 8 and 10 WAT for 2018 and 2019.

It was observed that there was a general decrease for the branch count at 6, 8 and 10 WAT for the two varieties in 2018 while there was a general increase at 6, 8 and 10 WAT in 2019 in Table 4.24.

The effect of three fertilizer sources on branch count of tomato was not significantly different at 6, 8 and 10 WAT in 2018 and 6 and 8 WAT in 2019. However, the mean values of NPK fertilizer was significantly higher than zeolite A and phillipsie based fertilizer in the 10 WAT in 2019. The higher branch counts in NPK fertilizer source may be attributed to the effect of higher nutrient release pattern from the NPK fertilizers. Similar trend in agronomic growth was reported by Preetha and Balakrishnan (2017) that the nutrient release pattern for the conventional NPK fertilizer was faster and incremental than zeolite based nanofertilizers whose release rate was consistent. It was further observed that the maximum mean branch count of tomato for NPK 15:15:15 at 6 WAT was 12.57 in 2018 and followed by the mean of 12.21 at 10 WAT in 2019.

It was observed that the rate of application 150 kg/ha with mean value of 14.47 was significantly higher than rate of application of 300 and 600 kg/ha at 8 WAT in 2018. In 2019, the mean value at the rate of application of 150 kg/ha was also significantly higher than the control 0 kg/ha but not significantly different to rate of application 300 and 600 kg/ha at 6 WAT. There was no significant difference between the interactions in 2018 and 2019.

Table 4.23: Effect of varieties, fertilizer sources and rates of application on the branch count of tomato for 2018 and 2019.

	2018			2019		
WAT	**6**	**8**	**10**	**6**	**8**	**10**
Variety (V)						
UC82b	14.15a	13.97a	7.79a	8.53a	8.96a	11.08a
Roma VF	11.26b	11.56b	6.68b	7.52b	7.33b	9.14b
SE±	0.43	0.53	0.36	0.35	0.40	0.54
Fertilizer source						
Zeolite A based fertilizer	11.03a	11.84a	6.96a	8.25a	8.17a	9.92b
Phillipsite based fertilizer	11.54a	11.75a	6.63a	7.96a	7.17a	8.21b
NPK15:15:15	12.57a	11.27a	6.75a	7.96a	9.10a	12.21a
SE±	0.66	0.73	0.45	0.42	2.21	0.58
Rate of Application (kg/ha)						
0	11.57b	11.66b	6.44b	7.78ab	7.22b	9.44a
150	13.84a	14.47a	8.01a	9.16a	8.17ab	9.85a
300	13.17a	12.03b	6.97ab	7.50b	7.86ab	9.81a
600	14.05a	12.88ab	7.52ab	7.78ab	9.33a	11.36a
SE±	0.82	0.79	0.48	0.51	0.52	0.81
Interaction						
V*F	NS	NS	NS	NS	NS	NS
V*R	NS	NS	NS	NS	NS	NS
F*R	NS	NS	NS	NS	NS	NS
V*F*R	NS	NS	NS	NS	NS	NS
CV (%)	21.19	25.67	25.91	25.30	27.09	30.8

Means with unlike letter(s) in columns are significantly different at $p \leq 0.05$ by Duncan's Multiple Range Test (DMRT), NS stands for not significant, * stands for significant at 5%, V, Fand L stands for variety, fertilizer source and rate respectively.

4.9.5 Flower count

The UC82b and Roma Vf varieties were not significantly different with respect to flower count during 2018 whereas in 2019, UC82b recorded significantly higher number of flowers at 6 and 10 WAT as presented in Table 4.24.

Moreover, in year 2018, NPK 15:15:15 showed the highest mean of 4.24 at 6 WAT and it was not significantly different to zeolite A and phillipsite based fertilizers. In 2019, the NPK 15:15:15 had the highest mean of the flower count at 10 WAT and it was significantly different to the means of zeolite A and phillipsite based fertilizers. The difference between the zeolite based fertilizers and NPK 15:15:15 could be traced to slow release property of the zeolite carriers (Thirunavukkarasu and Subramanian, 2014). However, there was a decrease in the trend of mean values of flower count from the 6 to 10 WAT in 2018 as expected. The increase in the trend of mean values of the flower count from 6 to 10 WAT in 2019 may be attributed to the delayed onset of flowering which was probably due to the temperature and rainfall pattern of the year.

The was no significant difference between the rate of fertilizer application and the four different levels of application. There was interaction between fertilizer source and variety on flower count for 2019.

The interactive effect of fertilizer sources and varieties on flower count for 2019 is presented in Table 4.25. Results indicated that there was no significant difference between zeolite A and phillipsite based fertilizers and NPK 15:15:15 for UC82b and Roma VF varieties. Maximum fruit count (143.5) was recorded with the application of NPK 15:15:15 followed by zeolite A that recorded 120.4.

Table 4.24: Effect of varieties, fertilizer sources and rates of fertilizer application on the flower count of tomatoes for 2018 and 2019 seasons

	2018			2019		
Treatment	**6**	**8**	**10**	**6**	**8**	**10**
Variety (V)						
UC82b	4.12a	0.82a	0.02a	0.50a	0.56a	2.56a
Roma VF	4.04a	0.44a	0.02a	0.00b	0.11a	1,22b
SE±	0.34	0.31	0.01	0.11	0.17	0.51
Fertilizer source						
Zeolite based fertilizer	3.36a	1.47a	0.00a	0.21a	0.29a	0.96b
Phillipsite based fertilizer	3.15a	1.24a	0.04a	0.29a	0.46a	1.42b
NPK15:15:15	4.24a	0.76a	0.04a	0.25a	0.25a	3.29a
SE±	0.37	0.25	0.00	0.26	0.23	0.60
Rate of Application (Kg/ha)						
0	3.65a	0.98a	0.04a	0.33	0.56a	0.50a
150	4.23a	1.04a	0.00a	0.17a	0.17a	1.44a
300	3.92a	1.02a	0.00a	0.00a	0.00a	1.72a
600	4.46a	1.59a	0.04a	0.50a	0.61a	3.89a
SE±	0.57	0.35	0.00	0.18	0.23	0.63
Interaction						
V*F	NS	NS	NS	*	NS	NS
V*L	NS	NS	NS	NS	NS	NS
F*L	NS	NS	NS	NS	NS	NS
V*F*L	NS	NS	NS	NS	NS	NS
CV (%)	45.67	64.22	24.64	37.1	33.5	12.3

Means with unlike letter(s) in columns are significantly different at $p \leq 0.05$ by Duncan's Multiple Range Test (DMRT). NS stands for not significant, * stands for significant at 5%, V, Fand L stands for variety, fertilizer source and rate respectively

Table 4.25: Interaction of fertilizer source and variety on flower count for 2019

	6 WAT	
Fertilizer source	**UC82b**	**Roma VF**
Zeolite A based fertilizer	120.42a	75.33bc
Phillipsite based fertilizer	112.92ab	66.25c
NPK 15:15:15	143.50a	103.20ac
SE+	6.07	6.16

Means with unlike letter(s) in columns or rows are significantly different at $p \leq 0.05$ by Duncan's Multiple Range Test (DMRT).

4.9.6 Fruit count

It was observed from Table 4.27 that tomato variety, UC82b was significantly higher than Roma VF at 6 and 8 WAT in 2018 and 2019 respectively. There was no significant difference between the means of the two varieties at 8 and 10 WAT and 6 and 10 WAT in 2018 and 2019 respectively.

There was no significant difference between the means of the fertilizer sources in 2018 and 6 WAT in 2019, however, zeolite A based fertilizer and NPK 15:15:15 were significantly different to phillipsite in 10 WAT in 2019. Phillipsite based fertilizer produced the highest fruit count at 10 WAT with a mean of 2.53 and it was followed closely by Zeolite A based fertilizer with a mean value of 2.36 at 10 WAT in 2018. The NPK fertilizer had its highest fruit count with a mean value of 2.11 at 10 WAT. The difference in mean values of the zeolite based fertilizers to the conventional NPK fertilizers is traceable to the steady nature the zeolite based fertilizers release their nutrients to the plant. Leaching of plant nutrients is reduced largely because the plant nutrients are occluded in the pores of the zeolite framework and not exposed easily as conventional NPK are mainly supported by fillers for handling purposes. It was also observed that the rate of application of 300 kg/ha which was the recommended rate for

applying NPK 15: 15:15 produced the highest fruit count at 10 WAT as also reported by Isah *et al*. (2014). There was interactive effect for variety and fertilizer at 10 WAT in 2019 as shown in Table 4.28. The mean of the interaction of NPK at 150 and 600 kg/ha were significantly higher than zeolite A and phillipsite based fertilizer at 600 kg/ha though zeolite A and phillipsite based fertilizers at 150 and 300 kg/ha were less significant.

Table 4.26: Effect of varieties, fertilizer sources and rates of fertilizer application on the fruit count of tomatoes for 2018 and 2019 at Minna

	2018			**2019**		
WAT	**6**	**8**	**10**	**6**	**8**	**10**
Variety(V)						
UC82b	1.02a	2.57a	2.65a	0.08a	0.75a	0.94a
Roma VF	0.32b	2.54a	2.53a	0.03a	0.36b	0.56a
SE±	0.13	0.26	0.22	0.04	0.56	0.18
Fertilizer source						
Zeolite based fertilizer	0.59a	2.26a	2.36a	0.04a	0.33b	0.92
Phillipsite based fertilizer	0.58a	2.46a	2.53a	0.13a	0.33b	0.33b
NPK15:15:15	0.70a	2.00a	2.11a	0.00	1.00a	1.00a
SE±	0.24	0.22	0.23	0.04	0.18	0.22
Rate of application (kg/ha)						
0	0.47a	2.29a	2.22b	0.11a	0.22b	0.33a
150	0.56a	2.57a	2.54ab	0.00a	0.50b	0.61a
300	0.83a	2.86a	3.05a	0.00a	0.50b	1.00a
600	0.94a	2.54a	2.53ab	0.11a	1.00a	1.06a
SE±	0.34	0.31	0.30	0.05	0.20	0.31
Interaction						
V*F	NS	NS	NS	NS	NS	NS
V*R	NS	NS	NS	NS	NS	NS
F*R	NS	NS	NS	NS	NS	*
V*F*R	NS	NS	NS	NS	NS	NS

CV (%)	16.43	23.16	38.77	15.3	11.4	12.3

Means with unlike letter(s) in columns are significantly different at p≤0.05 by Duncan's Multiple Range Test (DMRT), NS stands for not significant, * stands for significant at 5 %, V, Fand L stands for variety, fertilizer source and rate respectively

Table 4.27: Interaction of fertilizer source and rate of fertilizer application on fruit count in 2019

		10 WAT	
	Zeolite A	**Phillipsite**	**NPK**
0	0.11c	0.33c	0.00c
150	0.33c	0.00c	2.00a
300	0.33c	0.33c	0.80bc
600	0.50bc	0.66bc	1.33ab
SE+		0.94	

Means with unlike letter(s) in columns or rows are significantly different at p≤0.05 by Duncan's Multiple Range Test (DMRT)

4.9.7 Fruit yield

The mean values of the fruit yield of tomato variety shown in Table 4.29 indicates that UC82b produced the highest fruit yield (g/plant) with mean value of 92.71 and 71.87 while Roma VF produced the lowest yield with mean value of 87.66 and 68.00 in 2018 and 2019 respectively. The mean values of the two varieties were not significantly different to each other in 2018 and 2019. It was however observed that the fruit yield (g/plant) was much higher in 2018 than 2019.

The fruit yield of Zeolite A and Phillipsite based fertilizer with mean values of 84.69 and 83.36 respectively were significantly higher than NPK 15:15:15 fertilizer with mean value of 69.34 in 2018. The result was consistent with Bernardi and Verruma (2013)'s report where there were increased yields in tomato cultivated with KH_2PO_4 – enriched zeolite in an inert sand substrate. Similarly, in 2019, zeolite A and phillipsite based fertilizer with mean values of 65.70 and 64.70 respectively were significantly higher than NPK 15:15:15 with mean value of 53.80. The decrease in mean values

observed in 2019 might be attributed to the time of planting and the temperature variations in the weather.

The fruit yields according to the rate of application of 150, 300, and 600 kg/ha were significantly higher than 0 kg/ha which was the control where no fertilizer was added in 2018 and 2019. The rate of application of fertilizer (300 kg/ha) which was the recommended rate had the highest mean values of 103.57 and 80.30 in 2018 and 2019 respectively.

Table 4.28: Effect of varieties, fertilizer sources and rates of fertilizer application on fruit yield of tomatoes for 2018 and 2019

	Fruit yield (g/plant)	
Variety (V)	**2018**	**2019**
UC82b	92.71a	71.87a
Roma VF	87.66a	68.00a
SE±	7.58	7.48
Fertilizer Source		
Zeolite A based fertilizer	84.69a	65.70a
Phillipsite based fertilizer	83.36a	64.70a
NPK15:15:15	69.34b	53.80b
SE±	4.93	3.81
Rates of application (kg /ha)		
0	70.36b	54.56c
150	97.57a	75.40a
300	103.57a	80.30a
600	89.25ab	69.22b
SE±	12.19	5.58
Interaction		
V*F	NS	NS
V*L	NS	NS
F*L	NS	NS
V*F*R	NS	NS
CV (%)	25.30	30.2

Means with unlike letter(s) in columns are significantly different at $p \leq 0.05$ by Duncan's Multiple Range Test (DMRT), NS stands for not significant, * stands for significant at 5%, V, Fand L stands for variety, fertilizer source and rate respectively

4.9.8 Fruit nutrient content

It was observed in Table 4.30 that Roma VF tomato variety had the highest nutritive values for calcium, potassium, and phosphorous though they were not statistically different to UC82b variety. The UC82b tomato variety had the highest mean nutritive content for nitrogen, magnesim and vitamin C.

The zeolite A and phillipsite based fertilizer sources were observed to have the highest mean nutritive contents for all the selected macronutrients and they were statistically significant in comparison to the conventional NPK 15:15:15. This difference might be attributed to the different carriers of nutrients in each of the fertilizer source considered. The zeolite carrier in zeolite A and phillipsite based fertilizer releases its nutrients slowly as a result of its ion exchange and porosity properties. The ability of the fertilizers to delay nutrient leaching beyond the root zone provides the advantage for more plant nutrients to be available during fruit development thereby increasing their nutritive contents (Khan *et al*., 2017; Cole *et al*., 2016).

The recommended rate of application, 300kg/ha had the highest mean fruit content for nitrogen, phosphorous and vitamin C while rate of application 600 kg/ha had the highest mean fruit content for calcium, magnesium and phosphorous.

Table 4.29: Effect of varieties, fertilizer sources and rates of fertilizer application on tomato fruit contents

	Tomato fruit content (mg/100g)					
Treatment	**Nitrogen**	**Calcium**	**Magnesium**	**Potassium**	**Phosphorous**	**Vit.C**
Variety(V)						
Uc82b	4.18a	86.34a	137.39a	358.39a	65.31a	112.2a
Roma VF	4.02a	86.54a	134.82a	372.85a	67.21a	111.82a
SE±	1.09	0.91	1.47	8.79	0.80	4.26
Fertilizer Source						
Zeolite A based fertilizer	4.35a	44.45a	141.71a	371.17a	67.14a	123.34a
Phillipsite based fertilizer	4.31a	44.47a	137.93a	383.83a	66.90a	126.34a
NPK15:15:15	3.64b	37.33b	124.67b	342.65b	64.65b	84.60b
SE±	0.12	0.30	4.08	8.33	0.96	1.02
Rates of application (kg/ha)						
0	3.27c	88.15a	128.14c	317.97d	63.80c	90.52b
150	3.97b	85.39a	132.08bc	342.37c	65.38b	114.66a
300	4.48a	85.15a	137.44b	368.57b	71.85a	120.23a
600	4.67a	87.07a	146.77a	433.55a	64.02bc	122.69a
SE±	0.12	1.03	2.56	6.86	0.49	3.06
Interaction						
F x R	NS	NS	NS	NS	NS	NS
F x V	NS	NS	NS	NS	NS	NS
V x R	NS	NS	NS	NS	NS	NS
F x R x V	NS	NS	NS	NS	NS	NS

Means with unlike letter(s) in columns are significantly different at $p \leq 0.05$ by Duncan's Multiple Range Test (DMRT), NS stands for not significant, * stands for significant at 5%, V, Fand L stands for variety, fertilizer source and rate respectively

4.9.9 Effects of zeolite A, phillipsite based fertilizers and NPK 15:15:15 fertilizer on the soil nutrient content after the harvest

The result of the physical and chemical properties of the soil used in this study is presented in Table 4.31. The initial soil parameters of the study area was analysed according to the rating chart for analytical soil nutrient values for soil pH, organic carbon, available phosphorous and potassium parameters reported by (Onwudike *et al*., 2016). The soil texture is sandy loam and slightly acidic with a pH of 6.83. The organic carbon value of 6.7 g/kg is rated low. The total nitrogen value of 1.46 mg/kg is rated low. The available Phosphorous value of 5.86 mg/kg is rated low. The value for Potassium is 3.80 mg/kg and it is rated very high. The cation exchange capacity of the soil is 14.88 cmol/kg and it is rated as moderate (Abah and Petja, 2015).

The major plant nutrients of the soil were measured after harvesting the tomatoes as shown in Table 4.30. The comparisons of the initial nitrogen content of the soil with those of post-harvest revealed that most of the zeolite based fertilizers applied retained more nitrogen than the nitrogen content in the initial soil. It was generally observed that Zeolite A based fertilizer retained the highest nitrogen content and it was followed by phillipsite based fertilizer and conventional NPK fertilizer had the least nitrogen content. The reason for the observed decrease in nitrogen content from zeolite A fertilizers to NPK fertilizers is that zeolite based fertilizers have zeolite carriers which have their negative surface charge reversed to positive with a surfactant (HDTMA-Br) in order to adsorb the nitrogen molecules in their nitrate form on its exchange sites. In contrast, conventional fertilizers with their nitrogen content in nitrate forms were repelled by the negative framework charge of the clay in the soil. The nitrogen in nitrate forms are therefore highly susceptible to leaching of

plant nutrient beyond the root zone due to their high solubility in water. This trend is in agreement with Rajonee *et al*. (2016) report that nano fertilizers retain higher content of inorganic nitrogen than conventional ones.

It was also observed in Table 4.30 that zeolite A and phillipsite based fertilizers had higher phosphorous content than the conventional NPK fertilizer. This might be traceable to the zeolite based fertilizers possessing zeolite surface modified for adsorption of phosphate molecules whereas in conventional NPK fertilizers, the available phosphate anions are ordinarily supported by fillers and not adsorbed to them. These fillers are sometimes made up of saw dust, limestone and clay which are mixed with these negatively charged plant nutrients and they are easily leached from the soil because of negative charge repulsion. The high phosphorous content in the soil with phillipsite based fertilizer could be explained by the high selectivity of phillipsite for the phosphate anion.

The potassium content in the soil where zeolite A and phillipsite based fertilizer were applied were higher than those of conventional NPK fertilizer as shown in Table 4.30. The observed increase in potassium content of the zeolite based fertilizers could be traced to the fact that the potassium cations are not easily leachable in the soil. This observation can be further explained by the negative surface charge of zeolites framework which allows potassium ion which are cations to be readily attracted to the negative sites of the zeolite and the clay in the soil. The large surface areas of the zeolite framework have nano-pores in form of cavities and channels whose diameters are small enough to adsorb the small size potassium cations. HDTMA molecules are adsorbed on the zeolite external surface areas and therefore they could not assess the inner pores due to their large molecular sizes. The high potassium content observed in phillipsite based

fertilizers could be attributed to the addition of the mineralizing agent, potassium hydroxide during the phillipsite synthesis. The chart for analysing the soil parameters were shown in Table 4.31

Table 4.30: Effects of Zeolite A and Phillipsite based fertilizers and conventional NPK 15:15:15 fertilizer on the soil nutrients after the harvest of tomatoes

Fertilizer Sources	Initial Soil Analysis	Moderate Limits	Roma VF Zeolite A	Phillipsite	NPK 15:15:15	UC82b Zeolite A	Phillipsite	NPK 15:15:15
Soil Parameters								
Soil pH	6.83	6.6 – 7.3	6.88	6.98	6.63	7.08	7.14	6.50
Conductivity (uS/cm)	30.9	40 - 80	82	83	114	99	70	117
Organic Carbon (g/kg)	6.70	10 - 15	8.60	6.60	6.90	6.40	9.80	3.50
Total Nitrogen (mg/kg)	1.46	1.5 – 2.0	2.10	1.70	1.40	2.00	1.80	1.50
Available Phosphorous (mg/kg)	5.86	10 - 20	8.15	9.93	6.16	7.84	9.59	5.63
Exchangeable Bases								
Na (mg/g)	34.5	23 - 69	110.40	78.20	96.60	105.8	280.60	105.8
K (mg/g)	3.80	5.85 – 11.70	4.20	5.00	3.20	3.90	5.20	3.80
Mg (mg/g)	93.00	36 - 120	120.00	96.00	156.00	216.00	108.00	132.00
Ca (mg/g)	550.00	400 - 1000	480.00	540.00	540.00	540.00	500.00	540.00
Exchangeable Acid (cmol/Kg)	0.05	0.03 – 0.08	0.06	0.08	0.08	0.06	0.06	0.08
Effective Cation Exchange Capacity(cmol/Kg)	4.21	6 - 12	4.30	4.42	4.08	5.38	5.20	4.66
Cation Exchange capacity (CEC)	15.91	12 - 25	18.47	20.10	17.88	18.99	19.03	17.60

Table 4.31: Critical Limits for interpreting levels of soil nutrients

Parameter	Low	Medium	High
Calcium (mg/kg)	< 400	400 – 1000	1000
Magnesium (mg/kg)	< 36	36 - 120	> 120
Potassium (mg/kg)	<5.85	5.85 – 11.7	> 11.7
Sodium (mg/kg)	< 23	23 - 69	> 69
Cation Exchange Capacity (cmol/kg)	< 6.0	12 - 25	>40
Organic Carbon (g/kg)	< 10.00	10 – 15	>15
Total Nitrogen (mg/Kg)	< 1.5	1.5 – 2.0	>2.0
Available Phosphorous (mg/kg)	< 5.00	10 - 20	>20
B. S (%)	< 50	– 80	>80
Soil pH	< 6.5	6.6 – 7.3	>7.4

(Afolabi *et al*.2014; Abah and Petja, 2015)

PLATE XII: Image of Zeolite A, Phillipsite based fertilizer and NPK 15: 15: 15 fertilizer treatments at 11 (WAT)

CHAPTER FIVE

5.0 CONCLUSION AND RECOMMENDATIONS

5.1 Conclusion

The lack of good agricultural practices and high solubility of inorganic fertilizer are probable the most common sources of ground water nitrate pollution caused by excessive use of fertilizer. The challenge has led to the selection of low cost materials such as Ahoko kaolin which are converted into low silica zeolites with high surface area and high cation exchange. The surfaces of these low silica zeolites such zeolite A and phillipsite were functionalized with surfactant hexadecyltrimethylammonium bromide (HDTMA-Br) in order to adsorb potassium, phosphates and nitrates necessary to enhance soil fertility. The slow release property of synthesised zeolite A and phillipsite based fertilizers were evaluated on tomato crop for its effect on growth, fruit yield and quality, and delay of plant nutrient leaching out of the root zone. The results from the study shows the following objectives were met.

A high crystalline zeolite A was synthesised from Ahoko Kaolin from a statistical designed experimental 30 runs revealed an optimised product with a cubic morphology from SEM analysis and intensed zeolite A characterisitcs peak from XRD results. The high crystallinity of zeolite A is in correlation with its high cation exchange capacity.

A low silica phillipsite with spherical and prismatic morphology was synthesised from locally sourced Ahoko Kaolin having varied the synthesis parameters within the design space using central composite design of 20 experimental runs. The high surface area of phillipsite is a potential for high adsorption capacity. The increasing contribution of the synthesis variable of crystallisation time is an indication of higher orderliness of the crystalline atoms.

The functionalisation of the zeolite A and phillipsite surfaces with HDTMA were carried out successfuly through the use of Central Composite Design. The highly stable surfactant whose polar head is made to adsorb on the negative charged zeolites makes it serve as an enduring plant nutrient carrier. FTIR confimes that bulky molecule of HDTMA was adsorbed on the zeolite and it was not hidden in the micropores of the zeolites. The reduced BET surface area of the modified zeolites also reveal modification that took place. The simultaneous propery of cations and anions on the functionalised zeolite reveal the potential to carry both cationic and anionic plant nutrients.

The isotherm, kinetics and thermodynamic parameters obtained from the adsorption process of HDTMA on zeolite A and Phillipsite provides insight into the mechanism adsorption. The kinetics provides information on how fast the spontaneous adsorption process will go. The isotherm constants give an estimate of the adsorption capacity of the zeolites and further insight into the pore filling nature of the adsorption.

The desorption of oxyanions from phosphate and nitrate loaded zeolite A and phillipsite based fertilizers revealed that phosphate loaded zeolite A based fertilizer showed slower release effect with the rate constant k_2 of 1.8 x $10^{-3}h^{-1}$ compared with potassium dihydrogen phosphate (KH_2PO_4) fertilizer with its rate constant k_2 of 3.84 x$10^{-3}h^{-1}$. The nitrate loaded zeolite A based fertilizer with rate constants k_2 of 5.51 x $10^{-2}h^{-1}$ were slower than ammonium nitrate (NH_3NO_3) fertilizer with rate constants k_2 of 9.70 x $10^{-2}h^{-1}$.

The effect of the nutrient release from the zeolite based fertilizers and NPK fertilizers were carried out on two tomato crop varieties. It was observed that more leaf counts of the zeolite based fertilizers were observed to be greener in comparison to the NPK 15:15:15 fertlizer at post-harvest (11WAT). There was also significant difference in the tomato fruit yield for

zeolite A and Phillipsite based fertilizers in comparism to NPK 15: 15:15 fertilizer. It was further observed that the nutritive fruit contents of nitrogen, potassium, calcium, magnesium, potassium, phosphorous and vitamin C showed that plants treated with zeolite A and phillipsite based fertilizers were significantly higher than plants treated with NPK 15:15 15 fertilizers. The slow releasing property of the zeolite A and phillipsite based fertilizers were evaluated on the soil at post harvest and the results indicated that their nitrogen, potassium and phophorous contents were higher than that of conventional NPK fertilizers as a result of the delaying effect of the zeolite carriers.

5.2 Recommendations

The following recommendations are made to further support the discussion in this subject area

i). Investigation on other High-silica zeolites such as ZSM-5 that could give higher surface areas could be studied

ii). Synthesis conditions that could enhance side products with high percentages that are formed in the course of synthesizing phillipsite such as zeolite P could be investigated as a potential source for fertilizer carrier.

iii). Zeolitic products from the precursor of kaolin are usually accompanied by impurities. Further works could be carried out on how to purify zeolite A and phillipsite and thereby enhancing their crystallinity

iv). Zeolites are reported in literature to have high moisture retention. Studies on the effects of moisture retention property of zeolite based fertilizers on the growth, fruit yield and quality of short and long gestation crops cultivated during the peak of dry season or in arid regions.

v). The slow release property of zeolite based fertilizers had denied the nutrients demanded by the plant. Therefore the timing of the application of zeolite based fertilizers could be studied to determine the optimum period which would enhance adequate plant health and growth.

vi). The effect of the fertilizer sources on the shelf life of the tomatoes would futher add information on the zeolite based fertilizer developed.

5.3 Contributions to Knowledge

i). The production and functionalisation of zeolite A and phillipsite obtained from Ahoko Kaolin with appropriate cation exchange and nutrients embolic capacities.

ii). The development of slow release fertilizers from the functionalized zeolites A and phillipsite possessing low nutrients leaching rates in the soil.

iii). The establishment of enhanced agronomic impacts of the synthesised fertilizer on Tomato (*Lycopersicon esculentum*) as well as their optimal process conditions

iv). Zeolite A and Phillipsite as a slow released fertilizers were synthesised and characterized from Ahoko Kaolin for the first time and the mechanism of desorption of plant nutrient determined.

v). The synthesis of phillipsite with crystallinity of 72.26% from Ahoko Kaolin for the first time and used as a fertilizer carrier with a steady desorption rate constant of $1.05 \times 10^{-3} h^{-1}$ for nitrate ions

vi). The application of Zeolite A based fertilizer on tomato resulted in a significant high vitamin C nutritive fruit content with mean 123.24 statistically significant with respect to NPK 15:15:15 with mean 84.60

REFERENCES

Abah, R. C. and Petja, B. M. (2015). The socio-economic factors affecting agricultural development in the lower river Benue Basin. *Journal of Biology, Agriculture and Healthcare*, *5*(24), 12-23.

Abdullahi, T., Harun, Z., Othman, M. H. D., Nuhu, A. H. and Usman, J. (2017a). Conversion and characterization of synthetic zeolite using low grade kaolin from Mersing area of Johor. In *AIP Conference Proceedings*, 68(1), 201-209.

Abdullahi, T., Harun, Z. and Othman, M. H. D. (2017b). A review on sustainable synthesis of zeolite from kaolinite resources via hydrothermal process. *Advanced Powder Technology*, *28*(8), 1827-1840.

Abukhadra, M. R. and Mostafa, M. (2019). Effective decontamination of phosphate and ammonium utilizing novel muscovite/phillipsite composite; equilibrium investigation and realistic application. *Science of the Total Environment*, 667(1), 101-111.

Acquafredda, P. (2019). XRF technique. *Physical Sciences Reviews*, 4(8). 31 - 62

Adhikari, T. A. and Ramana, S. I. (2019). Nano Fertilizer: Its impact on crop growth and soil health. *Journal of Research Pjtsau,* 47(1), 1-70.

Adisaputra, M. K. and Kusnida, D. (2010). Paleocene postgenetic Accumulation of Nannoplankton on the Phillipsite Minerals in Roo Rise, Indian Ocean. *Indonesian Journal on Geoscience*, 5(1), 49-56.

Afolabi, S. G., Adeboye, M.K. A., Adekanmbi, A. A., Yusuf A. A., and Tsado, P. A. (2014). Evaluation of some soils of Minna production. *National Journal of Agriculture, Food and Environment* 10(4), 6 – 9

Agbede, T. M., Adekiya, A. O., Ale, M. O., Eifediyi, E. K. and Olatunji, C. A. (2018). Soil properties, growth, fruit yield, mineral, lycopene and vitamin C contents of tomato (*Lycopersicon esculentum mill*) grown with green manures and NPK fertilizer. *Agriculturae Conspectus Scientificus,* 83(4), 291-297.

Agbenin, J.O. (1995). Laboratory Manual for soil and plant analysis (selected methods and data analysis). *Faculty of Agriculture/Institute of Agricultural Research*, *Ahamadu Bello University*, *Zaria*, 5(2), 7-71.

Ahmadkhaniha, D., Sohi, M. H., Zarei-Hanzaki, A., Bayazid, S. M. and Saba, M. (2015). Taguchi optimization of process parameters in friction stir processing of pure Mg. *Journal of Magnesium and Alloys*, 3(2), 168-172.

Ahmadishoar, A., Bahrami, S. H., Movassagh, B., Amirshahi, S. H. and Arami, M. (2016). Effect of Spacer and Alkyl Chain Groups of the Synthesised Cationic Gemini Surfactants on the Surface Modification of Nano Na-Montmorillonite and its Dye Adsorption from Textile Waste Water. *Indian Journal of Science and Technology*, *9(1)*, 1-10.

Ahmed, M., Rauf, M., Mukhtar, Z. and Saeed, N. A. (2017). Excessive use of nitrogenous fertilizers: an unawareness causing serious threats to environment and human health. *Environmental Science and Pollution Research*, *24*(35), 26983-26987.

Akbari, H., Modarres-Sanavy, S. A. M. and Heidarzadeh, A. (2021). Fertilizer systems deployment and zeolite application on nutrients status and nitrogen use efficiency. *Journal of Plant Nutrition*, 44(2), 196-212.

Alaba, P. A., Sani, Y. M., and Daud, W. M. A. W. (2015). Synthesis and characterization of hierarchical nanoporous HY zeolites from acid-activated kaolin. *Chinese Journal of Catalysis*, 36(11), 1846-1851

Alhawary, H. F., Abobaker, A. M., Rizk, S. A., Hegazi, A. Z. and Agoor, A. A. (2017). Field application of trivalent foot and mouth disease vaccine adjuvant with Zeolite. *Journal of Virology Science*, 2(1), 32-41.

Ali, S., and Danafar, F. (2015). Controlled-release fertilizers: advances and challenges. *Life Science Journal*, 12(11), 33-45.

Alsawalha, M. (2019). Overview of current and future perspectives of Saudi Arabian natural clinoptilolite zeolite: a case review. *Journal of Chemistry*, 2(1), 20 - 28.

Aminiyan, M. M., Sinegani, A. A. S. and Sheklabadi, M. (2015). Aggregation stability and organic carbon fraction in a soil amended with some plant residues, nanozeolite, and natural zeolite. *International Journal of Recycling of Organic Waste in Agriculture*, 4(1), 11-22.

Amir, Z.K., Khan, H., Nigar, S., Saeed, B.H., Guli, A., Wahab, S. A., Muhammad, M.A, Henmi, T. (2011). Morphology and yield of soybean grown on allophonic soil as influenced by synthetic zeolite application. *Pakistan Journal of Botany*, 43(4), 2099-2107.

Amir, Z.K., Nigar, S., Shad, K., Khalil, S., Wahab, A., Rab, M.K., Khattak and Teru, H. (2013). Influence of synthetic zeolite application on seed development profile of soybean grown on allophonic soil. *Pakistan Journal of Botany*, 45(3), 1063-1068.

Anari-Anaraki, M. and Nezamzadeh-Ejhieh, A. (2015). Modification of an Iranian clinoptilolite nano-particles by hexadecyltrimethyl ammonium cationic surfactant and dithizone for removal of Pb (II) from aqueous solution. *Journal of Colloid and Interface Science*, *440(1)*, 272-281.

Ande, O. T., Huising, J., Ojo, A. O., Azeez, J., Are, K. S., Olakojo, S. A. and Ojeniyi, S. O. (2017). Status of integrated soil fertility management (ISFM) in southwestern Nigeria. *International Journal of Sustainable Agricultural Research*, 4(2), 28-44.

AOAC (2002). Official Method of Analysis 16th Edition, Association of Official Analytical Chemist, Washington DC USA

Arogundade O.A. (2014), *Development of kinetic parameters for the dealumination of Elefun kaolinite clay*, (Master's thesis), Covenant University, Ota, Ogun State, Nigeria.

Aroke, U. O. and El-Nafaty, U. (2014). XRF, XRD and FTIR properties and characterization of HDTMA-Br surface modified organo-kaolinite clay. *International Journal of Emerging Technology and Advanced Engineering*, *4(4)*, *817-825*

Asiedu, O. (2016). Removal of Fluoride from water using Surfactant Modified Synthetic Zeolites (Doctoral dissertation), Kwame Nkrumah University of Science and Technology, Kumasi, Ghana.

Asgari, G., Roshani, B., and Ghanizadeh, G. (2012). The investigation of kinetic and isotherm of fluoride adsorption onto functionalize pumice stone. *Journal of Hazardous Materials*, 217(1), 123-132.

Atugoda, T., Wijesekara, H., Werellagama, D. R. I. B., Jinadasa, K. B. S. N., Bolan, N. S. and Vithanage, M. (2020). Adsorptive interaction of antibiotic ciprofloxacin on polyethylene microplastics: Implications for vector transport in water. *Environmental Technology and Innovation*, 19(1), 10 - 19.

Auta, M. and Hameed, B. H. (2011). Optimized waste tea activated carbon for adsorption of Methylene Blue and Acid Blue 29 dyes using response surface methodology. *Chemical Engineering Journal*, 175(1), 233-243.

Ayele, L., Pérez-Pariente, J., Chebude, Y., and Díaz, I. (2015). Synthesis of zeolite A from Ethiopian kaolin. *Microporous and Mesoporous Materials*, 215(1), 29-36.

Ayele, L., Pérez-Pariente, J., Chebude, Y. and Díaz, I. (2016). Conventional versus alkali fusion synthesis of zeolite A from low grade kaolin. *Applied Clay Science*, *132(1)*, 485-490.

Ayawei, N., Ebelegi, A. N., and Wankasi, D. (2017). Modeling and interpretation of adsorption isotherms. *Journal of Chemistry*, 10(1), 57- 65

Azman, N. A. N., Malek, N. A. N. N., Noor, N. S. M. and Javed, M. A. (2018). *Asian Journal of Agriculture and Biology*, 6(1), 55-65.

Baerlocher, C., McCusker, L. B. and Olson, D. H. (2007). *Atlas of zeolite framework types* (pp 51 -61). Elsevier.

Bakhtiary, S., Shirvani, M. and Shariatmadari, H. (2013). Characterization and 2, 4-D adsorption of sepiolite nanofibers modified by N-cetylpyridinium cations. *Microporous and mesoporous materials*, 168(1), 30-36.

Balarak, D., Mostafapour, F. K., Azapira, H., and Joghataei, A. (2017). Langmuir, freundlich, temkin and dubinin-radushkevich isotherms studies of equilibrium sorption of amplicillin unto montmorillonite nanoparticles. *Journal of Pharmaceutical Research International*, 2(1), 1 – 9

Bamaniya, B., Ali, S. A., Ramgiri, S. R., Shrivastava, A. and Bain, R. P. (2019). Performance of Tomato Hybrids for Growth, Yield and Quality under Western Track of Vindhyan

Plateau of Madhya Pradesh, India. *International Journal of Current Microbiology Applied Science*, 8(12), 2226-2232.

Bandura, L., Franus, M., Jozefaciuk, G., and Franus, W. (2015). Synthetic zeolites from fly ash as effective mineral sorbents for land-based petroleum spills cleanup. *Fuel*, 147(12), 100-107

.

Bansiwal, A. K., Rayalu, S. S., Labhasetwar, N. K., Juwarkar, A. A., and Devotta, S. (2006). Surfactant-modified zeolite as a slow release fertilizer for phosphorus. *Journal of Agricultural and Food Chemistry*, 54(1), 4773-4779.

Baruah, A., Chaudhary, V., Malik, R. and Tomer, V. K. (2019). Nanotechnology based solutions for wastewater treatment. In *Nanotechnology in Water and Wastewater Treatment* (pp. 337-368).

Basaldella, E. I., Kikot, A. and Pereira, E. (1990). Synthesis of zeolites from mechanically activated kaolin clays. *Reactivity of solids*, *8*(2), 169-177.

Bazgaou, A., Fatnassi, H., Bouharroud, R., Ezzaeri, K., Gourdo, L., Wifaya, A. and Bouirden, L. (2021). Effect of active solar heating system on microclimate, development, yield and fruit quality in greenhouse tomato production. *Renewable Energy*, 165, 237-250.

Berar, V. and Posta, G. (2011). Research concerning the zeolites influence, used in the culture substratum, upon the quality of green house grown tomato, *Journal of Horticulture*, *Forestry and Biotechnology*, 15(4), 45 – 47

Bernardi, A.C.C., Carlos, G.W., Patrick, G.H., Neide, B. J., Oiano-Neto, M. B., Maria, R. V. (2007). Yield and fruit quality of tomato grown in substrate with zeolite. *Horticultura Brasileira,* 25(12), 306-311.

Bernardi, A. C. C., Mota, E. P., Souza, S. C. H., Cardoso, R. D., and Oliviera, P. P. A. (2010). Ammonia volatilization, dry matter yield and nitrogen levels of Italian ryegrass fertilized with urea and zeolite. *19th world congress of soil science*, *soil solutions for a changing world 1-6 August 2010*, 22-26. Brisbane, Australia.

Bernardi, A.C., and Verruma-Bernardi, M.R. (2013). Increases in Yield and Vitamin C levels of Tomato Grown on K_2HPO_4 –enriched Zeolite in an inert-sand substrate, The Electronic International Fertilizer Correspondent (e-ifc) of the Edition Number 33: 3: Research Findings.

Bhardwaj, D., and Tomar, R. (2011). Use of surface modified inorganic nano materials as slow release nitrogen fertilizer. *In Sustainable Agricultural Development* (pp. 171-184). Springer, Dordrecht.

Bharadwaj, D. N. (2016). Sustainable agriculture and plant breeding. In *Advances in Plant Breeding Strategies: Agronomic*, *Abiotic and Biotic Stress Traits* (pp. 3-34). Springer, Cham.

Bilgin, O. and Koc, E. (2013). Zeolites in medicine and Turkey zeolites, *International Multidisciplinary Scientific GeoConference: SGEM: Surveying Geology and mining Ecology Management*, *2*, 673.

Biramo, G. (2018). The role of integrated nutrient management system for improving crop yield and enhancing soil fertility under small holder farmers in Sub-Saharan Africa: A review article. *Mod Concep Dev Agrono*. MCDA, 54(7), 2 - 7.

Biswas, S., and Mishra, U. (2015). Effective remediation of lead ions from aqueous solution by chemically carbonized rubber wood sawdust: equilibrium, kinetics, and thermodynamic study. *Journal of Chemistry*, 2(5), 19 -21

Bortolatto, L. B., Santa, R. A. B., Moreira, J. C., Machado, D. B., Martins, M. A. P., Fiori, M. A. and Riella, H. G. (2017). Synthesis and characterization of Y zeolites from alternative silicon and aluminium sources. *Microporous and Mesoporous Materials*, 248, 214-221.

Bosch, P., Ortiz, L., and Schifter, I. (1983). Synthesis of faujasite type zeolites from calcined kaolins. *Industrial and Engineering Chemistry Product Research and Development*, *22*(3), 401-406.

Bouakham, S., Carmelita, M. R., Antonio, J. A. and Maria, V. O. (2015). Land cover changes and resource use patterns of selected communities in Phanang national protected area, Sangthong district, Vientiane capital, Lao PDR. *Journal of Environmental and Science and Management*, 18(3), 33 – 43.

Bumbac, M., Nicolescu, C. M., Gheboianu, A. I., Olteanu, R. L., Hossu, A. M. and Setnescu, T. (2016). Evaluation of ammonium exchange capacity for agricultural soils treated with zeolites. INCD ECOIND – International symposium – SIMI 2006 The "Environment and Industry", Proceeding's book, Valahia University of Targoviste, Romania.

Bunaciu, A. A., Udristioiu, E. G. and Aboul-Enein, H. Y. (2015). X-ray diffraction: instrumentation and applications. *Critical reviews in analytical chemistry*, 45(4), 289-299.

Burton, A. (2018). Recent trends in the synthesis of high-silica zeolites, *Catalysis Reviews*, 60(1), 132-175.

Cairo, P. C., de Armas, J. M., Artiles, P. T., Martin, B. D., Carrazana, R. J. and Lopez, O. R. (2017). Effects of zeolite and organic fertilizers on soil quality and yield of sugarcane. *Australian Journal of Crop Science*, *11*(6), 7 -16

Celik, F.E., Kim, T.J. and Bell, A.T. (2010). Effect of zeolite framework type and Si/Al ratio on dimethoxymethane carbonylation. *Journal of Catalysis*, 270(1), 185 – 195.

Chan, M. T., Selvam, A. and Wong, J. W. (2016). Reducing nitrogen loss and salinity during 'struvite'food waste composting by zeolite amendment. *Bioresource technology*, 20(3), 838-844.

Chao, H. P. and Chen, S. H. (2012). Adsorption characteristics of both cationic and oxyanionic metal ions on hexadecyltrimethylammonium bromide-modified NaY zeolite. *Chemical Engineering Journal*, 19(3), 283-289.

Chandrasekhar, S., and Pramada, P. N. (2008). Microwave assisted synthesis of zeolite A from metakaolin. *Microporous and Mesoporous Materials*, *108*(3), 152-161.

Channabasavaraj, W. and Reddy, R. (2017). Review on Characterization and Application of Fly Ash Zeolites. *International Journal of Development Research, 7(1),* 14294-14300.

Chaudhuri, A. R., Dey, G. K., and Pal, T. K. (2002). Synthesis and Characterization of Detergent-Grade Zeolite from Indian Clay. *Chemical Engineering and Technology*, *25*(1), 91-95.

Chen, J., Lu, S., Zhang, Z., Zhao, X., Li, X., Ning, P. and Liu, M. (2018). Environmentally friendly fertilizers: A review of materials used and their effects on the environment. *Science of the Total Environment*, 61(3), 829-839.

Chen, H. F., Lo, H. J., Song, S. R., Fang, J. N., Chen, Y. L., Li, L. J., Lee, Y. T. (2002). The synthesis of phillipsite. *Western Pacific Earth Sciences*, *2*(4), 381-392

Chen, T., Xia, G., Wu, Q., Zheng, J., Jin, Y., Sun, D. and Chi, D. (2017). The influence of zeolite amendment on yield performance, quality characteristics, and nitrogen use efficiency of paddy rice. *Crop Science*, 57(5), 2777- 2787.

Chojnacka, M., Warchoł, J., and Sobolewska, P. (2018). Effect of the pH on the Cr (VI) Sorption on HDTMA-zeolites. *Journal of Environmental Science and Engineering*, 1(7) 261 – 267

Clough, M., Pope, J. C., Lin, L. T. X., Komvokis, V., Pan, S. S., and Yilmaz, B. (2017). Nanoporous materials forge a path forward to enable sustainable growth: Technology advancements in fluid catalytic cracking. *Microporous and Mesoporous Materials*, *254(1)*, 45-58.

Cole, J. C., Smith, M. W., Penn, C. J., Cheary, B. S., and Conaghan, K. J. (2016). Nitrogen, phosphorus, calcium, and magnesium applied individually or as a slow release or controlled release fertilizer increase growth and yield and affect macronutrient and micronutrient concentration and content of field-grown tomato plants. *Scientia horticulturae*, *2(1)*, 420-430

Comboni, D., Gatta, P., Lotti, M., Merlini, H.P. (2016). On the P - induced behavior of the zeolite phillipsite : an in situ single - crystal synchrotron X - ray diffraction study, *Physcal and Chemical Minerals*, 17(2), 89 – 96.

Colella, B., De Gennaro, S. R., Salvestrini, C.(2015). Surface interaction of humic acids with natural and synthetic phillipsite, *Clay Minerals*, 13(7), 36-44.

Cornelius, M. L. U., Price, L., Wells, S. A., Petrik, L. F., and Sartbaeva, A. (2019). The steric influence of extra-framework cations on framework flexibility: an LTA case study. *Zeitschrift für Kristallographie-Crystalline Materials*, *234*(7), 461-468.

Cvetko, Z., Jelena, K., Simo, M., Dragoman, R. (2013). A Preliminary study on the effect of the natural clinoptilolite and bentonite additions on the Tomato "Nemo Netta" growth. In *Proceedings of the 5th Serbian-Croatian-Slovenian Symposium on Zeolites. Geoloski zavod Srbije*, Belgrade, Serbia.

Darvanjooghi, M. H., Davoodi, S. M., Dursun, A. Y., Ehsani, M. R., Karimpour, I., and Ameri, E. (2018). Application of treated eggplant peel as a low-cost adsorbent for water treatment toward elimination of Pb^{2+}: Kinetic modeling and isotherm study. *Adsorption Science and Technology*, *36*(3-4), 1112-1143.

Das, B., Mondal, N. K. and Chattaraj, P. R. S. (2013). Equilibrium, kinetic and thermodynamic study on chromium (VI) removal from aqueous solution using Pistia stratiotes biomass. *Chemical Science Transactions*, *2*(1), 85-104.

Ditta, A. and Arshad, M. (2016). Applications and perspectives of using nanomaterials for sustainable plant nutrition. *Nanotechnology Reviews,* 5(2), 209-229.

Demirçivi, P. and Saygılı, G. (2014). Sorption isotherms and modeling studies of HDTMA for adsorption onto vermiculite, perlite and zeolite clays. *Sigma Journal of Engineering and Natural Sciences*, *32(7)*, 311-320

Drevkova, M., Bencoova, B., Tudos, D., Puzder, M. and Slosar, D. (2017). Traditional and innovative applications of natural zeolites in household products. *International Multidisciplinary Scientific GeoConference: SGEM: Surveying Geology and Mining Ecology Management*, *17(1)*, 651-658.

Dusselier, M., and Davis, M. E. (2018). Small-pore zeolites: synthesis and catalysis. *Chemical reviews*, 118(11), 5265-5329.

Elemike, E. E., Uzoh, I. M., Onwudiwe, D. C.and Babalola, O. O. (2019). The role of nanotechnology in the fortification of plant nutrients and improvement of crop production. *Applied Sciences*, 9(3), 49 - 57.

Epp, J. (2016). X-ray diffraction (XRD) techniques for materials characterization. In Materials characterization using nondestructive evaluation (NDE) methods (pp. 81-124). Woodhead Publishing.

Eroglu, N., Emekci, M., and Athanassiou, C. G. (2017). Applications of natural zeolites on agriculture and food production. *Journal of the Science of Food and Agriculture*, 97(11), 3487-3499.

Faccini, B., Di Giuseppe, D., Ferretti, G., Coltorti, M., Colombani, N. and Mastrocicco, M. (2018). Natural and NH 4+-enriched zeolitite amendment effects on nitrate leaching from a reclaimed agricultural soil (Ferrara Province, Italy). *Nutrient cycling in agroecosystems*, 110(2), 327-341.

Felipe, S. D., Jadir N. S., Luiz F. T., Albino, J.M. and Luciano, B.M. (2015). Air pollution and their mitigation measures in Brazilian poultry production. *African Journal of Agricultural Research*, 10(50), 4522-4531.

Ferreira, S. L., Lemos, V. A., de Carvalho, V. S., da Silva, E. G., Queiroz, A. F., Felix, C. S. and Oliveira, R. V. (2018). Multivariate optimization techniques in analytical chemistry-an overview. *Microchemical Journal*, 140(1), 176-182.

Ferretti, G., Keiblinger, K. M., Faccini, B., Di Giuseppe, D., Mentler, A., Zechmeister-Boltenstern, S. and Coltorti, M. (2020). Effects of Different Chabazite Zeolite Amendments to Sorption of Nitrification Inhibitor 3, 4-Dimethylpyrazole Phosphate (DMPP) in Soil. *Journal of Soil Science and Plant Nutrition*, 1(1), 1-6.

Fletcher, R. E., Ling, S., and Slater, B. (2017). Violations of Löwenstein's rule in zeolites. *Chemical science*, 8(11), 7483-7491.

Fuerjierfu, B. (2016). The effect of the grit stone on feed passage rate in broiler chickens (Master's thesis, Norwegian University of Life Sciences) As

Fungaro, D. A. and Magdalena, C. P. (2014). Counterion Effects on the Adsorption of Acid Orange 8 from Aqueous Solution onto HDTMA-Modified Nanozeolite from Fly Ash. *Environment and Ecology Research*, *2*(2), 97-106

Gan, F., Zhou, J., Wang, H., Du, C. and Chen, X. (2009). Removal of phosphate from aqueous solution by thermally treated natural palygorskite. *Water Research*, 43(11), 2907-2915.

Gao, Li., Sun, D., and Huang, J. (2017). Impact of Land tenure policy on agricultural investments in China: Evidence from a panel data study, *China Economic Review*, 45(3), 244 – 252.

Georgiev, D., Bogdanov, B., Markovska, I. and Hristov, Y. (2011). Synthesis of NaA Zeolite from Natural Kaolinite, *Oxidation Communications*, 34(4), 812–819.

Ghadamnan, E., Nabavi, S. R. and Abbasi, M. (2019). Nano LTA Zeolite in Water Softening Process: Synthesis, Characterization, Kinetic studies and process optimization by Response Surface Methodology (RSM). *Journal of Water and Environmental Nanotechnology*, 4(2), 119-138.

Ghomashi, P., Charkhi, A., Kazemeini, M. and Yousefi, T. (2020). Removal of fluoride from wastewater by natural and modified nano clinoptilolite zeolite. *Journal of Water and Environmental Nanotechnology*, 5(3), 270-282.

Gholamhoseini, M. and Gholamhoseini, M. (2018). Zeolite Applications in Agriculture. *Horticulture and Arboriculture*, 1(1), 1-2.

Gordina, N. E., Prokof'ev, V. Y., Hmylova, O. E., and Kul'pina, Y. N. (2017). Effect of ultrasound on the thermal behavior of the mixtures for the LTA zeolite synthesis

based on metakaolin. *Journal of Thermal Analysis and Calorimetry*, *129* (3), 1415-1427

Gougazeh, M., and Buhl, J. C. (2014). Synthesis and characterization of zeolite A by hydrothermal transformation of natural Jordanian kaolin. *Journal of the Association of Arab Universities for Basic and Applied Sciences*, 15(1), 35-42.

Gu, B., Bai, J., Yang, W., and Li, C. (2019). Synthesis of ANA-zeolite-based Cu nanoparticles composite catalyst and its regularity in styrene oxidation. *Microporous and Mesoporous Materials, 274(3),* 318-326.

Gupta, V. K., Sadegh, H., Yari, M., Shahryari, G. R., Maazinejad, B. and Chahardori, M. (2015). Removal of ammonium ions from wastewater a short review in development of efficient methods. *Global Journal of Environmental Science and Management*, 2(1), 149 – 158.

Gulten, C. (2014). Removal of Hardness of Earth Alkaline Metals from Aqueous Solutions by Ion Exchange Method. International Scholarly Research Notices, *Analytical Chemistry*, (2)4, 12 – 19.

Guo, Y., Liu, Z., Zhang, M., Tian, X., Chen, J. and Sun, L. (2018). Synthesis and application of urea-formaldehyde for manufacturing a controlled-release potassium fertilizer. *Industrial and Engineering Chemistry Research*, 57(5), 1593-1606.

Hadigavabar, A. D., Tabatabaeian, K., Zanjanchi, M. A. and Mamaghani, M. (2018). Molybdenum anchored onto zeolite beta: an efficient catalyst for the one-pot synthesis of octahydroquinazolinone derivatives under solvent-free conditions. *Reaction Kinetics*, *Mechanisms and Catalysis*, *124*(2), 857-871.

Hailu, S. L., Nair, B. U., Redi-Abshiro, M., Diaz, I. and Tessema, M. (2017). Preparation and characterization of cationic surfactant modified zeolite adsorbent material for adsorption of organic and inorganic industrial pollutants. *Journal of Environmental Chemical Engineering*, *5*(4), 3319-3329.

Ham, K., Kim, B. S. and Choi, K. Y. (2018). Enhanced ammonium removal efficiency by ion exchange process of synthetic zeolite after Na+ and heat pretreatment. *Water Science and Technology*, 78(6), 1417-1425.

Hasanuzzaman, M., Bhuyan, M. H. M., Nahar, K., Hossain, M., Mahmud, J. A., Hossen, M. and Fujita, M. (2018). Potassium: A vital regulator of plant responses and tolerance to abiotic stresses. *Agronomy*, 8(3), 31 – 39.

Hawkesford, M. J. (2014). Reducing the reliance on nitrogen fertilizer for wheat production. *Journal of Cereal Science,* 59(3), 276-283.

He, K., Chen, Y., Tang, Z. and Hu, Y. (2016). Removal of heavy metal ions from aqueous solution by zeolite synthesised from fly ash. *Environmental Science and Pollution Research* 3(2), 2778 – 2788.

Heller-Kallai, L. and Lapides, I. (2007). Reactions of kaolinites and metakaolinites with NaOH—comparison of different samples (Part 1). *Applied Clay Science*, *35*(2), 99-107.

Heller-Kallai, L. (2013). Thermally modified clay minerals. *In Developments in Clay Science*, 5(1), 411-433.

Higashiyama, H., Sano, M., Nakanishi, F., Takahashi, O. and Tsukuma, S. (2017). Surface temperature on asphalt pavements with colored cement-based grouting material containing ceramic waste powder and zeolite. *Nonlinear Analysis*, *1490*, 61881.

Hoeung, P., Yazid, B., Semuel, P. S. (2011). Development of Granular Urea-zeolite slow release fertilizer using inclined pan granulator. *Jurnal Teknik Kimia Indonesia*, 10(2), 102-111.

Holler, A., Barth-Wirsching, U. (2010): *Forthschritte der Miner*al 63(4), 21- 43.

Hommaid, O., and Hamdo, J. Y. (2014). Adsorption of chromium (VI) from an aqueous solution on a Syrian surfactant modified zeolite. *International Journal of Chemical Technological Research*, 6(7), 3753–3761.

.

Hossain, K., and Rameeja, S. (2015). Importance of nanotechnology in civil engineering. *European Journal of Sustainable Development*, 4(1), 161-161.

Huang, P. S., Su, C. Y., Lam, C. H., Lee, W. Y., Wang, D. M., Hua, C. C. and Kang, D. Y. (2018). Direct wet deposition of zeolite FAU thin films using stabilized colloidal suspensions. *Microporous and Mesoporous Materials*, 272, 286-295.

Hussain, N. A. and Radi, A. M. A. (2019). Effect of natural zeolite mineral and ground zeolite in physical properties of soil. *Plant Archives*, *19*(2), 135-139.

Ibrahim, (2014). Geology and mineralogy of zeolitic tuff in Tulul Unuqar Rustum Ash Shmaliyya, NE JORDAN, Jordan. *Journal of Earth Environmental Science*. 6, 29–34

Imbert, F. E., Moreno, C., Montero, A., Fontal, B. and Lujano, J. (1994). Venezuelan natural alumosilicates as a feedstock in the synthesis of zeolite A. *Zeolites*, *14*(5), 374-378.

Inan, H., Yazici, E., and Yigit, Z. (2016). Zinc removal from aqueous solutions by Turkish Clinoptilolite, *Journal of Hazardous Material*, 136(13), 938-945.

Inglezakis, V. and Antonis Z. (2012). Handbook of Natural Zeolites, 3 -10

Inglezakis, V. J. and Zorpas, A. A. (2012). Heat of adsorption, adsorption energy and activation energy in adsorption and ion exchange systems. *Desalination and water treatment*, *39*(1-3), 149-157.

Iqbal, M. and Umar, S. (2019). Nano-fertilization to enhance nutrient use efficiency and productivity of crop plants. *In Nanomaterials and Plant Potential* (pp. 473-505). Springer, Cham.

Iqbal, A., Sattar, H., Haider, R. and Munir, S. (2019). Synthesis and characterization of pure phase zeolite 4A from coal fly ash. *Journal of Cleaner Production*, 219, 258-267.

Iqra, J., Faryal, M., Uzaira, R., and Noshaba, T. (2014). Preparation of zeolite from incinerator ash and its application for the remediation of selected inorganic pollutants: A greener approach. *In IOP Conference Series: Materials Science and Engineering* (Vol. 60, No. 1, p. 012060). IOP Publishing.

Isah, A. S., Amans, E.B., Odion, E. C. and Yusuf, A. (2014). Growth rate and yield of two tomato varieties (*lycopersicon esculentum Mill*) under green manure and NPK fertilizer rate, Samaru Northern Guinea Savanna, *International Journal of Agronomy,* 8(1), 17 -25.

Jalil, R. U., Sameer, H. K., Sahar, S. H. (2013). Adsorption of Hydrogen Sulphide on the Zeolite type A synthesised from Iraqi kaolinite, *Baghdad Science Journal*, 10(3), 1023 – 1033.

Jakkula, V., Sandeep, W., Craig, D.H., Trevor, J., Fullen, M. A. (2011). High selectivity and affinity of synthetic Phillipsite compared with natural Phillipsite towards ammonium (NH_4^+) and its potential as a slow release fertilizer. *Archives of Agronomy and Soil Science*, 57(1), 47–60.

Jakkula, V. S. and Wani, S. P. (2018). Zeolites: Potential soil amendments for improving nutrient and water use efficiency and agriculture productivity. *Scientific Reviews and Chemical Communications*, *8*(1), 1-15.

Jami, M. G., Baghbani-Arani, A., Karami Borz-Abad, R. and Saadatkhah, A. (2019). Towards Improving the Vegetative and Qualitative Traits of Sunflower Using Amending Soil (Zeolite and Manure Farmyard) under Water Deficit Stress. *Communications in Soil Science and Plant Analysis*, 50(18), 2227-2237.

Janda, A., Vlaisavljevich, B., Lin, L. C., Smit, B. and Bell, A. T. (2016). Effects of zeolite structural confinement on adsorption thermodynamics and reaction kinetics for monomolecular cracking and dehydrogenation of n-butane. *Journal of the American Chemical Society*, 138(14), 4739-4756.

Jankauskiene, J., Brazaityte, A. and Viskelis, P. (2015). Effect of different growing substrates on physiological processes, productivity and quality of tomato in soilless culture. *Soilless culture: Use of substrates for the production of quality horticultural crops. InTech*, *Rijeka*, *Croatia*, 99-124.

Jiang, J., Yun, Y., Zou, X., Jorda, J.L. and Corma, A. (2015). A multi-dimensional extra-large pore zeolite with 20 X 14 X 12-ring channels. *Chemical Science*, 6(2), 480 –485

Jiang, N., Shang, R., Heijman, S. G. and Rietveld, L. C. (2018). High-silica zeolites for adsorption of organic micro-pollutants in water treatment: A review. *Water research*, 144(3), 145-161

.

Jie, L. Y., Nik, A. N., Teo, W. S., Noor, H. (2015). Effect of Surfactant Modified Zeolite (SMZ) added in propagating substrate for the germination of some vegetables. Proceedings of THeIRES 4th International Conference, Kuala Lumpur, Malaysia. 16th – 19th November, 2015. pp 51 - 73

Jiménez-Castañeda, M. E. and Medina, D. I. (2017). Use of surfactant-modified zeolites and clays for the removal of heavy metals from water. *Water*, *9*(4), 235.

Johnson, E. B. G., and Arshad, S. E. (2014). Hydrothermally synthesised zeolites based on kaolinite: a review. *Applied Clay Science*, 97(1), 215-221.

Johan, E., Yamada, T., Munthali, M. W., Kabwadza-Corner, P., Aono, H. and Matsue, N. (2015). Natural zeolites as potential materials for decontamination of radioactive cesium. *Procedia Environmental Sciences*, 28, 52-56.

Jumadi, O., Hartono, H., Masniawati, A., Iriany, R. N., Makkulawu, A. T. and Inubushi, K. (2019). Emissions of nitrous oxide and methane from rice field after granulated urea application with nitrification inhibitors and zeolite under different water managements. *Paddy and Water Environment*, *17*(4), 715-724.

Kacem, M., Pellerano, M. and Delebarre, A. (2015). Pressure swing adsorption for CO_2/N_2 and CO_2/CH_4 separation: Comparison between activated carbons and zeolites performances. *Fuel Processing Technology*, 13(8), 271-283.

Kalotra, S., Mehta, R. G. and Sangal, V. K. (2014). *Adsorption Study for the Treatment of Wastewater Using Cloisite 15A as an Adsorbent* (Doctoral dissertation) Thapar University, Punjah, India.

Kam, S.K., Kim, K.S., Ahn, B.J., Lee, M.G. (2002). Adsorption and desorption of hexadecyltrimethylammonium bromide by natural and synthetic zeolite. *Hwahak Konghak*, 40(2), 265 -273.

Kamal, M. S., Hussein, I. A. and Sultan, A. S. (2017). Review on surfactant flooding: phase behavior, retention, IFT, and field applications. *Energy and Fuels*, 31(8), 7701-7720.

Katsiki, A. (2019). Aluminosilicate phosphate cements–a critical review. *Advances in Applied Ceramics*, 118(5), 274-286.

Kaushik, G., Vishnu, J. and Arslan, R. (2014). Manufacture and categorization of nanoporous zeolite based N fertilizer. *African Journal of Agronomy*, 2 (7) 180-187

Khaleque, A., Alam, M. M., Hoque, M., Mondal, S., Haider, J. B., Xu, B. and Moni, M. A. (2020). Zeolite synthesis from low-cost materials and environmental applications: A review. *Environmental Advances*, 2(2), 10 - 19.

Khivantsev, K., Jaegers, N. R., Kovarik, L., Wang, M., Hu, J. Z., Wang, Y. and Szanyi, J. (2021). The superior hydrothermal stability of Pd/SSZ-39 in low temperature passive NOx adsorption (PNA) and methane combustion. *Applied Catalysis B: Environmental*, 280, 119 - 129.

Koshy, N. and Singh, D.N. (2016). Fly ash zeolites for water treatment applications. *Journal of Environmental Chemical Engineering*, 4(3), 1460 – 1472.

Kowalak, S., Szyld, M., Jankowska, A., Zalewska, A., Colella, A. and De Gennaro, B. (2015). Embedment of Methylene Blue in natural and synthetic phillipsite. *Clay Minerals*, 50(1), 23-30.

Kovo, A. S., and Edoga, M. O. (2005). Production and Characterisation of Zeolite from Ahoko Clay in Kogi State, Nigeria. *Leonardo Electronic Journal of Practices and Technologies, 7(1),* 31-40.

Kovo A. S. and Holmes, S. M. (2009). Synthesis and characterization of zeolite A from Ahoko Nigerian kaolin using novel dehydroxylation technique, *Advanced Powder Technology*, 27(2), 750-755.

Kovo, A. S. (2011). Development of zeolites and zeolite membranes from Ahoko Nigerian Kaolin. Doctoral dissertation, The University of Manchester, United Kingdom.

Kovo, A. S., Abdulkareem, A. S. and Salami, H. (2017). Statistical analysis of zeolite A and Y synthesised from Ahoko kaolin using two different hydrothermal methods and the study of their ion exchange capacities, *Journal of Nigeria Society of Chemical Engineers*, *32*(2), 82-82.

Krivovichev, S. V. (2017). Structure description, interpretation and classification in mineralogical crystallography. *Crystallography Reviews*, *23*(1), 2-71.

Kulasekaran, R., Ashis, k., Jayaraman, S., Annagi, S. (2010). Nanoporous Zeolites in Farming: Current Status and Issues Ahead. *Current Science*, 6(1), 760-764.

Kusumastuti, Y., Istiani, A. and Purnomo, C. W. (2019). Chitosan-based polyion multilayer coating on NPK fertilizer as controlled released fertilizer. *Advances in Materials Science and Engineering*, 20(5), 19.- 26.

Kwakye-Awuaha, B., Adzabea F. J. K., Nkrumaha N. and William B. (2013). Application of Laboratory-Synthesised Ammonium Zeolite LTX as Soil Amendment Additive. *International Journal of Sciences: Basic and Applied Research (IJSBAR)*, 12(1), 67-81

Kwakye-Awuah, B., Von-Kiti, E., Buamah, R., Nkrumah, I. and Williams, C. (2014). Effect of crystallisation time on the hydrothermal synthesis of zeolites from kaolin and bauxite. *International Journal of Scientific and Engineering Research*, 5(2), 734- 741

Lafrenière, C., Surrage, V., Dixon, M.A. and Zheng, Y. (2011). Evaluation of Zeolite as a component in organic growing substrates for tomato transplant production. *Acta Horticulturae*, 89(3), 1215-1222

Lateef, A., Nazir, R., Jamil, N., Alam, S., Shah, R., Khan, M. N., and Saleem, M. (2016). Synthesis and characterization of zeolite based nano–composite: an environment friendly slow release fertilizer. *Microporous and Mesoporous Materials*, *232(6)*, 174-183.

Latifah, O., Ahmed, O. H. and Majid, N. M. A. (2017). Enhancing nitrogen availability from urea using clinoptilolite zeolite. *Geoderma*, 306(1), 152-159.

Lee, M. G., Park, J. W., Kam, S. K., and Lee, C. H. (2018). Synthesis of Na-A zeolite from Jeju Island scoria using fusion/hydrothermal method. *Chemosphere*, *207*, 203-208.

Leghari, S. J., Wahocho, N. A., Laghari, G. M., HafeezLaghari, A., MustafaBhabhan, G., HussainTalpur, K. and Lashari, A. A. (2016). Role of nitrogen for plant growth and development: A review. *Advances in Environmental Biology*, 10(9), 209-219.

Li, H., Hou, R., Chen, Y. and Chen, H. (2019). Removal of hexavalent chromium from aqueous solutions using sulfonated peat. *Water*, 11(10), 19 - 30.

Li, Y., Li, L., and Yu, J. (2017). Applications of zeolites in sustainable chemistry. *Chemical Materials*, 3(6), 928-949.

Li, Z., Zhang, Y. and Li, Y. (2013). Zeolite as slow release fertilizer on spinach yields and quality in a greenhouse test. *Journal of Plant Nutrition, 36*(10), 1496-1505.

Li, Z., Wen, X., Hu, C., Li, X., Li, S., Zhang, X. and Hu, B. (2020). Regional simulation of nitrate leaching potential from winter wheat-summer maize rotation croplands on the North China Plain using the NLEAP-GIS model. *Agriculture*, *Ecosystems and Environment*, *294(1)*, 106 - 121.

Lima, C., Bieseki, L., Melguizo, P. V. and Pergher, S. B. C. (2019*). Environmentally Friendly Zeolites.pp 22 -28*, Springer International Publishing.

Lin, Q., Bu, X., Mao, C., Zhao, X., Sasan, K., and Feng, P. (2015). Mimicking high-silica zeolites: highly stable germanium-and tin-rich zeolite-type chalcogenides. *Journal of the American Chemical Society, 137*(9), 6184-6187

Lisa Rydenheim (2007). Effects of Zeolites on the growth of cucumber and tomato seedlings. Unpublished theses, Department of Horticulture, Swedish University of Agriculture (SLU), Box 44 SE-230 53 Alnarp.

Liu, J., Huang, H., Huang, R., Zhang, J., Hao, S., Shen, Y. and Chen, H. (2016). Mechanisms of CPB modified zeolite on mercury adsorption in simulated wastewater. *Water Environment Research*, 88(6), 490-499.

Liu, Y., Pan, Z., Zhuang, Q., Miralles, D. G., Teuling, A.J., Zhang, A. J. (2015). Agriculture intensifies soil moisture decline in Northern China, *Scientific Reports* 5(1), 11261 - 11268

Loiola, A.R., Andrade, J.C., Sasaki, J.M., Silva, L.R. (2012). Structural analysis of zeolite NaA synthesised by a cost-effective hydrothermal method using kaolin and its use as water softener. *Journal of Colloid and Interface Science*, 367(3), 34 – 39.

Lozinska, M. M., Miller, D. N., Brandani, S. and Wright, P. A. (2020). Hiding extra-framework cations in zeolites L and Y by internal ion exchange and its effect on CO_2 adsorption. *Journal of Materials Chemistry*, 8(6), 3280-3292.

Ltifi, I., Ayari, F., Hassen Chehimi, D. and Ayadi, M. (2017). Study of the adsorption of bright green by a natural clay and modified. *Journal of Material Science Engineering*, 6(2), 21-32.

Lubkowski, K. (2014). Coating fertilizer granules with biodegradable materials for controlled fertilizer release. *Environmental Engineering and Management Journal* (EEMJ), 13(10), 11- 19.

Mahesh, M., Thomas, J., Kumar, K. A., Bhople, B. S., Saresh, N. V., Vaid, S. K., and Sahu, S. K. (2018). Zeolite Farming: A Sustainable Agricultural Prospective. *International Journal of Current Microbiology and Applied Science*, 7(5), 2912-2924.

Maheswari, M., Murthy, A. N. G. and Shanker, A. K. (2017). Nitrogen Nutrition in Crops and Its Importance in Crop Quality. In *The Indian Nitrogen Assessment* (pp. 175-186). Elsevier.

Maia, A. Á. B., Dias, R. N., Angélica, R. S. and Neves, R. F. (2019). Influence of an aging step on the synthesis of zeolite NaA from Brazilian Amazon kaolin waste. *Journal of Materials Research and Technology*, *8*(3), 2924-2929.

Maleki Dizaj, S., Lotfipour, F., Barzegar-Jalali, M., Zarrintan, M. H. and Adibkia, K. (2016). Application of Box–Behnken design to prepare gentamicin-loaded calcium carbonate nanoparticles. *Artificial cells*, *nanomedicine*, *and biotechnology*, 44(6), 1475-1481.

Malhotra, H., Sharma, S. and Pandey, R. (2018). Phosphorus nutrition: plant growth in response to deficiency and excess. In Plant nutrients and abiotic stress tolerance (pp. 171-190). Springer, Singapore.

Mcevoy, J. E. and Mills, G. A. (1970). *U.S. Patent No. 3,532,459*. Washington, DC: U.S. Patent and Trademark Office

Mehrab, N., Chorom M. and Hojati, S., (2016). Effect of Raw and NH_4^+-enriched Zeolite on Nitrogen Uptake by Wheat and Nitrogen Leaching in Soils with Different Textures, *Communications in Soil Science and Plant Analysis*, 47(10), 1306-1316.

Manikandan, A., and Subramanian, K. S. (2014). Fabrication and characterisation of nanoporous zeolite based N fertilizer. *African Journal of Agricultural Research*, 9(2), 276-284.

Manikandan, A. and Subramanian, K. (2016). Evaluation of zeolite based nitrogen nano-fertilizers on maize growth, yield and quality on inceptisols and alfisols. *International Journal of Plant and Soil Science*, 9(4), 1-9.

Manjaiah, K. M., Mukhopadhyay, R., Paul, R., Datta, S. C., Kumararaja, P. and Sarkar, B. (2019). Clay minerals and zeolites for environmentally sustainable agriculture. *In Modified clay and zeolite nanocomposite materials* (pp. 309-329). Elsevier.

Maina, E. W. (2016). *Studies on photo stabilization of pyrethrum flower extracts using clay*, (Unpublished Master's thesis), Jomo Kenyatta University of Agriculture and Technology,Nairobi, Kenya.

Mattioli, M. and Cenni, M. (2020). Mineralogical dataset of natural zeolites from Lessini Mounts, Northern Italy: Analcime, natrolite, phillipsite and harmotome chemical composition. *Data in Brief*, 31(1), 10 - 15.

Mees, F. (2018). Authigenic silicate minerals–sepiolite-palygorskite, zeolites and sodium silicates. In Interpretation of Micromorphological Features of Soils and Regoliths (pp. 177-203). Elsevier.

Mehrab, N., Chorom, M. and Hojati, S. (2016). Effect of Raw and NH_4^+-enriched zeolite on nitrogen uptake by wheat and nitrogen leaching in soils with different textures. *Communications in Soil Science and Plant Analysis, 47*(10), 1306-1316.

Menezes, R. A., Paz, S. P. A., Angélica, R. S., Neves, R. F., Neumann, R., Faulstich, F. R. L. and Pergher, S. B. C. (2017). Synthesis of ultramarine pigments from Na-A zeolite derived from kaolin waste from the Amazon. *Clay Minerals*, *52*(1), 83-95.

Mikhak, A., Sohrabi, A., Kassaee, M. Z. and Feizian, M. (2018). Effect of Nanoclinoptilolite/Nanohydroxyapatite mixtures on phosphorus solubility in soil. *Journal of Plant Nutrition*, *41*(10), 1227-1239.

Mikula, K., Izydorczyk, G., Skrzypczak, D., Mironiuk, M., Moustakas, K., Witek-Krowiak, A. and Chojnacka, K. (2020). Controlled release micronutrient fertilizers for precision agriculture–A review. *Science of the Total Environment*, 71(2), 13 - 22.

Milani, P., França, D., Balieiro, A. G., and Faez, R. (2017). Polymers and its applications in agriculture. *Polímeros*, 27(3), 256-266.

Minkara, K. (2017). *Zeolite Facies and Environmental Change in the Plio-Pleistocene Baringo Basin*, *Kenya Rift*, (Master's Thesis), Georgia State University, Georgia

Mirfendereski, S.M. (2018). Synthesis of zeolite NaA Nano-crystals: Effect of synthesis parameters on crystallinity and crystal size. *Iranian Journal of Chemical Engineering*, 16(1), 22 – 38.

Mirfendereski, M.and Mohammadi, T. (2016). Effects of synthesis parameters on the characteristics of NaA Type zeolite nanoparticles. In *Proceedings of the World Congress on Recent Advances in Nanotechnology (RAN'16)* (pp. 1-8).

Mohebbi, S., Rostamizadeh, M. and Kahforoushan, D. (2020). Efficient sulfated high silica ZSM-5 nanocatalyst for esterification of oleic acid with methanol. *Microporous and Mesoporous Materials*, 29(4), 98 - 105.

Moliner, M., Martínez, C., and Corma, A. (2015). Multipore zeolites: synthesis and catalytic applications. *Angewandte Chemie International Edition*, *54*(12), 3560-3579.

Moshoeshoe, M., Nadiye-Tabbiruka, M. S., and Obuseng, V. (2017). A Review of the Chemistry, Structure, Properties and Applications of Zeolites, *American Journal of Materials Science*, *7*(5), 196-221.

Mostafa, A. A., Youssef, H. F., Sorour, M. H., Tewfik, S. R. and Shalaan, H. F. (2011). Utilization of Egyptian kaolin for zeolite-A preparation and performance evaluation. *In 2nd International conference on environmental science and technology*, (6), 1- 8

Munir, J.M., Nabila S. K., Nabil, K. A. (2004). Response of Croton Grown in a Zeolite-Containing Substrate to Different Concentrations of Fertilizer Solution. *Communications in Soil science and Plant Analysis*, 35 (15), 2283 – 2297.

Muraoka, K., Chaikittisilp, W. and Okubo, T. (2016). Energy analysis of aluminosilicate zeolites with comprehensive ranges of framework topologies, chemical compositions, and aluminum distributions. *Journal of the American Chemical Society*, 138(19), 6184-6193.

Murat, M., Amokrane, A., Bastide, J. P. and Montanaro, L. (1992). Synthesis of zeolites from thermally activated kaolinite. Some observations on nucleation and growth. *Clay Minerals*, *27*(1), 119-130.

Murray, J. S. and Politzer, P. (2017). Molecular electrostatic potentials and noncovalent interactions. *Wiley Interdisciplinary Reviews*: *Computational Molecular Science*, 7(6), 13 - 26.

Musyoka, N. M. (2012). *Zeolite A, X and Cancrinite from South African coal fly ash: mechanism of crystallisation, routes to rapid synthesis and new morphology*. (Doctoral dissertation), University of the Western Cape, South Africa

Musyoka, N. M., Petrik, L.F., Hums, E.A.K., and Schwieger, W. (2013). Thermal Stability studies of zeolite A and X synthesised from South African Coal fly ash. *Research Chemistry Intermediate*, 2(3), 7 - 18

Musyoka, N. M., Missengue, R., Kusisakana, M. and Petrik, L. F. (2014). Conversion of South African clays into high quality zeolites. *Applied Clay Science*, *97(2)*, 182-186.

Musyoka, N. M., Petrik, L. F., Balfour, G., Ndungu, P., Gitari, W. M., and Hums, E. (2012). Synthesis of zeolites from coal fly ash: Application of a statistical experimental design. *Research on Chemical Intermediates*, 38(2), 471-486.

Naderi, M. R. and Danesh-Shahraki, A. (2013). Nano-fertilizers and their roles in sustainable agriculture, *International Journal of Agricultural Crop Science*, 5(19), 2229-2232.

Nadziakiewicza, M., Kehoe, S. and Micek, P. (2019). Physico-chemical properties of clay minerals and their use as a health promoting feed additive. *Animals*, 9(10), 7 - 14.

Nair, A. T., Makwana, A. R., and Ahammed, M. M. (2014). The use of response surface methodology for modelling and analysis of water and wastewater treatment processes: a review. *Water Science and Technology*, *69*(3), 464-478.

Nagrockiene, D. and Girskas, G. (2016). Research into the properties of modified with natural zeolite addition. *Construction and Building Materials, 113(1)*, 964-969.

Nakhli, S. A. A., Delkash, M., Bakhshayesh, B. E. and Kazemian, H. (2017). Application of zeolites for sustainable agriculture: a review on water and nutrient retention. *Water, Air and Soil Pollution*, 228(12), 1-34.

Narimani, F. and Kharamesh, M. (2014). Synthesis of nano-porous molecular sieve from some natural materials. *International Journal of Nano Dimension*, 5(1), 69-75.

Naz, M. Y. and Sulaiman, S. A. (2016). Slow release coating remedy for nitrogen loss from conventional urea: a review. *Journal of Controlled Release*, 225, 109-120.

Nigussie, A. (2018). *Removal of Nitrate from Groundwater Using Modified Natural Zeolite, the Case of Dire Dawa City, Ethiopia* (Doctoral dissertation, Addis Ababa University), Ethiopia.

Nimibofa, A., Tobin, E. A., David, S. N., Donbebe, W. and Dixon, D. E. (2017). Equilibrium, kinetic and thermodynamic studies of the uptake of copper by layered double hydroxide. *Hemijska Industrija*, 71(5), 429-437.

Naranjo, P. M., Sham, E. L., Castellón, E. R., Torres Sánchez, R. M. and Farfán, E. M. (2013). Identification and quantification of the interaction mechanisms between the cationic surfactant HDTMA-Br and montmorillonite. *Clays and Clay Minerals, 61*(2), 98-106.

Nokkoul, R. and Wichitparp, T. (2015). Research Article Effects of Zeolite Application on Seed Yield and Yield Component of Organic Upland Rice. *Research Journal of Applied Sciences, Engineering and Technology*, 11(8), 879-884

Notario, J.S., Garcia, J.E., Ceceres, J.M., Arteaga, I.J., Gonzales, M.M. (1995). Characterisation of Natural Phillipsite Modified with Orthophosphoric Acid. *Applied Clay Science*, 10(3), 209-217.

Omar, L., Ahmed, O. H., Jalloh, M. B. and Nik Muhamad, A. M. (2020). Soil nitrogen fractions, nitrogen use efficiency and yield of Zea mays L. grown on a tropical acid soil treated with composts and clinoptilolite zeolite. *Applied Sciences*, 10(12), 4 - 13.

Olutoye, (2012). *Synthesis, Characterization and Activity of Mixed metal oxide (Mg, Zn, Al) catalysts for Transesterification of Waste cooking palm oil*, *Edible and non-edible o ils*, (Doctoral dissertification), University of Malaysia, Ethiopia

Onuche, P. U., Okibe, F. G., and Ajibola, V. O. (2016). Biodegradation of Cetyltrimethylammonium Bromide and Methylparaben in Shampoo and Hair Dressing Salon Waste Using Bacteria Isolated from Sewage Treatment Sludge. *Archives of Current Research International*, 3(3), 1-9.

Onwudike, S. U., Uzoho, B. U., Ihem, E. E., Ahukaemere, C. M., Nkwopara, U., Irokwe, I. F. and Echeanyanwu, G. I. (2016). Evaluation of the fertility status of selected soils in Mbaise, Imo State southeastern Nigeria using nutrient index method. *Agrosearch*, 16(1), 75-86.

Onyia, V. N., Chukwudi, U. P., Ogwudu, V. C., Atugwu, A. I., Eze, S. C., Ene, C. O. and Umeh, S. (2019). Evaluation of Tomato Genotypes Growth, Yield, and Shelf Life Enhancement in Nigeria. *Journal of Agricultural Science and Technology*, 21(1), 143-152.

Ogunleye, O.O., Adeniyi, A.G., Durowoju, M.O. (2016). Factorial design based optimisation of crevice corrosion for type 304 stainless steel in chloride solutions. *Advances in Material Science*, 16(2), 48 – 67.

Ogunleye, O., Babatunde, K. and Agbede, O. (2016). Ricinus cummunis as feedstock for raw vegetable oil expression via mechanical extraction process. Optimization study. *Journal of Engineering and Technology*, 10(1), 74-81.

Oyinade, A., Kovo, A. S., and Hill, P. (2015). Synthesis, characterization and ion exchange isotherm of zeolite Y using Box–Behnken design. *Advanced Powder Technology*, 27(2), 750-755.

Ozdemir, D.O. and Piskin S. (2013). Zeolite X synthesis from different sources. *International Journal of Chemical, Environmental and Biological Sciences*, 1(2), 229 -232.

Paolini, V., Petracchini, F., Guerriero, E., Bencini, A., and Drigo, S. (2016). Biogas cleaning and upgrading with natural zeolites from tuffs. *Environmental technology*, *37*(11), 1418-1427.

Park, M. A. N., and Choi, I, J. (1995). Synthesis of Phillipsite from fly ash. *Clay Science*, *9*(4), 219-229

Park, J. I. N., Kim, B. C., Park, S. S. and Park, H. C. (2001). Conventional versus ultrasonic synthesis of zeolite 4A from kaolin. *Journal of Materials Science Letters*, *20*(6), 531-533.

Peng, S., Tang, Z., Jiang, W., Wu, D., Hong, S. and Xing, B. (2017). Mechanism and performance for adsorption of 2-chlorophenol onto zeolite with surfactant by one-step process from aqueous phase. *Science of the Total Environment*, *581(1)*, 550-558.

Peng, Y. L., Chen, L., Shen, G. Z., Li, Y. N., Yao, J. J., Xiao, W. W. and Deng, X. W. (2018). Interobserver variations in the delineation of target volumes and organs at risk and their impact on dose distribution in intensity-modulated radiation therapy for nasopharyngeal carcinoma. *Oral oncology*, 82, 1-7.

Preetha, P. S., and Balakrishnan, N. (2017). A Review of Nano fertilizers and their use and functions in Soil. *International Journal of Current Microbiology and Applied. Science*, *6*(12), 3117-3133.

Polat, E., Karaca, M., Demir, H., Naci-onus, A. (2004). Use of natural zeolite (clinoptilolite) in agriculture. *Journal of Fruit Ornament*, 12(6), 183 – 189.

Rabai, K.A., Ahmed O, H., and Kasim, S. (2012). Improving formulated nitrogen, phosphorous and potassium compound fertilizer using zeolite. *African Journal of Biotechnology*, 11(65), 1288-12829.

Rajan, M., Shahena, S., Chandran, V. and Mathew, L. (2021). Controlled release of fertilizers—concept, reality, and mechanism. *In Controlled Release Fertilizers for Sustainable Agriculture* (pp. 41-56). Academic Press.

Rajonee, A., Farah, N., Samma, A., Imamul, H. (2016). Synthesis of Nitrogen Nano-Fertilizer and its Efficacy. *Canadian Journal of Pure and Applied Sciences*,10(2), 3913-3919

Ramadoss, R. and Subramaniam, D. (2018). Adsorption of chromium using blue green algae-modeling and application of various isotherms. *International Journal of Chemical Technology*, 10(2), 1-22

Ramesh, V., James G., Jissy S., Jyothi., and Shibli, S.M.A. (2015). Effect of Zeolites on Soil quality, Plant growth and Nutrient uptake efficiency in Sweet Potato. *Journal of Root Crops*, 41(1), 25 -31.

Ramesh, K., Biswas, A. K., Somasundaram, J. and Subba Rao, A. (2010). Nanoporous zeolites in farming: Current status and issues ahead. *Current Science*, 99(6), 760-765.

Ramesh, K. and Reddy, D. D. (2011). Zeolites and Their Potential Uses in Agriculture, *Advances in Agronomy*, 113(5), 219- 235.

Rees, L. V. and Chandrasekhar, S. (1993). Hydrothermal reaction of kaolinite in presence offluoride ions at pH< 10. *Zeolites*, 13(7), 534-541.

Reeve, P. J. and Fallowfield, H. J. (2018). Natural and surfactant modified zeolites: a review of their applications for water remediation with a focus on surfactant desorption and toxicity towards microorganisms. *Journal of Environmental Management*, *205(1)*, 253-261.

Riley, R. D., Snell, K. I., Ensor, J., Burke, D. L., Harrell Jr, F. E., Moons, K. G. and Collins, G. S. (2019). Minimum sample size for developing a multivariable prediction model: PART II-binary and time-to-event outcomes. *Statistics in medicine*, 38(7), 1276-1296.

Ruman, M., Olkowska, E., Pytel, S. and Polkowska, Ż. (2018). Surfactants in Klodnica River (Katowice, Poland). Part II. Quaternary Ammonium Compounds. *Ecological Chemistry and Engineering*, *25*(2), 229-242.

Rujiwatra, A. (2004). A selective preparation of phillipsite and sodalite from perlite. *Materials Letters*, *58*(14), 2012-2015

Rodrigues, M. I. and Iemma, A. F. (2014). *Experimental design and process optimization*. (pp 9 – 21). CRC Press.

Rodrigues, M., Souza, A.G.and Santos, I. M. G. (2016). Brazilian Kaolin Wastes: Synthesis of Zeolite P at Low-Temperature, *American Chemical Science Journal* 12(4),1-11

Ruthiraan, M., Abdullah, E. C., Mubarak, N. M. and Nizamuddin, S. (2018). Adsorptive removal of methylene blue using magnetic biochar derived from agricultural waste biomass: equilibrium, isotherm, kinetic study. *International Journal of Nanoscience*, 17(05), 18 - 25.

.

Saadi, R., Saadi, Z., Fazaeli, R., and Fard, N. E. (2015). Monolayer and multilayer adsorption isotherm models for sorption from aqueous media. *Korean Journal of Chemical Engineering*, 32(5), 787-799.

Saha, P. and Chowdhury, S. (2011). Insight into adsorption thermodynamics. *Thermodynamics*, 12(1), 349-364.

Salmiaton, A. and Firoozeh, D., (2015). Controlled – Release Fertilizer: Advances and Challenges, *Life Science Journal*, 12(11), 33- 35

Samal, D. P. (2014). *Characterization of activated carbon and study of adsorption of methylene blue dye using activated carbon* (Doctoral dissertation). National Institute of Technology, Rourkela, India

Sangeetha, C. and Baskar, P. (2016). Zeolite and its potential uses in agriculture: A critical review. *Agricultural Reviews*, *37*(2), 101-108.

Sangita, K., Prasad, B. and Udayabhanu, G. (2016). Synthesis of zeolite from waste fly ash by using different methods. *Asian Journal of Chemistry*, 28(7), 14 - 35.

Sanhueza, V., Kelm, U. and Cid, R. (1999). Synthesis of molecular sieves from Chilean kaolinites: 1. Synthesis of NaA type zeolites. *Journal of Chemical Technology and Biotechnology: International Research in Process, Environmental and Clean Technology*, *74*(4), 358-363.

Schick, J., Caullet, P., Paillaud, J. L., Patarin, J. and Mangold-Callarec, C. (2010). Batch-wise nitrate removal from water on a surfactant-modified zeolite. *Microporous and Mesoporous Materials*, 132(3), 395-400.

Schulze, A., Strakos, L., Vystavel, T., Loo, R., Pacco, A., Collaert, N. and Caymax, M. (2018). Non-destructive characterization of extended crystalline defects in confined semiconductor device structures. *Nanoscale*, 10(15), 7058-7066.

Sebastian, O., Mariusz, K., Marek, S., Zbigniew, D., Roman, K. (2015). Application of aluminosilicates for mitigation of ammonia and volatile organic compound emissions from poultry manure, *Open Chemistry*, 13(4), 967–973.

Selim, M. M., EL-Mekkawi, D. M., Aboelenin, R. M., Sayed Ahmed, S. A., and Mohamed, G. M. (2017). Preparation and characterization of Na-A zeolite from aluminum scrub and commercial sodium silicate for the removal of Cd2+ from water. *Journal of the Association of Arab Universities for Basic and Applied Sciences*, 24(1), 19-25.

Selva-Preetha, P., Subramanian, K. S. and Sharmila Rahale, C. (2014). Sorption characteristics of nanozeolite based slow release sulphur fertilizer. *International Journal of Devevelopment Research*, *4(5)*, 225-228.

Selva-Preetha, P. and Balakrishnan, N. (2017). A Review of Nano Fertilizers and Their Use and Functions in Soil. *International Journal of Current Microbiology and Applied Sciences*. 6(12), 3117-3133.

Sempeho, S. I., Kim, H. T., Mubofu, E., and Hilonga, A. (2014). Meticulous overview on the controlled release fertilizers. *Advances in Chemistry*. 12(2), 78 -85

Seyed, A. H. (2015). Optimization of Synthesis Conditions of Zeolite 4A from Nepheline Syenite, *International Journal of Materials Chemistry and Physics*, 1(2), 93-98

Shaban, M., Abukhadra, M. R., Shahien, M. G. and Ibrahim, S. S. (2018). Novel bentonite/zeolite-NaP composite efficiently removes methylene blue and Congo red dyes. *Environmental chemistry letters*, *16*(1), 275-280.

Shah, B., Pandya, D., Patel, H., Ayalewa, A., Shah., A. (2016). Zeolitic Composites from Agricultural Detritus for pollution Remedy: A Review, *Journal of Critical Reviews*, 3(3). 33 – 39.

Shahmohammadi-Kalalagh, S. and Babazadeh, H. (2014). Isotherms for the sorption of zinc and copper onto kaolinite: comparison of various error functions. *International Journal of Environmental Science and Technology*, 11(1), 111-118.

Shaila, K., Dawle, N., Patil, P., Panhekar, D. (2015). Zeolite Synthesis Strategies from Coal Fly Ash: A Comprehensive Review of Literature. *International Research Journal of Environmental Sciences*, 4(3), 93 – 99.

Sharma, S.K. and Sambi, S.S. (2010). Conversion of low grade clays to zeolite NaA The IUP, *Journal of Chemistry*, 3(2), 32 – 41.

Shi, J., Zhang, N., Zhang, C. and Wei, B. (2016). Study on the effect of different modified zeolite to phosphorus activation in red soil. *Journal of Environmental Protection*, 7(13), 2036.

Sherafatmand, S., Hoodaji, M., Eghtedari, A. (2014). The effect of Iron riched zeolite application on tomato yield and quality in soilless culture. The first International Conference on New Ideas in Agriculture, Islamic Azad University, khorasgan Branch, 26 – 27, Jan 2014, Isfahan, Iran.

Silva Filho, S. H. D., Bieseki, L., Maia, A. A. B., Treichel, H., Angelica, R. S. and Pergher, S. B. C. (2017). Study on the NaOH/metakaolin ratio and crystallisation time for zeolite a synthesis from kaolin using statistical design. *Materials Research*, 20(3), 761-767.

Sonmez,I., Mustafa, K., Halil, D. and Erdem, Y.(2010). Effects of zeolite on seedling quality and nutrient contents of tomato plant (Solanum lycopersicon cv. Malike F1) grown in different mixtures of growing media. *Journal of Food, Agriculture and Environment*, 8 (2), 1162-1165.

Souri, M. K. and Dehnavard, S. (2018). Tomato plant growth, leaf nutrient concentrations and fruit quality under nitrogen foliar applications. *Advances in Horticultural Science*, 32(1), 41-47.

Subramanian, K. S., Manikandan, A., Thirunavukkarasu, M., and Rahale, C. S. (2015). Nano-fertilizers for balanced crop nutrition. In *Nanotechnologies in Food and Agriculture* (pp. 69-80). Springer, Cham.

Subbarao, C. V., Kartheek, G. and Sirisha, D. (2013). Slow release of potash fertilizer through polymer coating. *International Journal of Applied Science and Engineering*, 11(1), 25-31

Suek, N. W., Guillaume, M. C., Delannoy, J. Y. P. and Tielens, F. (2018). Characterization of hydroxylated amorphous silica: A numerical approach. *Adsorption*, 24(3), 267-278.

Swarnkar, V. and Tomar, R. (2013). Sorption of Chromate by Surfactant Modified Willhender-sonite. *Acta Chim Pharmceutical Indica*, *3*, 40-51.

Szabo, K., Catoi, A. F. and Vodnar, D. C. (2018). Bioactive compounds extracted from tomato processing by-products as a source of valuable nutrients. *Plant foods for human nutrition*, 73(4), 268-277.

Szala, B., Bajda, T., Jelen, A, (2015). Removal of chromium (VI) from aqueous solutions using zeolites modified with HDTMA and ODTMA surfactants. *Clay Minerals*, 50(1), 103 – 115

Taaca, K. L. M., Nakajima, H., Thumanu, K., Janphuang, P., Chanlek, N. and Vasquez Jr, M. R. (2020). Spectroscopic studies of plasma-modified silver-exchanged zeolite and chitosan composites. *Materials Chemistry and Physics,* 250(2), 122 - 134.

Tan, I. A. W. and Hameed, B. H. (2010). Adsorption isotherms, kinetics, thermodynamics and desorption studies of basic dye on activated carbon derived from oil palm empty fruit bunch. *Journal of Applied Sciences (Faisalabad)*, *10*(21), 2565-2571

Tan, K. L. and Hameed, B. H. (2017). Insight into the adsorption kinetics models for the removal of contaminants from aqueous solutions. *Journal of the Taiwan Institute of Chemical Engineers*, 74(1), 25-48.

Tarafdar, J. C. (2015). Nanoparticle production, characterization and its application to horticultural crops. Compendium of winter school on utilization of degraded land and soil through horticultural crops for improving agricultural productivity and environmental quality. *NRCSS*, *Ajmer*, India, 222-229.

Taheri-Soudejani, H., Heidarpour, M., Shayannejad, M., Shariatmadari, H., Kazemian, H. and Afyuni, M. (2019). Composts Containing Natural and Mg-Modified Zeolite: The Effect on Nitrate Leaching, Drainage Water, and Yield. *CLEAN–Soil, Air, Water*, 47(8), 18 - 27.

Thakkar, K., Bharatiya, B., Ray, D., Aswal, V. K. and Bahadur, P. (2017). Cationic surfactants modulate aqueous micellization and wetting on PTFE by Triton X-100: Effect of alkyl chain length, headgroup and counterion. *Journal of Molecular Liquids*, *241(1)*, 136-143.

Thakur, A. (2017). *Evaluation of biological control strategies against a range of plant pathogens*. (Masters theses). Agricultural university of Athens.Greece

Thirunavukkarasu, M. and Subramanian, K.S. (2014). Surface modified nano-zeolite used as carrier for slow release of sulphur. *Journal of Applied and Natural Science* 6 (1), 19-26.

Timilsena, Y. P., Adhikari, R., Casey, P., Muster, T., Gill, H. and Adhikari, B. (2015). Enhanced efficiency fertilisers: a review of formulation and nutrient release patterns. *Journal of the Science of Food and Agriculture*, 95(6), 1131-1142.

Tontisirin, S. (2017). Synthesis and characterization of co-crystalline zeolite composite of LSX/A. *Microporous and Mesoporous Materials*, *239(1)*, 123-129.

Tran, Y. T., Lee, J., Kumar, P., Kim, K. H. and Lee, S. S. (2019). Natural zeolite and its application in concrete composite production. Composites Part B: *Engineering*, 165(2), 354-364.

Treacy, M. M., Higgins, J. B., and von Ballmoos, R. (1996). Collection of simulated XRD powder patterns for zeolites. *Zeolites*, *5*(16), 330-802.

Ugonna, C. U., Jolaoso, M. A. and Onwualu, A. P. (2015). Tomato value chain in Nigeria: Issues, challenges and strategies. *Journal of Scientific Research and Reports*, 1(2), 501-515.

Ushakumary, E. R. (2013). *Waste water treatment using low-cost natural adsorbents*. (Doctoral dissertation), The Cochin University of Science and Technology, Kerala, India.

Valpotic, H., Gracner, D., Turk, R., Đuricic, D., Vince, S., Folnozic, I. and Getz, I. (2017). Zeolite clinoptilolite nanoporous feed additive for animals of veterinary importance: potentials and limitations. *Periodicum biologorum*, *119*(3), 159-172.

Villarroel-Rocha J., Barrera D., Arroyo-Gómez J.J., Sapag K. (2020) Critical Overview of Textural Characterization of Zeolites by Gas Adsorption. In: Valencia S., Rey F. (eds) New Developments in Adsorption/Separation of Small Molecules by Zeolites. Structure and Bonding, vol 184. Springer, Cham

Volova, T. G., Prudnikova, S. V. and Boyandin, A. N. (2016). Biodegradable poly-3-hydroxybutyrate as a fertiliser carrier. *Journal of the Science of Food and Agriculture*, 96(12), 4183-4193.

Wato, T. (2019). Improvements of Crop Production through Integrated Soil Fertility Management in Ethiopia. *Asian Journal of Environment and Ecology*, 1(1), 2-11.

Wang, J., Huang, Y., Pan, Y. (2014). Hydrothermal synthesis of high purity zeolite A from natural kaolin without calcinations. *Microporous and Mesoporous Materials*, 199 (2), 50 – 56.

Wang, J. and Guo, X. (2020). Adsorption isotherm models: Classification, physical meaning, application and solving method. *Chemosphere*, 12(7), 2 - 9.

Wang, X., Yun, J., Shi, P., Li, Z., Li, P. and Xing, Y. (2019). Root growth, fruit yield and water use efficiency of greenhouse grown tomato under different irrigation regimes and nitrogen levels. *Journal of Plant Growth Regulation*, 38(2), 400-415.

Wołowiec, M., Muir, B., Zięba, K., Bajda, T., Kowalik, M. and Franus, W. (2017). Experimental study on the removal of VOCs and PAHs by zeolites and surfactant-modified zeolites. *Energy and Fuels*, *31*(8), 8803-8812.

Wu, D., Sun, Y., Wang, L., Zhang, Z., Gui, J. and Ding, A. (2019). Modification of NaY zeolite by lanthanum and hexadecyl trimethyl ammonium bromide (HDTMA) and its removal performance for nitrate. *Water Environment Research* 8(2), 73 – 82.

Wu, Q., Chi, D., Xia, G., Chen, T., Sun, Y. and Song, Y. (2019). Effects of Zeolite on Drought Resistance and Water–Nitrogen Use Efficiency in Paddy Rice. *Journal of Irrigation and Drainage Engineering*, 145(11), 41 - 52.

Wu, Q. S., Srivastava, A. K., Zou, Y. N. and Malhotra, S. K. (2017). Mycorrhizas in citrus: Beyond soil fertility and plant nutrition. *Indian Journal of Agricultural Sciences*, 87(4), 427-443.

Wyszkowski, M. and Sivitskaya, V. (2019). Effect of sorbents on the content of trace elements in maize cultivated on soil contaminated with heating oil. *International Agrophysics*, 33(1), 437-444.

Xia, H., Yan, X., Xu, S., Yang, L., Ge, J.W., and Zuo, S. (2015). Effect of Zn/ZSM-5 and $FePO_4$ catalysts on cellulose pyrolysis. *Journal of Chemistry*, 15(1), 749 – 765.

Xing, X., Chang, P. H., Lv, G., Jiang, W. T., Jean, J. S., Liao, L. and Li, Z. (2016). Ionic-liquid-crafted zeolite for the removal of anionic dye methyl orange. *Journal of the Taiwan Institute of Chemical Engineers*, 59(1), 237-243.

Yadav, K. K. and Sarkar, S. (2019). Biofertilizers, impact on soil fertility and crop productivity under sustainable agriculture. *Environment and Ecology*, 37(1), 89-93.

Yılmaz, E., Ozen, N. and Ozen, M. (2017). Determination of changes in yield and quality of tomato seedlings (*Solanum lycopersicon cv. Sedef* F1) in different soilless growing media. *Mediterranean Agricultural Sciences, 30*(2), 163-168.

Younas, M., Sohail, M., Leong, L. K., Bashir, M. J., and Sumathi, S. (2016). Feasibility of CO_2 adsorption by solid adsorbents: a review on low-temperature systems. *International Journal of Environmental Science and Technology*, 13(7), 1839-1860.

Young, A. M. (2011). *Zeolite Based Algae Biofilm Rotating Photo bioreactor for Algae and Biomass Production*. (Masters Theses). Utah State University, United States.

Youssef, H., Ibrahim, D. and Komarneni, S. (2008). Microwave-assisted versus conventional synthesis of zeolite A from metakaolinite. *Microporous and Mesoporous Materials, 115*(3), 527-534.

Yousef, R. I., El-Eswed, B. and Ala'a, H. (2011). Adsorption characteristics of natural zeolites as solid adsorbents for phenol removal from aqueous solutions: kinetics, mechanism, and thermodynamics studies. *Chemical Engineering Journal*, 171(3), 1143-1149.

Yuna, Z. (2016). Review of the natural, modified, and synthetic zeolites for heavy metals removal from wastewater. *Environmental Engineering Science*, *33*(7), 443-454.

Yuvaraj, M. and Subramanian, K. S. (2018). Development of slow release Zn fertilizer using nano-zeolite as carrier. *Journal of plant nutrition*, 41(3), 311-320.

Zahoor, F., Malik, M. A., Anser, R., Shehzad, M., Saleem, A., Anser, M. and Raza, S. H. (2015). Water use efficiency and rain water productivity of wheat under various tillage-glyphosate interactive systems. *Cercetari Agronomice in Moldova*, 48(1), 25-36.

Zhang, Y., Zhao, L. and Chen, Y. (2017). Synthesis and characterization of starch-g-Poly (acrylic acid)/Organo-Zeolite 4 A superabsorbent composites with respect to their water-holding capacities and nutrient-release behavior. *Polymer composites*, *38*(9), 1838-1848.

Zheng, Y., Xiaogan, Li., and Prabir, K., (2012). Exploitation of Unique Properties of Zeolites in the Development of Gas Sensors. *Sensors*, 12(1), 5170-5194.

Zhaohu, L., Yingpeng, Z and Yan, L. (2013). Zeolite as slow release fertilizer on spinach yields and quality in a greenhouse test, *Journal of Plant Nutrition*, 36 (10), 1496-1505.

Zhihui, Z., Yan, C., Yan, J. and Yunsong, Y. (2014). Crystallisation mechanism of zeolite A from coal kaolin using a two-step method. *Applied Clay Science*, 8(2), 421 – 434.

Appendix A

List of Publications

Patent: Submitted

Salako, O., Kovo, A.S., Abdulkareem, A.S., Yusuf, S.T., Afolabi, E.A. and Auta, M. (2020). The Effect of Synthesised NPK loaded Surfactant Modified zeolite A based Fertilizer in Tomato (*Lycopersicon esculentum*) cultivation. *Journal of the Nigeria Soceity of Chemical Engineering*, 35(1), 50 – 63.

Salako, O., Kovo, A.S., Abdulkareem, A.S., Yusuf, S. T. (2017). Synthesis of LTA Zeolite from Ahoko Kaolin: Application of Statistical Analysis. Proceedings of 2nd International Engineering Conference, Federal University of Technology, Minna, Niger State, Nigeria, 17th – 19th October, 2017, pp 39-47

Salako, O., Kovo, A. S., Abdulkareem, A. S., Yusuf, S.T., Afolabi, E. A. and Auta, M. (2019). The Effect of Synthesised NPK Loaded Surfactant Modified Zeolite A based Fertilizer in Tomato (*Lycopersicon esculentum*) Cultivation. Proceedings of the 49th NSChE Annual Conference (KADA 2019), Kaduna, Nigeria, 13 -16 November, 2019.pp 56 – 72

Appendix B: Phillipsite synthesis recipe by (Jakkula *et al.*, 2011)

$6.95Na_2O: 3.50K_2O: Al_2O_3 : 18.5SiO_2 : 325H_2O$

40g of NaOH = 1 mole of NaOH

1g of NaOH = 1/40 mole of NaOH

= 0.025 mole g NaOH

= 0.025 x Purity

= 0.025 x 99 %

=0.02475 mole of NaOH (1)

Source of Na_2O

NaOH was used to supply the required Na_2O

$Na_2O + H_2O$ = 2NaOH (2)

i.e. 1 mole of Na_2O = 2 moles of NaOH

6.95 moles of Na_2O = 6.95 x 2 moles of NaOH

= 13.90 moles of NaOH

From Equation (1)

0.02475 mole of NaOH = 1g of NaOH

13.90 moles of NaOH = 1/0.02475 x 13.90

= 561.616g of NaOH

Source of K_2O

$K_2O + H_2O$ = 2KOH (3)

KOH was used to supply the required K_2O

i.e. 1 mole of K_2O = 2 moles of KOH

3.50 moles of K_2O = 2 x 3.50 moles of KOH

= 7.0 moles of KOH (4)

56 g of KOH = 1 mole of KOH

1g of KOH = 1/56 mole of KOH

= 0.0178 mole of KOH

= 0.0178 mole x purity

= 0.0178 mole x 99 %

= 0.0176 mole of KOH (5)

From equation (5)

0.0176 mole of KOH = 1g of KOH

1 mole of KOH = 1/0.0176 g of KOH

.: 7 mole of KOH = 1/0.0176 x 7 g of KOH

= 397g of KOH

Mass of water

18g of H_2O = 1 mole of H_2O

1 mole of H_2O = 18 g of H_2O

.: 325 moles of H_2O = 325 x 18g = 5850g of H_2O

Removing 1 mole of H_2O each from the introduction of NaOH and KOH

= 5850g – 36g of H_2O = 5814g of H_2O

Metakaolin is basically SiO_2	=	60.08 x 18.50	= 1111.48
Al_2O_3		101.96 x1	+101.96
			1,213.44g of metakaolin

Therefore			scale down to	
Mass of needed Kaolin	=	1,213.44g	=	2.999 g
Mass of needed NaOH	=	561.616g	=	1.3884 g
Mass of needed KOH	=	397g	=	0.9815g
Mass of needed H_2O	=	5814g	=	14.3740g

Appendix C: Zeolite A recipe reported by (Oyinade *et al*., 2015)

3.75 Na_2O: Al_2O_3: 2.1 SiO_2: 243.7 H_2O

$2NaOH = H_2O + Na_2O$

$H_2Al_2Si_2O_8H_2O = Al_2O_3 + 2SiO_2 + 2H_2O$

Basis: 10g of kaolin.

Mole SiO_2 in 10g of kaolin = (0.60958 x10)/60 = 0.1015mol

.: **Mass of kaolin** to give 2.1 SiO_2 = (2.1 x 10)/ 0.1015 = 206.896 g

Mass of Al_2O_3 = 0.33832 x 206.896

= 69.997g/102

= 0.6862mol

1 – 0.6862 = 0.3137mol

= 0.3137mol x 102g

= 32g to add to make up 1 mol Al_2O_3

Mass of Na_2O = 0.0012 x 206.896/62

= 0.004 mol of Na_2O

3.75 – 0.004 = 3.7459mol of Na_2O to add up to make 3.75Na_2O

From 2NaOH = $Na_2O + H_2O$

Mass of NaOH required = 2(3.7459) x 0.96 x 40

= 287.68g of NaOH to make up to 3.75 Na_2O

Mole of H_2O in Kaolin = 2(0.1015mol.)

Mass of H_2O = 0.0146 x 206.896 = 3.0206816g

Mol of H_2O = 3.0206816/18 = 0.1678mol of H_2O

Mol of H_2O required from (metakaolin (OH)group) = 243.7 – 0.1678 = 243.532mol

= 243.532 – 3.7459 = 289.786/mol

.: Mass of H_2O required = 239.7861 x 18

= 4316.1498g

Therefore

Mass of needed Kaolin = 206.896g = 206.896g/100 = 2.0689g

Mass of needed NaOH	=	287.68g	=	287.68g/100	= 2.8768g
Mass of H_2O needed	=	4316.1498g	=	4316.1498/100	= 43.1614g

To further scale down	=	2.0689/x = 3;
x	=	2.0689/3
	=	0.689

Metakaolin=	2.0689/0.689	=	3g	
NaOH =	2.8768/0.689	=	4.175g	
H_20 =	43.1614/0.689	=	62.6435g	